

Dynamics in growth and metabolism of adherent MDCK cells unraveled by an integrated modeling approach

Dissertation
zur Erlangung des akademischen Grades

**Doktoringenieur
(Dr.-Ing.)**

von Dipl.-Ing. Markus Rehberg
geb. am 14.08.1984 in Ilmenau

genehmigt durch die Fakultät für Verfahrens- und Systemtechnik
der Otto-von-Guericke-Universität Magdeburg

Promotionskommission:

Jun.-Prof. Dr. rer. nat. Timo Frensing	(Vorsitz)
Prof. Dr.-Ing. Andreas Kremling	(Gutachter)
Prof. Dr. Manuel Freitas Oliveira	(Gutachter)
Prof. Dr.-Ing. Udo Reichl	(Mitglied)

eingereicht am 29. Juni 2015

Promotionskolloquium am 27.11.2015

simplicity is the ultimate
sophistication

(William Gaddis)

Danksagung

Die vorliegende Arbeit entstand im Rahmen meiner Tätigkeit in der Arbeitsgruppe Bioprozesstechnik am Max-Planck-Institut für Dynamik komplexer technischer Systeme in Magdeburg in der Zeit von Dezember 2009 bis Juni 2015. Ich möchte allen Danken, die daran mitgewirkt und meine Promotion unterstützt haben.

Mein ganz besonderer Dank gilt Herrn Prof. Dr.-Ing. Udo Reichl für die Gelegenheit, unter exzellenten Bedingungen und großzügiger thematischer Freiheit, meine Arbeit anfertigen und in seiner Gruppe mitwirken zu dürfen. Die vielen konstruktiven Diskussionen, seine inspirierenden Blickwinkel sowie seine Unterstützung in schwierigen Zeiten haben maßgeblich zum Gelingen der Arbeit beigetragen.

Ebenso gilt mein Dank Herrn Prof. Dr.-Ing. Kremling und Herrn Prof. Dr. rer. nat. Rui Oliveira für Ihr Interesse an der Arbeit und die Übernahme des Koreferats. Herrn Jun.-Prof. Dr. rer. nat. Timo Frensing danke ich für die Übernahme des Prüfungsvorsitzes.

Weiterhin bedanke ich mich herzlich bei Frau PD Dr. rer. nat. Yvonne Genzel für die fachliche Unterstützung zu Zellkulturen und Ihre Erfahrung im Umgang mit umfangreichen Forschungsprojekten.

Einen ausdrücklichen Dank verdient auch mein Bürokollege und Freund Dr.-Ing. Stefan Heldt für die tiefgründigen Diskussionen zur mathematischen Modellierung, die die Qualität dieser Arbeit an vielen Stellen geschärft hat, aber auch für das gemeinsame Feiern von Erfolgen wie Ertragen von Fehlschlägen.

Ebenfalls danke ich Prof. Dr. rer. nat. Dr. rer. nat. Dietrich Flockerzi, Dr. rer. nat. Hauser und Prof. Dr.-Ing. Stefan Streif für die konstruktiven Ideen und Analysen die mir eine erhellende Hilfestellung in der mathematischen Modellierung von Zellwachstum und Stoffwechsel waren.

Ein sehr herzliches Dankeschön gilt auch Maria Wetzels und Jan Mares Klassen für das große Engagement im Rahmen ihrer Abschlussarbeiten und für ihren wertvollen Beitrag zu Teilen dieser Arbeit.

Zusätzlich danke ich Dr.-Ing. Joachim Ritter, Alexander Rath, Anne Blechert und Thomas Bissinger für die unschätzbaren experimentellen Vorarbeiten auf diesem Thema sowie die Mühe mir die Untiefen experimenteller Messmethoden nahezubringen. Auch die zusätzlichen Experimente durch Frau Claudia Best möchte ich an dieser Stelle dankend erwähnt wissen.

In der Verbundenheit einer solch herausfordernden Aufgabe möchte ich auch den Kollegen der Bioprozesstechnik Arbeitsgruppe für ihre Geduld, Aufopferung und Motivation danken. Das freundschaftliche Verhältnis und das angenehme Arbeitsklima haben viele Hürden kleiner wirken lassen.

Mein größter Dank gilt meiner Familie ohne die mir diese Arbeit kaum möglich erscheint.

Abstract

The central carbon metabolism is the driving force of cellular processes as it covers the essential generation of energy and biomass from extracellular substrates. Understanding its capacity and regulation provides an enormous potential to the design of efficient biotechnological processes as well as to remedy metabolic diseases. Unfortunately, the complexity and versatility of metabolism conceals the interplay of different regulatory layers and leaves the field of metabolic research with numerous, partially competing hypotheses, which calls for an integrated analysis.

This work aims at unraveling the interplay of regulation mechanisms in the central carbon metabolism of adherent Madin-Darby canine kidney (MDCK) cells for a broad range of growth conditions and relies on the development of mathematical models for the quantitative description of experimental measurements.

With the objective to find an initial concept for an integrated modeling approach, this work characterizes in a first step the growth and metabolism of MDCK cells cultivated in two different media. Surprisingly, this analysis reveals an identical growth behavior as well as comparable dynamics in intracellular metabolite concentrations. The data, thus, implicitly suggests that extracellular substrate levels may have a minor influence on the metabolic activity. Also the hypothesis of an energy homeostasis is rendered as less relevant for describing the MDCK cell metabolism. It rather seems that substrate uptake rates, which change with culture duration, and key enzyme metabolite interactions constitute salient features of intracellular metabolite dynamics.

To fully account for cell growth and uptake of substrates, this work develops in a second step a segregated model that describes the proliferation of adherent cells in number and volume by taking into account the mean cell diameter. The process of growth involves that cells pass through different diameter classes, while consuming substrates and releasing byproducts. In addition to the substrate availability, growth is also limited by the cell density on the attachment surface. The derived model is simply structured, easy to compute and recapitulates the data of three independent experiments using a single parameter set. Apart from evaluating and predicting cell cultivations, the model also

provides macroscopic functions for complex cellular processes such as substrate uptake, biosynthesis and change in cell size and is, thus, particularly suited for a growth-related analysis of the cellular metabolism.

Coupling the segregated cell growth model to simple, biologically relevant descriptions of the central carbon metabolism supports the analysis of metabolite dynamics for a variety of growth conditions and time scales. The derived model covers central parts of glycolysis and glutaminolysis, accounts for links to associated metabolic pathways and takes into account *in vitro* measurements of enzyme activities. Based on an advanced simulation scheme and sequential model fitting, the approach suggests that metabolic activity is mainly driven by a growth-dependent substrate transport while the distribution of fluxes to biosynthesis and energy generation is determined by the properties of the involved enzymes. In case substrates are limiting, the metabolic activity reduces and enzyme-metabolite-interactions enable the supply of the central carbon metabolism with intracellular amino acids and biomass precursor, which guarantees a minimum activity. Therefore, the shift in metabolic control is an essential property of the cellular metabolism that consistently describes metabolite dynamics of three cell cultivations, two substrate limitation experiments and one substrate pulse experiment. Furthermore, the approach considers the preculture of cells, which explains variations among replicate experiments. Based on the model's performance in describing the data, its simple structure and its power to predict the metabolic activity, the model enables a reliable evaluation of strategies that aim at a faster or more efficient metabolism.

Overall, the modeling approach realizes a combined analysis of growth and metabolism of MDCK cells that contributes to the field of metabolic research. By placing relevant hypotheses on the metabolic regulation into the context of various experimental conditions, this work delivers conclusive insights into the mechanisms of metabolic pathways and illuminates the turnover of metabolites as well as the supply of the cell with energy and biomass precursors.

Kurzfassung

Der zentrale Kohlenstoffwechsel einer Zelle wandelt extrazelluläre Substrate zu Energie und Biomasse um und ist damit die Triebkraft zellulärer Prozesse. Ein umfassendes Verständnis von Kapazität und Regulation des Stoffwechsels besitzt daher ein enormes Potential sowohl für die Auslegung effizienter biotechnologischer Prozesse als auch für die Behandlung metabolischer Erkrankungen. Bedauerlicherweise verdecken seine Komplexität und Vielseitigkeit das Zusammenspiel der verschiedenen regulatorischen Ebenen, was der Metabolismusforschung unzählige, zum Teil konkurrierende Hypothesen einbrachte und nach einer ganzheitlichen Analyse verlangt.

Diese Arbeit zielt darauf ab, das Zusammenspiel von Regulationsmechanismen im Zentralstoffwechsel der adhärenen Madin-Darby canine kidney (MDCK) Zelle über einen weiten Bereich von Wachstumsbedingungen aufzuklären und stützt sich dabei auf die Entwicklung mathematischer Modelle zur quantitativen Beschreibung experimenteller Messungen.

Mit dem Ziel, ein initiales Konzept für den ganzheitlichen Modellierungsansatz zu finden, werden im ersten Schritt dieser Arbeit Wachstum und Stoffwechsel der MDCK Zelle für zwei unterschiedlichen Kultivierungsmedien charakterisiert. Überraschenderweise zeigen sich übereinstimmende Wachstumsphasen und vergleichbare Dynamiken in den intrazellulären Metabolitkonzentrationen. Die Daten legen damit implizit nahe, dass der Einfluss der Substrate auf die Stoffwechselaktivität begrenzt ist. Auch die Hypothese einer Energie-Homeostase ist minder relevant für die Beschreibung des MDCK Zellstoffwechsels. Vielmehr scheinen die Substrataufnahmeraten, welche sich mit der Kultivierungsdauer ändern, im Zusammenspiel mit entscheidende Enzym-Metabolit-Interaktionen bereits wesentliche Dynamiken in den intrazellulären Metaboliten auszumachen.

Um Wachstum und Substratbedarf der Zellen vollständig nach zu bilden, wird ein segregiertes Modell entworfen, welches das adhärenente Wachstum in Zahl und Volumen durch die Berücksichtigung des mittleren Durchmessers beschreibt. Der Wachstumsprozess beinhaltet das Durchlaufen verschiedener Zelldurchmesser-Klassen, was Substrate verbraucht und Nebenprodukte freisetzt. Zusätzlich zur Substratverfügbarkeit ist das

Wachstum auch durch die Zelldichte auf der Anheftungsfläche begrenzt. Dabei besitzt das Modell eine relativ einfache Struktur, ist schnell zu berechnen und gibt die Daten von drei unabhängigen Experimenten unter Verwendung eines einzigen Parametersatzes wieder. Neben dem Evaluieren und Vorhersagen von Zellkultivierungen kann das Modell komplexe zelluläre Prozesse wie Substrataufnahme, Biosynthese und Zellgrößenänderung durch einfache, makroskopische Funktionen abbilden und ist damit ideal für wachstumsabhängige Analysen des Zellstoffwechsels geeignet.

Die anschließende Kopplung des segregierten Zellwachstumsmodells mit einer einfachen, biologisch relevanten Beschreibung des Zentralstoffwechsels erlaubt es, Dynamiken in den Metabolitkonzentrationen über verschiedene Kultivierungsbedingungen und Zeitskalen hinweg aufzuklären. Hierbei werden zentrale Bestandteile von Glykolyse und Glutaminolyse als auch deren Verbindung zu assoziierten metabolischen Wegen berücksichtigt und *in vitro* Messungen von Enzymaktivitäten einbezogen. Basierend auf einem erweiterten Simulationsschema und sequentieller Modellanpassung legt der angewandte Ansatz nahe, dass die Aktivitäten des Stoffwechselnetzwerkes im Wesentlichen durch wachstumsabhängige Substrattransporte bestimmt sind. Die exakte Verteilung der Stoffflüsse zu Biosynthese oder Energiegenerierung hängt hingegen von den Eigenschaften der involvierten Enzyme ab. Im Falle einer Substratlimitierung verringert sich die metabolische Aktivität wobei Enzym-Metabolit-Interaktionen eine minimale Versorgung der Stoffwechselwege mit intrazellulären Aminosäuren und Biomassevorläufern ermöglichen. Die Verlagerung der metabolischen Kontrolle ist somit eine essentielle Eigenschaft des zellulären Stoffwechsels, welche Metabolitdynamiken für drei Zellkultivierungen, zwei Substratlimitierungen und einem Substratpuls Experiment konsistent beschreibt. Weiterhin berücksichtigt der Ansatz die Vorkultur der Zelle, was experiment-spezifische Unterschiede erklärt. Basierend auf der Leistungsfähigkeit im Beschreiben der Daten, der einfachen Modellstruktur und der erzielten Vorhersagekraft für Kultivierungen ist das entwickelte Modell auch geeignet, Strategien die auf einen schnelleren oder effizienteren Stoffwechsel abzielen verlässlich zu evaluieren.

Zusammengefasst realisiert der hier vorgestellte Modellierungsansatz eine kombinierte Analyse von Wachstum und Metabolismus der MDCK Zelle und trägt zur Erforschung des Zellstoffwechsels bei. Relevante Hypothesen zur Stoffwechselregulation werden in den Kontext verschiedenster Kultivierungsbedingungen gesetzt, was Aufschluss über die Kontrolle der metabolischen Netzwerke gibt und die Metabolitumsetzung als auch die Versorgung der Zelle mit Energie und Biomassevorläufern beleuchtet.

Contents

Abstract	V
Kurzfassung	VII
List of abbreviations	XIII
List of symbols	XVII
1. Introduction	1
2. Theory	5
2.1. Madin Darby canine kidney cells	5
2.1.1. Biotechnological application of MDCK cells	6
2.1.2. Growth phases during cell cultivation	6
2.2. Metabolism of continuously growing cells	8
2.2.1. Hierarchical control	9
2.2.2. Extracellular substrates	10
2.2.3. Transport processes	11
2.2.4. Glucose metabolism	12
2.2.5. Glutamine metabolism	17
2.2.6. Nucleotide metabolism	20
2.3. Systems biology approach to cell growth and metabolism	21
2.3.1. Cell growth models	22
2.3.2. Dynamic models of metabolism	23
2.3.3. Model construction and analysis	25
3. Models and methods	29
3.1. Model definitions	29
3.1.1. Segregated cell growth model	29
3.1.2. Structured central carbon metabolism model	33
Glycolysis	33
Glutaminolysis	39
Energy metabolism and respiration	46
3.1.3. Coupling of models	48
3.2. Model simulation	51
3.2.1. Considering the preculture of cells	52

3.2.2.	Substrate limitations through medium dilution	53
3.2.3.	Hierarchy of model parts and sequential model fitting	54
3.3.	Theoretical tools	55
3.3.1.	Algorithms and objective function	55
3.3.2.	Model analysis	55
3.3.3.	Limit of quantification	56
4.	Results and discussion	57
4.1.	Observations for MDCK cell cultivations in different media	57
4.1.1.	Growth, nutrient supply and byproduct release	57
4.1.2.	Response of metabolism to growth and media	60
4.1.3.	Discussion	64
4.1.4.	Summary	68
4.2.	A segregated model for cell growth	70
4.2.1.	Relation between cell number, diameter and volume changes	70
4.2.2.	Extracellular substrate and byproduct dynamics	73
4.2.3.	Substrate uptake rates during cell cultivation	74
4.2.4.	Discussion	76
4.2.5.	Summary	80
4.3.	Dynamics in central carbon metabolism	81
4.3.1.	Glycolysis	81
4.3.2.	Pentose phosphate pathway	91
4.3.3.	Glycogenesis	92
4.3.4.	Sensitivity analysis for glycolysis	93
4.3.5.	Discussion part I	94
4.3.6.	Glutaminolysis	102
4.3.7.	Pyruvate metabolism	111
4.3.8.	Sensitivity analysis for glutaminolysis	113
4.3.9.	Energy metabolism	114
4.3.10.	Model performance	116
4.3.11.	Discussion part II	118
4.3.12.	Summary	126
5.	Conclusion	127
6.	Outlook	131
	List of figures	134
	List of tables	136
	List of publications	137
	Bibliography	140

A. Supplementary studies	173
A.1. Sedimentation and attachment of MDCK cells to 6-well plate surface . . .	173
A.2. Adjusting the segregated cell growth model to growth in DMEM medium	174
A.3. Fit of segregated cell growth model to MDCK.SUS growth	177
A.4. Parameter correlation analysis	178
B. Supplementary data	180
B.1. Limits of quantification for metabolite measurements	180
B.2. Adenosine pool dynamics during substrate perturbation	181
C. Local and global model parameters	182

List of abbreviations

13DGP	1,3-Bisphosphoglyceric acid
2PG	2-Phosphoglycerate
3PG	3-Phosphoglycerate
6PGDH	6-Phosphogluconate dehydrogenase
αKG	α -Ketoglutarate
AA	Amino acid pool
AAex	Exchange between AA and α KG
ACCoA	Acetyl-CoA
ACO	Aconitase
ADK	Adenylate kinase
ADP	Adenosine diphosphate
AGE1.HN	Designer cell developed by ProBioGen
Akt	Protein kinase B
ALA	Alanine
ALD	Aldolase
AMP	Adenosine monophosphate
AS30D	Tumor ascite
ASP	Aspartate
ATA	Aspartate/Alanine transaminase
ATP	Adenosine triphosphate
ATPase	Adenylpyrophosphatase
B⁰AT	Amino acid transporter family
BHK	Baby hamster kidney
BPE group	Bioprocess engineering group
CAC	Cis-aconitate
CDP	Cytidine diphosphate
CHO	Chinese hamster ovary
CIT	Citrate

CL	Citrate lyase
CMP	Cytidine monophosphate
CS	Citrate synthase
CTP	Cytidine triphosphate
DAP	Dihydroxyacetone phosphate
E4P	Erythrose 4-phosphate
EC	Energy charge
ENO	Enolase
EpiSerf	Serum-free cell culture medium
ERK	Extracellular-signal-regulated kinases
F16BP	Fructose 1,6-bisphosphate
F6P	Fructose 6-phosphate
FAD	Flavin adenine dinucleotide
FADH₂	Reduced flavin adenine dinucleotide
FIM	Fisher information matrix
FMA	Fumarase
FUM	Fumarate
G6P	Glucose 6-phosphate
G6PDH	Glucose 6-phosphate dehydrogenase
GAP	Glyceraldehyde 3-phosphate
GAPDH	Glyceraldehyde phosphate dehydrogenase
GDH	Glutamate dehydrogenase
GDP	Guanosine diphosphate
GLC	Intracellular glucose
GLC^x	Extracellular glucose
GLN	Intracellular glutamine
GLNase	Glutaminase
GLNT	Glutamine transporter
GLN^x	Extracellular glutamine
GLT	Glutamate transporter
GLU	Intracellular glutamate
GLUT	Glucose transporter
GLU^x	Extracellular glutamate
GLYS	Glycogen synthase
GMEM	Glasgow's MEM (Eagle's Minimal Essential Medium)

GMEM-Z	Serum-containing cell culture medium
GMP	Guanosine monophosphate
GPI	Glucose-6-phosphate isomerase
GS	Glutamine synthase
GTP	Guanosine triphosphate
HEK	Human embryonic kidney
HeLa	Cells derived from Henrietta Lacks
HIF-1	Hypoxia-inducible factor 1
HK	Hexokinase
ICDH	Isocitrate dehydrogenase
ICIT	Isocitrate
IMP	Inosine monophosphate
KDH	α -Ketoglutarate dehydrogenase
LAC	Intracellular lactate
LAC^x	Extracellular lactate
LDH	Lactate dehydrogenase
LOQ	Limit of quantification
M	Arbitrary metabolite
MAL	Malate
MDCK	Madin Darby canine kidney
MDH	Malate dehydrogenase
ME	Malic enzyme
mTOR	Mechanistic target of rapamycin
myc	Oncogene
NAD	Nicotinamide adenine dinucleotide
NADH	Reduced nicotinamide adenine dinucleotide
NADP	Nicotinamide adenine dinucleotide phosphate
NADPH	Reduced nicotinamide adenine dinucleotide phosphate
NH₄	Intracellular ammonium
NH₄^x	Extracellular ammonium
OAA	Oxaloacetate
ODE	Ordinary differential equation
P	Arbitrary product
p53	Tumor suppressor protein
PBS	Phosphate buffered saline

PC	Pyruvate carboxylase
PDH	Pyruvate dehydrogenase
PEP	Phosphoenolpyruvate
PEPCK	Phosphoenolpyruvat-carboxykinase
PFK	Phosphofructokinase
PGK	Phosphoglycerate kinase
PGM	Phosphoglycerate mutase
PI3K	Phosphatidylinositide 3-kinases
PK	Pyruvate kinase
PPP	Pentose phosphate pathway
PSP	Purine salvage pathway
PYR	Pyruvate
R5P	Ribose 5-phosphate
ras	Oncogene
RDPK	Ribose 1,5-bisphosphate phosphokinase
Rul5P	Ribulose 5-phosphate
S	Arbitrary substrate
S7P	Seduheptulose 7-phosphate
SDH	Succinate dehydrogenase
SNAT3	Transporter family
src	Oncogene
SUC	Succinate
SUCCoA	Succinyl-COA
TATK	Transaldolase and transketolase
TPI	Triosephosphate isomerase
UDP	Uridine diphosphate
UDPGalNAc	UDP N-acetylgalactosamine
UDPGlcNAc	UDP N-acetylglucosamine
UGLC	Uridine diphosphate glucose
UMP	Uridine monophosphate
UT	Uridyl transferase
UTP	Uridine triphosphate
X5P	Xylulose 5-phosphate

List of symbols

Symbol	Unit	Description
α	-	scaling factor for transition rate
γ_{GLNT}	-	scaling factor for variable GLNT capacity
γ_{GLUT}	-	scaling factor for variable GLUT capacity
Θ	-	unit step function
λ	-	scaling factor that accounts for water evaporation
μ	1/min	specific growth rate
μ_{max}	1/min	maximum specific growth rate
σ		maximum data point
$\tilde{\sigma}$		maximum simulation point
ϕ	-	parameter vector
ϕ'	-	perturbed parameter vector
Φ	-	matrix of model parameterizations
$\chi^2(\phi)$	-	sensitivity coefficients for ϕ
b_{syn}	-	relative biosynthesis activity
b_{NAD}	-	relative NADH level
\bar{d}	μm	mean cell diameter
d_c	μm	critical cell diameter
d_m	μm	minimum cell diameter
E_{level}	-	enzyme level
f	-	growth inhibition factor
F_{evap}	L/min	water evaporation rate constant
FQS	-	weighted sum of squared residuals
K_{AAex}	1/min	specific activity of AAex
K_{ACO}	1/min	specific activity of ACO
K_{ATA}	1/min	specific activity of ATA
K_{ATPase}	1/min	specific activity of ATPase

List of symbols

Symbol	Unit	Description
k_{dGLN^x}	1/min	specific GLN ^x decomposition rate
k_{dPYR}	1/min	specific PYR degradation rate
K_e	1/min	specific activity of enzyme e
K_{ENO}	1/min	specific activity of ENO
K_{GLT}	1/min	specific activity of GLT
K_{GLYS}	1/min	specific activity of GLYS
K_{KDH}	1/min	specific activity of KDH
$k_{m/ATP}$	cell/L/min	specific ATP consumption rate for cell maintenance
K_{PSP}	1/min	specific activity of PSP
K_{RDPK}	1/min	specific activity of RDPK
K_{SDH}	1/min	specific activity of SDH
k_{sett}	1/min	specific sedimentation rate
$K_{TATK3PG}$	1/min	specific activity of TATK3PG
$K_{TATKF6P}$	1/min	specific activity of TATKF6P
$k_{X/ATP}$	1/min	specific ATP consumption rate for growth
k_{PK}^a	L ² mmol ²	activation constant of PK
k_{LDH}^a	L ² mmol ²	activation constant of LDH
k_{AAex}^{eq}	-	equilibrium constant of AAex
k_{ACO}^{eq}	-	equilibrium constant of ACO
k_{ACO2}^{eq}	-	equilibrium constant of ACO2
k_{ADK}^{eq}	-	equilibrium constant of ADK
k_{ENO}^{eq}	-	equilibrium constant of ENO
k_{FMA}^{eq}	-	equilibrium constant of FMA
k_{GPI}^{eq}	-	equilibrium constant of GPI
k_{ICDH}^{eq}	-	equilibrium constant of ICDH
k_{PSP}^{eq}	-	equilibrium constant of PSP
k_{SDH}^{eq}	-	equilibrium constant of SDH
$k_{TATK3PG}^{eq}$	-	equilibrium constant of TATK3PG
$k_{TATKF6P}^{eq}$	-	equilibrium constant of TATKF6P
k_{ADK}^m	mmol/L	affinity constant of ADK
k_{ALD}^m	mmol/L	affinity constant of ALD
k_{CL}^m	mmol/L	affinity constant of CL
k_{FMA}^m	mmol/L	affinity constant of FMA

Symbol	Unit	Description
k_{G6PDH}^m	mmol/L	affinity constant of G6PDH
$k_{GLC^x}^m$	mmol/L	Monod constant for GLC^x
k_{GLNT}^m	mmol/L	affinity constant of GLNT
$k_{GLN^x}^m$	mmol/L	Monod constant for GLN^x
k_{GLUT}^m	mmol/L	affinity constant of GLUT
k_{GPI}^m	mmol/L	affinity constant of GPI
k_{HK}^m	mmol/L	affinity constant of HK
k_{ICDH}^m	mmol/L	affinity constant of ICDH
k_{LDH}^m	mmol/L	affinity constant of LDH
k_{MDH}^m	mmol/L	affinity constant of MDH
k_{PDH}^m	mmol/L	affinity constant of PDH
k_{eP}^m	mmol/L	affinity constant of enzyme e for product P
k_{PFK}^m	mmol/L	affinity constant of PFK
k_{PK}^m	mmol/L	affinity constant of PK
k_{eS}^m	mmol/L	affinity constant of enzyme e for substrate S
k_{UT}^m	mmol/L	affinity constant of UT
K_{ADK}^{max}	mmol/L/min	maximum cell-volume-specific activity of ADK
K_{ALD}^{max}	mmol/L/min	maximum cell-volume-specific activity of ALD
K_{CL}^{max}	mmol/L/min	maximum cell-volume-specific activity of CL
K_e^{max}	mmol/L/min	maximum cell-volume-specific activity of enzyme e
K_{FMA}^{max}	mmol/L/min	maximum cell-volume-specific activity of FMA
K_{G6PDH}^{max}	mmol/L/min	maximum cell-volume-specific activity of G6PDH
K_{GLNT}^{max}	mmol/L/min	maximum cell-volume-specific activity of GLNT
K_{GLUT}^{max}	mmol/L/min	maximum cell-volume-specific activity of GLUT
K_{GPI}^{max}	mmol/L/min	maximum cell-volume-specific activity of GPI
K_{HK}^{max}	mmol/L/min	maximum cell-volume-specific activity of HK
K_{ICDH}^{max}	mmol/L/min	maximum cell-volume-specific activity of ICDH
K_{LDH}^{max}	mmol/L/min	maximum cell-volume-specific activity of LDH
K_{MDH}^{max}	mmol/L/min	maximum cell-volume-specific activity of MDH
K_{PDH}^{max}	mmol/L/min	maximum cell-volume-specific activity of PDH
K_{PFK}^{max}	mmol/L/min	maximum cell-volume-specific activity of PFK
K_{PK}^{max}	mmol/L/min	maximum cell-volume-specific activity of PK
K_{UT}^{max}	mmol/L/min	maximum cell-volume-specific activity of UT

List of symbols

Symbol	Unit	Description
LOQ_M	mmol/L	volume-specific limit of quantification for metabolite M
LOQ_M^{mmol}	mmol	limit of quantification for metabolite M
m_{GLC^x}	mmol/L/ μ L/min	cell-volume-specific uptake rate of GLC^x for maintenance
m_{GLN^x}	mmol/L/ μ L/min	cell-volume-specific uptake rate of GLN^x for maintenance
$m_{NH_4^x}$	mmol/L/ μ L/min	cell-volume-specific use of NH_4^x for maintenance
NAD_{basal}	-	adjustable parameter for influence of NAD/NADH
N^c	-	number of classes
N_{lm}^j	-	number of measured time points for state variable m in experiment l
N^l	-	number of experiments
N_l^m	-	number of state variables measured in experiment l
r_{AAex}	mmol/L/min	cell-volume-specific reaction rate for AAex
r_{ACO}	mmol/L/min	cell-volume-specific reaction rate for ACO
r_{ACO2}	mmol/L/min	cell-volume-specific reaction rate for ACO2
r_{ADK}	mmol/L/min	cell-volume-specific reaction rate for ADK
r_{ALD}	mmol/L/min	cell-volume-specific reaction rate for ALD
r_{ATA}	mmol/L/min	cell-volume-specific reaction rate for ATA
r_{ATPase}	mmol/L/min	cell-volume-specific reaction rate for ATPase
$r_{bsyn/PPP}$	mmol/L/min	cell-volume-specific efflux from PPP for biosynthesis
r_{CCM}	mmol/L/min	cell-volume-specific net ATP production rate by central carbon metabolism
r_{CL}	mmol/L/min	cell-volume-specific reaction rate for CL
r_{dATP}	mmol/L/min	cell-volume-specific ATP consumption rate for biosynthesis and cell maintenance
r_{dGLN^x}	mmol/L/min	medium-volume-specific GLN^x decomposition rate
r_{ENO}	mmol/L/min	cell-volume-specific reaction rate for ENO
r_{FMA}	mmol/L/min	cell-volume-specific reaction rate for FMA
r_{G6PDH}	mmol/L/min	cell-volume-specific reaction rate for G6PDH

Symbol	Unit	Description
r_{GLC^x}	mmol/L/min	cell-volume-specific uptake rate of GLC^x
r_{GLNT}	mmol/L/min	cell-volume-specific transport rate for GLNT
r_{GLN^x}	mmol/L/min	cell-volume-specific uptake rate of GLN^x
r_{GLT}	mmol/L/min	cell-volume-specific transport rate for GLT
r_{GLUT}	mmol/L/min	cell-volume-specific transport rate for GLUT
r_{GLU^x}	mmol/L/min	cell-volume-specific uptake rate of GLU^x
r_{GLYS}	mmol/L/min	cell-volume-specific reaction rate for GLYS
r_{GPI}	mmol/L/min	cell-volume-specific reaction rate for GPI
r_{HK}	mmol/L/min	cell-volume-specific reaction rate for HK
r_{ICDH}	mmol/L/min	cell-volume-specific reaction rate for ICDH
r_{KDH}	mmol/L/min	cell-volume-specific reaction rate for KDH
r_{LAC^x}	mmol/L/min	cell-volume-specific release rate of LAC^x
r_{LDH}	mmol/L/min	cell-volume-specific reaction rate for LDH
$r_{m/ATP}$	mmol/L/min	cell-volume-specific ATP consumption rate for cell maintenance
r_{m/GLC^x}	mmol/L/min	medium-volume-specific uptake rate of GLC^x for maintenance
r_{m/GLN^x}	mmol/L/min	medium-volume-specific uptake rate of GLN^x for maintenance
r_{m/NH_4^x}	mmol/L/min	medium-volume-specific use of NH_4^x for maintenance
r_{MDH}	mmol/L/min	cell-volume-specific reaction rate for MDH
r_{NADH}	mmol/L/min	cell-volume-specific net NADH production rate by central carbon metabolism
$r_{NH_4^x}$	mmol/L/min	cell-volume-specific release rate of NH_4^x
r_{PDH}	mmol/L/min	cell-volume-specific reaction rate for PDH
r_{PFK}	mmol/L/min	cell-volume-specific reaction rate for PFK
r_{PK}	mmol/L/min	cell-volume-specific reaction rate for PK
r_{PSP}	mmol/L/min	cell-volume-specific reaction rate for PSP
r_{RDPK}	mmol/L/min	cell-volume-specific reaction rate for RDPK
r_{SDH}	mmol/L/min	cell-volume-specific reaction rate for SDH
$r_{TATK3PG}$	mmol/L/min	cell-volume-specific reaction rate for TATK3PG
r_{TATK6P}	mmol/L/min	cell-volume-specific reaction rate for TATK6P

List of symbols

Symbol	Unit	Description
r_{trans}	1/h	specific transition rate
r_{UT}	mmol/L/min	cell-volume-specific reaction rate for UT
$r_{X/ATP}$	mmol/L/min	cell-volume-specific ATP consumption rate for growth
r_{X/GLC^x}	mmol/L/min	medium-volume-specific uptake rate of GLC^x for growth
r_{X/GLN^x}	mmol/L/min	medium-volume-specific uptake rate of GLN^x for growth
r_{X/NH_4^x}	mmol/L/min	medium-volume-specific use of NH_4^x for growth
s	-	adjustable parameter for growth function
t	min	time
$v_{\alpha DH}$	L/cell/min	cell-number-specific activity of αDH
v_{AAex}	L/cell/min	cell-number-specific activity of AAex
v_{ACO}	L/cell/min	cell-number-specific activity of ACO
v_{ATA}	L/cell/min	cell-number-specific activity of ATA
v_{ATPase}	L/cell/min	cell-number-specific activity for ATPase
v_e	L/cell/min	cell-number-specific activity of enzyme e
v_{ENO}	L/cell/min	cell-number-specific activity of ENO
v_{GLT}	L/cell/min	cell-number-specific activity of GLT
v_{GLYS}	L/cell/min	cell-number-specific activity of GLYS
v_{RDPK}	L/cell/min	cell-number-specific activity of RDPK
v_{SDH}	L/cell/min	cell-number-specific activity of SDH
$v_{TATK3PG}$	L/cell/min	cell-number-specific activity of TATK3GP
$v_{TATKF6P}$	L/cell/min	cell-number-specific activity of TATKF6P
v_{HK}	L/cell/min	cell-number-specific activity of HK
v_{ICDH}	L/cell/min	cell-number-specific activity of ICDH
v_{LDH}	L/cell/min	cell-number-specific activity of LDH
v_{MDH}	L/cell/min	cell-number-specific activity of MDH
v_{PDH}	L/cell/min	cell-number-specific activity of PDH
v_{PFK}	L/cell/min	cell-number-specific activity of PFK
v_{PK}	L/cell/min	cell-number-specific activity of PK
v_{UT}	L/cell/min	cell-number-specific activity of UT
V^C	μL	cell volume

Symbol	Unit	Description
V_*^C	μL	approximate cell volume for larger times
V_i^C	μL	volume of cells in class i
V_{model}^C	μL	cell volume derived from summation of V_i^c
V_s^C	L/cell	cell-specific volume
V^M	L	medium volume
V^W	L	well volume
v_{ADK}^{max}	mmol/cell/min	cell-number-specific maximum activity of ADK
v_{ALD}^{max}	mmol/cell/min	cell-number-specific maximum activity of ALD
v_{CL}^{max}	mmol/cell/min	cell-number-specific maximum activity of CL
v_e^{max}	mmol/cell/min	cell-number-specific maximum activity of enzyme e
v_{FMA}^{max}	mmol/cell/min	cell-number-specific maximum activity of FMA
v_{G6PDH}^{max}	mmol/cell/min	cell-number-specific maximum activity of G6PDH
v_{GLNT}^{max}	mmol/cell/min	cell-number-specific maximum activity of GLNT
v_{GLUT}^{max}	mmol/cell/min	cell-number-specific maximum activity of GLUT
v_{GPI}^{max}	mmol/cell/min	cell-number-specific maximum activity of GPI
v_{HK}^{max}	mmol/cell/min	cell-number-specific maximum activity of HK
v_{ICDH}^{max}	mmol/cell/min	cell-number-specific maximum activity of ICDH
v_{LDH}^{max}	mmol/cell/min	cell-number-specific maximum activity of LDH
v_{MDH}^{max}	mmol/cell/min	cell-number-specific maximum activity of MDH
v_{PDH}^{max}	mmol/cell/min	cell-number-specific maximum activity of PDH
v_{PFK}^{max}	mmol/cell/min	cell-number-specific maximum activity of PFK
v_{PK}^{max}	mmol/cell/min	cell-number-specific maximum activity of PK
v_{UT}^{max}	mmol/cell/min	cell-number-specific maximum activity of UT
x	cell	cell number of a standard growth model
X_i	cell	number of cells in class i
X_{tot}	cell	total cell number
\tilde{y}_{lmj}	-	simulation value for time point j , state m and experiment l
y_{lmj}	-	data value for time point j , state m and experiment l
Y_{LAC^x/GLC^x}	-	GLC ^x -specific LAC ^x yield
Y_{X/GLC^x}	mmol/L/cell	cell-growth-specific yield coefficient of GLC ^x
Y_{X/GLN^x}	mmol/L/cell	cell-growth-specific yield coefficient of GLN ^x

List of symbols

Symbol	Unit	Description
Y_{X/NH_4^x}	mmol/L/cell	cell-growth-specific yield coefficient of NH_4^x

1 Chapter

Introduction

Cell culture processes represent an advanced technology platform for developing and producing diagnostic and therapeutic biologicals that improve human and animal health. Fundamental to any cell culture-based process is the robust and efficient growth of cells in an artificial environment to produce, for example, insulin with *E. coli* [1], antibodies with CHO or hybridoma cells [2, 3] and viral vaccines with BHK or MDCK cells [4, 5]. To enable growth, division and response to stress, the cell requires a steady supply with energy and biomass precursors from metabolism to fuel numerous biosynthetic reactions and physiological functions [6]. Therefore, the metabolic conversion of nutrients is the driving force of cellular life and organized in cellular reaction pathways. These reaction pathways consist of enzymes that catalyze the conversion of one metabolic intermediate to another [7, pp. 90-119] and compose a metabolic network that is supplied by uptake of substrates via facilitated transports across cellular membranes. Based on the individual properties of the involved enzymes, the resulting production rates for cellular energy and biomass precursors are determined by the network properties and adjusted to cellular needs by sophisticated regulation mechanisms, which together enable biosynthesis in a changing environment.

The *in vitro* properties of single enzymes were investigated by biochemists since many years to unravel the network architecture and regulation mechanisms of metabolic pathways. These studies delivered a detailed description of substrate and cofactor use of enzymatic reactions, while regulation mechanisms and overall dynamics of the *in vivo* metabolism remained largely hypothetical [8–10]. Firstly, because *in vitro* measurements barely reflect the *in vivo* behavior [11] and, secondly, many of the identified cofactors and allosteric effects may not act as regulators of metabolism [12]. In parallel, biotechnologists analyzed in empiric studies the cellular need for extracellular nutrients under various cultivation conditions and achieve appreciable cell growth rates and product titers [13, 14]. Combined with knowledge of biochemical reaction pathways, the analysis of substrate uptake and byproduct release rates provides insights into metabolic pathway activities under (pseudo) steady state conditions and facilitates the design of cell feeding

strategies [15, 16]. During standard cultivations, however, cells easily adapt their growth and substrate uptake rates to environmental conditions, e.g. switch from growth to intermediary to stationary phase, with a concomitant adjustment of the metabolic activity through multiple regulatory mechanisms. For instance, the genomic, translational and proteomic level influences the abundance of enzymes and transporter as well as their degree of phosphorylation which, in addition to metabolite, cofactors and allosteric effector levels, determine the conversion rate within the reaction pathways. Since the pools and fluxes of the metabolic network represent the functional endpoints through all these regulatory layers, their quantification is key for a comprehensive systems level analysis of the cellular metabolism [17, 18]. Together with the measurement of enzyme activities, such data can illuminate many facets of metabolism and can indirectly unravel regulatory principles. However, it involves the acquisition of large data sets from different analytical methods and for a variety of experiments, which often impedes conclusive insights unless integrated into a systematic data analysis framework.

Mathematical models can organize information in a comprehensive system description and offer a predictive rationalization for bioprocesses [19]. Current metabolic models (e.g. [20]) elegantly explain general phenomenological aspects such as metabolic steady states, the response of metabolism to substrate, enzyme and effector level perturbations or the connection between transcriptome and metabolome. These models were largely developed for yeast or bacteria and deliver conclusive insights into regulatory principles of the central carbon metabolism. However, for mammalian cells only very few data-driven models are available and explanations for the metabolic regulation in a broader physiological context, where cells undergo changes in growth and substrate uptake rates, are rare. Whilst the correlation between specific growth rate and metabolic activity is widely accepted, the question of what actually regulates the metabolic activity is still difficult to answer [21].

Over the past decade, the BPE group from the Max Planck Institute for Dynamics of Complex Technical Systems in Magdeburg collected a profound data set for adherently growing MDCK cells that covers enzyme activities [22], metabolite pools [23] and intracellular fluxes [16] for a variety of growth conditions. Although MDCK cells are only sparsely considered in metabolic research, their adherent nature provides an ideal opportunity to study the metabolic activity in dependence of the cellular growth status. In contrast to suspension cells such as CHO, the growth status of adherent cultures can exclusively depend on the available attachment surface if well defined media are used, which ultimately allows to distinguish the influence of growth and extracellular substrate

levels on metabolism. It is the aim of this work to develop a mathematical model that incorporates the available data for adherent MDCK cells and that unravels the interplay of regulatory principles of the cellular metabolism. Provided that the model is capable to predict the metabolic behavior of MDCK cells, this work also seeks to evaluate strategies for a faster or more efficient cell growth. The initial step towards these objectives is the pre-analysis of cell cultivations in GMEM-Z and EpiSerf medium to strengthen or reject hypotheses on the regulation of metabolism. Based on these observations, the second step is to develop and evaluate a simple kinetic model for the central carbon metabolism that explains metabolite pools upon substrate limitations and substrate pulses with the regulation of single enzymes. In a third step, cell growth dynamics are coupled to the kinetic model of metabolism to evaluate whether the derived mechanisms of enzyme regulation also explain metabolite pool dynamics during cell cultivation or if additional, hierarchical influences need to be considered.

The following theoretical part explains the physiology and metabolism of MDCK cells and provides an overview on systems biological approaches to cell growth and metabolism (Chapter 2). Afterwards, the structure of the established mathematical models, the applied simulation strategies and the required theoretical methods are specified (Chapter 3). The modeling as well as its implications to the MDCK cell metabolism start with observations for MDCK cell cultivations and proceed with the analysis of cell growth, glycolysis and glutaminolysis (Chapter 4). Each part of Chapter 4 is provided with a separate discussion and summary while the contribution of this work to the field of metabolic research and the opportunities for future studies are addressed in Chapter 5 and 6, respectively.

2 Chapter Theory

2.1. Madin Darby canine kidney cells

In 1958, Madin and Darby described a method to obtain continuously growing cells from domestic animal tissues [24]. The renal tubular cell analyzed in this work is derived from a cocker spaniel kidney, wherefore it is referenced as MDCK cell, and grows adherently (Fig. 2.1 A, B). Based on its fast and robust proliferation under standardized conditions and its high susceptibility for virus infections, the MDCK cell evolved as a host system for biotechnological virus production processes (see next section). Apart from its role as host system for virus production, the MDCK cell also finds attention as model system for studying a variety of biological phenomena such as the drug transport across the epithelial barrier [25], the regulation of cell-cell adhesion [26], the development of the cell surface polarity [27] or the localization of sugar transporter ([28], Fig. 2.1C).

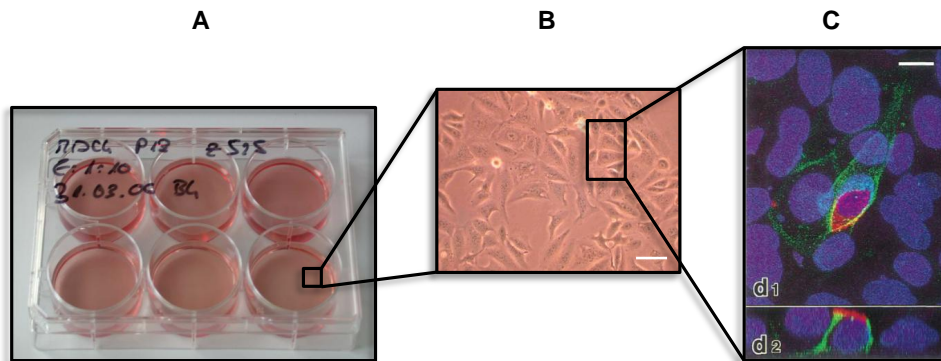


Figure 2.1.: Madin Darby canine kidney cells (MDCK) attached to a growth surface. (A) MDCK cell cultivation in 6-well plates (picture from BPE group). (B) Magnification of cell monolayer (picture from BPE group, scale bar: 40 μm). (C) MDCK cells (nucleus in green) co-transfected with glucose transporter GLUT1 (in green at basolateral membrane) and GLUT5 (in red at the apical membrane) are shown in d1 while d2 is the same picture as X-Z slice image, both taken from Takata et al. [28] (scale bar: 10 μm).

2.1.1. Biotechnological application of MDCK cells

The production of recombinant proteins, such as erythropoetin, insulin and antibodies, by cultivated mammalian cells is of great medical and industrial relevance as the extraction from animals is less efficient, less stable or simply not possible [29]. A second, equally important field of application is the production of viral vaccines that prevent the body from infections by pathogens where causal cures are not yet available. From a biotechnological point of view, the use of the MDCK cell is almost completely located and widely recognized in the field of influenza virus production [30] and is licensed for human vaccine production since 2001 [31]. Any production process relies upon cell cultivation in which the cells undergo several growth phases (see section 2.1.2) with changing substrate uptake and byproduct release rates. Typically, serum-containing (e.g. GMEM + fetal calf serum) or serum-free (e.g. EpiSerf) media are used to supply the cells with nutrients. To better understand the variations of the cultivation process, to optimize cell growth or the conditions for virus production and to establish new cultivation strategies, a deeper understanding of the growth-related metabolism is of key importance. Apart from the routine monitoring of the cultivation conditions and the growth status of the cells, measurements of intracellular metabolites, which are intermediates in the breakdown of, e.g., glucose in glycolysis or of glutamine in glutaminolysis (see section 2.2), provide an additional dimension for the identification of rate limiting intracellular reaction steps [32] or of mechanisms important for adaptation of cells to new cultivation media [33]. For MDCK and other cell lines, the bioprocess engineering group at the Max Planck Institute in Magdeburg developed an assay platform to gather data on cultivation conditions, growth status [14], intracellular metabolite levels [34–36] and enzyme activities [22, 37] to support a systems-level analysis of the MDCK cell metabolism.

2.1.2. Growth phases during cell cultivation

Cultivation processes start with inoculating cells in a bioreactor (e.g 6-well plate, T-Flask, roller bottle, stirred tank reactor). The subsequent growth of cells can be divided into the following characteristic phases:

Lag phase: Cultivation of cells starts with a lag phase in which adaption to the environment occurs prior to the initiation of biomass increase. In case of adherent cells in non-stirred bioreactors, the lag phase involves sedimentation to a surface, followed by an active attachment and flatening [38]. Afterwards, cells increase in biomass well before

the actual division [39, 40], which is already accompanied by an increased demand for substrates [41]. Since the cell only divides after a certain size is reached, the cell number is in many cases a delayed indicator for cell growth ([42], Fig. 2.2).

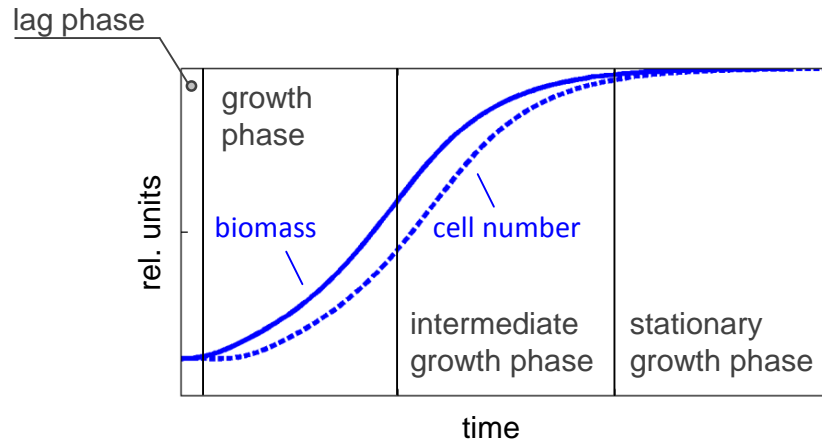


Figure 2.2.: Schematic representation of growth phases during cell cultivation.

Growth phase: The increase in biomass with a concomitant increase in cell volume [43] and protein content [44] marks the beginning of the growth phase. When reaching a certain cell-specific volume, a mother cell divides into two daughter cells, which start growing again. It is further observed that the relative number of cells in the S-phase of the cell cycle is increased [45]. On a population level, the amount of biomass increases in an exponential manner, which is close to the maximum growth rate. On the level of a single cell, however, the growth process unravels an unexpected degree of complexity. The cell-specific volume increase in the different cell cycle phases is far different from being monotonic [46]. Furthermore, larger cells have higher biomass growth rates than smaller cells which in consequence changes the distribution of the population with each generation [47]. Since cells still remain in a certain size range, mechanisms exist that limit the size variations [48]. However, the exponential growth of cells lasts until either substrates or byproduct levels become limiting. In case of adherent cells, growth can also be limited by the availability of free growth surface, which is formally defined as cell density-dependent growth inhibition [49].

Intermediate growth phase: Independent of which resource is limiting, when the growth rate decreases the cell passes into an intermediate growth phase that is characterized by a decreasing mean cell diameter and protein content [22, 25]. For example, a

significant reduction in the growth of mammalian cells is typically observed if the main substrates glucose and glutamine become limiting [50], which is, at least for hybridoma cells, expected to be at about 0.2 mmol/L [51]. Alternatively, growth inhibition can occur due to accumulation of byproducts from the breakdown of glucose and glutamine [52]. The incomplete oxidation of glucose yields lactate, which reduces the pH and impairs cell growth [51]. Also, ammonia, which is either released by thermal decomposition of glutamine [53] or by uptake and enzymatic conversion of glutamine, can reduce cell growth in the range of 2.3 – 7 mmol/L [41, 54] as it shifts the amino acid transport across cell membranes towards unfavorable conditions [55].

Stationary growth and decline phase: Under full growth inhibition, cells remain in a stationary growth phase which is characterized by maintenance metabolism with a minimum substrate consumption. A decline phase may follow if main substrates are depleted or byproducts reach toxic levels and cells start to lyse.

2.2. Metabolism of continuously growing cells

The growth of cells in the environment of both biotechnological processes and living organisms depends on the ability to convert substrates in a rapid and economic fashion into cellular energy and biomass precursors. Therefore, the study of cell growth implies the characterization of metabolism regarding its capacity and regulation. In case of continuously growing cells, which are cells with a permanent drive for growth, decades of research delivered deep insights into the enormously complex and versatile metabolism. The most prominent among these findings was made ninety years ago by Warburg et al. [56] and fits to most fast proliferating cells. It describes tumor cells, which also possess a permanent drive for growth, to secrete larger amounts of lactate under aerobic glycolysis than normal cells and is today exploited to mark cancers in surgery [57]. Since then, many facets of metabolism have been reported that contribute to an overflow metabolism and reduced mitochondrial respiration but a consistent explanation for these phenomena that fits to all continuously growing cells is still lacking, which could be due to genomic differences [58]. Perhaps, the efforts of studying metabolism suffer from the fact that characteristics change with the cell type [59], with the physiological status at time of measurement [21] and with the cultivation conditions [60]. Even after decades of research, the link between cell growth and metabolism remains an exciting area of research [61] with many important questions to be answered. The following sections

give an overview on how cell growth, cultivation conditions and metabolism influence each other (Fig. 2.3) and introduce hypotheses on how the central metabolic pathways glycolysis and glutaminolysis, which convert the largest portion of the overall substrate uptake [15, 62], are regulated. Particular emphasis is placed on hypotheses that cover hierarchical aspects, the direct influence of extracellular substrates, transport processes, supply and demand scenarios and intrinsic pathway properties. As data for the MDCK cell metabolism is sparse, the following summary relies upon findings for other, preferentially continuously growing cells such as AGE1, BHK, CHO and hybridomas. However, plausible observations for cancer cells are also taken into account and we refer to normal cells or even yeast cells if very general observations were made that possibly also apply to MDCK cells.

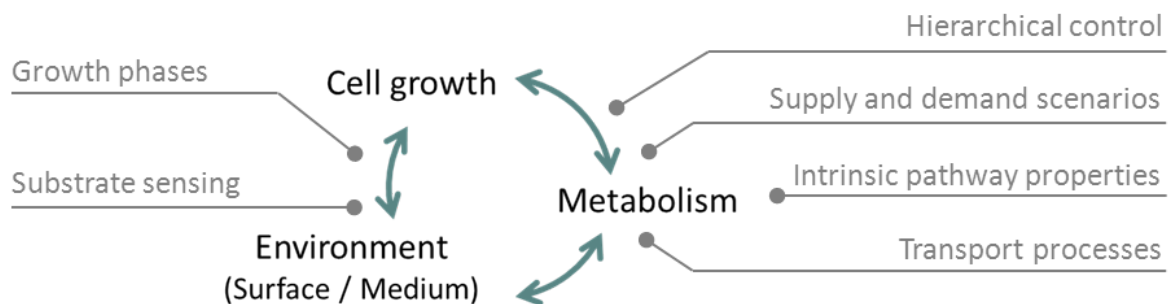


Figure 2.3.: Mutual influence of cell growth, metabolism and environment. Well-known cellular processes/mechanisms that interact with the metabolic activity are placed next to the arrows (gray, see text for further explanations).

2.2.1. Hierarchical control

A long standing question is whether cell growth controls metabolism or whether the activity of metabolism modulates the biosynthesis machinery (Fig. 2.3), which Suarez and Moyes described as "cart and horse" phenomenon as both influence each other [21]. In principle, mammalian cells possess sophisticated mechanisms to act on the level of genomes, transcripts [63, 64], proteins [13], and by enzyme phosphorylation [65] on the activity of metabolic pathways, which are often recognized as hierarchical control mechanisms. Several reviews comprehensively discuss, for example, the Mth1 enzyme to enable the amplification of the glucose transporter (GLUT) in yeast [57]. Also, the transcription factor HIF-1, oncogenes (*myc* family), and the PI3K/Akt/mTOR signaling pathway are involved in the activation of several enzymes and the GLUT in mammalian

cells [66–68]. In an antagonistic way tumor suppressor genes, such as p53, can be involved in switching the metabolic activity of cancer cells [69] towards, for example, higher GLUT expression levels [70]. Some of these factors integrate extracellular stimuli such as Akt signaling in hepatoma cells, which responds to insulin [71], or HIF-1, which responds to growth factors and low oxygen levels [67]. Another example is the ERK signaling cascade, which is involved in cell proliferation and stimulated by glucose sensing through the glucose transporter (GLUT, [72]). Accordingly, hierarchical mechanisms integrate different sources of information like a hub and, in response, influence the metabolic activity to better suit the conditions for cell proliferation. In contrast to such hierarchical influences, it is suggested that the control over metabolism lies within the properties of the network itself (see section 2.2.4 and 2.2.5), e.g. a control shared by several enzymes [73] or a control exerted by mechanisms for flux sensing [74]. In particular, enzymes are suggested to switch in activity with changing energy and precursors levels ([75], see section 2.2.6) and also metabolite levels may report back to the transcriptomic and proteomic level, as reviewed by Grüning et al. [76]. So both, hierarchical mechanisms as well as intrinsic pathway properties, are discussed to control metabolic activity as well as biosynthesis (Fig. 2.3). Although the mutual influence is not yet fully resolved, a correlation between metabolic activity and cell growth seems evident and calls for a growth-related analysis of metabolism [77], which is a central element of this work.

2.2.2. Extracellular substrates

Glucose and glutamine are main substrates for continuously growing cells and their presence is fundamental to a normal metabolic activity. Glucose is suggested to provide most of the cellular energy through the breakdown to pyruvate in the glycolysis pathway [78] while glutamine is expected to provide essential building blocks for biosynthesis [50], e.g. as protein and peptide constituent and as nitrogen carrier [79]. However, substrate labeling experiments of continuously growing cells revealed that glutamine, which is metabolized by glutaminolysis and subsequently by the citric acid cycle, not only supports protein and nucleotide synthesis but can replace the energy production of glycolysis such that glucose is solely used for the synthesis of biosynthetic precursors [80], e.g. macromolecule and lipid synthesis [81]. Other studies reported that glutamine is the major ATP source [82, 83], which however depends on the assumed ATP yield from glutamine [84]. Furthermore, the abundance of glutamine can stimulate the uptake of glucose [85, 86]. The opposite, i.e. an activation of glutamine uptake by increasing glucose levels, is not observed and minimal glutamine levels are essential to stimulate

cell growth [87, 88]. In conclusion, both substrates contribute to the cellular energy and precursor generation and are to a certain degree complementary but cannot necessarily replace each other [89]. Besides glutamine, a wide range of essential and non-essential amino acids are metabolized by MDCK cells [15].

Mammalian cells are not only flexible in the use of substrate sources but also in the efficiency to catabolize glucose. It is shown for many continuous cell lines that the glucose-specific lactate yield is influenced by the media composition [90, 91], e.g. by ammonium [85] and pyruvate [14]. Under limiting glucose concentrations, much lower relative lactate release rates [87, 92] and higher glutamine uptake rates were found [93]. It seems that high glucose levels impair the full oxidation of glucose for ATP production [78], which is described as Crabtree effect [94]. Renner et al. [95] concluded that a high glycolytic flux easily saturates the synthetic and oxidative pathways, which utilize glucose-derived pyruvate, and, hence, increases the glucose-specific lactate yield. However, also the depletion of substrates, which may induce a rewiring of metabolic routes and a reduction in metabolic activity, is an example for the influence of extracellular substrate levels on the mammalian cell metabolism.

2.2.3. Transport processes

Transport of molecules across membranes is a prerequisite of living cells and is facilitated by entire protein families. The hexose transporters of kidney cells that predominantly transfers glucose and fructose between the medium and the cytosol are GLUT1, GLUT2 and GLUT5 [96]. In principle, the cell can modulate the influx by changing the transporter's affinity for its substrate, translocate GLUT to the plasma membrane and activate preexisting GLUT [97, 98]. For fibroblasts it is described that modulation of the influx mainly depends on changes in the maximum activity of GLUT [99], for example by hierarchical regulation through the transcription factor HIF-1, oncogenes or extracellular stimuli, while for HEK cells the GLUT1 activity is influenced by the ATP level [100]. For fibroblasts it was also shown that overexpression of *ras* or *src* drives the glucose uptake [101]. Independent of which mechanisms modulate the influx, the transport of glucose is a potential target for the design of bioprocess and is an often overseen element that exhibits significant control over glycolysis in well studied systems, such as yeast, as shown by Reijenga et al. [102] and by Galazzo and Bailey [103]. Even in cases where the transport may not be rate limiting for the glucose metabolism (e.g. in BHK, CHO or hybridoma cells [86, 92, 104]), reducing the high glucose uptake rates through molecular biological tools [105] or by chemical inhibition [106] may yield a more eco-

nomic breakdown of glucose with lower lactate secretion rates as it potentially interferes with the Crabtree effect. In cancer cells, it is commonly perceived that the GLUT has substantial control over glycolysis [107, 108] and is, therefore, studied as potential target for therapy [109–111]. For example, Matsushita and coworkers inhibited GLUT1 with 3-bromopyruvate acid and found significantly suppressed proliferation rates for tumor cells with high GLUT1 expression levels [112]. In turn, an increase in GLUT1 expression levels yields a faster increase in tumor size [113]. Also, cells from the immune system show higher fluxes in upper glycolysis and the pentose phosphate pathway (PPP) after activation of GLUT with concanavalin A [114]. In turn, genetic deletion of GLUT1 yields reduced glucose uptake with concomitantly reduced growth rates and ATP levels [115]. Taken together, the fields of bioprocess, cancer and diabetes research [116] describe the GLUT as a central element in understanding a highly active metabolism.

In contrast to glucose, there is no mammalian cell transporter that is specific to glutamine [117]. Furthermore, incorporation of glutamine into cellular building blocks is difficult to track, which complicates direct measurements. Normal kidney cells realize the glutamine uptake through the B⁰AT transporter, which has a wide specificity as it transports also hydrophobic and aromatic neutral amino acids, and through the SNAT3 transporter, which is electrogenic and ion-dependent. For tumor cells, it is reported that glutamine uptake is facilitated by the ASCT2 transporter [117], and the expression of ASCT2 transporter is stimulated by oncogenes (*myc* family) to maintain cellular viability and citric acid cycle anaplerosis¹ [117, 118]. For cultured HeLa and hybridoma cells, it is assumed that glutamine transport is the rate limiting step for glutaminolysis [82, 104]. Finally, the uptake of glutamate is an electroneutral (ion-dependent) transport in kidney cells and suggested to be rate-limiting in analogy to the glutamine transport [119].

2.2.4. Glucose metabolism

The breakdown of intracellular glucose (GLC) to pyruvate (PYR) through several intermediate metabolites with the concomitant production of ATP and precursors for anabolic processes is a well studied metabolic conversion route and denoted as glycolysis (Fig. 2.4). A high activity in glycolysis supports the growth of cells [120] and is, therefore, often found in cancer or transformed cells but also in cells of the body, e.g. enterocytes [121] and lymphocytes [114], that show high rates of proliferation. On the one hand an increase in glycolytic activity readily outpaces the capacity for oxidative

¹**anaplerosis:** reactions that supply the citric acid cycle with precursor.

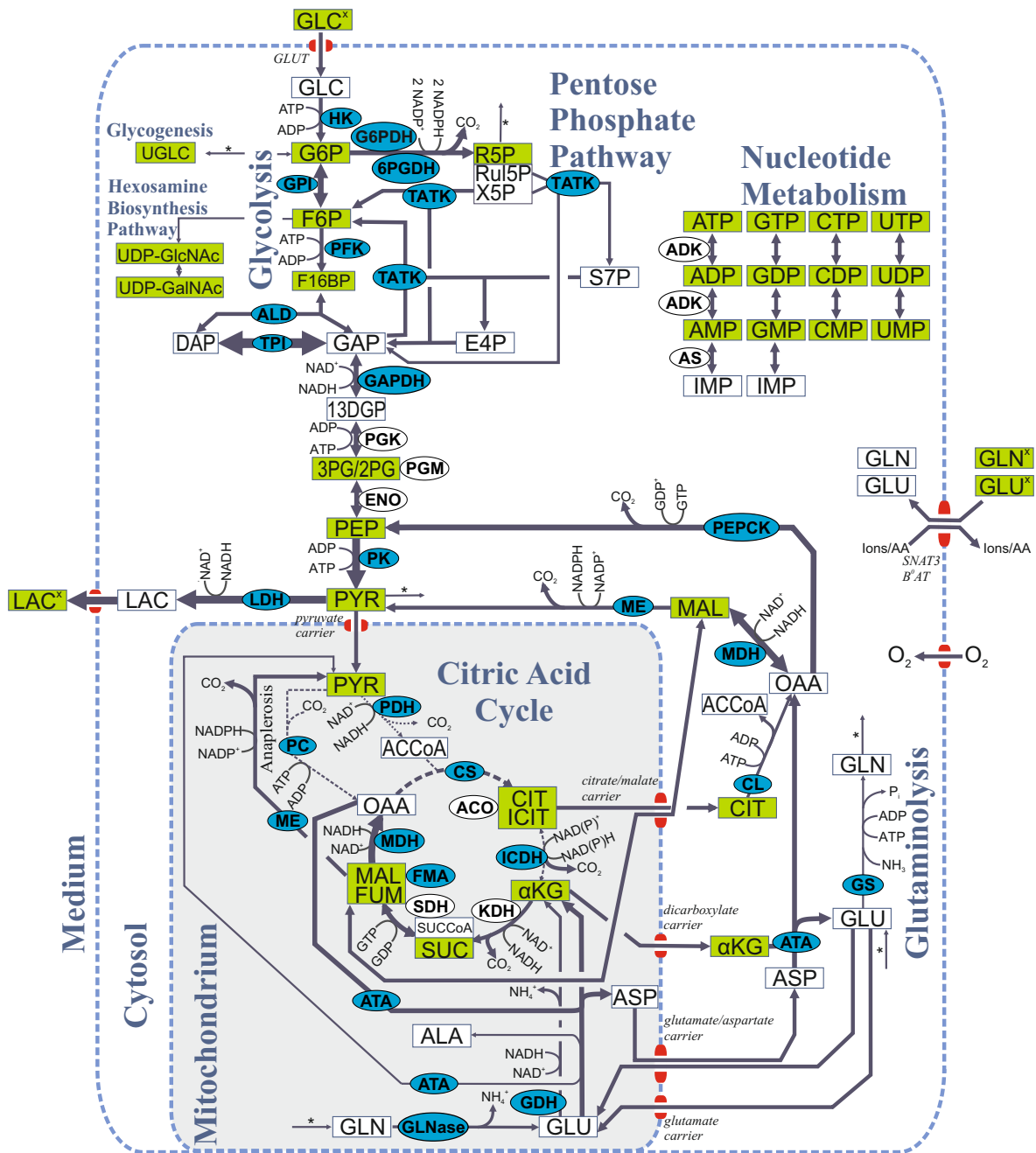


Figure 2.4.: Simplified reaction network of the central carbon metabolism of MDCK cells (modified from Wahl et al. [15]). Square symbols represent metabolites and are illustrated in green if quantified by Ritter [23]. Oval symbols represent enzymes and are illustrated in blue if measured by Janke et al. [22]. Lines represent reactions and thickness of lines indicates the relative enzyme activity measured *in vitro* for cultivation in GMEM-Z medium. Reactions with asterisks are not further specified but are part of the model. Abbreviations are explained in the text.

phosphorylation or of low flux branches [67] but on the other hand enables a robust and steady supply with biomass precursors [122]. Curi et al. [123] described the influx into the citric acid cycle to compete with a highly active lactate dehydrogenase (LDH). Thus, cytosolic PYR is not accumulating but rather secreted as lactate into the medium (LAC^x). It is discussed that the high activity of glycolysis is enabled by overexpression of enzymes [124, 125] or expression of certain isoenzymes [126, 127] and seems to correlate with the malignancy of tumor cells [128]. In contrast to these findings, it is hypothesized that cells rather modulate the specific activity of enzymes than their abundance [129]. For example, an overexpression of single enzymes by molecular biological tools may not enhance the metabolic activity simply because they have diminishing flux control [130], which is defined as follows: each pathway consists of a reaction cascade where enzymes and intermediates interact. The conversion rate of intermediates is determined by the properties of the involved enzymes. Thus, enzymes exert a certain control over the substrate abundance [131]. On a higher level, some of these substrates also participate in other reactions or act as allosteric modifier of enzymes such that the control spreads over several reactions (example given in [122]). Another example are rate limiting steps that dictate the conversion speed of follow up reactions and can, thus, control the activity of entire pathways. The more the control is located at a single enzymatic step the less control have the remaining reactions. In the following, we describe the metabolic network of upper and lower glycolysis as well as of closely related metabolic pathways and illuminate whether the involved enzyme-mediated reactions are expected to be flux controlling.

Upper glycolysis: In the first step of upper glycolysis, hexokinase (HK) phosphorylates GLC to glucose 6-phosphate (G6P, Fig. 2.4) and preferentially relies on mitochondrial ATP [132]. Depending on the cell, the HK is highly active such that any GLC is rapidly converted [91, 95] and trapped intracellularly, which would indirectly point towards the GLUT as rate-limiting step. However, with changing cell growth conditions the control can shift between the GLUT and HK, for example in rat heart cells [60], and it is difficult to distinguish the influence of both reactions on the metabolic activity, as reviewed by Rodríguez-Enríquez et al. [133] and by Marín-Hernández et al. [108]. In BHK and hybridoma cells, for example, the maximum activity of HK was observed to be close to the flux through glycolysis and, therefore, assumed to be rate-limiting [86, 104]. With the subsequent phosphoglucose isomerase (GPI) mediated conversion to fructose 6-phosphate (F6P), the hexose can continue to follow the glycolytic pathway where it

serves as a substrate for the phosphofructokinase (PFK). The PFK catalyzes an essentially irreversible reaction of F6P and ATP to fructose 1,6-bisphosphate (F16BP) and ADP. It consists of three subunits [134] and is regulated in many ways. Among others, by adenosine-based nucleotides, fatty acids, citrate and fructose 2,6-bisphosphate [135]. The latter is reversibly generated from F6P and the most potent activator of the PFK [136]. Although the PFK is observed to be rate limiting in normal cells, as reviewed by Dunaway [137], it seems that glycolysis of continuously growing cells is not limited by the PFK activity [86, 104]. Rate limiting or not, an inhibition by, e.g. citrate, can increase metabolite pools of upper glycolysis and yield higher fluxes into the PPP, which is shown for endothelial cells by Wu et al. [138], and indicates a certain flux control.

Lower glycolysis: In the lower part of glycolysis, the hexose F16BP is split into 3-carbon sugars, or trioses, while their subsequent degradation is mostly reversible and exerts only a minor control over the glycolytic activity in AS-30D [108] and HeLa cells [139]. In particular, the products of the aldolase (ALD) mediated reaction are dihydroxyacetone phosphate (DAP) and glyceraldehyde 3-phosphate (GAP), which can be interconverted by the triosephosphate isomerase (TPI). GAP is further degraded by glyceraldehyde phosphate dehydrogenase (GAPDH) to 1,3-bisphosphoglyceric acid (13DGP), which concomitantly oxidizes NAD to NADH. Afterwards, phosphoglycerate kinase (PGK) converts 13DGP to 3-phosphoglycerate (3PG) and an equimolar amount of ADP to ATP. It seems that rapidly growing tumor cells keep 3PG at low levels by a highly active phosphoglycerate mutase (PGM) as it inhibits the PPP and the serine production [140]. The PGM reversibly converts 3PG into 2-phosphoglycerate (2PG) and targeting the PGM with inhibitors arrests cancer cell proliferation [141]. The intermediate 2PG is a substrate to enolase (ENO), which produces phosphoenolpyruvate (PEP). The subsequent conversion of PEP to PYR is mediated by the pyruvate kinase (PK) and phosphorylates ADP to ATP. It is assumed that fast proliferating cells keep the PK at low activities to increase upstream metabolite concentrations, which then fuel nucleic acid synthesis with precursor [120]. The decrease in activity can be achieved by changing from a tetrameric to a dimeric form of the embryonic PK type M2 [142], which is assumed to be induced by low F16BP levels [143]. In MDCK cells, PYR is mainly metabolized to lactate (LAC) by the LDH, which is the natural end product of glycolysis [144]. Only minor amounts of PYR enter the citric acid cycle by conversion to citrate (CIT) or oxaloacetate (OAA) [16, 22]. The activity of the LDH converts NADH to NAD and supports the cell in maintaining a proper redox balance. A high LDH

activity is often indirectly observed as high lactate secretion rate, e.g. for MDCK [145] or hybridoma [104] cells. Apart from glycolysis, mammalian cells are also capable to perform gluconeogenesis, which is the synthesis of hexoses from PYR and an important feature of liver cells [146]. However, gluconeogenesis is not engaged by renal epithelial cells when brought to tissue culture [147] and also not by tumor cells [148].

Pathways fueled by glycolysis: Possible metabolic branches for the glycolytic intermediate G6P are glycogenesis for a possible glycogen storage or the PPP for nucleotide, nucleic acid and macromolecule synthesis as well as NADPH generation. Glycogen levels are low in kidney cells [149] and glycogenesis is initiated by an isomerization of G6P to glucose 1-phosphate followed by a reaction with uridine triphosphate (UTP) to uridine diphosphate glucose (UGLC). Afterwards glycogen is produced and serves as glucose storage. The first reactions of the PPP are mediated by the glucose 6-phosphate dehydrogenase (G6PDH) and 6-phosphogluconate dehydrogenase (6PGDH) yielding ribulose 5-phosphate (Ru5P) with its isomers ribose 5-phosphate (R5P) and xylulose 5-phosphate (X5P). Both enzymes constitute the oxidative entry point into the PPP and especially 6PGDH is inhibited by glycolytic intermediates such as F16BP and 3PG [140]. The metabolites F6P and 3PG are also part of the PPP such that glycolysis and the PPP overlap to a certain degree. The interconversion of metabolites in the PPP is mediated by the transaldolase and transketolase (TATK) reactions yielding erythrose 4-phosphate (E4P) and seduheptulose 7-phosphate (S7P). The influx into the PPP ranges from 4 % to 40 % of the glycolytic flux [150–152] for most continuously growing cells and even higher contributions are estimated for CHO cells by metabolic flux analysis [2, 153]. A large fraction of the glucose-derived pentose phosphate metabolites are found in nucleic acids and adenosine-based nucleotides and, thus, their contribution to lactate production is diminishing [13, 82]. In transformed mammalian cell lines, the generated NADPH covers 30 – 50 % of the total cellular production and is predominantly used for lipid synthesis [154]. The glycolytic intermediate F6P is in addition used for generation of UDP N-acetylhexosamines denoted as hexosamine biosynthesis pathway [85]. In particular, F6P is used for amination with intracellular ammonium (NH_4) and linked to UTP under consumption of glutamine (GLN) such that UDP N-acetylglucosamine (UDPGlcNAc) and its isomer UDP N-acetylgalactosamine (UDPGalNAc) are derived. Both metabolites are important for oxygen-linked protein glycosylation and play a role in signal transduction [155] as well as sensor mechanisms [156]. It is, for example, suggested that hexosamines influence growth factor signalling

and, thus, indirectly couple glucose with glutamine metabolism [157]. In CHO cell-based anti-body production processes, it is observed that the glycosylation of products depends on the UDP N-acetylhexosamine levels, which in turn correlate with extracellular glutamine (GLN^x) levels and the glycolytic flux [158]. However, also a dependence of UDP N-acetylhexosamines on NH₄ is described [78]. Finally, lower glycolysis fuels the serine and glycine production, which is enhanced in tumor cells to support biosynthesis [159] as well as the ability to reduce osmotic [160] and oxidative stress [154].

2.2.5. Glutamine metabolism

It is frequently observed in mammalian cell cultures that the secreted lactate exceeds the theoretical maximum of two molecules per molecule of consumed glucose [104, 124]. Although puzzling at first glance, it indicates that cells produce lactate from sources other than glucose [13]. One reason lies in their permanent drive for growth that builds upon an alternative use of the citric acid cycle, which comes along with a supply different from glycolysis. The role of the citric acid cycle changes in fast proliferating cells from a highly efficient energy production system (fueled from glucose) towards a hub that ubiquitously supplies biosynthesis [67]. Thus, intermediates of the citric acid cycle are only partly used for oxidation in mitochondria and the concomitant reduction in respiratory activity is misinterpreted as defect [56], which has become a central dogma of tumor cell research [58]. Neither elevated mitophagy² nor reduced enzyme activities, which are perceived as causal explanation, are evidenced [161, 162]. Furthermore, Barnabé and Butler [78] could show that continuously growing cells engage in respiration and derive most of the cellular energy from the citric acid cycle when glycolysis is limited in substrates. So, the citric acid cycle can engage in energy production and replace glycolysis as main energy generating pathway depending on the cell and the culture conditions, as summarized by Moreno-Sanchez et al. [58]. However, the constant efflux of intermediates for biosynthetic purposes, which is called cataplerosis [67], is refilled with the uptake and degradation of glutamine, a preferred substrate of cancer cells [163], and also supported by the uptake of other amino acids [13, 164]. Therefore, glutamine is one of the largest contributor to biosynthesis in mammalian cell culture and minimal levels are required to enable cell proliferation [78]. In analogy to glycolysis, glutamine is only partially oxidized and yields PYR as end product, which can be converted to LAC [121, 150]. Motivated by these observations, McKeehan [89] denoted the path from glutamine to pyruvate as "glutaminolysis". The incomplete oxidation in

²mitophagy: degradation of mitochondria

the citric acid cycle is described as "truncation" although the capability for oxidative phosphorylation is still given [165]. Within this definition, glutaminolysis consists not of a single reaction sequence but of a network with at least four active routes in kidney cells ([166], out of eight possible routes [84]) and resides partly in the cytosol and partly in the mitochondrion. Therefore, the description that follows is condensed to central reactions.

Glutaminolysis: In the first part of glutaminolysis, glutamate (GLU) is generated from GLN and serves as a source for the second part known as citric acid cycle. The transport of both intermediates across the mitochondrial membrane is found to work near equilibrium and, thus, seems to have almost no flux control [167]. The conversion of GLN to GLU is mediated by glutaminase (GLNase) and releases NH_4 . Afterwards, GLU is converted to α -ketoglutarate (α KG) either by a second release of NH_4 through the glutamate dehydrogenase (GDH) yielding NADH or by transferring the amino group to PYR or OAA under the production of alanine (ALA) or aspartate (ASP), respectively [124]. Such a transfer of amino groups is facilitated by transaminases³, which are located in the cytosol and the mitochondrion. In principle, ALA is a nitrogen acceptor that is secreted by cancer cells [148] as well as by CHO [32], AGE1.HN [168] and MDCK cells [15] while ASP is used for biosynthesis. It is reported for tumor cells that glutamate is mainly degraded by transamination and not by the dehydrogenase route [169]. In line with these observations, MDCK cells were found to have high transaminases activity [22, 170]. Therefore, release of NH_4 results largely from the conversion of glutamine and not from glutamate [171], which could be due to the negative inhibition of GDH by guanosine triphosphate (GTP, [172]). Since extracellular ammonium (NH_4^x) impairs cell growth, cultivation of cells with a sole supply by extracellular glutamate (GLU^x) is suggested as an alternative worth testing [173] but requires the synthesis of GLN via an active glutamine synthase (GS, a premise that is given for MDCK cells [22]) to continue purine, pyrimidine [154] and UDP N-acetylhexosamine synthesis.

Lower citric acid cycle and oxidative phosphorylation: Since the use of the citric acid cycle is changed in continuously growing cells, the descriptions often follows the reaction paths starting with α KG. In principle, glutamine-derived α KG either takes the energy producing path in the lower citric acid cycle or the lipid synthesis path in the upper citric acid cycle [174] and constitutes 50–90 % of the metabolite pools

³**transaminases:** alanine transaminase (AlaTA), aspartate transaminase (AspTA)

[148]. The other part of the metabolite pools is generated from non-essential amino acids [13]. However, the lipid generating route is often denoted as reversed citric acid cycle flux and exhibits a reductive carboxylation of GLN, which is not found in normal cells. This route is expected to rely on a reverse functioning of the NADPH-dependent isocitrate dehydrogenase (ICDH, [175, 176]). In normal cells of the body, the ICDH converts isocitrate to α KG using either NAD or NADP to produce NADH or NADPH. However, Yan and coworkers discovered that more than 70 % of gliomas (tumor cells) harbor a mutation in genes encoding for the ICDH [177]. On the contrary, Moreno-Sánchez et al. [68] describes the reversibly working ICDH to be thermodynamically infeasible and casts doubt on this reaction. They propose that an alternative reaction exists that facilitates a reductive carboxylation of glutamine which is not yet discovered. However, the degradation of α KG in the lower part of the citric acid cycle is initiated by the α -ketoglutarate dehydrogenase (KDH) and yields succinyl-CoA (SUCCoA) while transforming NAD to NADH. Apart from the influence of substrates and products on the KDH activity [178], ions and adenosine-based nucleotides are also reported to influence the conversion of α KG by the KDH [179]. In the following reaction steps, SUCCoA is reversibly converted to succinate (SUC), oxidized to fumarate (FUM) and hydrated to malate (MAL), and involves, amongst others, the enzymes succinyl-CoA synthase, succinate dehydrogenase (SDH), fumarase (FMA) and malate dehydrogenase (MDH), which is in detail described by Nelson and Cox [180, pp. 571-579]. The released energy from these reactions is stored in GTP (or ATP) as well as NADH and FADH₂, which both drive the oxidative phosphorylation under mitochondrial respiration [181] using oxygen. Thus, oxidative phosphorylation links ATP with NADH (1 NADH = 2.5 ATP, 1 FADH₂ = 1.5 ATP [6]) and the respiratory chain can exert significant flux control over the citric acid cycle under physiological conditions [182, 183] by controlling both the NADH to NAD ratio and the ATP to ADP ratio. Studies for cancer therapy recognized the oxidative phosphorylation as a potential target to impair cell proliferation [184]. Furthermore, it is hypothesized that alterations in enzymes such as SDH contribute to the emergence of cancer [185]. However, the control in the citric acid cycle not only resides in the oxidative phosphorylation but also in metabolites that act allosterically on enzymes [167, 186]. The end product of the lower citric acid cycle, MAL, is either converted to mitochondrial OAA or PYR (which are required for AspTA or AlaTA activity in glutaminolysis) or to cytosolic PYR with synthesis of NADPH, which supports lipid synthesis.

Upper citric acid cycle: The upper part of the citric acid cycle involves the reversible turnover of CIT to isocitrate (ICIT) by aconitase with cis-aconitate (CAC) as an intermediate product. Interestingly, CIT interacts with several branch points of metabolism (extensively reviewed by [187]) and is produced by the citrate synthase (CS) using OAA and acetyl-CoA (ACCoA), which is derived from PYR through the pyruvate dehydrogenase (PDH). Alternatively, ICIT can be produced from a reductive flux from α KG. It is shown for melanoma cells that appreciable amounts of CIT are derived from α KG and used to produce cytosolic acetyl-CoA to support lipid synthesis [148]. The production of cytosolic acetyl-CoA involves an active transport of CIT into the cytosol [188] and a subsequent conversion by citrate lyase (CL) under the use of ATP and the formation of ADP. Disruption of the CL in tumor cells suppresses proliferation [189]. In CHO cells, Dean and Reddy discovered that 30 % of the CIT is derived from GLN and ASP while PYR is a negligible source [13]. Icard et al. [187] even anticipate that cytosolic CIT is converted to PYR, which again enters the citric acid cycle forming a so called vicious cycle to support cytosolic NADPH synthesis [187]. However, the contribution of PYR to the citric acid cycle is low and either explained with an impaired mitochondrial uptake [190] or an inhibition of PDH, for example by HIF-1 induced phosphorylation [191] or by NADH, ATP and ACCoA [172].

2.2.6. Nucleotide metabolism

Fast proliferating cells need to generate certain levels of energy carriers to fuel biosynthetic reactions and physiological functions. The most famous carriers are the adenosine-based nucleotides, adenosine triphosphate (ATP), adenosine diphosphate (ADP) and adenosine monophosphate (AMP), which are partly interconverted by the adenylate kinase (ADK, [192]). Similarly, the cell uses guanosine-based nucleotides (GTP, GDP, GMP) as energy carriers, which also belong to the purines, and AMP as well as GMP are generated from the same precursor, i.e. inosine monophosphate (IMP), by the purine salvage pathway (PSP). Both purines are main energy acceptors during the conversion of glycolytic as well as citric acid cycle metabolites and the abundance of ATP relative to ADP is thought to be involved in the regulation of metabolic processes [94]. Similarly, Hofmeyr and Cornish-Bowden [193] describe a supply-demand scenario where the rate of ATP syntheses is controlled by the demand reactions (biosynthesis) and where ATP in turn controls the synthesis pathway such that the demand is compensated by the supply. Atkinson and coworkers even anticipate for rat liver cells that the energy charge (EC), which is a ratio between ATP, ADP and AMP (see Eq. (2.2.1)), changes

enzyme activities in favor of energy generation or biosynthesis depending on what is most required (control by energy charge, [194, 195]).

$$EC = \frac{[ATP] + [ADP]/2}{[ATP] + [ADP] + [AMP]} \quad (2.2.1)$$

In hybridoma and CHO cells the EC and especially the ATP level was found to mainly depend on the extracellular glucose (GLC^x) level [13, 78]. Interestingly, the EC is usually kept between 0.8 and 1 by vital cells [196], although environmental perturbations can induce considerable changes in the nucleotide levels. Walther and colleagues unraveled for yeast cells that large amounts of AMP are transferred to the PSP to maintain a proper nucleotide balance [197]. For cancer cells, it is further hypothesized that ATP is never limiting but that the ATP production rate dictates the biosynthesis activity [61, 198], which is also found for yeast cells [199]. Also, for rat liver cells, it is suggested that the rate of glycolysis determines the level of ATP and not vice versa [200]. So the question whether the metabolic activity is mostly independent of the ATP level or fully determined by the energy status is not yet resolved (addressed later in this work) and the answer may depend on the cell type [59]. Another group of high energy molecules are the pyrimidines consisting of uridine-based nucleotides (UTP, UDP, UMP) and cytidine-based nucleotides (CTP, CDP, CMP). Although their role as energy carriers is limited compared to the purines, their contribution to biosynthesis is equally important.

2.3. Systems biology approach to cell growth and metabolism

Understanding intrinsically complex biological systems, which typically arise from a large number of functionally diverse elements that interact symbiotically [201], requires the integration of experimental and computational approaches in a multidisciplinary environment. In this regard, systems biology complements molecular biosciences and addresses the missing link between molecules and physiology with mathematical models [202]. Such models express hypotheses through the choice and parameterization of relationships and reach their ultimate sophistication by successfully predicting the biological process. The actual experience is an iterative cycle of model development and hypothesis testing that requires multiple rounds of data generation and model adjustment until the predictive power reaches an acceptable agreement with experimental data [203]. However, succeeding in the development of such models opens up the avenue for a rational, systematic and efficient design of bioprocesses [204] or of medication strategies

[205]. In case of dynamic phenomena that involve a sufficiently high number of species molecules, such models can be composed of ordinary differential equations (ODEs) to integrate experimental data and structural information of the network. The application of dynamic mathematical models spans from the analysis of heterogeneous cell populations (segregated models, cf. [206]) to the investigation of intracellular components (structured models) and may touch multiple scales (multi-scale model). In the following sections, standard models on cell growth and metabolism are introduced regarding their complexity and field of application. Afterwards, examples for the mathematical description of enzyme kinetics and methods for the analysis of ODE-based models are introduced.

2.3.1. Cell growth models

For the understanding of yeast, bacteria or mammalian cell growth, models are desired that precisely recapitulate the growth process, metabolite consumption and byproduct release over the course of cultivation. The structure of cell growth models has a mainly empirical form where the biological system is viewed as a catalyst for the conversion of substrates into products [19, 207]. This conversion of substrates is directly linked to an increase and maintenance of cell numbers or biomass.

Cell number-based models: In biotechnology, cell growth models often consist of a growth function for the cell number that is linked to substrate uptake and byproduct release rates in order to reflect changes in the culture and to evaluate yield coefficients [51]. Due to their simple structure and the wide accessibility of data, such models find application in many studies and were developed for various cells and growth inhibiting aspects [208–210]. For adherent cells, cell number-based models can reflect the growth in bioreactors [211] and can take into account the cell number distribution on microcarriers [212]. Such models are also used to study growth on flat surfaces [213] and are — besides ODE-based approaches — also available as stochastic [214] and cell automata models [215]. The lag phase in cell number growth (see section 2.1.2) is typically realized by implementing delay functions [211] (to account for cell settling, attachment or size increase until division). Delay functions, however, can fail in rendering the uptake and release of metabolites experimentally identified during the initial phase of cultivation where biomass growth precedes cell division. Towards the end of cultivations, cell density-dependent growth inhibition can occur and cells enter a stationary growth phase. If cell density-dependent growth inhibition is calculated on the basis of cell num-

bers, a distorted view on growth phases may result, as cell numbers can increase while the biomass remains constant [216]. Furthermore, higher cell concentrations can be achieved if cells have smaller mean cell diameters [44] and, thus, final cell numbers can differ among replicate cultivations (e.g. [211]). Therefore, cell number-based models can explain several aspects of cultivations but only in a very restrictive way.

Biomass-based models: Some of the above-mentioned problems are solved by using biomass-based models, e.g. by Baltes et al. [217] to support the experimental design of yeast cultivations or by Dhir et al. [3] as well as Frame and Hu [39] to study hybridoma cell growth. However, these models can hardly distinguish between cell-specific mass changes and the cell number increase. Since parameters of intracellular biochemical processes can correlate with the cell mass (e.g. protein synthesis, membrane composition, metabolite concentrations) as well as with the cell number (e.g. activities located in the nucleus, signaling pathways), pure biomass-based models have a limited field of application when it comes to the analysis of intracellular phenomena. Nevertheless, cell number-based and biomass-based models are simple and, have without question, a certain power in analyzing cultivations of mammalian cells.

Cell mass models: Population balance equations are an elegant way to comprehensively characterize the growth in cultivation processes described in section 2.1.2 regarding the time course of cell mass and cell number changes [218, 219]. Many different "cell mass models" for microbial populations in culture have been developed [220–223] and numerical methods have been established to reduce the computational effort involved [224, 225]. Nevertheless, the validation of the underlying model functions, namely the growth rate function, the cell division probability function and the partitioning probability function is still challenging, mainly due to the lack of experimental data. Furthermore, the influence of substrate depletion, inhibitor accumulation or growth surface limitation on the respective functions remains to be characterized. Nielsen et al. [42] therefore suggest for yeast cells a middle course that links the cell number to the biomass using a delay function to induce an artificial diameter increase.

2.3.2. Dynamic models of metabolism

One of the first computational attempts to simulate the metabolism of tumor cells was made in 1959 by Chance et al. [226]. Since then, dynamic models for metabolism have been developed for many pathways and organisms. In the following, we introduce a

selection of the most insightful models for the cellular metabolism.

Glycolysis models: Since the first computational attempt by Chance et al. [226], glycolysis became the most intensively modeled metabolic pathway. For erythrocytes, which have a relatively stable cell composition, a first core model of glycolysis was developed by Rapoport and colleagues [227] in 1974 and was gradually extended by including detailed aspects of enzyme kinetics [228, 229] as well as the energy metabolism and ion transport [230–232]. The last versions integrate also the PPP and steady state metabolite data and are used to predict the impact of enzyme deficiencies [233, 234]. More recent models of mammalian cell glycolysis were developed for liver cells to analyze the blood glucose homeostasis [71, 146] and for skeletal muscle cells to illuminate glycogenolysis [235]. However, the largest part of glycolytic models were developed for yeast and *E. coli*, perhaps because of the large amount of available data, the ease of experiments and the wide options for genetic modifications, and cover a broad field of phenomena. The most advanced models on metabolism describe the response to glucose pulse experiments [20, 236, 237], the link between transcriptome and metabolism [238, 239] or the emergence of an oscillatory activity under glucose starvation [240, 241]. One of the best validated models for yeast glycolysis is proposed by Teusink et al. [242] and van Eunen et al. [20] and considers enzyme kinetics, which were measured under *in vivo*-like conditions [11]. It largely agrees with steady state flux and metabolite data, which were derived from labeling experiments. Although in many of the above cases the existent experimental data sets do not allow for a full validation of the complex kinetics used (especially not for a broader physiological context), their benefit lies in the integration of complex regulatory mechanisms and their explanation for general phenomenological aspects that are typically found in the respective cell type. However, an apparently complex metabolic behavior must not result from complex regulatory mechanisms [243]. In case of glycolysis, it seems that few regulatory mechanisms dominate the dynamics of intracellular pools and readily explain salient features of experimental measurements [12]. Furthermore, with an increasing number of powerful assays, e.g. to determine intracellular metabolite concentrations or to measure enzyme activities in yeast and animal cells, changes in glycolytic activity during cell growth or substrate perturbations can be monitored at an unprecedented level. Integrating such data under consideration of extracellular metabolite changes as well as cell growth dynamics may support mathematical modeling in the systematic analysis of metabolic pathways under various cultivation conditions.

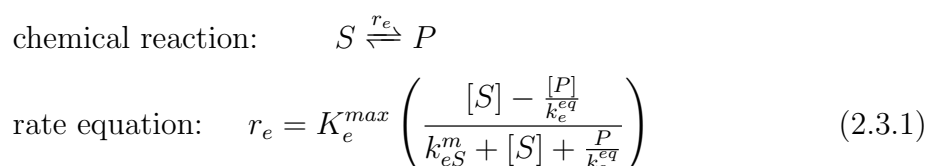
Citric acid cycle models: In a pioneering work, Garfinkel [244] proposed a computer model for the Krebs cycle and the closely related metabolism. The intention was to illuminate the control exerted by the different compounds with the use of steady state metabolite pool data. In the following studies performed with rat heart cells, the kinetic descriptions of the citric acid cycle were preferentially used to evaluate pathway fluxes from labeling experiments [245, 246]. Since then, the models were more and more refined by more detailed enzyme kinetics [167], extended by aspects of electrophysiology [247] and volume dynamics [248], and transferred to cells other than rat heart and muscle [249]. The most recent model proposed by Bazil and coworkers [248] incorporates an impressively large data set that covers *in vitro* enzyme activities, flux data as well as metabolite and ion concentrations, which are mostly derived from isolated mitochondria from rat heart and other cells to calibrate the involved kinetics comprising about 400 parameters. However, considerable differences in structure and parameterization of enzyme kinetics can be observed when using *in vitro* and *in vivo* data for model calibration, as described by Mauch et al. [250, pp. 571-579] and van Eunen et al. [11]. Since such models are usually too complex for validation with *in vivo* data, Nazaret et al. [251] proposed a simplified model for the citric acid cycle and its link to the oxidative phosphorylation that successfully renders the observed metabolic steady states. It shows that simple models can also explain salient features of experimental measurements for the citric acid cycle.

Central carbon metabolism models: With a model for the citric acid cycle at hand, a connection to glycolysis models seems intuitively attractive since both pathways are central to the generation of cellular energy and biomass. For *E. coli*, such models are validated with knockout mutants [252] and used to evaluate strategies that aim at re-designing metabolic routes [253], which was similarly done for yeast [237] and relies on metabolite pool data after a glucose pulse. Although detailed kinetic models of the central carbon metabolism also exist for CHO cells [254], macroscopic (sometimes unstructured) descriptions are already sufficient to study process strategies that aim at higher growth and antibody production rates for hybridoma cells [255, 256].

2.3.3. Model construction and analysis

Kinetics of enzyme-catalyzed reactions: The detailed *in vitro* characterization of glycolytic enzymes, such as HK [10], PFK [8] and PK [9], with respect to their catalytic

properties in the presence of substrates, products and allosteric effectors⁴ represents an important step towards a kinetic description of metabolic phenomena of cells. However, the most simple description for the conversion of substrates into products is provided by the law of mass action. Depending on the molecule number of reactants involved, the reactions have a certain order. For enzyme-mediated conversions the different steps, e.g. substrate binding, change in conformation and product release, can be individually represented by mass-action kinetics, which, unfortunately, yields large sets of differential equations and parameters. Under a few simplifying assumptions, Michaelis and Menten derived a rate-law that links the product formation with the substrate conversion. Cleland [257–259] extended that approach by introducing a nomenclature with full steady-state rate equations for arbitrary complex reactions by taking into account the number of reactants and products (e.g. uni-uni, bi-uni,...), the reaction sequence (ordered or random), the isomerization of the enzyme (iso, ping-pong) and the reversibility. The laborious mathematical derivation of these kinetics motivated King and Altman [260] to develop a relatively simple, graph-based method which mostly relies on the chemical reaction scheme. However, cooperative⁵ as well as allosteric effects are an important regulatory function of cells and not adequately covered by this approach. In 1910, Hill [261] discovered that the aggregation of hemoglobin yields sigmoid binding curves for oxygen. Motivated by this observation the authors proposed the Hill kinetic, which takes into account cooperativity and is an important discovery that contributes to the characterization of glycolytic enzymes such as the PK and the PFK. Since glycolytic enzymes are additionally regulated by many allosteric effectors, Monod et al. [262] proposed the Monod-Wyman-Changeaux model where the affinity for a substrate is a function of all the above highlighted influences. Taken together, the conversion of a substrate S into a product P can be expressed with an arbitrary complexity in corresponding kinetics depending on which effects are considered as relevant. An example of translating a reversible reaction into a simple enzyme kinetic is given here:



⁴**allosteric effector:** molecule that binds to the enzyme at an allosteric center, which changes the catalytic activity without a direct influence on ligands

⁵**cooperative effect:** aggregation of single units leading to a modification of the catalytic activity

The basic equation for the rate equation r_e of enzyme e stems from the simple Michaelis-Menten kinetic with a maximum cell-volume-specific activity K_e^{max} and an affinity constant for the substrate k_{eS}^m . Since the back reaction $S \leftarrow P$ cannot be neglected (in contrast to a standard Michaelis-Menten kinetic), the difference between S and P influences the velocity of the reaction and whether r_e has a positive or negative sign. Due to the Haldane relationship, the equilibrium constant k_e^{eq} between S and P is defined as

$$k_e^{eq} = \frac{k_{eP}^m}{k_{eS}^m} = \frac{[P^{ss}]}{[S^{ss}]} \quad (\text{ss} = \text{steady state}). \quad (2.3.2)$$

Such a kinetic is, among others, used in the structured model of this work. An overview for more detailed kinetics of enzyme mediated reactions is given in the book of Bisswanger [263].

Estimation and identifiability of model parameter: The sparsity of experimental data in combination with the complex nature of biological observations imposes great challenges for modeling and analysis of biochemical networks [203]. Models, which by definition are an abstraction of reality, have a great chance to fail in explaining observations at first simulation either because experimentally measured parameters were derived under experiment conditions different than required for the simulation scenario or are simply not available (which is mostly the case). The gap between observation and model simulation leads to the parameter estimation problem, as for instance described by Bellman and Åström [264]. The estimation of parameters typically requires non-linear optimization methods where the objective is to find a parameter set that minimizes a function quantifying the goodness of fit, usually a least squares function [204]. A large number of algorithms for solving optimization problems are currently available, either of deterministic or stochastic nature, and designed to find local or even global minima in the parameter space [265]. However, the ability to estimate parameters is not only a question of the optimization method but also of the underlying model structure and the data available for the analysis, which is further known as identifiability problem [266]. In particular, two formally distinct but functionally redundant mechanism of a model, which can replace each other in generating a certain response, may impose "structural" identifiability problems if both mechanisms cannot be distinguished with the available data (independent of the data quality, [267]). In consequence, the algorithms yield non-unique parameter solutions with strong correlations for the parameter estimation problem. In contrast, "practical" identifiability problems result from low

quality data that leaves parameters with large uncertainties. Practical identifiability problems can be identified by analyzing the change in model fit upon infinitesimal parameter perturbations and solved by acquiring data of higher quality. Note that Sontag [268] once stated that $2r + 1$ of highly informative data points are enough to identify r unknown parameters. However, since a reliable parameter identification is of utmost importance for the inference of biological meanings as well as for the quality of model predictions, uncertainty estimates should always be provided together with the parameter values [269]. A simple way of obtaining these uncertainty estimates is the Fisher Information Matrix (FIM) derived from the parameter sensitivities and the measurement error of the observables. The FIM can be used to support the design of most informative experiments [270]. However, the inverse of the FIM only yields a lower bound on the variance of the parameter, which is known as the Cramer Rao bound. More reliable parameter confidence intervals are obtained from bootstrap methods, as described by Efron and Tibshirani [271], the parameter likelihood-function [272] or by using the Bayesian approach to parameter identification and identifiability analysis [273]. Since these methods also unravel parameter correlations, model reduction can be facilitated such that more precise parameter confidence intervals are achieved. Counterintuitively, also sloppy parameter estimates⁶ can enable tight quantitative predictions (since highly sensitive parameters are also fragile sites [203]) and, thus, are not necessarily optional or removable degrees of freedom, as shown by the work of Brown et al. [274]. As long as the understanding of the system is tentative and incomplete, the focus should be on the predictive power of the model rather than on its parameter values [269]. It should be born in mind that sloppy parameter estimates may be a central feature of biological systems to achieve robustness against fluctuations in components or the environment, which is primarily achieved by functionally redundant or insensitive mechanisms [275].

⁶**sloppy parameter estimates:** the simulation result is mostly insensitive to changes in the corresponding parameter

3 Chapter

Models and methods

3.1. Model definitions

3.1.1. Segregated cell growth model

The segregated cell growth model established in the scope of this work simulates data that is obtained with automated cell counting devices, including cell diameters, and comprises parameters that are typically used for cell number-based models. It describes cell populations with growth and maintenance metabolism based on a set of ordinary differential equations.

Cell growth: To account for differences in cell diameter, several classes of cells X_i are introduced,

$$\frac{dX_1}{dt} = r_{trans}(-X_1f + 2X_{N^c}), \quad (3.1.1)$$

$$\frac{dX_2}{dt} = r_{trans}(X_1f - X_2), \quad (3.1.2)$$

$$\frac{dX_i}{dt} = r_{trans}(X_{i-1} - X_i), \text{ for } i = 3, \dots, N^c, \quad (3.1.3)$$

$$f := \begin{cases} 0 & \text{if } V^C > V_*^C \\ f(V^C) & \text{if } V^C \leq V_*^C \end{cases} . \quad (3.1.4)$$

The factor f accounts for the cell volume-dependent (V^C -dependent) growth inhibition, which we will discuss in the next paragraph. V_*^C is the approximate cell volume for larger times ($t \approx 200$ h). The cells pass with a transition rate r_{trans} through the classes X_1, \dots, X_{N^c} with linearly increasing diameter until a critical diameter d_c is reached and the cells divide. The transition rate itself is based on Monod's equation [276] where the specific growth rate μ is a function of the maximum specific growth rate μ_{max} , of the Monod constant $k_{GLC^x}^m$ and of the GLC^x concentration. Alternative growth kinetics might be appropriate for other cell lines [210], but were not required for fitting of our experimental data. Multiplication with α transforms the commonly used specific growth

rate μ into r_{trans} ,

$$r_{trans} = \mu\alpha = \frac{\mu_{max}[GLC^x]}{k_{GLC^x}^m + [GLC^x]} \frac{1}{2^{1/N^c} - 1}, \quad (3.1.5)$$

to obtain a cell growth model that is asymptotic in cell growth to $\dot{x} = \mu x$ (provided by D. Flockerzi, see Rehberg et al. [216] for mathematical explanation). Note that μ_{max} is an effective growth rate that considers the loss of cells due to death [277].

Growth inhibition as a function of cell volume: The transition between the exponential and the stationary growth phase of adherent MDCK cells can depend on the availability of free surface. Accordingly, cells will grow with μ_{max} as long as all essential substrates are available in sufficient amounts and surface is not limiting [211–213, 278, 279]. In this work, the inhibition is assumed to be a function of the cell volume. Note that biomass and cell volume are linearly correlated as long as changes in the density due to osmolality effects can be excluded [42]. The cell volume can be calculated on the basis of the cell numbers and the cell diameters. The cell number, which is the sum of cells in all classes X_i corresponds to

$$X_{tot} = \sum_{i=1}^{N^c} X_i \quad (3.1.6)$$

and is monotonically increasing over time. Assuming that the class-specific diameters are equidistant between the minimum diameter d_m and the critical diameter d_c , the mean diameter \bar{d} of all cells can be calculated with

$$\bar{d} = \sum_{i=1}^{N^c} \left(d_m + \frac{d_c - d_m}{N^c - 1} (i - 1) \right) \frac{X_i}{X_{tot}}. \quad (3.1.7)$$

Note that d_m and d_c may vary with every experiment. The cell volume V_{model}^C now follows with summation of all class-specific volumes V_i^C , given by $V_{model}^C = \sum_{i=1}^{N^c} V_i^C$. However, measurement of cells may only yield mean cell diameters and hence only allows to observe an 'experimental' cell volume (e.g. Niklas et al. [164]). Therefore, V^C is introduced as an estimator for V_{model}^C and defined as

$$V^C = \pi \frac{\bar{d}^3}{6} X_{tot} 10^{-9}, \quad (3.1.8)$$

with the unit μL . Note that Eq. (3.1.8) underestimates the true cell volume, $V^C < V_{model}^C$ (Jensen's inequality) but allows a larger applicability in the field of biotechnology where diameter distributions are not available. In cultivation processes monitored using coulter counters, e.g. for the data published by Frame and Hu [43], a deviation of up to 13 % can result. However, this is here within the error bars provided for the data of V^C . The cell-specific volume V_s^C (unit: L) follows with:

$$V_s^C = \frac{V^C}{X_{tot}} 10^{-6} \quad (3.1.9)$$

To describe an inhibition by cell density, Frame and Hu [278] proposed a nonlinear term, which is dependent on the cell number concentration. Here, a transformation based on V^C is used on $[0, V_*^C]$ to derive a cell volume-dependent growth inhibition factor f :

$$f = f(V^C) = 1 - \exp\left(\left(-s\right)\frac{V_*^C - V^C}{V^C}\right). \quad (3.1.10)$$

The adjustable parameter s is cell line-dependent and shapes the sensitivity of the (*in silico*) cell to extracellular limitations. Furthermore, we assume that growth inhibition only affects the initiation of cell proliferation at the first transition $X_1 \rightarrow X_2$ (Eq. (3.1.1) and (3.1.2)). Hence, cells that are already in the division process have passed the early checkpoint of cell growth and continue to increase in size.

Metabolic uptake and release rates: Cells consume substrates to sustain or increase their biomass. Thus, the substrate uptake rates are commonly linked to the cell number concentration or its increase [211, 212]. Nielsen et al. [42] hypothesized that cells with larger biomass consume and release more metabolites. Accordingly, we link the medium-volume-specific uptake rates for maintenance ($r_{m/S}$) to V^C , leading to

$$r_{m/S} = m_S V^C \Theta([S]) \lambda \text{ with } S \text{ out of } \{GLC^x, GLN^x, NH_4^x\}, \quad (3.1.11)$$

where m_S is the cell-volume-specific uptake rate of substrate S for maintenance metabolism, where S stands for GLC^x , extracellular glutamine (GLN^x) or NH_4^x . Θ is a unit step function, which is one for $[S] > 0$ and zero otherwise. Each reaction is scaled by λ to account for water evaporation (see Eq. (3.1.21)). Furthermore, the medium-volume-specific uptake rate ($r_{X/S}$) of substrate S is linked to the number of

growing cells (as discussed later) by

$$r_{X/S} = \mu \left(X_1 f + \sum_{i=2}^{N_c} X_i \right) Y_{X/S} \lambda, \quad (3.1.12)$$

where $Y_{X/S}$ is the cell-growth-specific yield coefficient for S . Apart from these commonly used definitions, the uptake of extracellular glutamate (GLU^x) seems to be best represented by

$$r_{GLT} = K_{GLT} [GLU^x] (1 - f), \quad (3.1.13)$$

according to the results of Maria Wetzel [280], and can be interpreted as a GLU^x transporter (GLT) that is inhibited as long as the cell proliferates. Note that r_{GLT} is a cell-volume-specific rate and, thus, different to $r_{m/S}$ or $r_{X/S}$. The specific activity K_{GLT} is further explained in section 3.1.3. The change in extracellular metabolite concentrations is thus given with

$$\frac{d[GLC^x]}{dt} = -r_{X/GLC^x} - r_{m/GLC^x} + \frac{F_{evap}[GLC^x]}{V^M}, \quad (3.1.14)$$

$$\frac{d[GLN^x]}{dt} = -r_{X/GLN^x} - r_{m/GLN^x} - r_{dGLN^x} + \frac{F_{evap}[GLN^x]}{V^M}, \quad (3.1.15)$$

$$\frac{d[GLU^x]}{dt} = -r_{GLT} \frac{V_s^C X_{tot}}{V^M} + \frac{F_{evap}[GLU^x]}{V^M}, \quad (3.1.16)$$

$$\frac{d[LAC^x]}{dt} = (r_{X/GLC^x} + r_{m/GLC^x}) Y_{LAC^x/GLC^x} + \frac{F_{evap}[LAC^x]}{V^M}, \quad (3.1.17)$$

$$\frac{d[NH_4^x]}{dt} = 2(r_{X/GLN^x} + r_{m/GLN^x}) + r_{dGLN^x} - r_{X/NH_4^x} - r_{m/NH_4^x} + \frac{F_{evap}[NH_4^x]}{V^M}. \quad (3.1.18)$$

Here, F_{evap} represents the measured water evaporation in 6-well plates (data not shown) and V^M stands for the medium volume during cultivation, defined by

$$\frac{dV^M}{dt} = -F_{evap}, \quad (3.1.19)$$

and thus by

$$\Rightarrow V^M(t) = V^M(0) - F_{evap} t \stackrel{!}{>} 0. \quad (3.1.20)$$

Note that $V^M(0)$ corresponds to the well volume V^W , which allows to define λ with:

$$\lambda = \frac{V^W}{V^M} \quad (3.1.21)$$

According to Ozturk and Palsson [53], glutamine decomposition can occur and was explicitly taken into account with

$$r_{dGLN^x} = k_{dGLN^x}[GLN^x], \quad (3.1.22)$$

where k_{dGLN^x} is the specific decomposition rate, estimated for GMEM-Z at 37 °C by Bock et al. [212]. Y_{LAC^x/GLC^x} is the glucose-specific lactate yield. Note that the accumulation of NH_4^x depends on a maximum stoichiometric production from GLN^x and its incorporation into biomass during cell growth and maintenance. A release of NH_4^x from GLU^x is not considered in the model (discussed later).

3.1.2. Structured central carbon metabolism model

In order to derive conclusive insights into the regulation of the central carbon metabolism of adherent MDCK cells, this work seeks a simple kinetic description of the enzyme catalyzed reactions that agrees with the most basic characteristics reported for the corresponding enzymes and pathways. Therefore, differential algebraic equations of the model, which describe enzyme activities in dependence of metabolite concentrations and allosteric influences, were composed as far as possible using first order rate laws. In cases where measurements on maximum enzyme activities are available Michaelis-Menten and Hill kinetics were used. All metabolite levels and flux rates are related to the cell-specific volume, which is preferred by many scientists [94, 195, 281], as it allows an adequate comparison of metabolite pools under varying cell sizes but assumes an even distribution of metabolites within the intracellular space [44]. In the following we also assume that the cell population reflects the metabolite pool dynamics of a single cell.

Glycolysis

The kinetics for glycolysis consider the metabolic conversion of GLC to PYR as well as the closely related metabolism of PPP and glycogenesis:

$$\frac{d[GLC^x]}{dt} = -r_{GLUT} \frac{V_s^C X_{tot}}{V^M} \quad (3.1.23)$$

$$\frac{d[GLC]}{dt} = r_{GLUT} - r_{HK} - \mu f[GLC] \quad (3.1.24)$$

$$\frac{d[G6P]}{dt} = r_{HK} - r_{GPI} - r_{G6PDH} - r_{UT} - \mu f[G6P] \quad (3.1.25)$$

$$\frac{d[F6P]}{dt} = r_{GPI} + r_{TATKF6P} - r_{PFK} - \mu f[F6P] \quad (3.1.26)$$

$$\frac{d[F16BP]}{dt} = r_{PFK} - r_{ALD} - \mu f[F16BP] \quad (3.1.27)$$

$$\frac{d[3PG]}{dt} = 2r_{ALD} + r_{TATK3PG} - r_{ENO} - \mu f[3PG] \quad (3.1.28)$$

$$\frac{d[PEP]}{dt} = r_{ENO} - r_{PK} - \mu f[PEP] \quad (3.1.29)$$

The term $\mu f[M]$ expresses the dilution of intracellular metabolite M by the approximate cell volume growth (μ is here used in 1/min). The dilution by cell volume growth only occurs during the cell cultivation experiments and not during the perturbation experiments. The enzyme kinetics for the metabolic conversion rates r are defined as follows:

Glucose transporter (GLUT): The GLUT diffuses within the cell membrane and transports glucose between the cytosol and the extracellular medium depending on the glucose gradient. For yeast cells, a complex kinetic description was developed to reflect this process mechanistically [282], while the corresponding data is equally well represented by a simple Michaelis-Menten kinetic that considers G6P inhibition (simulation not shown). As intracellular GLC could not be detected experimentally (see HK), the transport across the membrane seems rate limiting and is, according to simulations, insensitive against changes in G6P (simulations not shown). Therefore, and in agreement to findings for pancreatic β -cells by Luni et al. [116], a simple Michaelis-Menten kinetic was used and complemented with a variable capacity for the substrate uptake (γ_{GLUT} , explained in section 3.1.3) for an uni-directional glucose transport r_{GLUT} :

$$r_{GLUT} = K_{GLUT}^{max} \gamma_{GLUT} \frac{[GLC^x]}{k_{GLUT}^m + [GLC^x]} \quad (3.1.30)$$

K_{GLUT}^{max} is the maximum cell-volume-specific activity of the GLUT with affinity k_{GLUT}^m for GLC^x . Because of the multiplication of K_{GLUT}^{max} with γ_{GLUT} , structural identifiability problems occurred and a unique estimation of the cell-specific maximum ac-

tivity of the GLUT (v_{GLUT}^{max}) is not possible. Therefore, v_{GLUT}^{max} was chosen to be 1.60×10^{-11} mmol/cell/min according to findings for other mammalian cells [104, 107].

Hexokinase, (HK, EC number: 2.7.1.1): GLC could not be detected experimentally in MDCK cells, which was similarly reported for other cell lines [91, 95, 283]. Therefore, a possible influence by ATP, as measured by Fromm and Zewe [10] for yeast cells, may reduce the HK activity but presumably not to a degree sufficient to limit the glycolytic activity. Due to the lack of appropriate data for GLC and the lack of any indication regarding a possible regulation by ATP we chose a simple Michaelis-Menten kinetic that considers the maximum *in vitro* enzyme activity measured by Janke et al. [22] for MDCK cells and an affinity constant for glucose of $k_{HK}^m = 0.02$ mmol/L [86], which together yield a highly active HK and low GLC levels.

$$r_{HK} = K_{HK}^{max} \frac{[GLC]}{k_{HK}^m + [GLC]} \quad (3.1.31)$$

K_{HK}^{max} is the maximum cell-volume-specific activity of the HK with affinity k_{HK}^m for GLC.

Glucosephosphate isomerase (GPI, EC number: 5.3.1.9): A reversible kinetic of Michaelis-Menten type was used to describe the isomerization of G6P and F6P, as suggested by Richter et al. [241] for yeast cells and with the maximum *in vitro* activity measured by Janke et al. [22].

$$r_{GPI} = K_{GPI}^{max} \left(\frac{[G6P] - \frac{F6P}{k_{GPI}^{eq}}}{k_{GPI}^m + [G6P] + \frac{F6P}{k_{GPI}^{eq}}} \right) \quad (3.1.32)$$

K_{GPI}^{max} is the maximum cell-volume-specific activity of the GPI with affinity k_{GPI}^m for G6P and equilibrium constant k_{GPI}^{eq} .

Glucose 6-phosphate dehydrogenase (G6PDH, lumped reaction): The conversion of G6P to R5P involves G6PDH and other enzymes with an accompanying production of two NADPH molecules. For cancer cells, a negative regulation of the reaction sequence by 3PG is reported [140]. Our data, however, does not support a negative correlation between 3PG and R5P, which indicates that this mechanisms may not have a significant influence in adherent MDCK cells. Assuming that G6PDH is rate limiting within the reaction sequence allows the model to use a Michaelis-Menten kinetic with

the maximum *in vitro* activity measured by Janke et al. [22]:

$$r_{G6PDH} = K_{G6PDH}^{max} \frac{[G6P]}{k_{G6PDH}^m + [G6P]} \quad (3.1.33)$$

K_{G6PDH}^{max} is the maximum cell-volume-specific activity of the G6PDH with affinity k_{G6PDH}^m for G6P.

Uridyl transferase (UT, lumped reaction): In glycogenesis, UT is involved in the generation of UGLC from G6P. A Michaelis-Menten kinetic close to saturation was necessary to describe the experimental data of this work:

$$r_{UT} = K_{UT}^{max} \frac{[G6P]}{k_{UT}^m + [G6P]} \quad (3.1.34)$$

K_{UT}^{max} is the maximum cell-volume-specific activity of the UT with affinity k_{UT}^m for G6P.

Phosphofructo kinase (PFK, EC number: 2.7.1.11): The PFK is a highly regulated enzyme in glycolysis and often assumed to be best represented by kinetics that consider a certain cooperativity. According to measurements of Otto et al. [228] for erythrocytes and a review by Boiteux and Hess [284], a cooperativity of four seems to suit the PFK and is analogously used in this work. A very potent regulator of the PFK is fructose 2,6-bisphosphate [135], which is synthesized from F6P by phosphofructokinase-2. For simplicity, it is assumed that F6P and fructose 2,6-bisphosphate are linearly positively correlated in their dynamics through a fast and reversible working phosphofructokinase-2, which allows us to implement the PFK as a Hill kinetic with sole activation by F6P. During development of the model, other less efficient regulators such as ATP, ADP, AMP or CIT [135, 228] were tested, and finally withdrawn as the model fit was not improved.

$$r_{PFK} = K_{PFK}^{max} \frac{[F6P]^4}{k_{PFK}^m + [F6P]^4} \quad (3.1.35)$$

K_{PFK}^{max} is the maximum cell-volume-specific activity of PFK with affinity k_{PFK}^m for F6P.

Transaldolase and transketolase (TATK, EC number: 2.2.1.2 / 2.2.1.1): Both enzymes are responsible for the reversible conversion of metabolites of the PPP such as F6P, R5P and GAP. Because of the unknown flux distribution and unknown concentrations of many PPP metabolites, we decided to use individual reversible first order

rate laws for F6P and GAP formation and degradation (see "Pentose Phosphate Pathway" for further constraints). As GAP is not explicitly incorporated in the model, we assumed a strong correlation to 3PG (see "Aldolase") and, hence, coupled the activity of the TATK to 3PG. The equilibrium between consumption and production depends on the level of F6P (or 3PG) as well as a threshold defined by the equilibrium constants $k_{TATKF6P}^{eq}$ (or $k_{TATK3PG}^{eq}$) assuming a constant pool size of pentose phosphate metabolites of about 1 mmol/L:

$$r_{TATKF6P} = K_{TATKF6P} \left(1 - \frac{[F6P]}{k_{TATKF6P}^{eq}} \right) \quad (3.1.36)$$

$$r_{TATK3PG} = K_{TATK3PG} \left(1 - \frac{[3PG]}{k_{TATK3PG}^{eq}} \right) \quad (3.1.37)$$

$K_{TATK3PG}$ and $K_{TATKF6P}$ are the cell-volume-specific activities of the TATK for F6P and 3PG conversion.

Aldolase (ALD, lumped reaction): Since DAP, GAP and 13DGP could not be quantified for MDCK cells by Ritter [23], we assume that the enzymes, which are involved in the generation of 3PG, highly correlate in their activity with ALD. High *in vitro* enzyme activities of the TPI and GAPDH were indeed reported by Janke et al. [22] and support the idea of a diminishing flux control. Furthermore, all reactions are reversible and expected to have a minor flux control over glycolysis in tumor cells [108]. Therefore, we chose a Michaelis-Menten kinetic that represents the net flux from F16BP to 3PG using the *in vitro* enzyme activity measured by Janke et al. [22]. A larger model that explicitly integrates additional reaction steps requires seven additional parameters, while showing only a minor improvement in fitting the data of this work.

$$r_{ALD} = K_{ALD}^{max} \frac{[F16BP]}{k_{ALD}^m + [F16BP]} \quad (3.1.38)$$

K_{ALD}^{max} is the maximum cell-volume-specific activity of ALD with affinity k_{ALD}^m for F16BP.

Enolase (ENO, lumped reaction): In yeast, reversible Michaelis-Menten kinetics are used to describe the ENO activity [241]. Under the assumption that the isomerization of 3PG to 2PG is usually a very fast and reversible step, the model describes the generation of PEP from 3PG using a single reversible kinetic for ENO. A first order rate law

sufficiently describes the data of this work:

$$r_{ENO} = K_{ENO} \left([3PG] - \frac{[PEP]}{k_{ENO}^{eq}} \right) \quad (3.1.39)$$

K_{ENO} is the cell-volume-specific activity of ENO with equilibrium constant k_{ENO}^{eq} .

Pyruvate kinase (PK, EC number: 2.7.1.40): The PK is another strongly regulated enzyme in tumor cell glycolysis with four subunits and high affinity for PEP [126]. The most prominent control over the PK activity is exerted by a feedforward activation through F16BP [69]. Since the cofactors ATP and ADP as well as a higher cooperativity (e.g. four) could not improve the model fit (simulation not shown), we only considered a Michaelis-Menten kinetic with an activation by F16BP that considers the *in vitro* enzyme activity measured by Janke et al. [22]:

$$r_{PK} = K_{PK}^{max} \frac{[PEP]}{k_{PK}^m + [PEP] + \frac{k_{PK}^a}{F16BP}} \quad (3.1.40)$$

K_{PK}^{max} is the maximum cell-volume-specific activity of PK with affinity k_{PK}^m for PEP and activation constant k_{PK}^a for F16BP.

Pentose phosphate pathway

The link of glycolysis with the PPP through the G6PDH reaction eventually yields R5P, which is degraded by TATK or used for biosynthesis, and changes with

$$\frac{d[R5P]}{dt} = r_{G6PDH} - r_{RDPK} - \mu f[R5P]. \quad (3.1.41)$$

Corresponding biosynthetic needs for PPP intermediates ($r_{X/PPP}$) are indirectly given with:

$$r_{X/PPP} = r_{G6PDH} - r_{TATKF6P} - 0.5r_{TATK3PG}. \quad (3.1.42)$$

Furthermore, the metabolite exchange between glycolysis and PPP is constrained to be in a typical biologically feasible range of 0 % to 40 % of the glycolytic activity (here hexokinase activity, [150–152]):

$$0 < \frac{r_{X/PPP}}{r_{HK}} < 0.4 \quad (3.1.43)$$

During glucose limitation, the PPP can fuel glycolysis but presumably at a very low rate. Therefore, the activity of the pyruvate kinase should be as low as possible (at 6 min) but high enough to satisfy the experimental data (see section 3.3.2).

Ribose 1,5-bisphosphate phosphokinase (RDPK, EC number: 2.7.4.23): The degradation of R5P by ribose 1,5-bisphosphate phosphokinase (RDPK) is implemented as first order rate law and is representative for all possible conversion reactions.

$$r_{RDPK} = K_{RDPK}[R5P] \quad (3.1.44)$$

K_{RDPK} is the cell-volume-specific activity of RDPK.

Glycogenesis

The generation of glycogen from UGLC, which is mainly derived from G6P by a UT-mediated reaction (see Eq. (3.1.34)), is mediated by the glycogen synthase (GLYS):

$$\frac{d[UGLC]}{dt} = r_{UT} - r_{GLYS} - \mu f[UGLC] \quad (3.1.45)$$

Glycogen synthase (GLYS, EC number: 2.4.1.11): The degradation of UGLC by GLYS is implemented as first order rate law and is representative for all possible conversion reactions,

$$r_{GLYS} = K_{GLYS}[UGLC], \quad (3.1.46)$$

with the cell-volume-specific activity K_{GLYS} .

Glutaminolysis

The supply of the citric acid cycle relies upon anaplerotic reactions that use amino acids such as GLN, GLU or PYR as substrate. The conversion of GLN to GLU and subsequently to α KG are initial reaction steps of glutaminolysis and produce intracellular ammonium (NH_4). A fraction of NH_4 remains in the cell, either bound to amino acids or as O-GlcNAcylation [85], while the other fraction is secreted into the medium, which the model already covers with Eq. 3.1.18. The uptake of GLU^x and GLN^x and the

generation of GLU is described in the model with:

$$\frac{d[GLU^x]}{dt} = -r_{GLT} \frac{V_s^C X_{tot}}{V^M} \quad (3.1.47)$$

$$\frac{d[GLN^x]}{dt} = -r_{GLNT} \frac{V_s^C X_{tot}}{V^M} \quad (3.1.48)$$

$$\frac{d[GLU]}{dt} = r_{GLT} + r_{GLNT} - r_{ATA} - \mu f[GLU] \quad (3.1.49)$$

r_{GLT} is described in section 3.1.1 (Eq. 3.1.13), while r_{GLNT} and r_{ATA} are defined as follows:

Glutamine transporter (GLNT): The GLNT is not only important for the nutrient supply of mammalian cells but also crucial for the survival of tumor cells which over-express the ASCT2 transporter family [117]. Studies with hepatoma cells suggest a Michaelis-Menten kinetic [285], which we extend, similarly to GLUT, by a variable capacity for the substrate uptake (γ_{GLNT} , see section 3.1.3):

$$r_{GLNT} = K_{GLNT}^{max} \gamma_{GLNT} \frac{[GLN^x]}{k_{GLNT}^m + [GLN^x]} \quad (3.1.50)$$

K_{GLNT}^{max} is the maximum cell-volume-specific activity of GLNT with affinity k_{GLNT}^m for GLN^x .

Aspartate/Alanine transaminase (ATA, EC number: 2.6.1.1/2.6.1.2): The conversion of GLU to α KG can be exerted by a few enzymes which either release or transfer an amino group. Modeling the NH_4^x dynamics, however, suggests that mainly transaminases are used. As data on GLU and NH_4 release is not available, a first order rate law seems sufficient for this reaction:

$$r_{ATA} = K_{ATA}[GLU] \quad (3.1.51)$$

K_{ATA} is the cell-volume-specific activity of ATA.

Citric acid cycle

The rate equations for the lower citric acid cycle were taken from Wetzel [280], extended such that they include the upper citric acid cycle and slightly simplified, while yielding the same (or better) data fits. In principle, both parts of the cycle are fueled by GLU

(through a reversed ICDH activity) and, thus, show independent activities [286]. For our data, the citric acid cycle seems to be sufficiently represented by:

$$\frac{d[\alpha KG]}{dt} = r_{ATA} + r_{AAex} + r_{ICDH} - r_{KDH} - \mu f[\alpha KG] \quad (3.1.52)$$

$$\frac{d[SUC]}{dt} = r_{KDH} - r_{SDH} - \mu f[SUC] \quad (3.1.53)$$

$$\frac{d[FUM]}{dt} = r_{SDH} - r_{FMA} - \mu f[FUM] \quad (3.1.54)$$

$$\frac{d[MAL]}{dt} = r_{FMA} - r_{MDH} - \mu f[MAL] \quad (3.1.55)$$

$$\frac{d[ICIT]}{dt} = r_{ACO2} - r_{ICDH} - r_{CL} - \mu f[ICIT] \quad (3.1.56)$$

$$\frac{d[CAC]}{dt} = +r_{ACO} - r_{ACO2} - \mu f[CAC] \quad (3.1.57)$$

$$\frac{d[CIT]}{dt} = r_{PDH} - r_{ACO} - \mu f[CIT] \quad (3.1.58)$$

The enzyme kinetics underlying the various reaction rates r are suggested to depend on many different ions, cofactors, inhibitors and activators [248]. In agreement with a mathematical analysis of the system by Nazaret et al. [251] and the conceptual direction of this work, we chose simple kinetic descriptions that suit our data but may fail to cope with observations made for other cells or isolated mitochondria. Several of the reaction rates that are introduced on the following pages use the cofactors NAD and NADH, which are important energy carrier of the mitochondria and link oxidative phosphorylation with the citric acid cycle. To account for the influence of both carrier on the citric acid cycle, we assume that NAD levels correlate positively with the relative biosynthesis activity of the cell b_{syn} , which is introduced in section 3.1.3 with Eq. (3.1.94). In contrast to b_{syn} , NAD levels are not supposed to deplete or to drop below a basal level (NAD_{basal}). So the virtual, relative NAD level (b_{NAD}) is represented with:

$$b_{NAD} = \frac{b_{syn} + NAD_{basal}}{1 + NAD_{basal}}. \quad (3.1.59)$$

In case of very large values for NAD_{basal} , the citric acid cycle is not affected by NAD.

Amino acid exchange (AAex, lumped reaction): Intermediates of the citric acid cycle are linked to many other amino acids (AA) that are involved in protein synthesis

and degradation. For MDCK cells, Wahl et al. [15] observed relatively high uptake rates for the branched chain amino acids leucine, iso-leucine and valine, which are converted to GLU and α KG [6]. To account for this supply route, we implemented an exchange between AA (constant pool size: 1 mmol/L) and α KG

$$r_{AAex} = K_{AAex} \left(1 - \frac{[\alpha KG]}{k_{AAex}^{eq}} \right) \quad (3.1.60)$$

K_{AAex} is the cell-volume-specific activity of AAex with equilibrium constant k_{AAex}^{eq} .

α -ketoglutarate dehydrogenase (KDH, EC number: 1.2.4.23): The oxidative carboxylation of α KG is performed by KDH, a main regulatory enzyme in the citric acid cycle [248]. But neither activation by ADP nor inhibition by ATP [179] improved the model fits. So attributed to its dependence on NAD, we chose a first order rate law with the cell-volume-specific activity K_{KDH} and with an influence by b_{NAD} :

$$r_{KDH} = K_{KDH}[\alpha KG]b_{NAD} \quad (3.1.61)$$

K_{KDH} is the cell-volume-specific activity of KDH.

Isocitrate dehydrogenase (ICDH, EC number: 1.1.1.41 / 1.1.1.42): According to Filipp et al. [174], the ICDH is significantly changed in its characteristics in melanoma and fast proliferating cells compared to all other citric acid cycle enzymes [175]. The ICDH or another yet unknown enzyme [68] possibly mediate a reductive metabolism of α KG, which leads to a reversed TCA flux under normoxic conditions and produces ICIT. Its purpose lies in an enhanced lipid synthesis. Using a reversible Michaelis-Menten kinetic (used also by Chen and Plaut [287] for bovine heart cells) that depends on NAD in the forward direction (b_{NAD}) as well as on NADH ($1 - b_{NAD}$) in the back reaction suits our data and supports observations about a reversed flux. The kinetic also takes into account the *in vitro* activity measured by Janke et al. [22]. Neither an inhibition by ATP nor an activation by ADP, which is reported by Plaut et al. [288], improved the fit to a significant degree:

$$r_{ICDH} = K_{ICDH}^{max} \frac{[ICIT]b_{NAD} - \frac{[\alpha KG](1-b_{NAD})}{k_{ICDH}^{eq}}}{k_{ICDH}^m + [ICIT] + \frac{[\alpha KG]}{k_{ICDH}^{eq}}} \quad (3.1.62)$$

K_{ICDH}^{max} is the maximum cell-volume-specific activity of ICDH with affinity k_{ICDH}^m for α KG and with equilibrium constant k_{ICDH}^{eq} .

Succinate dehydrogenase (SDH, EC number: 1.3.5.1): The conversion of SUC to FUM is performed by the SDH and yields $FADH_2$, which can be converted to ATP during oxidative phosphorylation. The enzyme's activity is reversible with dependence on the FUM and SUC levels [248]. We used a reversible first order rate law for the SDH:

$$r_{SDH} = K_{SDH} \left([SUC] - \frac{[FUM]}{k_{SDH}^{eq}} \right) \quad (3.1.63)$$

K_{SDH} is the cell-volume-specific activity of SDH with equilibrium constant k_{SDH}^{eq} .

Fumarase (FMA, EC number: 4.2.1.2): For isolated cardiac mitochondria, a reversible Michaelis-Menten kinetic is proposed for the FMA [167] and here taken for MDCK cells using the *in vitro* measured enzyme activity of Janke et al. [22]:

$$r_{FMA} = K_{FMA}^{max} \frac{[FUM] - \frac{[MAL]}{k_{FMA}^{eq}}}{k_{FMA}^m + [FUM] + \frac{[Mal]}{k_{FMA}^{eq}}} \quad (3.1.64)$$

K_{FMA}^{max} is the maximum cell-volume-specific activity of FMA with affinity k_{FMA}^m for SUC and with equilibrium constant k_{FMA}^{eq} .

Malate dehydrogenase (MDH, lumped reaction): According to Sidorenko et al. [16], main routes of MAL conversion are either via the MDH to OAA, which yields NADH from NAD, or via the malic enzyme (ME) to PYR, which yields NADPH from NADP. Furthermore, PYR and OAA are linked via the pyruvate carboxylase (PC). Since data is missing for the intermediates and fluxes, the actual flux distribution cannot be identified based on the model and both routes are equally likely. To achieve high LAC^x secretion rates with a $Y_{LAC^x/GLC^x} > 2$, we assume a net reaction that is influenced by the abundance of NAD and eventually yields PYR. Therefore, we chose a Michaelis-Menten kinetic that considers the *in vitro* measured enzyme activity by Janke et al. [22] and a dependence on NAD (b_{NAD}):

$$r_{MDH} = K_{MDH}^{max} \frac{[MAL]}{k_{MDH}^m + [MAL]} b_{NAD} \quad (3.1.65)$$

K_{MDH}^{max} is the maximum cell-volume-specific activity of MDH with affinity k_{MDH}^m

Pyruvate dehydrogenase (PDH, lumped reaction): The PDH and the CS fuel the citric acid cycle by converting PYR to ACCoA and afterwards to CIT using OAA. A Michaelis-Menten kinetic and the *in vitro* measured enzyme activity from Janke et al. [22] for the PDH were used to account for the transfer of PYR into the citric acid cycle. Additionally, we consider that the reaction converts NAD to NADH and, thus, multiply the reaction with b_{NAD} . Inhibition by several compounds such as CIT, ATP, ADP and AMP, which are described for cardiac mitochondria [167], could not improve the model fit.

$$r_{PDH} = K_{PDH}^{max} \frac{[PYR]}{k_{PDH}^m + [PYR]} b_{NAD} \quad (3.1.66)$$

K_{PDH}^{max} is the maximum cell-volume-specific activity of PDH with affinity k_{PDH}^m for PYR.

Aconitase (ACO, EC number: 2.7.1.40): The ACO converts CIT to ICIT in a reversible fashion with CAC as intermediate and is suggested to be best represented by a reversible Michaelis-Menten kinetic [248]. As measurements for the enzyme's activity are missing for MDCK cells, we used a reversible first order rate law and assumed that CAC dissociates from ACO after the release of a water molecule and poses a substrate for the second reaction that is mediated by the same enzyme:

$$r_{ACO} = K_{ACO} \left([CIT] - \frac{[CAC]}{k_{ACO}^{eq}} \right) \quad (3.1.67)$$

$$r_{ACO2} = K_{ACO} \left([CAC] - \frac{[ICIT]}{k_{ACO2}^{eq}} \right) \quad (3.1.68)$$

K_{ACO} is the cell-volume-specific activity of ACO with equilibrium constants k_{ACO}^{eq} and k_{ACO2}^{eq} between CIT and CAC and between CAC and ICIT, respectively.

Citrate lyase (CL, lumped): In tumor cells, cytosolic CL reversibly converts CIT to ACCoA and OAA to meet the high demand for lipids [80]. OAA is then either converted to PEP or converted to PYR with the accompanying production of NADPH from NADP and of NAD from NADH (see "Malate dehydrogenase"). Also in MDCK cells the upper citric acid cycle is proposed to mainly yield cytosolic CIT [16], which may be attributed to the large demand in cytosolic ACCoA and NADPH. In agreement with findings by Metallo et al. [175] for tumor cells, we consider the conversion to PYR as main route and use a simple Michaelis-Menten kinetic that takes into account the enzyme activity

measured *in vitro* by Janke et al. [22] and a dependence on NADH ($1 - b_{NAD}$):

$$r_{CL} = K_{CL}^{max} \frac{[ICIT]}{k_{CL}^m + [ICIT]} (1 - b_{NAD}) \quad (3.1.69)$$

K_{CL}^{max} is the maximum cell-volume-specific activity of CL with affinity k_{CL}^m for ICIT.

Pyruvate metabolism

The glycolytic activity (r_{PK}) generates large amounts of pyruvate, which is mainly converted to lactate (r_{LDH}) and various amino acids (r_{dPYR}). A smaller portion can enter the upper part of the citric acid cycle (r_{PDH}) and consumes OAA, which can also be converted from PYR. Furthermore, PYR is produced by MDH and CL (see above descriptions) and, thus, connects glycolysis and the citric acid cycle:

$$\frac{d[PYR]}{dt} = r_{PK} + r_{MDH} + r_{CL} - r_{LDH} - 2r_{PDH} - r_{dPYR} - \mu f[PYR] \quad (3.1.70)$$

$$\text{with: } r_{dPYR} = k_{dPYR}[PYR]. \quad (3.1.71)$$

Here, k_{dPYR} is the specific PYR degradation rate. The macroscopic description of the lactate release of Eq. 3.1.17 can now alternatively be described with:

$$\frac{d[LAC^x]}{dt} = r_{LDH} \frac{V_s^C X_{tot}}{V^M} + \frac{F_{evap}[LAC^x]}{V^M} \quad (3.1.72)$$

Lactate dehydrogenase (LDH, EC number: 1.1.1.27): The LDH converts PYR to LAC and it is generally accepted that its high activity is essential for fast proliferating cells to maintain a certain redox balance (recouping of NAD). The accumulation of intracellular LAC was not quantified by Ritter [23] and the largest fraction is presumably secreted to the medium. Without measurements for LAC, the model is not extended by the cytosolic influence of NADH. Taken together, the model considers a Michaelis-Menten kinetic and the maximum activity measured *in vitro* by Janke et al. [22], which shows very high activities.

$$r_{LDH} = K_{LDH}^{max} \frac{[PYR]}{k_{LDH}^m + [PYR] + \frac{k_{LDH}^a}{F_{16BP}}} \quad (3.1.73)$$

K_{LDH}^{max} is the maximum cell-volume-specific activity with affinity k_{LDH}^m for PYR and activation constant k_{LDH}^a for F16BP.

Energy metabolism and respiration

For the production and degradation of adenosine-based nucleotides, we used a reaction network proposed by Verma and colleagues for yeast cells and adopted it such that it suits our kinetic description for central carbon metabolism [199]. The model considers the enzyme-mediated interconversion of adenosine-based nucleotides through the adenylate kinase (r_{ADK}), central carbon metabolism (r_{CCM}) and demands by the cells for growth, maintenance and futile cycles (r_{dATP}). Furthermore, the synthesis and degradation of AMP from and to IMP through the purine salvage pathway (r_{PSP}), which is in detail explained by Walther et al. [197], is taken into account:

$$\frac{d[ATP]}{dt} = r_{CCM} + \frac{r_{ADK}}{2} - r_{dATP} \quad (3.1.74)$$

$$\begin{aligned} \text{with: } r_{CCM} &= r_{ENO} + r_{PK} + 2.5r_{NADH} + 2r_{FADH} \\ &\quad - r_{HK} - r_{PFK}, \end{aligned} \quad (3.1.75)$$

$$\begin{aligned} r_{dATP} &= r_{X/ATP} + r_{m/ATP} + r_{ATPase} \\ &= (k_{X/ATP}b_{syn} + V_s^C k_{mATP})[ATP] + r_{ATPase} \end{aligned} \quad (3.1.76)$$

$$\frac{d[ADP]}{dt} = -r_{CCM} - r_{ADK} + r_{dATP} \quad (3.1.77)$$

$$\frac{d[AMP]}{dt} = \frac{r_{ADK}}{2} - r_{PSP} \quad (3.1.78)$$

$$\frac{d[IMP]}{dt} = +r_{PSP} \quad (3.1.79)$$

$k_{X/ATP}$ is the specific ATP consumption rate for cell growth, k_{mATP} is the cell-volume-specific ATP consumption rate for cell maintenance [242]. Here, the production of ATP by r_{ENO} is representative for the PGK mediated reaction, which is not explicitly taken into account. For convenience, the model assumes that the purine pool is constant (Eq. (3.1.74) – (3.1.79)) and, thus, also neglects dilution by growth. The remaining enzyme reaction rates are described below:

Respiration (NADH / FADH, lumped): Parts of the energy that is produced by reactions of the central carbon metabolism are indirectly transferred to ATP through the hydrogen carriers NAD and FAD. The exact stoichiometry of reactions that produce or consume NADH and FADH is, however, unclear as many of the mitochondrial reaction paths have alternatives that may not phosphorylate these hydrogen carriers or use it for purposes other than oxidative phosphorylation. Therefore, we rather calculate a max-

imum NADH and FADH production rate based on the reactions defined for glycolysis and the citric acid cycle:

$$r_{NADH} = r_{ENO} + r_{KDH} + r_{MDH} + r_{PDH} + 2r_{AAex} + r_{ICDH} - r_{LDH} - r_{CL} \quad (3.1.80)$$

$$r_{FADH} = r_{SDH} + r_{AAex} \quad (3.1.81)$$

Note that the conversion of NADH to NAD by r_{CL} is representative for an implicitly considered cytosolic MDH reaction. Furthermore, metabolism of branched chain amino acids by r_{AAex} allow for the production of 2 NADH molecules from NAD [6]. The oxidation of NADH yields 2.5 molecules ATP, while the oxidation of FADH yields 2 molecules of ATP ([6], cf. Eq. (3.1.75)). To enable a consistency check with experimental data, the cell-number-specific oxygen demand is calculated from the production rates of r_{NADH} and r_{FADH} (unit: fmol/cell/h):

$$r_{O_2} = \frac{r_{NADH} + r_{FADH}}{2} \times V_s^C \times 60 \times 10^{12} \quad (3.1.82)$$

If further data becomes available, it seems reasonable to integrate a simple model for the oxidative phosphorylation which considers a membrane potential that couples NADH to the ATP pool (e.g. Nazaret et al. [251]). The model was already tested in this work but too many parameters were not identifiable and several difficulties with the resulting regulation pattern remained.

Adenylpyrophosphatase (ATPase, EC number: 3.6.1.3): Although the model already considers ATP consumption for growth and maintenance, the MDCK cell is expected to have a large overproduction in ATP that is simply converted to ADP in futile cycles [15]. To account for this hypothesis, we implemented a degradation rate that is based on a first order rate law:

$$r_{ATPase} = K_{ATPase}[ATP]. \quad (3.1.83)$$

K_{ATPase} is the cell-volume-specific activity of the ATPase.

Adenylate kinase (ADK, EC number: 2.7.4.3): The ADK reversibly converts ATP and AMP into two molecules of ADP and maintains a certain ratio between the three adenosine nucleotides. In most cases, the ADK is realized with simple conversion kinetics

that enable a fast equilibrium [199, 242]:

$$r_{ADK} = K_{ADK}^{max} \frac{ADP - \frac{AMP}{k_{ADK}^{eq}}}{k_{ADK}^m + ADP + \frac{AMP}{k_{ADK}^{eq}}}. \quad (3.1.84)$$

K_{ADK}^{max} is the maximum cell-volume-specific activity with affinity k_{ADK}^m for ADP and with equilibrium constant k_{ADK}^{eq} .

Purine salvage pathway (PSP, lumped reactions): In yeast cells, it is observed that the sum of adenosines drops in response to a glucose pulse [289]. Presumably because of a conversion of AMP to IMP, which is part of the PSP [197]. As the overall adenosine pool also drops in MDCK cells in response to a sudden start of cell growth, we assume a similar mechanism and implemented a first order rate law for the exchange with the PSP:

$$r_{PSP} = K_{PSP} \left(AMP - \frac{IMP}{k_{PSP}^{eq}} \right). \quad (3.1.85)$$

K_{PSP} is the cell-volume-specific activity with equilibrium constant k_{PSP}^{eq} between AMP and IMP.

3.1.3. Coupling of models

For simulation of the cell cultivation experiments, we couple the kinetic description of the central carbon metabolism with the segregated cell growth model. In particular, we track the actual growth status and culture condition of the cell population during batch cultivation and apply the resulting properties of a mean cell to the structured central carbon metabolism model. What follows is an influence of the cell growth regime⁷ on the concentration of extracellular substances, their uptake and release, dilution of intracellular metabolites, consumption of cellular energy and biomass precursors as well as on the cell-volume-specific enzyme activities (Fig. 3.1). In the following, we describe modifications and additional definitions necessary for a consistent coupling of both models.

Transport kinetics of the structured model: During a cell cultivation, the uptake of GLC^x and GLN^x is solely defined by the macroscopic, growth-dependent functions.

⁷**growth regime:** an intracellular signal processing network that decides over cell growth phases

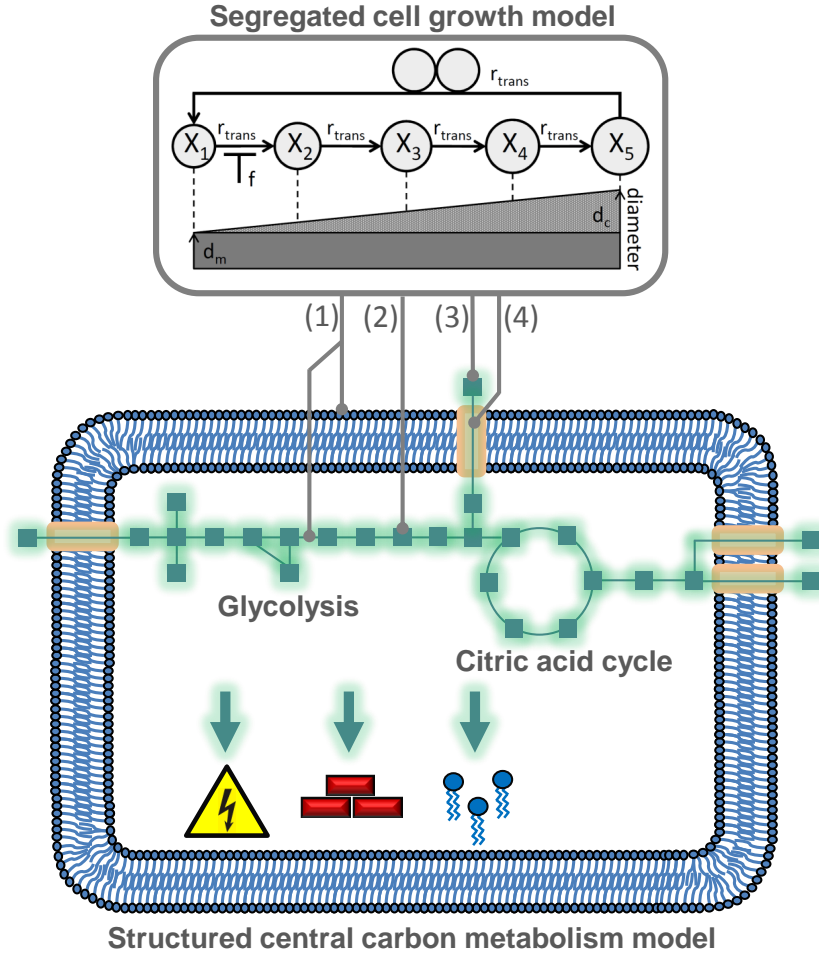


Figure 3.1.: Coupling of segregated cell growth and structured central carbon metabolism model. The segregated cell growth model influences: (1) the cell-specific volume (V_s^C) and, concomitantly, the cell-volume-specific enzyme activities (K_e^{max} , K_e); (2) the dilution of intracellular metabolite pools by cell growth; (3) the change in extracellular substrate levels; (4) the time-dependent uptake rates (r_{GLUT} , r_{GLNT} , r_{GLT}).

Therefore, the transport rate by GLUT and GLNT needs to fulfill the relation:

$$r_{GLUT} = (r_{X/GLC^x} + r_{m/GLC^x}) \frac{V^M}{V_s^C X_{tot}} \quad (3.1.86)$$

$$r_{GLNT} = (r_{X/GLN^x} + r_{m/GLN^x}) \frac{V^M}{V_s^C X_{tot}} \quad (3.1.87)$$

Note that $r_{X/S}$ and $r_{m/S}$ are here used with unit mmol/L/min. Furthermore, this relation only holds for the cellular uptake of substrates during cell cultivation experiments under excess of substrates. In scenarios characterized with low substrate concentrations (e.g.

< 0.2 mmol/L for hybridoma [51] or < 0.4 for BHK cells [290]) the uptake rates may strongly depend on the substrate affinity of the transporter and can differ significantly from the macroscopic descriptions given with Eq. 3.1.86 and 3.1.87. To simultaneously enable the use of a macroscopic description during cell cultivation and a mechanistic description during the perturbation experiments, we implemented variable capacities for the substrate transports (γ_{GLUT} and γ_{GLNT}), which are defined as follows:

$$\gamma_{GLUT} = \frac{(r_{X/GLC^x} + r_{m/GLC^x}) \frac{V^M}{V_s^C X_{tot}}}{K_{GLUT}^{max} \frac{[GLC^x]}{k_{GLUT}^m + [GLC^x]}} \quad (3.1.88)$$

$$\gamma_{GLNT} = \frac{(r_{X/GLN^x} + r_{m/GLN^x}) \frac{V^M}{V_s^C X_{tot}}}{K_{GLNT}^{max} \frac{[GLN^x]}{k_{GLNT}^m + [GLN^x]}} \quad (3.1.89)$$

Thus, multiplication of the mechanistic uptake rates with γ (Eq. (3.1.30) and (3.1.50)) adjusts their activity to the macroscopic description given by the segregated cell growth model. From a biological point of view, the GLUT and the GLNT have a variable transport capacity that is regulated by the cellular growth regime through a change in the transporter affinity, translocation of transporter to the membrane or molecule-based activation [97]. When it comes to the limitation experiments, γ remains constant (the cellular demand is still the same) and the depletion dynamics solely depend on the transporter kinetics. Therefore, γ is time-dependent for Cult1–3 simulations, where the growth of cells changes, and constant, experiment-specific for Lim1, Lim2 and Pulse simulations.

Calculation of specific enzyme activities: For a large portion of enzymes e , the cell-specific maximum activity v_e^{max} was measured *in vitro* by Janke et al. [22] for adherent MDCK cells cultivated in GMEM-Z. The transformation to K_e^{max} follows with

$$K_e^{max} = \frac{v_e^{max} E_{level}}{V_s^C}, \quad (3.1.90)$$

where E_{level} is the experiment-specific, relative enzyme level of the cell population. So, we take into account that cell cultures, which can already differ in d_m and d_c , may also show concerted variations in v_e^{max} . However, the variation in maximum enzyme activities is presumably limited. On the basis of the enzyme activity measurements by Janke et al. [22], we calculated a mean standard deviation for all enzyme activities of about $\pm 8\%$. Note that the K_e^{max} also change with V_s^C and are, hence, time-dependent.

The cell-volume-specific activity K_e similarly results from the cell-specific activity v_e :

$$K_e = \frac{v_e E_{level}}{V_S^C}. \quad (3.1.91)$$

Growth phases and biosynthesis activity of cells: Based on the segregated cell growth model, theoretical growth phases for a mean cell can be calculated and are important for the depiction of metabolite pool dynamics. The lag phase of V^C and X_{tot} is here the time span required by half of the cells to double in cell-specific volume or number, respectively. Afterwards, the growth phase follows and ends with the onset of the intermediate growth phase. The intermediate growth-phase for V^C is supposed to be in the time interval where

$$0.95 > f > 0.05 \quad (3.1.92)$$

holds. In case of X_{tot} , we use the relative growth rate of the cell number in the interval

$$0.95 \cdot \mu_{max} > \frac{X_5(t) r_{trans}(t)}{X_{tot}(t)} > 0.05 \cdot \mu_{max}, \text{ with: } t > 20 \text{ h.} \quad (3.1.93)$$

Afterwards, a stationary growth phase for X_{tot} and V^C follows. However, the degradation of citric acid cycle intermediates and ATP may not directly correlate with the increase of X_t or V^C but with the propagation of cells through the different classes X_i , which we define as relative biosynthesis activity (b_{syn}) that is

$$b_{syn} = \frac{X_1 f + \sum_{i=2}^5 X_i}{X_{tot}}. \quad (3.1.94)$$

The intermediate growth phase for b_{syn} shall be the time span that satisfies

$$0.95 > b_{syn} > 0.05. \quad (3.1.95)$$

3.2. Model simulation

Apart from the definition of the model structure, ODE-based models require the setting of initial conditions for each experimental scenario. In this work three cultivation experiments (Cult1–3) and three perturbation experiments (Lim1, Lim2, Pulse) are analyzed. For the sake of a clear overview, the initial conditions are divided into cultivation conditions, growth status and metabolic status.

3.2.1. Considering the preculture of cells

Cell cultivation experiments rely on the transfer of cells from a preculture into a new well or at least on changes in cultivation conditions, e.g. addition or removal of substrates. In both cases, the initial growth status (such as cell diameter, cell number, growth inhibition etc.) and metabolic status (intracellular metabolite concentrations) of the cells are pre-defined by the cultivation prior to the actual experiment (see Table C.1 and C.2). For a consistent simulation of the cellular behavior, the experiments conducted by Ritter [23] are set into the chronology shown in Figure 3.2. In particular, the simulation of the cultivation experiment (e.g. Cult1) provides (at individual time points t^*) the growth and metabolic status for the limitation experiments (Lim1 – 3), which in turn provide initial conditions and experiment-specific parameters for the pulse experiment. The corresponding culture conditions are given by Ritter [23] or estimated in the next section 3.2.2. For the inoculation of the cultivation experiments, however, the initial conditions were derived from different sources: The growth status and culture condition were determined with the segregated cell growth model during parameter estimation

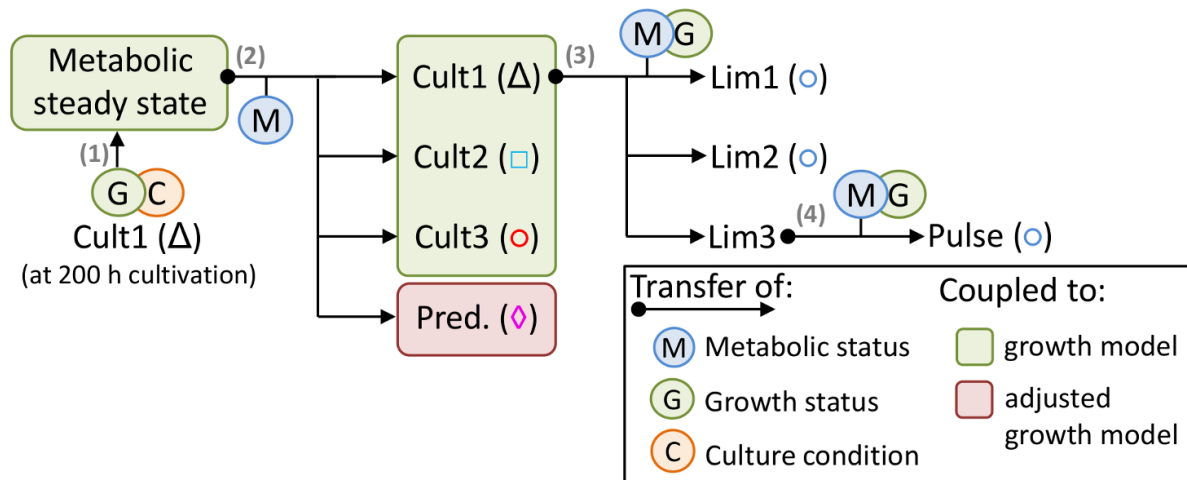


Figure 3.2.: Flow of information and link to experimental data. (1) Use of growth status and cultivation condition of Cult1 at 200 h to determine the metabolic status by steady state simulation. (2) Transfer of the metabolic steady state to the simulation of the Cult1 – 3 and the Pred. simulation. (3) At individual time points t^* , the metabolic and growth status of Cult1 is transferred to the respective simulation of the Lim1 – 3 experiments. (4) Simulation of pulse response with initial conditions determined with the Lim3 simulation. Green background: Coupling of segregated cell growth model and structured metabolism model; red background: coupling of adjusted segregated cell growth model, which renders cell growth under limited GLC^x concentrations, to the structured metabolism model.

and vary due to differences in the preculture device and the precultivation time [23]. The metabolic status was derived from a steady state simulation with the structured metabolism model using the culture conditions as well as the growth status present in Cult1 at $t = 200$ h. This, however, implies the assumption that cells achieve a reproducible metabolic status in the stationary growth phase of the precultures and that batch-to-batch variations during this growth phase are small and have a negligible impact on the metabolite pool levels. Both can be observed in the cultivation data (e.g. Fig. 4.11).

3.2.2. Substrate limitations through medium dilution

For the limitation experiments, the medium was discarded and replaced by phosphate buffered saline (PBS) [23]. At that time point of cultivation, e.g. 48 h, the activity of glycolysis is about 2.7 mmol/L/min which would deplete the G6P pool within seconds. Inspection of the corresponding G6P dynamics reveals high levels for about 0.3 min and a depletion of G6P after 0.6 min of cultivation (Figure 3.3A). Based on $V^C(t = 48 \text{ h}) = 5.9 \text{ }\mu\text{L}$, about $4.8 \times 10^{-6} \text{ mmol GLC}^x$ is required to satisfy the glycolytic activity for 0.3 min. Assuming that medium remains on the cellular surface and the intercellular space with a GLC^x concentration of 25 mmol/L (at 48 h) yields a $V^M = 4.8 \times 10^{-6} / 25 = 1.9 \times 10^{-7} \text{ L}$. Simulation studies with the structured metabolism model yield $3 \times 10^{-7} \text{ L}$ (simulation not shown). So instead of inducing the limitation with $\text{GLC}^x(t=0)=0 \text{ mmol/L}$ we simply set $V^M = 3 \times 10^{-7} \text{ L}$, which corresponds to a

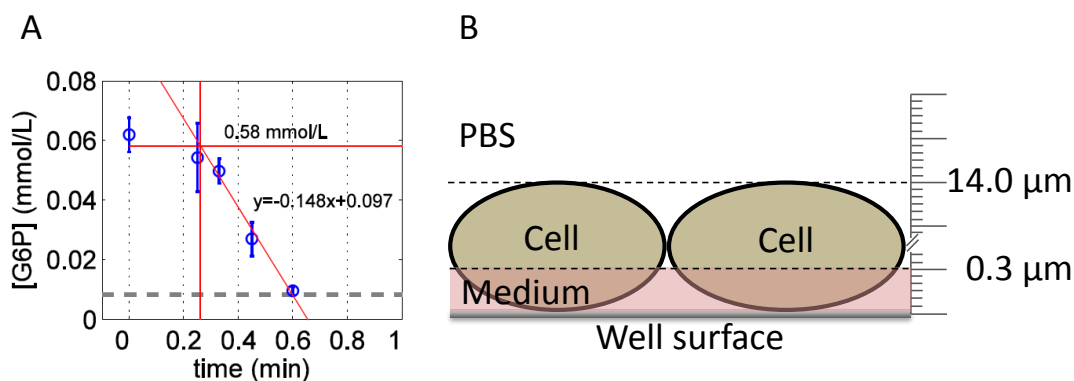


Figure 3.3.: A priori estimations for the substrate limitation experiments. (A) G6P time series (\circ) during the Lim1 experiment with mean and standard deviation of three wells (data taken from [23]). Red lines were derived by regression analysis and used to assess the time span of high G6P levels. Dashed gray line is the limit of quantification. (B) Illustration of remaining medium in the 6-well plate after medium depletion and addition of PBS.

height of $0.3\ \mu\text{m}$ in the well for a surface of $10\ \text{cm}^2$ (cell layer height $\approx 14.0\ \mu\text{m}$, Fig. 3.3B). Note that dilution of the medium by PBS is likely and may yield a V^M higher than 3×10^{-7} and a reduced GLC^x level, which, however, can be equally well realized with the model in case more detailed data becomes available.

To keep the simulations as simple as possible, we assume that cells remain constant in their initial growth status for the duration of the perturbation experiments (Table C.2).

3.2.3. Hierarchy of model parts and sequential model fitting

A reliable parameter estimation and an in-depth analysis of causal relationships is key to a proper model development but greatly hampered by a high model complexity. As a direct solution to that problem, we only considered simple enzyme kinetics (section 3.1.2) and used the cell's cultivation history (section 3.2.1) to both minimize the degree of freedom and focus on mechanisms that are essential to describe the data. However, the analysis of the full model (segregated growth + structured metabolism) was still difficult and we splitted the model into smaller, manageable parts (defined in section 3.1.2) and conducted a piecewise analysis. In particular, the macroscopic segregated cell growth model is by definition independent from intracellular changes. Glycolysis and glutaminolysis depend on the segregated cell growth model, while metabolites and nucleotides of the PPP, glycogenesis, pyruvate metabolism and energy metabolism depend on glycolysis and glutaminolysis but not on each other. The proposed hierarchy is illustrated in Figure 3.4. Using the hierarchy of model parts enables a sequential model fitting where only the actual model part is subject to parameter estimation. Model parts of lower hierarchy are disregarded, while model parts of higher hierarchy are not part of the parameter estimation as they already possess a final structure and parameterization. Note that the estimation of parameter confidence intervals takes into account the parameter uncertainty of model parts with higher hierarchy except of the segregated cell growth model. So the uncertainties in the segregated cell growth model and the overall

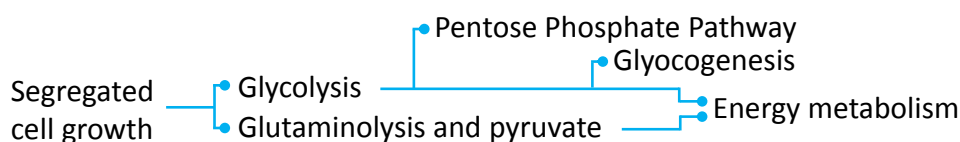


Figure 3.4.: Hierarchy of model parts. Blue lines indicate an unidirectional influence of a model part on another (from left to right).

kinetic description of central carbon metabolism are separately analyzed.

3.3. Theoretical tools

3.3.1. Algorithms and objective function

For model fitting, estimation of parameter confidence intervals, and visualization of results MATLAB® (Version R2012b, The MathWorks, Inc.) was used. Models and data were handled with the Systems Biology Toolbox 2 developed by Schmidt and Jirstrand [291]; integrations of the ordinary differential equations were performed with the CVODE from SUNDIALS [292]. The algorithm SSm [293] was used for stochastic global optimization of the parameters and experiment settings. All simulations were carried out on a Linux-based system (partly by using the Linux-Cluster "Otto" of the Max Planck Institute for Dynamics of Complex Technical Systems Magdeburg). By using this setup, a model simulation required less than 0.1 s.

3.3.2. Model analysis

Objective function: The fitness of the model trajectories \tilde{y}_{lmj} to the data y_{lmj} was evaluated based on a weighted sum of squared residuals (FQS), defined with

$$FQS = \sum_{l=1}^{N^l} \sum_{m=1}^{N_l^m} \sum_{j=1}^{N_{lm}^j} \left(\frac{y_{lmj} - \tilde{y}_{lmj}}{\sigma} \right)^2, \quad (3.3.1)$$

comprising the experiments $l = 1, \dots, N^l$, the states $m = 1, \dots, N_l^m$ measured in experiment l and the time points $j = 1, \dots, N_{lm}^j$ for state m in experiment l , while $\sigma = \max_{lm}([y_{lm1}, \dots, y_{lmN_{lm}^j}])$ is a weighting to the maximum data point for state m in experiment l . A violation of the constraint given in Eq. 3.1.43 increases FQS by a penalty value of 0.5. For low PK activities during the limitation experiments, $\frac{r_{PK}(6 \text{ min})}{10}$ of the Lim1 experiment was added to the FQS value.

Parameter confidence intervals: For assessment of the parameter confidence intervals a bootstrap method with at least 2000 runs was used [271, 294]. A total of 2000 runs is presumably sufficient for the parameter optimization problems of this work, especially when considering a sequential model fitting. Convergence of the parameter bounds was observed. The bootstrap method in short: 2000 *in silico* data sets were generated from the normal distribution of each y_{lmj} (defined by mean and standard deviation of

the measurement) and fitted with SSm yielding 2000 model parameterizations Φ . From these parameterizations, each parameter was sorted by value and the 0.025 and 0.975 quantile constitute the bounds of the 95 % confidence interval.

Local sensitivity analysis: According to Gutenkunst et al. [269], the change in model behavior χ^2 in response to a change in the parameter set ϕ is described with:

$$\chi^2(\phi) = \frac{1}{2} \sum_{l=1}^{N^l} \sum_{m=1}^{N_l^m} \sum_{j=1}^{N_{lm}^j} \frac{1}{N_l^m N_{lm}^t} \left(\frac{\tilde{y}_{lmj}(\phi) - \tilde{y}_{lmj}(\phi')}{\tilde{\sigma}} \right)^2 \quad (3.3.2)$$

where $\tilde{\sigma} = \max_{lm}([\tilde{y}_{lm1}(\phi), \dots, \tilde{y}_{lmN_{lm}^j}(\phi)])$ is a weighting with the maximum simulation point for state m in experiment l . In this work, a 1 % change in a single parameter value of ϕ was used (ϕ'). Note that only time points at which data points exist were considered for the sensitivity analysis.

3.3.3. Limit of quantification

The limit of quantification (LOQ) of the assays to determine the concentration of intracellular metabolites M is given in molar units in the Appendix B.1 (Table B.1) and here denoted as LOQ_M^{mmol} . As all adherent cells of a 6-well plate are quenched and analyzed, the LOQ used in the figures is related to V^C (taken from Cult1):

$$LOQ_M = \frac{LOQ_M^{mmol}}{V^C} \quad (3.3.3)$$

4 Chapter

4 Results and discussion

4.1. Observations for MDCK cell cultivations in different media

Current experimental approaches to the analysis of the MDCK cell metabolism comprise the quantification of extracellular and intracellular metabolites [23], the inferences of flux rates from flux balance analysis [15, 16], and the measurement of *in vitro* enzyme activities [22]. In this first part, we pre-analyze the data from all four sources to extract a working hypothesis for the integrated modeling approach of the following sections. Since a multitude of factors can influence metabolism, we concentrate in the pre-analysis on cell cultivation experiments where MDCK cells from the same preculture are seeded into a new well with either the serum-containing medium GMEM-Z or the serum-free medium EpiSerf to highlight similarities or dissimilarities. In particular, we examine the growth of the cells together with the uptake and release of metabolites, followed by the analysis of intracellular metabolite time series in glycolysis, glutaminolysis, and the closely related pathways as well as the level of purines. Finally, we discuss to which extent metabolism is influenced by the corresponding medium and the change in cell growth phase. Note that parts of the following analysis are taken from our original research article Rehberg et al. [295]. Copyright of these passages lies with the Journal of Applied Microbiology and Biotechnology (Springer-Verlag GmbH, Heidelberg).

4.1.1. Growth, nutrient supply and byproduct release

Cell number, diameter and volume: The time course of cell numbers of the two cultures (Fig. 4.1A) showed in mean a maximum specific growth rate for GMEM-Z cultures of 0.040 h^{-1} in the time interval of 21 – 54 h and for EpiSerf cultures of 0.035 h^{-1} in the time interval of 27 – 54 h, based on a logarithmic regression for the three experiments (Δ , \square , \circ , performed by Ritter [23]). The mean diameter of cells was similar for both media starting with 14 – 17 μm , increased to 17 – 21 μm after one day of cultivation, and afterwards decreased to its initial level ($t = 0 \text{ h}$). However, for EpiSerf cultures the mean cell diameter was initially lower and the maximum is slightly later achieved

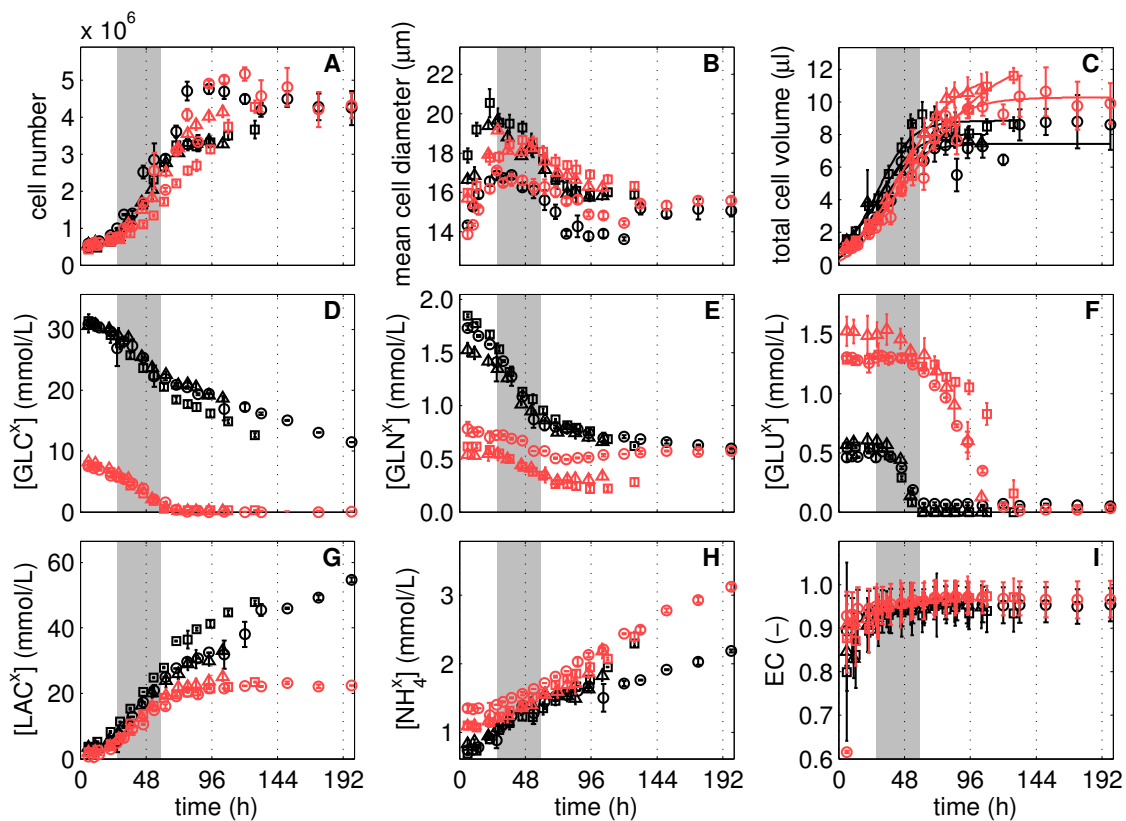


Figure 4.1.: Growth of adherent MDCK cells in 6-well plates with either GMEM-Z (black) medium or EpiSerf (red) medium. Time series of cell number (A), mean cell diameter (B), total cell volume (C, with splines used by Ritter [23] for calculation of intracellular metabolite concentrations), and extracellular metabolites glucose (D), glutamine (E), glutamate (F), lactate (G), and ammonium (H) were measured in three independent experiments by Ritter [23] marked with symbols Δ , \square and \circ (mean and standard deviation of three wells). The energy charge (I) is calculated from intracellular concentrations of ATP, ADP and AMP (Eq. (2.2.1)). Light gray field between 30 – 58 h illustrates the intermediate growth phase of the total cell volume (V^C in Table 4.2).

(Fig. 4.1B). In contrast to the increase in cell numbers, growth in total cell volume (Fig. 4.1C) occurred at a similar time interval for both media (6 – 46 h) with nearly the same maximum specific growth rate (0.040 h^{-1} in GMEM-Z; 0.039 h^{-1} in EpiSerf based on a logarithmic regression performed by Ritter [23]). Note that the time interval of the regression analysis of Ritter [23] overlaps with the gray fields of Fig. 4.1, which illustrate the intermediate growth phase and are derived from simulating the GMEM-Z cultivations with the model of section 4.2. After 58 h of cultivation, the cell volumes in the EpiSerf cultures reached higher levels of about 10 – 11 μL (GMEM-Z: 7 μL) due to slightly higher mean cell diameters and apparently higher cell numbers with 4×10^6 –

5×10^6 cells per well (GMEM-Z: $3 \times 10^6 - 4 \times 10^6$).

Substrate uptake and byproduct release: Both media differ significantly in the initial concentration of GLC^x , GLN^x and GLU^x (Fig. 4.1D – F). Nevertheless, the total cell-volume-specific uptakes of GLC^x (r_{GLC^x}) and GLN^x (r_{GLN^x}) are similar (Table 4.1) and the decrease in GLC^x and GLN^x correlates with the increase in cell volume until 58 h of cultivation. Afterwards, the GLC^x concentration decreased more or less linearly in GMEM-Z indicating cell maintenance (stationary growth phase, 58 – 200 h, Fig. 4.1D). According to Baggetto [50], cancer cells require no or only marginal amounts of GLN^x during stationary growth phase and the linear decrease of GLN^x after 58 h fits exactly to the spontaneous decomposition present in GMEM-Z medium (0.0036 h^{-1} , Fig. 4.1E, [51, 212]) and loss of water (water evaporation rate constant: $2.75 \times 10^{-6} \text{ L/h}$, [23]). In EpiSerf cultures, however, GLC^x was depleted after cells reached the stationary growth phase (72 h, Fig. 4.1D) while the GLN^x concentration was constant during stationary growth phase (Fig. 4.1E). Obviously, spontaneous decomposition of GLN^x does not play a role in EpiSerf medium. The uptake of GLU^x (Fig. 4.1F) started shortly after onset of cell growth inhibition (gray field) and lasted until GLU^x was depleted (GMEM-Z: 58 h, EpiSerf: 96 h). The corresponding uptake rate of GLU^x (r_{GLU^x}) was slightly lower in EpiSerf cultures compared to GMEM-Z (Table 4.1) and the uptake lasted longer due to higher initial GLU^x levels. The accumulation of LAC^x correlates with the drop in GLC^x (Fig. 4.1G) and, therefore, ceased after about 58 h of cultivation in EpiSerf medium while in GMEM-Z a linear increase until the end of the cultivation was observed. Extracellular ammonia (NH_4^x) levels showed a linear increase during cultivation, even at late time points where GLN^x and GLU^x were not consumed. In GMEM-Z cultures, the spontaneous decomposition of GLN^x may explain this increase in NH_4^x after 58 h. In EpiSerf cultures, however, the increase in NH_4^x most likely reflects the consumption of

Table 4.1.: Total cell-volume-specific uptake rate of substrates and release rate of byproducts in two different media, derived by polynomial regression analysis of three independent cultivations (units: mmol/L/min). Depicted are mean and standard deviation of the three regression analyzes.

	$r_{\text{GLC}^x}^a$	$r_{\text{GLN}^x}^a$	$r_{\text{GLU}^x}^b$	$r_{\text{LAC}^x}^a$	$r_{\text{NH}_4^x}^a$
GMEM-Z	3.12 ± 1.17	0.27 ± 0.10	0.20 ± 0.02	6.82 ± 1.22	0.13 ± 0.02
EpiSerf	2.78 ± 0.33	0.12 ± 0.08	0.13 ± 0.03	6.42 ± 0.35	0.20 ± 0.02

^acalculated for the time interval 0 – 48 h

^bcalculated for the time interval 35 – 62 hour (GMEM-Z), 61 – 132 hour (EpiSerf)

other amino acids. The EC showed values above 0.8 over the complete time course of cultivations (Fig. 4.1I), which is within the typical limits found for mammalian cells [192].

4.1.2. Response of metabolism to growth and media

Glycolysis and associated pathways: During cultivation in GMEM-Z and EpiSerf, the intermediates G6P, F6P and F16BP (Fig. 4.2A – C) of upper glycolysis showed a strong increase for the first 24 h of cultivations. With the onset of the intermediate growth phase (gray field) all three intermediates decreased in concentration and remained in the subsequent stationary growth phase at more or less constant levels. Interestingly, Sellick et al. [32] similarly observed for CHO cells that levels of glycolytic intermediates decrease during the transition to the stationary growth phase. With depletion of GLC^x in EpiSerf medium, the measured levels of G6P and F16BP were lower than the limit of quantification and, thus, slightly different to that of the GMEM-Z culture. In the lower part of glycolysis, 3PG as well as PEP showed an increase in concentration until 48 h, which corresponded to the cease of cell volume growth (end of gray field, Fig. 4.2D, E).

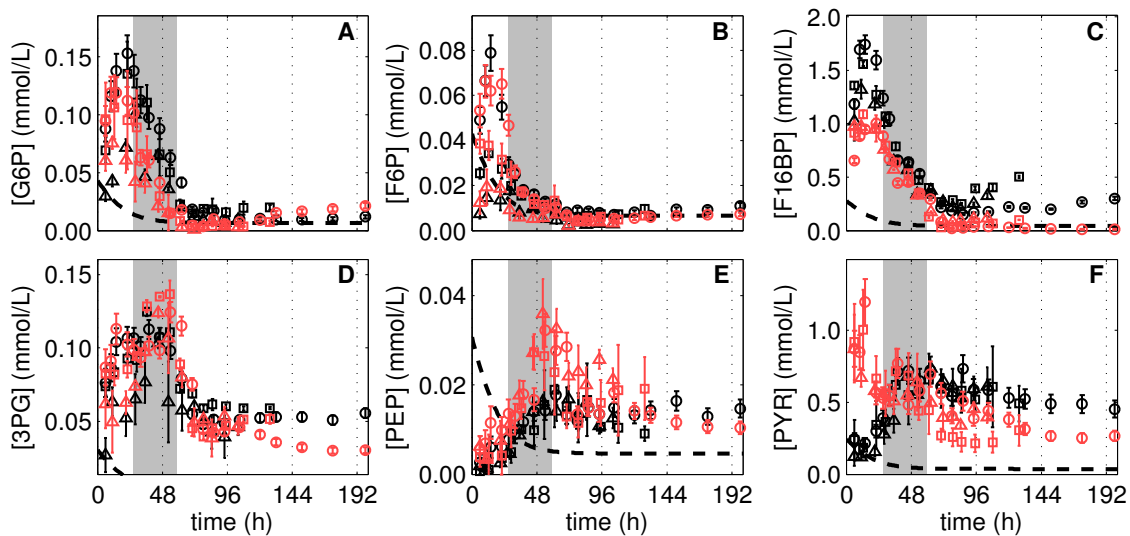


Figure 4.2.: Dynamics of glycolytic intermediates during cultivation of adherently growing MDCK cells in GMEM-Z and EpiSerf. The upper part of glycolysis with glucose 6-phosphate (A), fructose 6-phosphate (B), fructose 1,6-bisphosphate (C) and the lower part of glycolysis with glyceraldehyde 3-phosphate (D), phosphoenolpyruvate (E) and pyruvate (F) are shown in the color code of Figure 4.1 (data taken from Ritter [23]). The limit of quantification is shown as dashed black line. Light gray field between 30 – 58 h illustrates the intermediate growth phase of V^C (Table 4.2).

In the EpiSerf culture, the time courses of PEP seemed to follow the peak behavior of 3PG concentrations. In GMEM-Z, the time series of PEP were rather similar to PYR as both increased to their maximum concentrations at about 48 h and remained constant afterwards (Fig. 4.2E, F). Albeit the fact that cells of both cultures originated from the same pre-culture, intracellular PYR concentrations of the cells in EpiSerf cultures were initially significantly higher with a fast drop to concentrations lower than in GMEM-Z cultures. Possible metabolic branches for the glycolytic intermediate G6P are glycogenesis or the PPP comprising UGLC and R5P, respectively. Interestingly, R5P and UGLC seem to correlate with intermediates of upper glycolysis, which is presumably attributed to the close linkage of these pathways (Fig. 4.3A, B). Both metabolites increased initially, achieved a maximum at 24 h and decreased with onset of cell growth inhibition (gray field) to a stationary level. In the EpiSerf culture, the level of UGLC was mostly below that of the GMEM-Z cultures (similarly to the intracellular metabolites of the upper glycolytic pathway). UDPGlcNAc and its stereoisomer UDPGalNAc (not shown since it is identical in its dynamics) are linked to F6P but showed a totally different time course. It seems that both metabolite pools performed a nearly inverse dynamic with a maximum for GMEM-Z medium and a minimum for EpiSerf medium at day three (Fig. 4.3C, D). Note that Ryll et al. [85] found the highest level of these hexosamines at the end of the growth phase for various other cell lines. Their results are, thus, in line with the GMEM-Z cultivation but not with the EpiSerf cultivation.

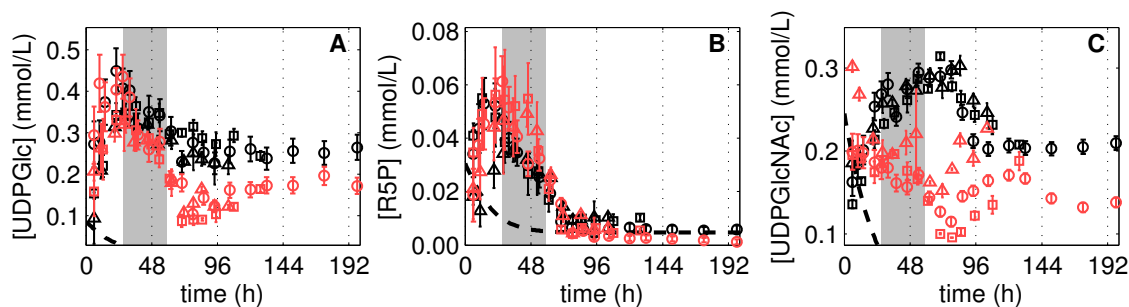


Figure 4.3.: Dynamics of intermediates of glycogenesis, pentose phosphate pathway and hexosamine biosynthesis pathway during cultivation of adherently growing MDCK cells in GMEM-Z and EpiSerf. Uridine diphosphate glucose (A), ribose 5-phosphate (B), and uridine diphosphate N-acetylglucosamine (C) are shown in the color code of Figure 4.1 (data taken from Ritter [23]). The limit of quantification is shown as dashed black line. Light gray field between 1 – 2.5 days illustrates the intermediate growth phase of V^C (Table 4.2).

Citric acid cycle: In MDCK cells, PYR is mainly metabolized to lactate and only minor amounts enter the citric acid cycle, according to the analysis of fluxes [16] and of enzyme activities [22]. Therefore, it is not surprising to find no correlations between metabolite pool dynamics of the citric acid cycle and glycolysis. The most prominent observation is the peak formation of α KG, SUC, FUM and MAL at about 24 h of cultivation (Fig. 4.4A – D). It appears that the peak coincides with the cease of cell volume growth (end of gray bar). Thus, the drop of metabolite pools may be related to the stop in GLN^x and GLU^x uptake. At least in case of the EpiSerf culture, the second drop at 96 h can be explained with the depletion of GLU^x . Thus, the intracellular concentrations of metabolites differ between both media after 96 h of cultivation. Unexpectedly, final levels of α KG in experiment \circ and \circ were generally higher compared to the other experiments. These high levels were not found for other metabolites of both experiments (Fig. 4.4A). SUC showed slightly lower levels for cells grown in EpiSerf, which indicates small differences among both media (Fig. 4.4B). In the upper part of the citric acid cycle, CIT and ICIT are highly correlated in their dynamics and showed decreasing concentrations over time (Fig. 4.4E, F). The concentrations in EpiSerf cultures were initially higher than that of GMEM-Z cultures. However, with increasing cultivation time CIT and

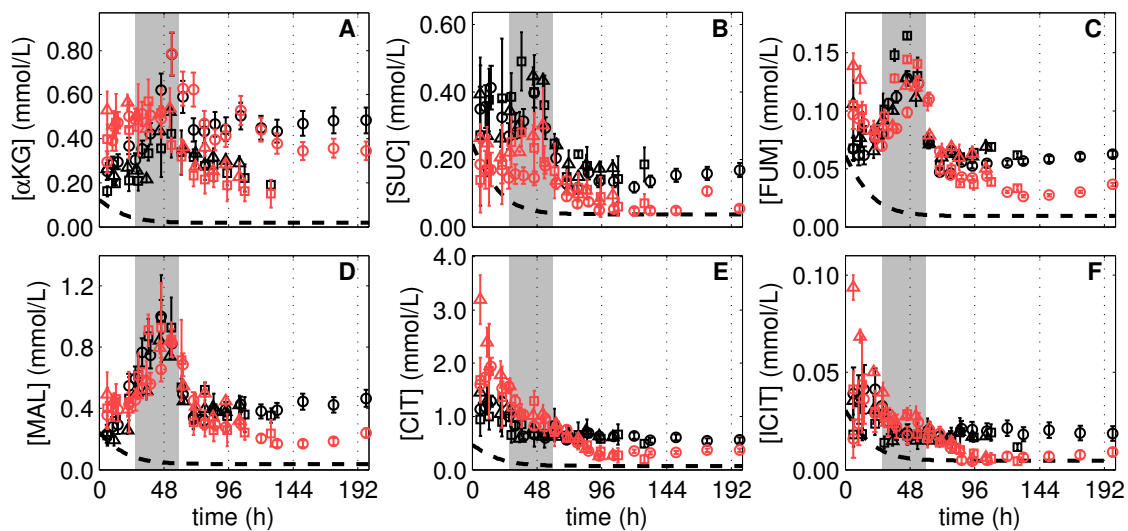


Figure 4.4.: Dynamics of citric acid cycle intermediates during cultivation of adherently growing MDCK cells in GMEM-Z and EpiSerf. The lower part of the citric acid cycle with α -ketoglutarate (A), succinate (B), fumarate (C), malate (D) and the upper part with citrate (E) and isocitrate (F) are shown in the color code of Figure 4.1 (data taken from Ritter [23]). The limit of quantification is shown as dashed black line. Light gray field between 1 – 2.5 days illustrates the intermediate growth phase of V^C (Table 4.2).

ICIT of EpiSerf cultures approached the same levels found in GMEM-Z cultures. With depletion of GLC^x in the EpiSerf culture after 72 h, it seems that concentration of both metabolites dropped again.

Purines: The nucleotides ATP, ADP and AMP showed significant changes in concentrations during the time course of cultivations (Fig. 4.5A – C). With the start of cultivations, concentrations of ATP increased roughly from 2 mmol/L to 4 mmol/L although large experiment-specific differences were observed. Experiment \circ , for example, showed the highest ATP levels at initial times of cultivation. For the other cultivations, however, the ATP level was highest when cells approach the stationary growth phase. In case of EpiSerf cultures, ATP concentrations dropped slightly after about 96 h while in GMEM-Z cultivations a minor increase towards later time points was measured. ADP and AMP concentrations were low in general (0.4 mmol/L; 0.1 mmol/L) with time courses more or less inverted to the ATP dynamics. Interestingly, neither a constant behavior of ATP nor a constant sum of adenosine-based nucleotides can be observed (the change in ATP is much larger than in AMP and ADP). In particular, the difference

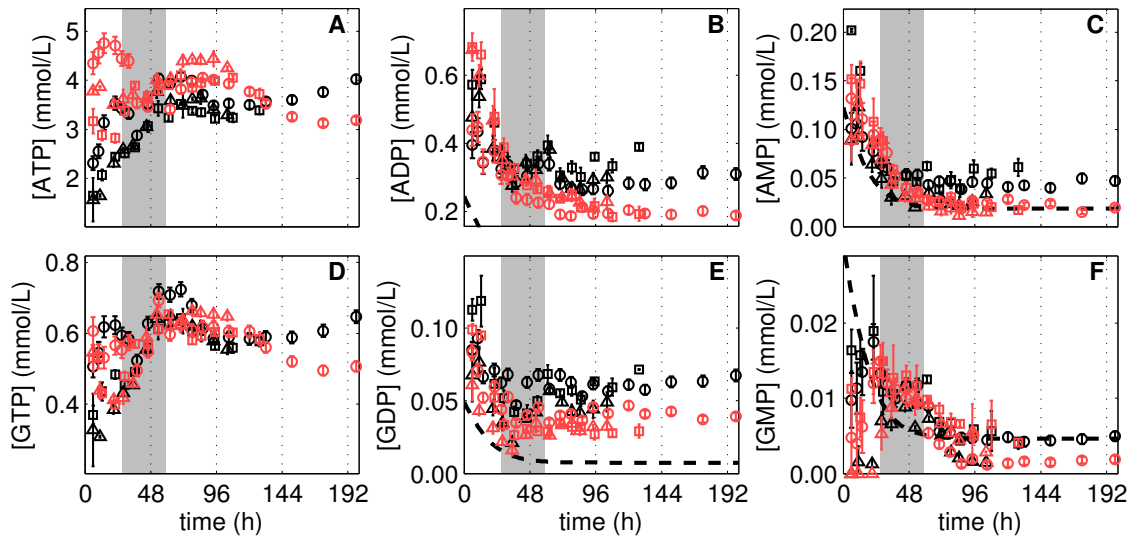


Figure 4.5.: Dynamics of purines during cultivation of adherently growing MDCK cells in GMEM-Z and EpiSerf. The adenosine-based nucleotides with adenosine triphosphate (A), adenosine diphosphate (B), and adenosine monophosphate (C) as well as the guanosine-based nucleotides with guanosine triphosphate (D), guanosine diphosphate (E) and guanosine monophosphate (F) are shown in the color code of Figure 4.1 (data taken from Ritter [23]). The limit of quantification is shown as dashed black line. Light gray field between 1 – 2.5 days illustrates the intermediate growth phase of V^C (Table 4.2).

in ATP levels reach up to 2 mmol/L, which cannot be fully explained with variations in ADP and AMP. The time series of the guanosines (Fig. 4.5D – F) were very similar to those of the adenosines but with much lower intracellular concentrations. In case of GMP (Fig. 4.5F), the concentration was mostly below the quantification limit but with a trend that might be similar to the AMP dynamics. The description of the pyrimidines is given elsewhere [295].

4.1.3. Discussion

Ritter [23] seeded MDCK cells from identical GMEM-Z precultures into 6-well plates to grow either in GMEM-Z or in EpiSerf medium. Thus, cells inoculated in EpiSerf medium grew without preliminary adaptation and faced substantial differences in the abundance of substrates and amino acids. In particular, the EpiSerf medium is serum-free. Therefore, the first aspect considered is to which extent the growth of cells cultivated in EpiSerf differs from cultivations with GMEM-Z. Next, it is discussed to which extent growth and substrate supply in both media can be linked to changes in the cellular metabolism and whether a robust regulation regime is present.

Cell growth and substrate uptake in two different media: In accordance to literature, we expected the cells to show clear differences in their growth behavior [4, 78, 168, 296], e.g. in lag phase, in specific growth rate or in time point of growth limitation by substrates or inhibitors with largely unknown effects on intracellular metabolite pool dynamics. Interestingly, however, the general growth behavior is very similar in both media. Minor differences are found in a slightly extended delay in cell number increase (about 6 h) and in a higher final cell volume of EpiSerf cultures, which may be attributed to differences in the osmolality (EpiSerf: 375 mOsm/kg; GMEM-Z: 320 mOsm/kg, measured by the group of Y. Genzel, Bioprocess Engineering Group, MPI Magdeburg, Germany) and missing factors for cell attachment in the serum-free EpiSerf medium. Also, the uptake of substrates appears to be qualitatively and quantitatively similar (Table 4.1), at least until GLC^x depletion occurs in the EpiSerf medium. In conclusion, a reduced cellular uptake or a more efficient breakdown of GLC^x , which is reported as Crabtree effect for many other cells [82, 87, 92, 95], is not observed in our data, although concentrations of substrates are far different. Therefore, the influence of the medium on cell growth and uptake rates is rather small, as long as substrate concentrations are not at limiting levels (< 0.2 mmol/L [51, 87]). However, an effect on intracellular metabolite pools can be expected at later stages of cultivation where either

GLC^x or GLU^x drop to very low levels.

Response of glycolysis to growth and media: Major amounts of G6P are converted in glycogenesis, the PPP and glycolysis to UDPGlc, R5P and F6P, respectively. Whilst these metabolites show fundamental changes in their pool size over time, differences between GMEM-Z and EpiSerf cultures are surprisingly small. All metabolites show a strongly correlated dynamic even though the involved enzyme-mediated reactions have different requirements for cofactors. A concerted regulation of these enzymes through cofactors, such as ATP or NADP, appears therefore unlikely. The peak-like response in several metabolites is, thus, rather a result of a reduction in the overall enzyme level or of rate limiting reactions, such as the HK or the GLUT facilitated transport, which is suggested for cancer cells by Rodríguez-Enríquez et al. [133]. For example, if none of the enzymes involved in G6P conversion are saturated or inhibited in their catalytic activity an increase in G6P levels should increase the production rate of UDPGlc, R5P and F6P. A rate limiting GLUT or HK may then exert flux control over this part of the network. Comparison of r_{GLC^x} (Table 4.1) with *in vitro* measured enzyme activities (e.g. of G6PDH and GPI, [22]) indicates a very high remaining capacity for G6P conversion and, thus, enzymes downstream of HK are presumably not rate limiting (and also not flux controlling). In line with this hypothesis, we recognized slightly lower GLC^x uptake rates in EpiSerf medium (Table 4.1) and found slightly lower metabolite pools in upper glycolysis and associated pathways, which also points towards a rate limiting GLUT or HK. Such a correlation between metabolite levels and fluxes, at least in the upper part of glycolysis, is also described by Munger et al. [297]. Taking into account that intracellular amounts of GLC were always below the detection limit, similarly described for other cell lines by Renner et al. [95] and Schmid and Blanch [91], renders the HK to be very active and the GLUT as rate limiting step. However, changes in intracellular metabolite levels can also be explained with concerted changes in the enzyme level. Nonetheless, the medium has only little influence and a rate limiting GLUT may represent a starting point for modeling. Interestingly, the strong influence of GLUT on the glycolytic activity was already shown for tumor cells [107, 108, 298]. In yeast cells, the GLUT transport is identified as a major effector of dynamics in glycolysis [102]. In the lower part of glycolysis, where the hexoses are split into trioses, the general picture of the metabolite dynamics is not as clear. The first measured component 3PG shows a broader peak than metabolites of upper glycolysis but is apparently decoupled from PEP dynamics (especially for GMEM-Z). It is established that F16BP is a po-

tent allosteric activator of the PK [142, 143]. Therefore, one explanation is that the decrease in F16BP reduces the PK activity and leads to higher PEP levels, which occurs in both media. Another explanation for differences in the PEP dynamics may lie in the linkage to the serine and glycine production, which can be responsible for medium-specific differences (a peak for PEP can be anticipated in the larger variations found for the EpiSerf cultures). A more pronounced medium-specific difference was observed for PYR, which started initially high in the EpiSerf culture and afterwards decreased to levels of the GMEM-Z culture. Amino acids such as alanine, glycine, serine and threonine are typically involved in the production or degradation of PYR in MDCK cells [15]. The conversion of these amino acids to cytosolic PYR, which results in the production of NH_4^x , may take place in the stationary growth phase of EpiSerf cultures when other substrates such as GLC^x and GLU^x were already depleted, and GLN^x was not taken up. Furthermore, providing an alternative source for intracellular PYR allows sustaining the glycolytic intermediates in the EpiSerf cultures under depletion of extracellular GLC^x . Therefore, in these cultures, the flux through glycolysis towards PYR may be comparatively low in the stationary growth phase, and even gluconeogenesis seems possible. Finally, also the hexosamines UDPGlcNAc and UDPGalNAc showed an inverse behavior in EpiSerf medium compared to GMEM-Z. However, almost no correlation was found with time series of other metabolites especially not to glycolytic intermediates, which is in agreement with observations of Barnabé and Butler [78]. Nonetheless, main parts of the glycolytic pathway as well as glycogenesis and the PPP show a similar behavior in both cultures. Differences in the lower glycolysis may be linked to differences in the amino acid metabolism, which may change with the media. Overall, it seems reasonable to assume that intracellular metabolite pools are mainly regulated by the GLUT activity and by a feed-forward activation of the PK by F16BP.

Two different parts of the citric acid cycle: The citric acid cycle is fed by anaplerotic reactions from the precursors GLN and PYR, which are produced by glutaminolysis and glycolysis with about 0.3 mmol/L/min and 3.0 mmol/L/min, respectively (Table 4.1). This large difference in glucose and glutamine conversion is a common feature of cancer cells [50, 58], hybridoma cells [104], BHK cells [86], and AGE1.HN cells [168]. Although PYR might be the main precursor for fueling the upper citric acid cycle in normal cells, the enzyme that is involved in this step (PDH) shows only an activity of 0.1 mmol/L/min in MDCK cells ([22], assuming a cell-specific volume of 3×10^{-12} L), and can limit the transfer speed, which is a phenomenon described by Warburg et al.

[56]. Moreover, a glucose-specific lactate yield coefficient above two was found, similarly reported by Genzel et al. [299] for MDCK cells in GMEM-Z, indicating that only low amounts of PYR are transferred to the citric acid cycle. Accordingly, we assume that fluxes in both parts of the citric acid cycle are relatively low compared to glycolysis and mainly fed from GLN, which agrees with the analysis of Sidorenko et al. [16].

In the lower part of the citric acid cycle, we again observed concerted changes in metabolite pools, which on the one hand excludes an influence by the medium and on the other points towards a robust regulation regime that either controls the transport steps or the enzyme level. Accordingly, we speculate that the observed peak behavior in α KG, SUC, FUM and MAL is linked to changes in GLN^x and especially in GLU^x consumption. The increase in metabolite pools started with beginning of GLU^x uptake (beginning of gray field), while depletion of GLU^x coincided with low intracellular metabolite pools. Interestingly, the EpiSerf cultures showed a clear drop in FUM and MAL pools with depletion of GLU^x ($t > 4$ days) that may further support its role as main substrate. In the stationary growth phase, constant levels of citric acid cycle intermediates were observed, although GLU^x is depleted and GLN^x is not taken up by the cell. To maintain constant levels, the cell may reduce the pathway activity, as the demand for biosynthesis is low, and may engage in the consumption of other substrates to compensate any cataplerotic effects, which presumably prevents apoptosis induced by depletion of these intermediates [300]. Either, pyruvate is used to compensate cataplerosis, which seems counterintuitive considering a lactate yield from glucose above two, or other amino acids are converted to GLN, which explains the NH_4^x release in EpiSerf cultures.

In the upper part, the pools of CIT and ICIT dropped more strongly in the EpiSerf culture, which might be linked to high PYR levels. However, it is established that ICIT is also generated from α KG to support lipid synthesis [175, 176]. Being produced from both pathways, CIT is presumably withdrawn from the mitochondrion such that the upper and lower part are uncoupled and that the citric acid cycle is truncated, which explains completely different metabolite dynamics in both parts. In the cytosol, CIT is transferred into glycolysis and may allow for a glucose-specific lactate yield coefficient that is above the theoretical maximum of two [121, 150].

The mutual influence of metabolism and purines: For the purines, significant changes were observed over the time course of cultivation. ATP and GTP, which are mostly identical in their dynamics, showed a negative correlation to their diphosphatic and monophosphatic counterparts and a adenosine (or guanosine) conservation seems

to be a rational explanation. Similar observations were also made for yeast cells after a GLC^x pulse [199, 289, 301]. The dynamics in ATP after inoculating cells in a new well may represent an interesting analogy to the GLC^x pulses in starved yeast cells. In both cases, the main growth inhibitor is suddenly removed. However, calculations revealed that the increase in ATP concentration is 66 % higher than the decrease in ADP and AMP. Thus, the total adenosine pool is not constant and apparently influenced by the purine salvage pathway [197] and by the usage of nucleosides for nucleic acid synthesis [302]. Regarding the dynamics in ATP, this raises the question to what extent the metabolism is subject to adenylate control [195] or whether energy-rich nucleotides serve as a mediator that adjusts biosynthesis depending on supply reactions [61, 198], e.g. glycolysis and oxidative phosphorylation. As an example for the first hypothesis, the PFK as well as the CL enzyme are both assumed to be controlled by the ATP/AMP ratio, a regulatory mechanism that is comprehensively described by Atkinson and Walton [194]. In this scenario, low levels in ATP during the growth phase may stimulate the PFK, which would yield reduced F6P levels but higher F16BP levels. Inspecting our data reveals a strong correlation in both metabolite pools with a prominent peak during the cell growth phase. Hence, adenylate control over the PFK may be superimposed by the large, GLUT-mediated carbon flux through glycolysis with generally elevated metabolite levels in upper glycolysis. Furthermore, with the depletion of GLC^x and GLU^x in the supernatant of EpiSerf cultures and a negligible GLN^x uptake the pools of ATP and GTP decreased slightly. In particular, dynamics of ATP seemed to correlate with the drop of citric acid cycle intermediates of the lower branch (> 72 h). However, the remaining citric acid cycle metabolites were not fully consumed to increase the ATP level and, hence, adenylate control was also not obvious during GLC^x and GLU^x depletion. Furthermore, a full control by adenosines implies rather constant ATP levels, which were not observed during cell growth. Therefore, it appears reasonable to assume that the importance of biomass growth as well as a cellular response to substrate depletions may overcome the necessity to maintain a constant nucleotide pool, at least on the time scale of days. Perhaps adenosines influence the biosynthesis activity but a strong influence on dynamics in metabolism seems unlikely for MDCK cells, which is an important observation for the development of a mathematical model.

4.1.4. Summary

By using two very different cultivation media, we expected cells from the same preculture to show significant changes in their growth behavior and metabolism. Firstly, because

cells that are passaged in different media adapt their physiology regarding enzyme activities and intracellular metabolite pools [33]. Secondly, because limitation in main substrates may occur at different time points of cultivation, which inevitably influences cell growth and metabolism. However, apart from minor differences in growth, which may be attributed to the osmolality or the lack of factors for cell attachment, and a few changes in metabolite pools, which indicate a slightly changed amino acid metabolism, the behavior of the cells is quite the same. Obviously, the media of this study provide sufficient amounts of main substrates such that limitations only occur at late stages of cultivation. As medium components have only a minor influence on intracellular metabolites, we, thus, anticipate that the metabolism of MDCK cells is robustly regulated by pathway properties, transport mechanisms or hierarchical processes that allow for a concerted change in metabolite pools. In particular, the growth phase-dependent substrate uptake rates together with few enzyme metabolite interactions may explain most of the experimental observations. Interestingly, we could neither observe a nucleotide balance nor a central role of purines for the regulation of central carbon metabolism. To which extent these hypotheses can cover the measured metabolite pool dynamics and whether they fit into a consistent picture of the metabolic regulation is part of the model-based analyzes in the following sections.

4.2. A segregated model for cell growth

From the observations made in the last chapter, the analysis of intracellular metabolite pools on the background of the cell's growth status is a line of investigation worth pursuing. It, however, calls for a model that precisely captures the growth of cells in number and volume over different phases of cultivation and that explains the uptake of substrates. Furthermore, a certain simplicity for fast and stable simulation results is required to enable the coupling with more complex structured models describing intracellular reaction processes. Since such a model has not yet been addressed for growth of adherent cells (see also section 2.3.1), we developed in section 3.1.1 a segregated model that can describe the growth of cultivated MDCK cells in diameter and number. The model assumes that the cell passes from one diameter class to the next with the concomitant consumption of substrates and release of byproducts (Fig. 4.6). After reaching the highest diameter class, the cell divides into two daughter cells of equal size. Growth inhibition can either occur due to limitation in GLC^x or due to the cell-volume dependent growth inhibition (f). Cells that pass the first transition proceed without this limitation. Note that parts of the segregated cell growth model are taken from our original research article Rehberg et al. [216]. Copyright of these passages lies with the Journal of Biotechnology (Elsevier).

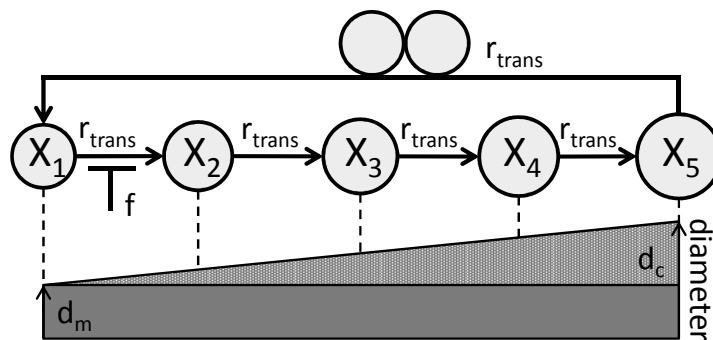


Figure 4.6.: Scheme of segregated cell growth model. Cells proceed through $N^c = 5$ classes with increasing diameter until they reach d_c and divide into two cells with diameter d_m . The transition from the minimum diameter d_m to the second class ($X_1 \rightarrow X_2$) is controlled by the cell volume-dependent growth inhibition factor f .

4.2.1. Relation between cell number, diameter and volume changes

In the following, experimental results of the GMEM-Z cultivations of section 4.1 were simulated with the model using the initial conditions of Table C.3 and a single set of

cell growth parameters of Table C.4. In the model simulation, the cell numbers per well show a lag phase of about 20 h in which cells attach to the growth surface and start to proliferate (Fig. 4.7A inset). Interestingly, the attachment of cells was found to be fast, as 50 % of cells were attached after 3 h and 80 % were attached after 6 h of cultivation, and, thus, constitutes only a small part of the 20 h delay (half of cells sedimented at: 2.4 h; mean duration of attachment process: 0.8 h; see Appendix A.1). Consequently, the remaining 17 h are more or less attributed to the cell size increase until division. According to the model simulations, exponential growth follows the lag phase with a maximum specific growth rate of $\mu_{max} = 0.039 \text{ h}^{-1}$ (Table C.4) until about 45 h of cultivation (Fig. 4.7A). The cell numbers reach their maximum in average after 82 h in the range of $3 \times 10^6 - 4 \times 10^6$ per well. The model can take into account that cultivations with higher final cell numbers show smaller mean cell diameters towards the end of cultivation (Fig. 4.7B). Another aspect of cell growth is the increase in cell volume (calculated with Eq. 3.1.8), which reaches similar levels of about 7 μL in all three experiments (Fig. 4.7C). Note that the cell volume dynamics in the experiments and in the model simulations show a very reproducible time course. The maximum specific growth rate of the cell volume is expected to (largely) correspond to that of the cell number. However, compared to the cell number the growth phases are different (already described in section 2.1.2), which will be important for later discussions. The increase in the cell volume starts immediately in the model simulation (5 h) and was also observed experimentally to start at 6 h of cultivation or even before, which is much earlier than

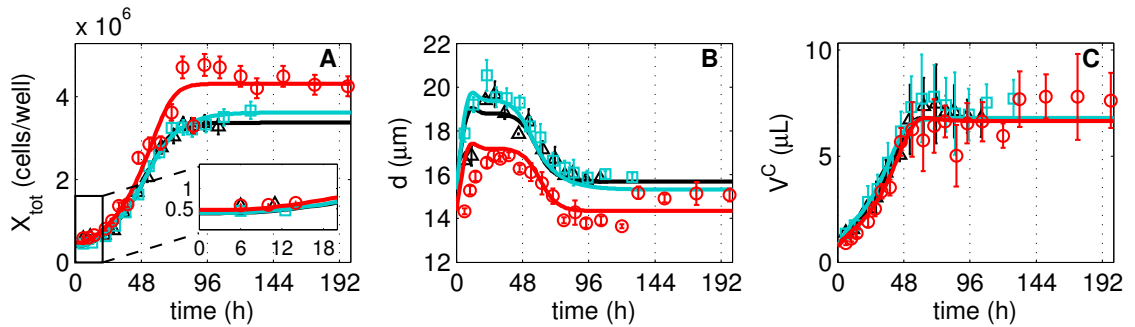


Figure 4.7.: MDCK cell growth in six-well plates with GMEM-Z medium. (A) Cell numbers (inset: first 20 h). (B) Mean cell diameter. (C) Volume of all cells calculated from the mean cell diameter and the cell number. Data of three independent experiments (Δ , \square , \circ) were taken from Ritter [23]. Error bars represent mean and standard deviation of three wells (in case of V^C error bars were calculated according to the error propagation law). Lines represent the corresponding model simulation (parameters of Table 1-2).

the increase in cell number. The exact delay between cell volume and cell number varies with cultivation time. Therefore, a summary of the obtained growth phases for X_{tot} , V^C and b_{syn} is given in Table 4.2 (for definitions see section 3.1.3). Taken together, the developed model is in good agreement with both, the time courses of cell numbers and of the cell volumes (Fig. 4.7A, 4.7C). In particular, it fits the delayed cell number increase and different final cell numbers using a single parameterization. Measurements of the mean cell diameters showed an increase from approximately 14 μm to 21 μm at 30 h of cultivation for all experiments (Fig. 4.7B). With onset of growth inhibition (after 30 h), the measured mean cell diameters decreased to their initial values. Preculturing in T-flasks (Cult1 (Δ), Cult2 (\square)) and roller bottles (Cult3 (\circ)) as well as different durations of the preculture (Cult1 (Δ): 6 days, Cult2 (\square): 3 days, Cult3 (\circ): 4 days) may have caused the systematic difference in the experimentally found mean cell diameters. Thus, the d_m and d_c of the cells division process vary with experiment and preculture and require estimation for every experiment (Table C.3). The step-like increase of the mean cell diameter at the end of experiment Cult3 (\circ) resulted presumably from an error during sample preparation (Fig. 4.7B, $t > 132$ h). The simulations show some disagreement to the measured mean cell diameter at the beginning of cultivations. The trajectories increase faster with a slight overshoot at about 12 h. Extending the model by cell sedimentation and attachment to the well surface may improve the model fit but

Table 4.2.: Calculated growth phases of cell number (X_{tot}), cell volume (V^C) and relative biosynthesis activity (b_{syn}).

		Lag ^a phase	Exponential growth phase	Intermediate ^b growth phase	Stationary growth phase
X_{tot}	Cult1 Δ	0 – 18 h	18 – 45 h	45 – 82 h	82 – 200 h
	Cult2 \square	0 – 18 h	18 – 43 h	43 – 98 h	98 – 200 h
	Cult3 \circ	0 – 18 h	18 – 47 h	47 – 84 h	84 – 200 h
V^C	Cult1 Δ	0 – 5 h	5 – 30 h	30 – 56 h	56 – 200 h
	Cult2 \square	0 – 5 h	5 – 27 h	27 – 59 h	59 – 200 h
	Cult3 \circ	0 – 5 h	5 – 32 h	32 – 58 h	58 – 200 h
b_{syn}	Cult1 Δ	-	0 – 37 h	37 – 76 h	76 – 200 h
	Cult2 \square	-	0 – 34 h	34 – 86 h	86 – 200 h
	Cult3 \circ	-	0 – 39 h	39 – 78 h	78 – 200 h

^athe lag phase is the time required for half of the cells to double in X_{tot} or V^C

^bintermediate phase is defined for V^C with Eq. 3.1.92; for X_{tot} with Eq. 3.1.92; for b_{syn} with Eq. 3.1.95

is not considered in this work as differences are small. Nevertheless, the model captures the maximum mean cell diameter and the decrease of the mean cell diameter towards constant values in the stationary growth phase.

4.2.2. Extracellular substrate and byproduct dynamics

The most essential substrates for cell growth are GLC^x and GLN^x . Until 30 h of cultivation, the model suggests a fast decrease in both substrates based on an exponentially increasing demand by the cells (Fig. 4.8A and 4.8B). Between 30 h and 58 h, the consumption of both substrates reduces, which coincides with the intermediate growth phase in V^C (Fig. 4.7C, Table 4.2). After 58 h the consumption of GLC^x reaches constantly low levels and is the demand for cellular maintenance. In contrast, the reduction in GLN^x is fully explained with water evaporation and spontaneous decomposition, which renders the maintenance metabolism of adherent MDCK cells to be independent from GLN^x . Final concentrations of 11 mmol/L for GLC^x and of 0.5 mmol/L for GLN^x were measured and not growth limiting in the model. Another substrate source for the citric

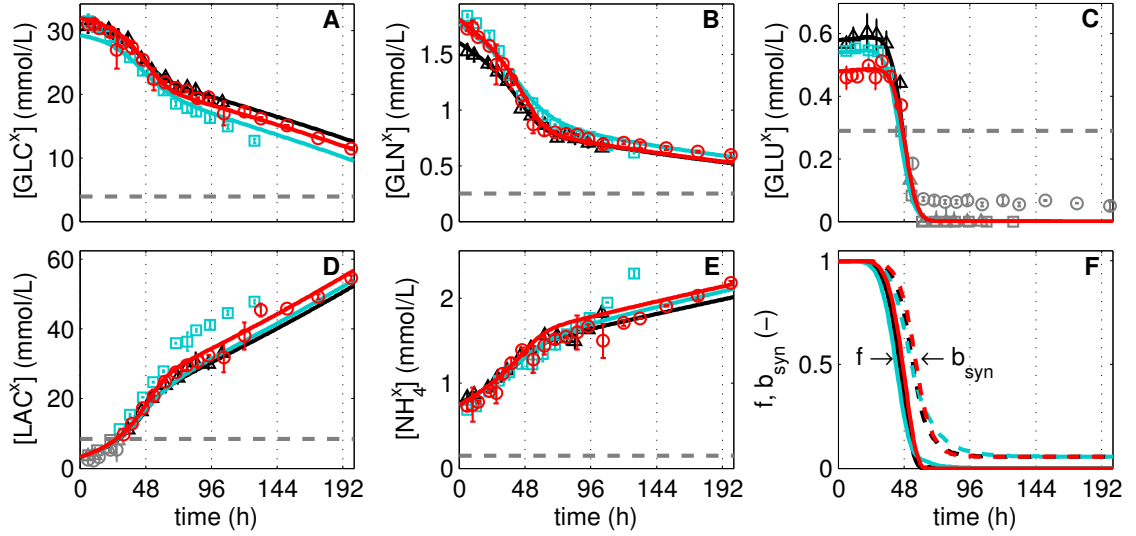


Figure 4.8.: Concentrations of extracellular substrates and byproducts. Glucose (A), glutamine (B), glutamate (C), lactate (D) and ammonia (E) during MDCK cell growth in six-well plate with cell growth medium (GMEM-Z). Data (Δ , \square , \circ) and error bars, which represent mean and standard deviation of three wells, were taken from Ritter [23]. (F) Cell volume-dependent growth inhibition (f , line) and relative biosynthesis activity (b_{syn} , dashed line) of the cells. Data and corresponding model simulations (based on parameters of Table C.3 and Table C.4) are shown in the color code of Fig. 4.7. Grey dashed lines are the limit of quantification (LOQ; data below LOQ marked in gray).

acid cycle is GLU^x . In contrast to GLC^x and GLN^x , the uptake of GLU^x is in the model dependent on a transporter activity that increases when cells are inhibited by f (Eq. 3.1.13, analyzed in Wetzel [280]). Therefore, GLU^x concentrations even increase slightly due to water evaporation until 30 h of cultivation and then sharply decrease to very low levels (below LOQ, Fig.4.8C). The model resembles the GLU^x data for the three cultivations with a single parameter value for the transporter activity (Table C.4). Simulations for LAC^x show initially low concentrations and an exponential increase due to the conversion of GLC^x (Fig. 4.8C). Between 30 h and 58 h, the formation of LAC^x ceases and reaches a final concentration of 52 mmol/L with a lactate yield from glucose of $Y_{\text{LAC}^x/\text{GLC}^x} = 2.14$. Experiment Cult3 (\circ) shows a LAC^x accumulation exceeding the simulation results. In case of NH_4^x , levels increase until 30 h of cultivation (Fig. 4.8D) and depend exclusively on the GLN^x consumption with a yield of roughly 0.8 molecules (cf. Fig. 4.8B, E). An additional contribution from GLU^x produces a peak in NH_4^x release at 48 h that is not observed experimentally and is, therefore, not implemented in the model. In the stationary growth phase, NH_4^x accumulates linearly until the end of cultivation due to spontaneous decomposition of GLN^x and water evaporation. Final levels of NH_4^x reach 2 mmol/L and are below growth limiting levels of about 2.4 mmol/L reported for MDCK cells by Butler et al. [54]. Thus, cell volume growth depends in the model simulations almost completely on the cell volume-dependent growth inhibition factor f , which is also used to control the GLU^x uptake. At the beginning of the cultivation, f is one and has thus no effect on cell volume growth (Fig. 4.8F). Surprisingly, growth inhibition starts early at about 30 h and f drops to zero within a day. The relative biosynthesis rate b_{syn} (explained in section 3.1.3) follows f although slightly delayed in time because cells can divide while the cell volume remains constant (Fig. 4.8F), e.g. a mother cell divides into two daughter cells that immediately stop proliferating. Overall, the model reflects the growth and metabolite dynamics of all three experiments with an intermediate phase that fits experimental observations. Experiment-specific differences are explained with variations in the initial conditions and experiment-specific parameters (Table C.3). Key growth parameters and metabolic parameters for adherent MDCK cells are within the range reported in literature (Table 4.3).

4.2.3. Substrate uptake rates during cell cultivation

In principle, uptake rates of cell growth models are based on causal relationships that hold for the entire course of cultivation and are, thus, more consistent and more precise compared to the polynomial regression analysis of Table 4.1 (section 4.1.1). The

Table 4.3.: Estimated parameters of adherent MDCK cell growth model compared to values given in literature

Parameter	Our model	Literature ^a	Unit
μ_{max}	0.039	0.029 – 0.082	1/h
Y_{X/GLC^x} ^b	$(1.23 - 1.43) \times 10^{-8}$	$(1.11 - 2.00) \times 10^{-8}$	mmol/cell
Y_{X/GLN^x} ^b	$(0.93 - 1.08) \times 10^{-8}$	$(0.61 - 1.81) \times 10^{-9}$	mmol/cell
m_{GLC^x} ^c	$(0.69 - 1.69) \times 10^{-10}$	$(0.02 - 2.18) \times 10^{-10}$	mmol/cell/h
m_{GLN^x} ^c	≈ 0	$(0.02 - 1.13) \times 10^{-10}$	mmol/cell/h

^aGlacken et al. [41], Butler et al. [54], Möhler et al. [211], Bock et al. [212]

^binterval results from multiplication of the optimal value with medium volume for all time points and cultivations

^cinterval results from multiplication of the optimal value with cell volume and medium volume and division by cell number for all time points and cultivations

derived cell-volume-specific uptake rates are main inputs to the structured model of central carbon metabolism and derived from a model that fits data for growth, intermediate and stationary phases. The cell-volume-specific uptake rates of GLC^x and GLN^x (r_{GLUT} and r_{GLNT} , respectively) are highest at the beginning of cultivation with approximately 5.8 mmol/L/min for GLC^x and 0.3 mmol/L/min for GLN^x (Fig. 4.9A – B). Afterwards, a two step decrease follows: technically, the first decrease is a result of an increasing cell-specific volume under a constant substrate uptake (cf. Eq. 3.1.12), which reaches a plateau at 24 h that represents the actual consumption for growth with about 3.5 mmol/L/min for GLC^x and 0.2 mmol/L/min for GLN^x ; the second decrease results from the cell volume-dependent growth inhibition f and ends in cellular maintenance, which requires about 0.7 mmol/L/min of GLC^x and no GLN^x . In contrast to GLC^x and GLN^x , the uptake of GLU^x (r_{GLT}) occurs only when cells are inhibited by f and drops as soon as the pool is depleted (Fig. 4.9C). In consequence, the corresponding cell-volume-specific uptake rate of GLU^x has a peak-like shape. Its maximum can reach similar values than the uptake rate for GLN^x . Some biotechnological studies use cell-specific substrate uptake rates to compare cell lines, which are also shown in Fig. 4.9D – F. Main features of the above described cell-volume-specific uptake rates are also observed for the cell-number-specific ones, i.e.: high uptake of GLC^x and GLN^x during growth, low or zero uptake of GLC^x and GLN^x during cell maintenance, and a peak-like uptake of GLU^x . Differences to the cell-volume-specific rates are the lack of the first, artificial decrease and smaller experiment-specific variations.

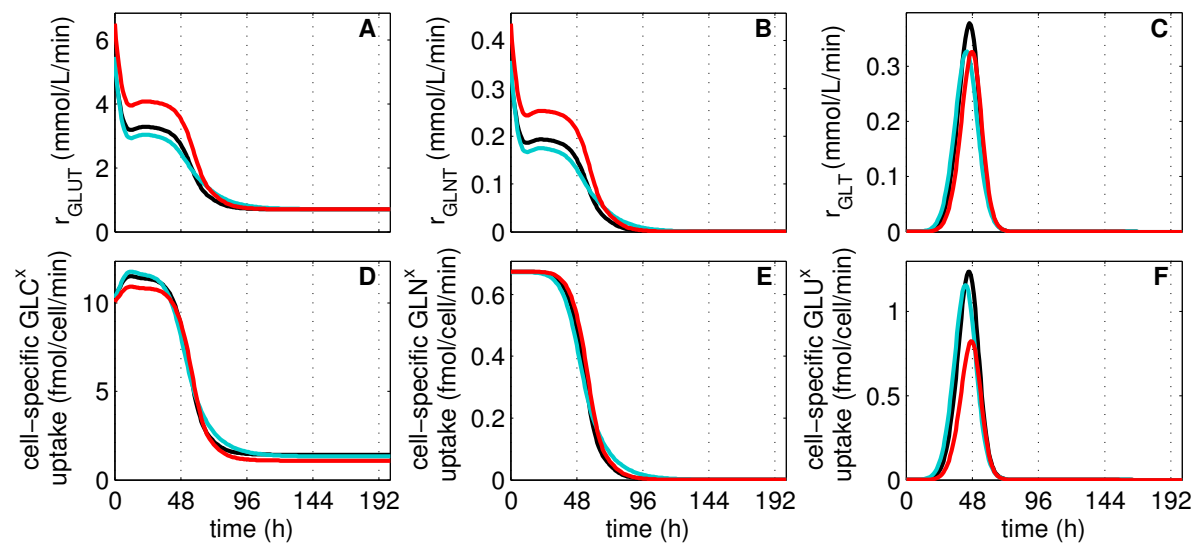


Figure 4.9.: Simulated substrate uptake rates during MDCK cell cultivation. Simulated cell-volume-specific uptake rates of glucose (A), glutamine (B) and glutamate (C). Simulated cell-number-specific uptake of glucose (D), glutamine (E) and glutamate (F). Model simulations (based on parameters of Table C.3 and Table C.4) are shown in the color code of Fig. 4.7.

4.2.4. Discussion

Model structure and possible modifications: We developed a model that accounts for different cell classes with varying cell diameters. The propagation through the classes depends on the density of cells on the attachment surface and the extracellular glucose concentration. However, none of the measured substrates or byproducts reached growth-limiting concentrations. Ammonia, for example, most likely does not inhibit MDCK cell growth below concentrations of 2.3 mmol/L [54] while GLC^x and GLN^x are available in sufficient amounts. The $k_{GLC^x}^m$ parameter of the Monod kinetic, which describes the influence of the glucose concentration on the specific growth rate, has a very low relative local sensitivity (Table C.4). Thus, the cell density is the major effector of growth under the cultivation conditions considered in this work. The underlying equation for f (Eq. 3.1.4) is based on an exponential function originally proposed by Frame and Hu [278] and allows the model to fit the experimental data. It relies on the adjustable parameter s , which is estimated with a large confidence interval ($2.14 < s < 4.15$) and low relative local sensitivity (Table C.4). A linear term for f , as proposed by Möhler et al. [211], results in a too slow transition from zero to maximum growth inhibition and was not able to describe our data (simulation not shown). Although the proposed

model is focused on adherently growing cells, which show a distinct growth inhibition by cell volume density, an application of the model to other adherent cells (MDBK cells, tested with data from IDT Biologika GmbH, results not shown) and even suspension cells seems possible (AGE1.HN cells, tested with data of Rath et al. [283] in Klassen [303]; MDCK.SUS cells, see appendix A.3). Note that the variable f might alternatively be, for example, a function of a metabolite, of another resource or of a limiting factor and can be applied to any of the N^c classes. Therefore, the model is a promising candidate for future applications considering growth dynamics of cultivated cells. Dynamics for cell attachment were not explicitly incorporated in the model but may be of interest if cell growth and metabolite uptake during the first hours of cultivation are under investigation [212]. However, the resulting delay of 3 h due to cell sedimentation and attachment (see appendix A.1) has only little influence on the simulation results and is partly covered by the intrinsic delay of 5 h for cell volume growth (see Table 4.2). The chosen number of classes $N^c = 5$ affects in combination with μ the delay between cell volume increase and cell number increase (for explanation see mathematical analysis provided by D. Flockerzi [216]). However, the dimension N^c of the model can be used to generate a set of nested models. All $N^c > 1$ dimensional models capture the qualitative behavior observed during cell growth. Considering the parameters of Table C.3 and C.4, the inspection of the model results suggests the use of low numbers for N^c . Low numbers for N^c yield a sufficient strong distribution in the growth rate of cells and, therefore, introduce some heterogeneity. With high values for N^c , cell growth becomes more and more synchronized leading to a step-like increase in cell number, which is not observed experimentally. Furthermore, N^c determines also a fraction of the growth cycle that is affected by f (Fig. 4.6). This has the following biological implication: Once cells have passed the first transition the subsequent growth process remains unaffected by cell volume density. Overall, model fits to the experimental data yielded $N^c = 5$ as best solution.

Metabolic parameters and uptake rates: the estimated parameters for MDCK cell growth are within the range published in literature. The cell-growth-specific yield coefficients Y_{X/GLC^x} and Y_{X/GLN^x} as well as the specific GLC^x uptake for maintenance m_{GLC^x} , for example, mirror values for MDCK cells grown in bioreactor systems (Table 4.3). The specific GLN^x uptake for maintenance m_{GLN^x} , is very small and therefore negligible. In particular, the drop in GLN^x in the stationary growth phase can be fully explained with spontaneous decomposition and water evaporation [23, 53]. Results ob-

tained in bioreactor cultivations show higher m_{GLN^x} , which can result from residual cell growth to compensate cell death by shear forces and other stressful conditions. However, a very small m_{GLN^x} suggests that glutamine is only required during cell growth as it is typically used for biosynthesis purposes [50, 87]. The Y_{LAC^x/GLC^x} is found to be high with 2.14. This may indicate, as discussed in the previous section 4.1.3, that GLC^x is primarily converted to LAC^x [16] and that glutaminolysis, which relies on GLN^x and GLU^x [58], increases the Y_{LAC^x/GLC^x} to values above 2. Overall, taking into account that simulations are based on a single set of parameters for all three cultivations, the model is in good agreement with the measured metabolite dynamics and is capable to predict each of the three cultivation processes if the other two are used for validation (shown in Rehberg et al. [216]). Furthermore, the applied bootstrap method yields narrow confidence intervals for most of the parameters (Table C.4), which indicates identifiability. For the uptake of GLU^x , we defined a transport kinetic that is activated by f , which may appear atypical for standard growth models. However, it is also recognized by Genzel et al. [14] that GLU^x uptake starts with growth inhibition. Together with the good fitting of the measured data, a kinetic that is inhibited by cell growth seems justified. Assuming that the transport is indeed inhibited by growth in turn validates the shape f with measurements for GLU^x . However, the model also takes into account the release of NH_4^x from the conversion of GLN^x . Based on the high transaminase activities in MDCK cells [22], which is also observed by Gstraunthaler et al. [170], and the accumulation dynamics of NH_4^x a contribution from GLU^x is presumably negligible.

Dynamics in cell growth: The model estimates a doubling time of 17.7 h ($\mu_{max} = 0.039 \text{ h}^{-1}$), which lies within the interval reported in literature [41, 54, 211, 212]. Note that differences in the doubling time, e.g. to the 24 h reported by Butler et al. [54], may result from differences in the cultivation conditions compared to 6-well plates, which have low shear stress and no risk of cell disruption by bubble bursting. Direct determinations of μ_{max} by logarithmic transformation for the exponential growth phase showed a similar average value of 17.3 h ($\mu_{max} = 0.040 \text{ h}^{-1}$, section 4.1.1). Based on the model, 80 % of cells are already inhibited by f within the regression interval chosen for the experimental determination of μ_{max} by Ritter [23] (20 h to 52 h). Nonetheless, the μ_{max} determined by regression analysis corresponds to the model-based estimation since the cell number is delayed and shows growth inhibition later than the cell volume. Before increase in cell number starts, a lag phase of roughly 20 h was observed, which is similarly described for MDCK cells in microcarrier cultivations [211], and presumably involves about 2.4 h for

sedimentation and 0.8 h for cell attachment (see Appendix A.1). Thus, about 17 h of the 20 h remain left for cell size increase and division, which corresponds to the 17.7 h estimated above. Nielsen et al. [42] developed a mathematical model that accounts for a time difference between the start of cell volume and cell number growth by using delay differential equations. In our data, however, the time shift between the growth phases of X_{tot} and V^C is not constant (cf. Table 4.2). The intermediate growth phase starts 15 h earlier and the stationary growth phase starts 30 h earlier for cell volume growth than for cell number growth. Thus, differences in growth phases may not be caused by a fixed delay and the dependencies may be time varying in a more general sense. Although a delay model, which requires the same number of parameters, yields seemingly similar fits (akaike information criterion evaluated in [216]: Rehberg model: 6.47×10^3 ; Nielsen model: 6.59×10^3), we prefer a finite (N^c) dimensional model. Another benefit lies in a much faster computation time (four magnitudes), which not only allows for a reliable and comprehensive parameter study but also for coupling with more complex structured models of metabolism. Moreover, it can take into account general class-specific effects, as shown by the implementation of f . In this regard, the proposed model has a better transferability and generality to incorporate diameter changes during cell growth.

Diameter changes during cultivation: To simulate the mean cell diameter during cultivation, we assume that all cells exhibit an identical linear increase from the minimum (d_m) to the critical diameter (d_c). Thus, heterogeneity in d_m or d_c as well as in r_{trans} is not considered but is typically observed in mammalian cells [47]. Ramirez and Mutharasan [45] as well as Boucrot and Kirchhausen [46] found that changes in cell size are correlated with the propagation through the cell cycle. Furthermore, d_m and d_c as well as the intermediate diameters do not change with each generation of cells but rather represent upper and lower limits. In consequence, the cell-specific volume of class N^c is more than the double of the cell-specific volume of the first class. The model pays indirectly tribute to a so called cell-sizing effect reported by Tzur et al. [48]. These discrepancies easily explain differences between model simulation and experimental data, especially until 12 h of cultivation. Nevertheless, the requirement for simulating mean cell diameter dynamics with a coarse-grained model is adequately met. It fits the measurements of all three cultivations and the observations of Rothen-Rutishauser et al. [25] of a decreasing cell diameter when cells pass into the stationary growth phase. For a more precise and deeper analysis of cell diameter dynamics, the use of mass distribution population-based models is an option worth considering [220, 223]. However, the information required

for such an analysis is currently not available for MDCK cells. Furthermore, to our knowledge none of the mass distribution population-based models were yet validated for batch cultivations of adherent cells.

4.2.5. Summary

From analyzing, in a previous section, MDCK cell cultivations in two different media, we derived the hypothesis of a growth-dependent regulation of intracellular metabolite pools. To support further investigations in this direction, we developed in this section a segregated model that describes cell growth in numbers and volume by considering the mean cell diameter. The model takes into account cell volume-dependent growth inhibition as well as the consumption of GLC^x , GLN^x and GLU^x for the progression through different diameter classes. The structure of the developed model is slightly more complex than conventional cell number-based models since additional information about the mean cell diameter are considered, which are, however, easily obtained from cell counting devices. For the three independent MDCK cell cultivations in GMEM-Z medium, the model successfully fits the experimental data using a single set of parameters. It also considers that cells may differ in their maximum and minimum diameter in dependence of their preculture. Analysis of the extracellular metabolite pool dynamics unraveled that substrates are not growth limiting under the chosen cultivation conditions and that cell growth ceases due to the limited availability of free surface for cell attachment. Furthermore, the model possesses a certain power in predicting cell cultivations and is applicable to other cell lines and cultivation systems. Therefore, it fills the gap between standard cell growth models and mass distribution population-based models with a certain generality and applicability that can support both the understanding of cell growth and the analysis of biotechnological processes. More importantly for this work, however, dynamics in cell growth can now be coupled to structured metabolic models, which facilitates studying the regulation of central carbon metabolism during cell cultivation.

4.3. Dynamics in central carbon metabolism

Analysis of MDCK cells indicated that many intracellular metabolite pools show the same dynamics, although cells are grown in two different media (see section 4.1). We hypothesized that the dynamics in metabolism depend on the uptake of substrates and on a few mechanisms for enzyme regulation. In the previous section 4.2, we developed a segregated model that describes adherent MDCK cell growth in volume and number and explains the uptake of main substrates. We now seek to evaluate whether the structured model for the central carbon metabolism, established in section 3.1.2, is able to explain intracellular metabolite pools when coupled to a segregated cell growth model (see section 3.1.3). To realize a proper balance between a detailed description of results and a conclusive discussion, the analysis is divided into two parts: first, we evaluate the simulation results for glycolysis and the closely related metabolic pathways and, afterwards, analyze to which extent the derived regulatory principles are also capable to explain metabolite dynamics in glutaminolysis, which includes the citric acid cycle, and the energy metabolism. In the following, parts of the structured glycolysis model published in PLoS Computational Biology [304] (open source) and of the structured glutaminolysis model published in the IFAC proceedings [305] (copyrights are with the International Federation of Automation and Control) are used.

4.3.1. Glycolysis

Due to its highly active and robust nature, glycolysis is an ideal candidate pathway to start evaluating general principles of metabolic regulation. The scenarios considered in the following sections cover a broad range of operation conditions including cell cultivation, substrate limitation and substrate pulse experiments. Afterwards, we estimate the capacity of the glycolytic pathway to unravel potential targets for the design of bioprocesses, e.g. higher growth rates or more efficient substrate use, and evaluate the predictive power of the model based on a cultivation in a second medium. The underlying model focuses on intermediates that were measured experimentally and is composed of a concise set of enzyme kinetics with few regulatory mechanisms, while taking into account the link to PPP and glycogenesis. A schematic overview of the considered enzyme reactions, metabolite pools and maximum *in vitro* enzyme activities is given in Fig. 4.10.

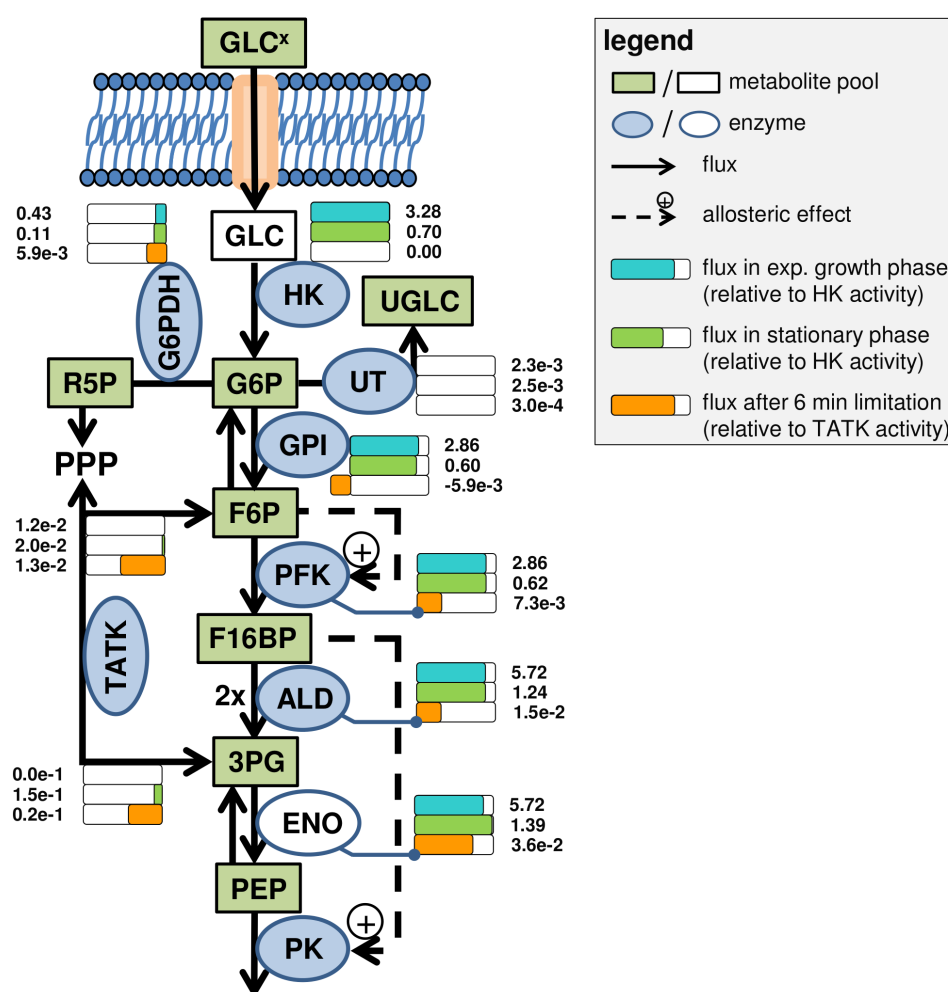


Figure 4.10.: Scheme of glycolysis model with calculated fluxes. Green boxes represent metabolite pools that were quantified experimentally, while white ones were not quantified. Enzymes are shown as ellipses with blue background if the maximum enzyme activity was measured *in vitro* and with white background otherwise. Reactions and their directions are shown as arrows. Dashed arrows represent allosteric regulation of enzymes by metabolites. Colored bars are attached to each reaction and express the relative flux compared to the largest flux in glycolysis (see legend, blue: cell growth at 24 h of Cult1; green: cell maintenance at 100 h of Cult1; orange: limitation after 6 min). Absolute flux rates (unit: mmol/L/min) are given next to the bars. Abbreviations are: GLC^x extracellular glucose; GLC glucose; G6P glucose 6-phosphate; UGLC uridyl diphosphate glucose; R5P ribose 5-phosphate; PPP pentose phosphate pathway; F6P fructose 6-phosphate; F16BP fructose 1,6-bisphosphate; 3PG 3-phosphoglyceric acid; PEP phosphoenol pyruvate; HK hexokinase; UT UTP-glucose-1-phosphate uridylyltransferase; G6PDH glucose 6-phosphate dehydrogenase; GPI glucose phosphate isomerase; ALD aldolase; ENO enolase; PK pyruvate kinase.

Metabolite pool dynamics and fluxes during cell cultivation: In three independent experiments, adherent MDCK cells were grown in 6-well plates with the serum-

containing medium GMEM-Z. The cells used for inoculation of Cult1 (Δ), Cult2 (\square) and Cult3 (\circ) originate from a preculture that has reached the stationary growth phase. According to the findings of previous section 4.2, the medium provides sufficient amounts of extracellular substrates over the chosen cultivation time and inhibition of cell growth is mainly induced by the cell density on the surface, which ultimately applies to the preculture. Assuming that the cells robustly achieve a certain metabolic status in the stationary growth phase of the preculture allows us to infer the metabolic starting conditions for the cultivation experiments by simulating the conditions at that time point of preculture (see also section 3.2.1). This simulation of starting conditions allows us to limit model fitting to 19 unknown parameters (as discussed later). The resulting metabolic status of the preculture is depicted in the time interval from -20 h to 0 h (Figure 4.11, Table C.1).

With the onset of cell growth, the simulation of the three experiments exhibits a peak-like behavior for G6P, F6P and F16BP concentrations that agrees well with the data for each cultivation (Fig. 4.11A – I). The maximum is reached at around 24 h and followed by a decrease during the intermediate biosynthesis phase where the growth rate of cells reduces, which is indicated by a gray bar (based on b_{syn} , Eq. (3.1.94), Table 4.2). In the model, the peak results from high cell-volume-specific glucose uptake rates and low maximum cell-volume-specific enzyme activities. The peak and the subsequent decrease of the metabolite pools is slightly different among the cultivations, although all three metabolites drop to the same final level that mostly corresponds to the initial level at 0 h (Fig. 4.11A – I). Due to the tight coupling of cell growth to glycolysis, the model considers experiment-specific differences, such as $X_{tot}(t=0)$ used for inoculation as well as d_m and d_c , which have a considerable influence on time point and height of the peak. Also, small differences in the relative enzyme level (E_{level} ; Table C.2) affect the maximum catalytic activity of every enzyme in the model (Eq. 3.1.90 and 3.1.91) and required estimation during data fitting for every cultivation. The E_{level} vary by $\pm 8\%$ for the three cultivations, which corresponds to the mean standard deviation for all enzyme activities based on the assay of Janke et al. [22]. Interestingly, cells with the lowest diameter also had the lowest enzyme level (Table C.2). Besides variations due to assay noise, the experiment-specific differences in X_{tot} , d and E_{level} explain batch-to-batch variations such as the lower peak height for Cult1 (Δ), a medium peak height for Cult2 (\square) and an increased peak height for Cult3 (\circ), which is most prominent for F6P. An exemplary intracellular flux from glycolysis into associated pathways is shown for Cult1 in Fig. 4.10. During cell growth the activity of HK (3.28 mmol/L/min) is roughly

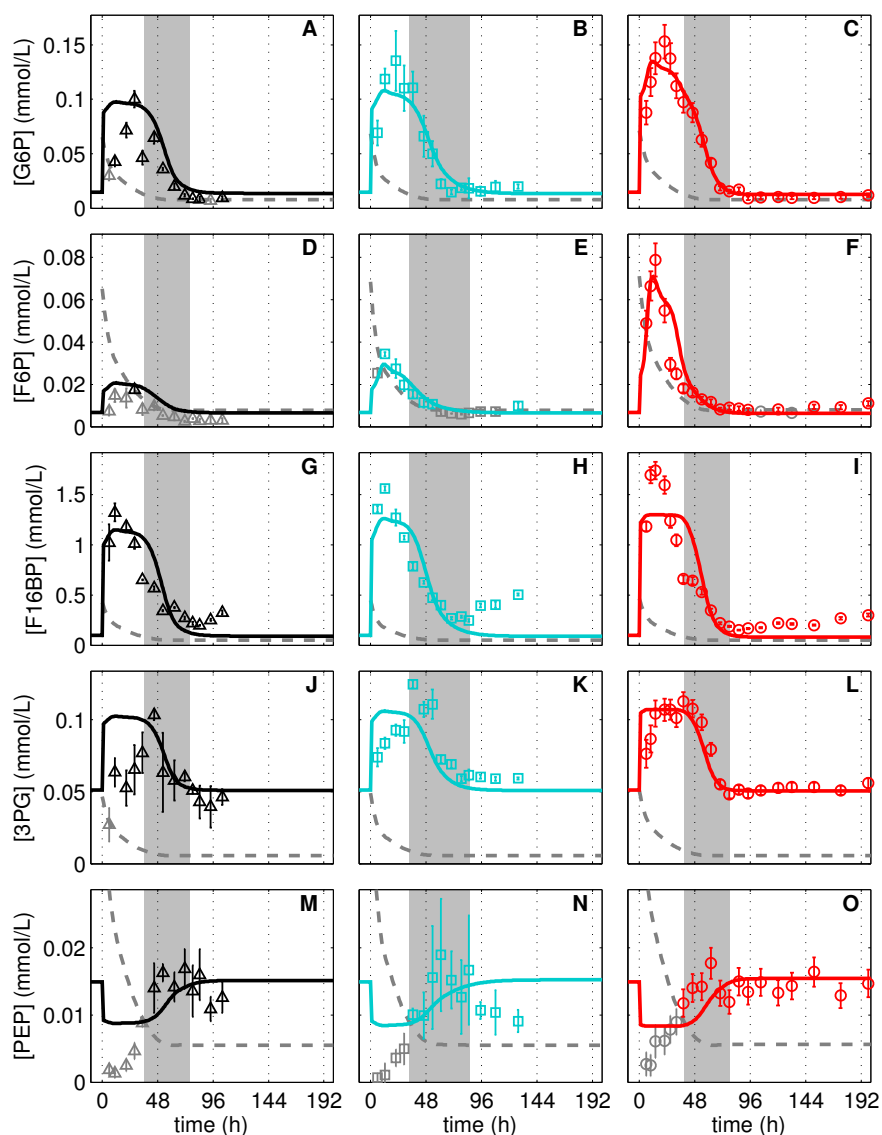


Figure 4.11.: Metabolite pools of glycolysis during adherent MDCK cell cultivation. Glucose 6-phosphate (A – C), fructose 6-phosphate (D – F), fructose 1,6-bisphosphate (G – I), 3-phosphoglyceric acid (J – L) and phosphoenolpyruvate (M – O) concentrations in three independent MDCK cell cultivations (Δ , \square , \circ) in 6-well plates and GMEM-Z. Data and error bars represent mean and standard deviation of three wells and were taken from Ritter [23]. Dashed lines are the limit of quantification (LOQ; data below LOQ marked in gray). Lines represent the respective simulation result based on the experiment-specific parameters in Table C.2 and parameters in Table C.5. The intermediate biosynthesis phase of the cells is indicated as gray bar for the respective cultivation (b_{syn} in Table 4.2).

five times higher than during stationary growth (0.7 mmol/L/min). The metabolite flux into the PPP is primarily mediated by the G6PDH route, which enables a net supply

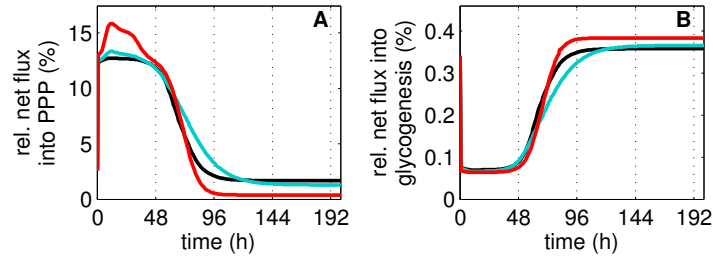


Figure 4.12.: Estimated fluxes into pentose phosphate pathway and glycogenesis during adherent MDCK cell cultivation. (A) Net flux into pentose phosphate pathway (PPP) relative to glucose transport activity and (B) net flux into glycogenesis relative to glucose transport activity are simulated for the three cultivations (Cult1 – 3) and shown in the color code of Fig. 4.11

($r_{X/PPP}$) that reaches 13–16 % of the glycolytic flux during cell growth and 0–3 % of the glycolytic flux during cell maintenance (Fig. 4.12A) and fulfills the constraint to be in the range of 0 % to 40 % (section 3.1.2). During cell growth, the TATK reactions transfer only a minor portion of PPP metabolites back to glycolysis. However, during the stationary growth phase the flux through the G6PDH route is completely compensated by the TATK reactions, which transfer all metabolites generated by this route back to glycolysis. It may indicate that the demand of biosynthesis for PPP metabolites is low and that GLC is completely converted to PYR. In comparison to the PPP, the relative net flux branched off from glycolysis for glycogenesis is low and reaches less than 0.1 % during cell growth with an increase to 0.4 % during cell maintenance (Fig. 4.12B). In the lower part of glycolysis, the level of 3PG follows the peak-like behavior of upper glycolysis albeit with a two-fold increase in concentration only, which is quite similar among the three cultivations (Fig. 4.11J–L). The data of Cult1 (Δ) have larger standard deviations and a peak-like behavior is not as obvious as for the other two cultivations (Cult2 (\square), Cult3 (\circ)). Assuming that the peak is also present in Cult1 (Δ) renders the model to be in general agreement with the 3PG dynamics for all three cultivations. The data for PEP are below the limit of quantification (LOQ) until 48 h of cultivation (indicated by gray symbols) but still support the hypothesis of a fast drop at the beginning of cultivation with a slow but steady increase until the stationary growth phase begins (Fig. 4.11M–O, 50–200 h). Under consideration of these data points, the model similarly suggests a decrease and increase in PEP levels due to an allosteric feed-forward activation of PK by F16BP. If data points below the LOQ are neglected, a straight line would be sufficient to describe the data. In the stationary growth phase,

the simulation result is slightly above the data points as higher levels of PEP in the cultivation simulations facilitates a more precise fitting of the perturbation experiments (see next section). In the model, the lower part of glycolysis shows a four-fold higher activity during cell growth (5.7 mmol/L/min) compared to the stationary growth phase (1.39 mmol/L/min).

Response of glycolysis to substrate limitations and a substrate pulse: At distinct time points of cultivation the medium was replaced by PBS, which removes substrates and byproducts. The model assumes that 3×10^{-7} L medium (0.008 % of original medium volume) remain on the cell's surface and the intercellular space (see section 3.2.2). If no medium remains, an activity of 3.28 mmol/L/min in glycolysis (Fig. 4.10) would, for example, deplete the G6P pool of 0.06 mmol/L within a second, which is not the case (Fig. 4.13A).

The intracellular metabolite pools of upper glycolysis, i.e. G6P, F6P and F16BP, show different starting concentrations in the first (Lim1; Fig. 4.13A, D, G) and the second limitation experiment (Lim2; Fig. 4.13B, E, H). The model, however, can readily explain the observed differences in the initial values for Lim1 and Lim2 by assuming that the cells originate from different time points (t^*) of Cult1 (Lim1: 48 h, Lim2: 60 h, see Table C.2, for explanation see section 3.2.1). Choosing Cult2 or Cult3 as a starting point for simulation of Lim1 and Lim2 would yield similar results (simulation not shown). Within one minute, the corresponding metabolite pools drop below the limit of quantification. Interestingly, traces of F6P and G6P are still detected by the assay, while the pool of F16BP seems to be empty. According to the model, a flux from PPP to F6P of about 0.013 mmol/L/min is sufficient to maintain the F6P and G6P pool under a reversed activity of the GPI (Fig. 4.10). However, G6PDH transfers metabolites back to the PPP and a cycle of metabolite exchange is created that is also described by Sengupta et al. [62]. The conversion of F6P by PFK is reduced due to a lack of an F6P-mediated activation and the remaining activity slowly generates 3PG (Fig. 4.10). Overall, we conclude that the model is in good agreement with experimental data for cells under glucose limitation, especially for the data above the limit of quantification.

In the lower part of glycolysis, 3PG and PEP remain comparatively constant or even increase in concentration until reaching a steady state after 3 min (Fig. 4.13J, K, M, N). In the model, the increase in PEP results from a reduction in the PK activity due to decreasing F16BP levels (Fig. 4.10). The initial concentration of PEP measured in both limitation experiments is higher than in the model simulations but also higher than the

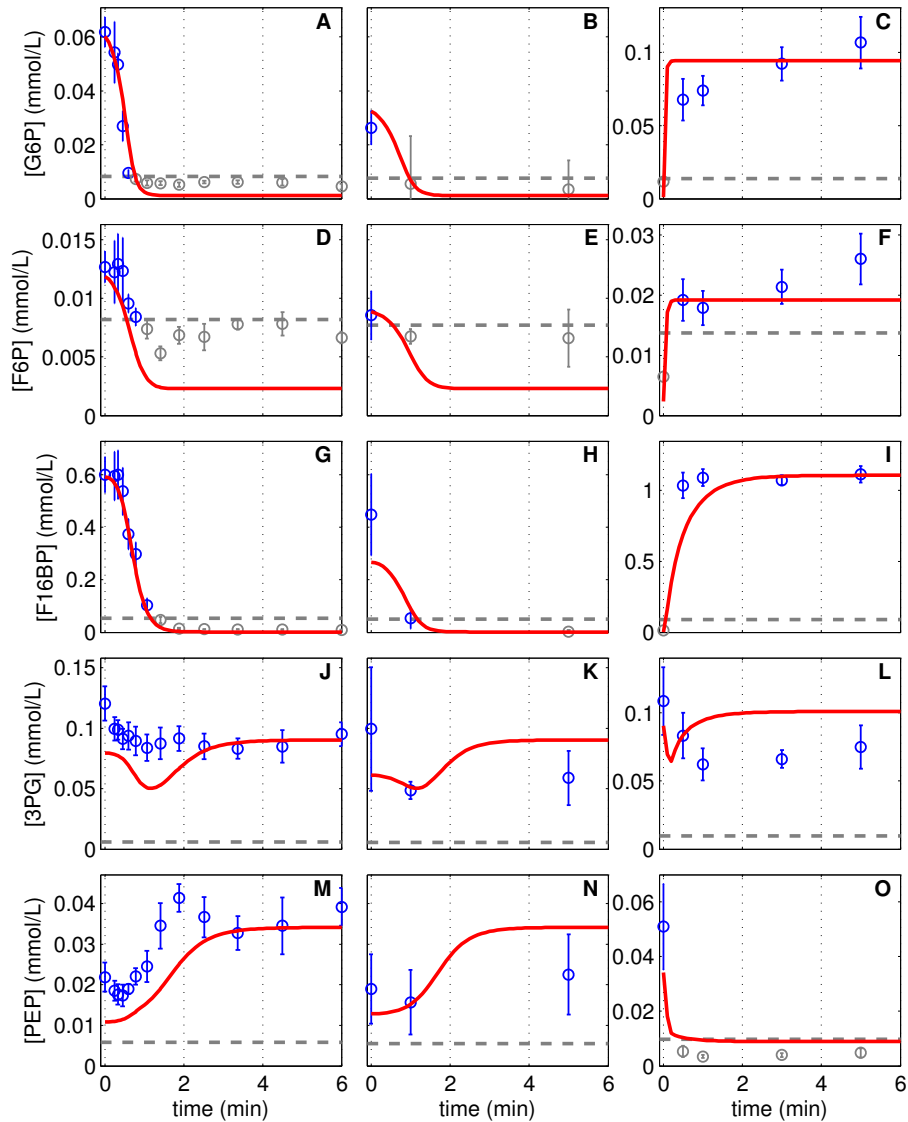


Figure 4.13.: Response of glycolytic metabolite pools to substrate limitations and a substrate pulse. Glucose 6-phosphate (A – C), fructose 6-phosphate (D – F), fructose 1,6-bisphosphate (G – I), 3-phosphoglyceric acid (J – L) and phosphoenolpyruvate (M – O) concentrations of three independent perturbation experiments with MDCK cells in 6-well plates. Cells, originating from a cultivation experiment (see Table C.2), were deprived of extracellular nutrients by removal of medium and addition of phosphate buffered saline (PBS), shown in the first (Lim1) and second column (Lim2). In a similar experiment, cells were exposed to a 2 h limitation and afterwards PBS was exchanged by fresh medium, shown in the third column (Pulse). Data (\circ) and error bars represent mean and standard deviation of three wells and were taken from Ritter [23]. Dashed lines are the limit of quantification (LOQ; data below LOQ marked in gray). Lines represent the respective simulation result based on the experiment-specific parameters in Table C.2 and parameters in Table C.5.

levels found in the cultivation experiment (Fig. 4.11M – O). To improve the fitting of the Lim1 and Lim2 experiments, the model realized slightly higher final PEP levels in the cultivation experiments than measured experimentally, which is a common problem in multi-experiment fitting that may indicate data inconsistencies. The simulation of 3PG showed a negative peak at 1 min of glucose limitation, which may also be present in the data although to a lesser extent.

The pulse experiment followed a limitation experiment conducted at 32 h of Cult1 (not shown). After two hours of limitation PBS was replaced with fresh medium, which provided the cells with glucose and other substrates. The model suggests that glycolysis almost immediately starts with the conversion of GLC to PYR (1.4 s until PK activity is 5 % of full operation) and returns to the cell status of Cult1 at 32 h. After one to two minutes, the metabolite pools reach the corresponding metabolic steady state (Fig. 4.13C, F, I, L, O). Such a fast increase in several glycolytic intermediates was also observed for tumor ascites [94]. As a result, the dynamic is mirroring the limitation experiment with increasing metabolite levels in upper glycolysis (Fig. 4.13C, F, I) and a decreasing PEP pool (Fig. 4.13O) due to the feed-forward activation of PK by F16BP. However, the slight, continuous increase measured for G6P and F6P pools is not reflected by the model and also the simulated dynamics in 3PG, which remains more or less constant in the simulation with a small drop at 0.5 min, is somewhat different compared to the experimental data (Fig. 4.13L). However, the model simulation simply returns to the metabolic status that was present in Cult1 at 32 h of cultivation, which fits most of the data of the pulse experiment.

***In silico* modulation of GLUT activity:** Up to this point, our model suggests that the GLUT controls the glycolytic activity during cell cultivation in GMEM-Z, which we exploit to assess the capacity of glycolysis. Modulation of the GLUT is not only recognized as a target for the improvement of production cell lines but also as an approach for cancer treatment with the intention to interfere with the high metabolic activity of cells, and eventually with tumor growth. For the subsequent analysis of glycolysis by *in silico* modulation of the GLUT activity, we chose cells from Cult1 at 24 h of cultivation. We also consider the impact of the parameter uncertainty by using the 2000 model parameterizations derived from the bootstrap method⁸ (section 3.3.2). All parameterizations are eligible to describe the data. The modulation of the GLUT activity in all these model parameterizations was chosen to range from 0 – 10 mmol/L/min, which ex-

⁸excluding the upper and lower 2.5 % of the results leaves a total of 1900 simulations for analysis

ceeds the typical uptake rates determined for Cult1 (0.7–3 mmol/L/min, Fig. 4.9A). The resulting steady state production rates of ATP and PPP metabolites were sorted in increasing ATP production rates and are shown in Fig. 4.14. Interestingly, an increase in GLUT activity until about 4 mmol/L/min enhances the production of ATP and PPP metabolites, depending on the model parameterization. A further increase in GLUT activity to 6 mmol/L/min saturates the PFK (for cells of Cult1 at 24 h). In consequence, the metabolic flux is directed into the PPP, which further increases the synthesis of metabolites but impairs the glycolytic ATP production. Note that the increase in PPP metabolite production results exclusively from an enhanced G6PDH activity, which, in cooperation with other enzymes, also yields NADPH. As a result, the PPP-based production of NADPH correlates linearly with the PPP metabolite production, which are both essential for biosynthesis. However, for a GLUT activity above 6 mmol/L/min, the HK becomes saturated as well and a further increase in GLUT activity is suggested to yield an accumulation of GLC.

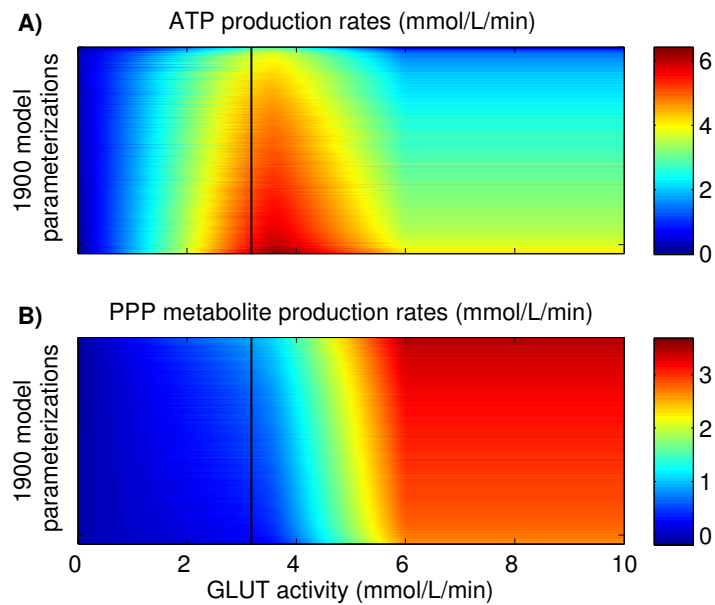


Figure 4.14.: Impact of *in silico* GLUT activity changes on energy and precursor production rates. ATP (A) and pentose phosphate pathway (PPP) metabolite production rates (B) in 1900 model parameterizations for the status of cells in Cult1 at 24 h. The model parameterizations were derived from the optimal result of each bootstrap run, which were also used to infer the parameter confidence intervals of Table C.5. The results were arranged from minimum to maximum ATP production rates (0.025-quantile to 0.975-quantile) and the colored bars on the right hand show the respective production rate, respectively; the vertical black line represents the original GLUT activity of cells of Cult1 at 24 h.

Predictions for DMEM cultivation: Validating the above made estimations for higher ATP or PPP metabolite production rates involves a considerable experimental effort, for instance by overexpression of GLUT or HIF-1 [97, 306] in combination with the measurement of ATP, NADPH and PPP metabolite production rates. To still evaluate the predictive power of the developed model, we simulate a cultivation with a second medium that has low initial GLC^x concentrations. This implies that neither initial conditions nor kinetic parameter of the structured glycolysis model were changed. Only the cell growth model was adjusted to reflect growth of cells in a GLC^x -limited culture (further information is given in the appendix A.2). Although initial conditions and kinetic parameter of the structured glycolysis model were not changed, the model resembles the shortened peaks in the metabolite pools and a transient shift into a limitation scenario (Fig. 4.15). In particular, the increase in metabolite pools and the time point of the maximum is correctly predicted. The subsequent decrease in metabolite levels cannot be attributed to the intermediate growth phase (gray bar) but to the limitation in GLC^x . However, the maximum peak height measured for F6P and F16BP exceeds that of the model prediction (Fig. 4.15B, C). Both peaks are also higher than those of the Cult1 – 3

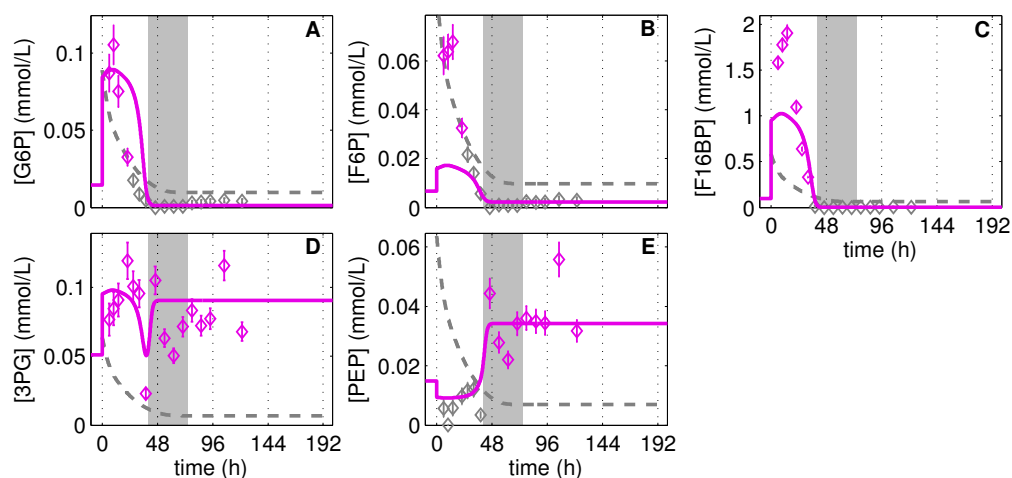


Figure 4.15.: Prediction for glycolytic metabolite pools during cultivation of adherent MDCK cells in DMEM with reduced glucose supplementation (2.5 mmol/L). Data on glucose 6-phosphate (A), fructose 6-phosphate (B), fructose 1,6-bisphosphate (C), 3-phosphoglyceric acid (D) and phosphoenolpyruvate (E) concentrations (\diamond) are depicted as mean and standard deviation of three wells and were taken from Ritter [23]. Dashed lines are the limit of quantification (LOQ; data below LOQ marked in gray). Lines represent the model prediction based on the modifications of the cell growth model described in the appendix (section A.2) and the parameters in Table C.2 and Table C.5. The intermediate biosynthesis phase of the cells is indicated as gray bar for the respective cultivation (b_{syn}).

cultivations and may point towards a reduction in the PFK activity. At later times of cultivation, the levels of G6P, F6P and F16BP are very low, which is similarly predicted by the model. Interestingly, the model prediction also supports the negative peak of 3PG at 48 h as well as the relatively high final level of PEP (Fig. 4.15D, E).

4.3.2. Pentose phosphate pathway

Apart from glycolysis, G6P can also be converted by G6PDH and enter the PPP such that it eventually fuels the R5P pool. The use of an additional model parameter for the RDPK-mediated degradation reaction (Eq. 3.1.44), which represents only one possible route in the PPP, enables the model to reflect the dynamics of R5P during cell cultivation (Fig. 4.16A – C). R5P mainly follows the peak-like behavior of G6P (cf. Fig. 4.11A – C) with similar experiment-specific variations. During the limitation experiments, the decrease of R5P is delayed in time (Fig. 4.16D, E) but still similar in its shape to G6P (cf. Fig. 4.13A, B). Although the model cannot render this delay, the shape of the decrease is reflected. After addition of fresh medium in the pulse experiment (Fig. 4.16F), the

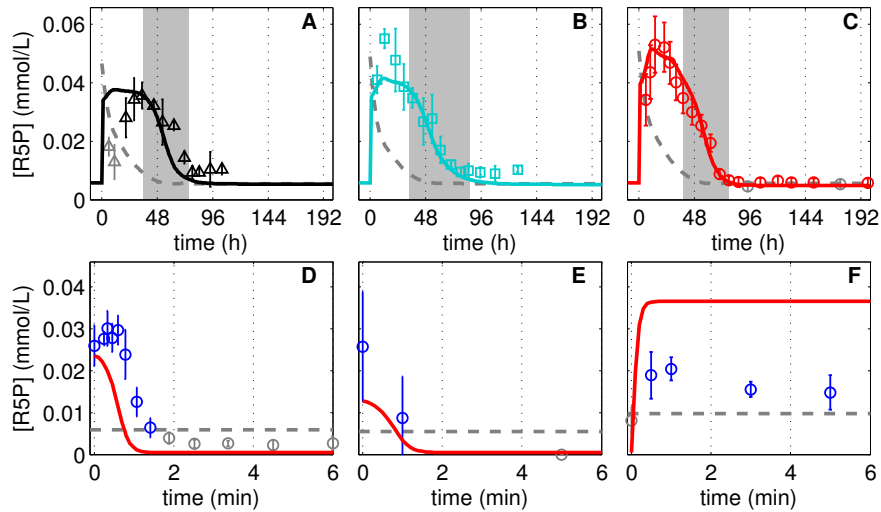


Figure 4.16.: Ribose 5-phosphate levels during adherent MDCK cell cultivation, substrate limitations and a substrate pulse. Each single plot illustrates an independent experiment. (A – C) Cultivation of MDCK cells in 6-well plates and GMEM-Z. (D, E) Substrate limitation. (F) Substrate pulse. Data (Δ , \square , \circ , \circ), which are depicted as mean and standard deviation of three wells, were taken from Ritter [23]. Dashed lines are the limit of quantification (LOQ; data below LOQ marked in gray). Lines represent the model simulation based on the parameters in Table C.1, Table C.2 and Table C.5. The intermediate biosynthesis rate of the cells in (A – C) is indicated as gray bar for the respective cultivation (b_{syn} in Table 4.2).

measured level of R5P increases rapidly to values above the LOQ but remains lower than suggested by the model. In all three cases, the differences between data and simulation results might be due to specific properties of the PPP, which were not considered by the model so far (for instance, the high number of reversible reactions, and the linkage of its intermediates to the biosynthesis machinery).

4.3.3. Glycogenesis

Another route for G6P is its transfer into glycogenesis through UT. Similar to the PPP, the use of an additional model parameter for a GLYS-mediated degradation reaction (Eq. 3.1.46), which lumps all possible degradation routes, enables the model to reflect the dynamics of UGLC during cell cultivation (Fig. 4.17A – C). Note that in contrast to other intracellular metabolites, UGLC is diluted by cell growth to a visible extent, which reduces the typical peak-like behavior compared to other metabolites. In other words, the synthesis and degradation rate for UGLC is such low that cell volume growth has an influence on its abundance. During substrate limitation and substrate pulse, the

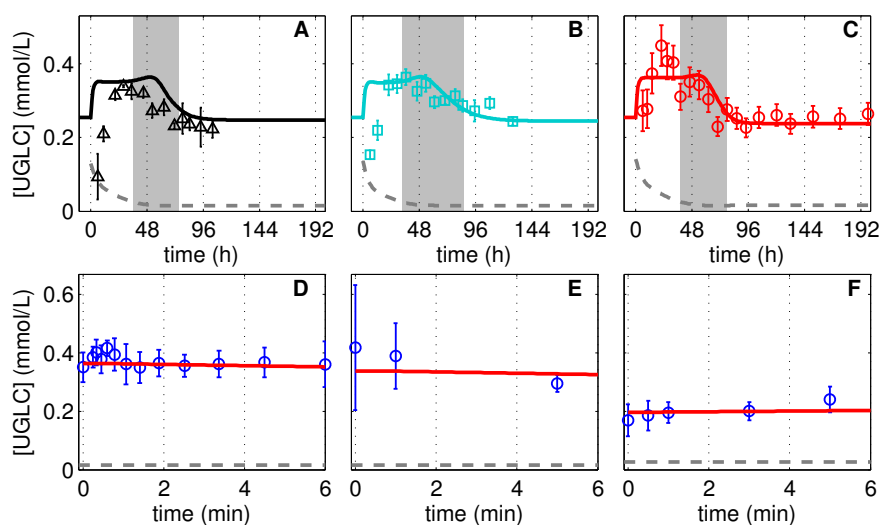


Figure 4.17.: UDP-glucose levels during adherent cell cultivation, substrate limitations and a substrate pulse. Each single plot illustrates an independent experiment. (A – C) Cultivation of MDCK cells in 6-well plates and GMEM-Z. (D, E) Substrate limitation. (F) Substrate pulse. Data (Δ , \square , \circ , \circ) are depicted as mean and standard deviation of three wells and were taken from Ritter [23]. Dashed lines are the limit of quantification (LOQ; data below LOQ marked in gray). Lines represent the model simulation based on the parameters in Table C.1, Table C.2 and Table C.5. The intermediate biosynthesis rate of the cells in (A – C) is indicated as gray bar for the respective cultivation (b_{syn} in Table 4.2).

data for UGLC show only a minor decrease and a minor increase, respectively, which is sufficiently described by the model (Fig. 4.17D – F) and attributed to the low pathway activity (Fig. 4.10).

4.3.4. Sensitivity analysis for glycolysis

To assess how the model behavior depends on the different model parameters and initial conditions, we performed a relative local sensitivity analysis by perturbing each parameter by 1 %. In particular, we analyzed parameters of the structured model of glycolysis (Table C.5), parameters of the segregated cell growth model (Table C.4) and initial conditions regarding culture condition, the growth status, and the metabolic status (Table C.2, Fig. 4.18A). The subsequent interpretation of the sensitivity analysis is based on the height of values relative to each other and not on absolute numbers. For the cultivation experiments, the model simulations are sensitive to growth and metabolic parameters but mostly insensitive to the initial metabolic status or initial culture conditions (for perturbations of 1 %). Also, the initial growth status has a certain influence on the simulation trajectories. The surprisingly low influence of the initial metabolic status on the metabolite pool dynamics can be explained with a high glycolytic activity and low metabolite pool sizes. Thus, any initial metabolic status is easily adjusted by the high flux rates. The reason for a low sensitivity regarding initial culture conditions is that a perturbation of 1 % is insufficient for obtaining substrate levels that limit cell growth or metabolism (see section 4.1). However, when it comes to the simulation of substrate perturbation experiments, the model behavior becomes sensitive to perturbations in the initial metabolic and growth status of the cells. Therefore, the preculture of cells affects the Lim1 and Lim2 experiment (Fig. 4.13). The growth parameters have, by definition, no influence on the model behavior. In contrast, parameters of the metabolic network rearrange the flux distribution towards a new steady state and, thus, also have a larger influence. Taken together, the sensitivity analysis illustrates that the sensitivity of glycolysis shifts with the experimental scenario. An in-depth analysis of glycolysis parameters reveals that the PFK has the largest influence on metabolite pool degradation (Fig. 4.18B). However, a certain sensitivity is also given for the remaining parameters, while parameter correlations are in general low (Fig. A.6), which together indicates parameter identifiability. The few exceptions of HK, TATK and GLUT are discussed in section 3.1.2.

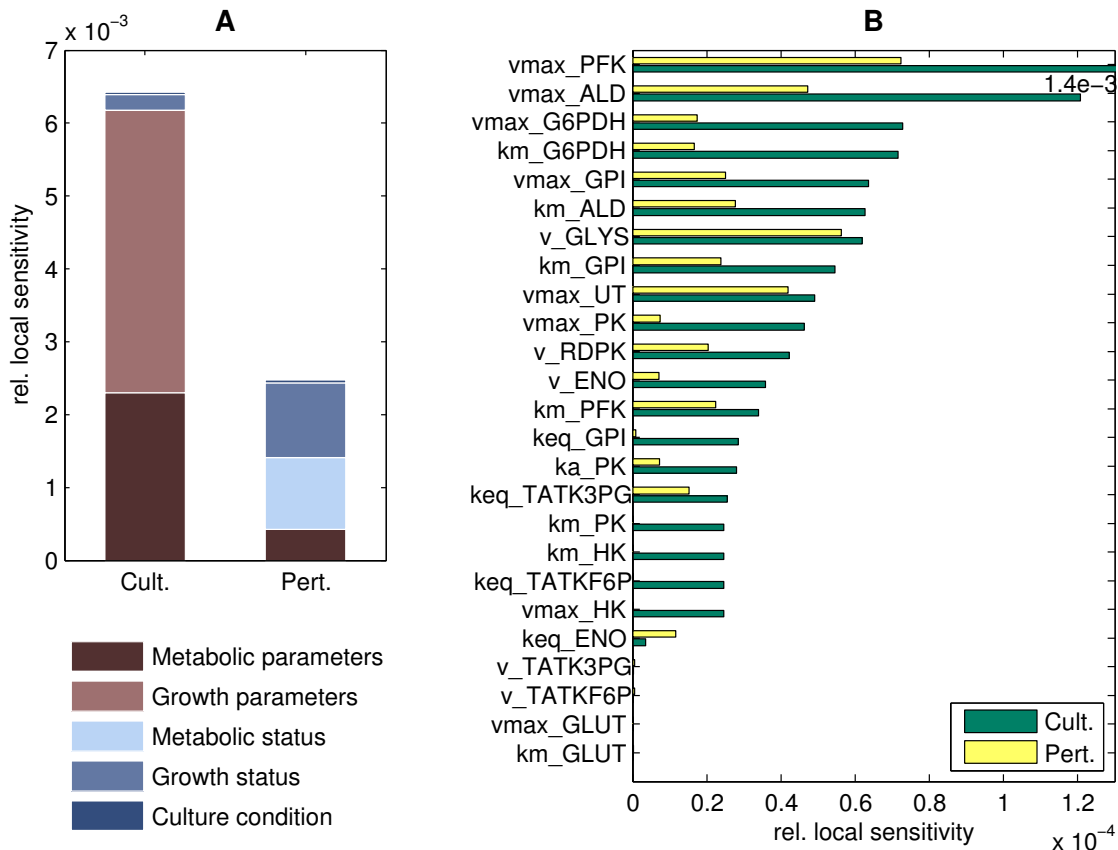


Figure 4.18.: Parameter sensitivity analysis of the structured model of glycolysis. (A) Relative local sensitivity of model simulations (for cultivation and perturbation experiments) to a 1 % perturbation in glycolysis parameters (Table C.5), parameters of the segregated cell growth model (Table C.4), culture conditions, growth status and metabolic status (Table C.2). (B) Relative local sensitivity of model simulations (for cultivation and perturbation experiments) to a 1 % perturbation of single glycolysis parameter.

4.3.5. Discussion part I

Glycolysis model structure: In this work, a kinetic description of glycolysis is developed that, coupled to a segregated cell growth model, enables describing and analyzing roughly 600 intracellular metabolite pool data points of Ritter [23] by using a single set of parameters for the enzyme kinetics. The description of dynamics in metabolite conversion can, however, rely on many different types of enzyme kinetics with arbitrary complexity [257, 260]. As a starting point and for simplicity, the model considers basic kinetics which only take into account basic regulatory mechanisms of glycolytic enzymes to reflect the dynamics of metabolite pools found during cultivation and perturbation experiments. In particular, the kinetics for TATK as well as for ENO represent lumped

reactions and were realized with reversible mass-action kinetics instead of using more complex kinetics (e.g. Monod-Wyman-Changeaux models [262]). The enzymes HK, GPI, G6PDH, UT, and ALD as well as the GLUT were defined as Michaelis-Menten kinetics, as they provide an upper activity bound that was measured *in vitro* by Janke et al. [22] (except for GLUT), and appear either as reversible or irreversible reaction. In analogy to mass action kinetics, only one or two parameters of the Michaelis-Menten kinetics required estimation. Only the PFK and PK, which are known to be strongly regulated enzymes, were considered to be influenced by allosteric effectors. For the PFK, a Hill-Kinetic with four subunits [234, 284], which takes a direct activation by F6P [12] and an indirect activation via F26BP into account [58, 135], was sufficient to fit all data. For the PK, the well-known F16BP-mediated activation [69, 143] was used. However, the chosen simplifications in enzyme kinetics render the used parameters to be more abstract, such that, for example, the affinity of an enzyme for its substrate rather represents a time invariant sum of influences than an explicit dependence on cofactors, ions or the degree of phosphorylation [65]. The benefit lies in obtaining a comparatively simple model that describes the experimental data with enzyme kinetics comprising only 19 unmeasured parameters (Table C.5). Thus, the resulting model features the identification of mechanisms that are involved in certain dynamics through an efficient and reliable estimation of parameters and a comprehensive model analysis. Furthermore, extension by additional reaction mechanisms is relatively easy in case further experimental data is available or other cellular functions are of interest, e.g. the response of primary metabolism to osmotic stress [160], and hypoxia [307] or its influence on the glycosylation of proteins [308]. Note that other models of glycolysis that take into account further, unmeasured metabolites or more complex enzyme reactions than used here may equally well describe the dynamics of the intracellular metabolite pools of this study.

Model coupling and simulation: The derived kinetic description of glycolysis considers data of three independent cell cultivation experiments, two limitation experiments and one pulse experiment and, therefore, required coupling to a model that takes explicitly into account the process of cell growth. Because of the many different experimental settings (6 experiments), simulations would normally require a large set of initial conditions about the cell status, which comprises the metabolic status (6×8 degrees of freedom) and growth status (6×7 degrees of freedom), and culture conditions (6×7 degrees of freedom) as listed in Table C.1 and Table C.2. Considering that the perturbation experiments were performed at a certain time point of cultivation and that cultivations

in turn were inoculated with cells from a defined preculture introduces a dependency of the cell status on the cultivation history. Accordingly, we transfer the required information from one simulation to another (Fig. 3.2 of section 3.2.1). First, the intracellular metabolite levels of the preculture were derived from a steady state simulation and, thus, depend only on the intrinsic pathway properties and the growth status. Second, the cultivations Cult1 – 3 provide the cell status for the limitation experiments, which in turn deliver the cell status for the pulse experiments. This modeling scheme not only reduced the number of kinetic parameters but also the total number of initial conditions that require estimation. Thus, modeling only involves a total of 21 degrees of freedom (not considering the parameters used in the segregated cell growth model and the structured model of glutaminolysis). In addition, using a certain cell cultivation history not only eliminates the search for adequate initial conditions but also supports consistent data simulation and can be used to evaluate biological variations [309]. However, inconsistent data sets or an unknown cell status (e.g. cell status different to those of Cult1 – 3) may pose a serious challenge for model fitting. For such scenarios, the individual selection or fitting of initial conditions might be a better option. In this work, however, the estimation of two experiment-specific parameters, which are the E_{level} for the respective cultivation and t^* as starting point for the perturbation experiments, as well as a consistent consideration of all data sets outweighed a perfect data fitting and greatly supported our systems-level analysis of glycolysis.

Enzymes control glycolysis during substrate limitation: The simulation of the limitation experiments was started with a growth status and a metabolic status that corresponded to a time point t^* of the Cult1 experiment. The selection of different time points t^* readily explains variations in the initial concentration of intracellular metabolite pools that were found between the Lim1 and Lim2 experiment. The actual limitation was induced in the simulations by reducing the medium volume to 3×10^{-7} L, which is estimated as liquid volume that remains on the cellular surface or in the intercellular space. In comparison, the volume of all cells is roughly 6×10^{-6} L. In principle, a dilution of the remaining medium with PBS can be realized by choosing lower GLC^x concentrations and a higher medium volume (V^M). The affinity of GLUT for GLC^x (k_{GLUT}^m) was found to have a large confidence interval (Table C.5) and, hence, lower concentrations of GLC^x under a higher V^M are likewise possible. The consideration of preculture conditions and of a remaining medium volume enables the model to reflect the data measured for the limitation experiments. It suggests that

with the limitation of glycolysis in substrates, the feed-forward regulations of PFK and PK stop the metabolite pool degradation, while the TATK reactions partially reverse and fuel glycolysis with 0.03 mmol/L/min, which leads to a new steady state within minutes. Thus, the control of the glycolytic activity shifts from the growth regime that regulates the GLUT activity (see next part of discussion) towards an inherent regulation of enzymes by substrates and products in the glycolytic pathway, which is further supported by the sensitivity analysis. Without the implementations for the TATK reactions, the remaining glycolytic activity eventually depletes the metabolite pools unless fueled from sources other than GLC. As the limitation applies to all possible extracellular substrates, the use of intracellular carbon sources from PPP, glycogenolysis or gluconeogenesis seems likely. The PPP shares already three metabolites with glycolysis (G6P, F6P, and GAP) which are most likely not depleted during the limitation experiments and may pose the most promising and simplest option among the aforementioned intracellular carbon sources. Also, the late decrease in R5P during the limitation experiment and its lower level during the pulse experiment may support a scenario in which the PPP fuels glycolysis under substrate limitation and, thus, can have a large influence on glycolytic intermediates, which is similarly found for hepatoma cells [73]. In turn, after addition of fresh medium, the PPP metabolite pools may be replenished by glycolysis and we hypothesize a certain buffering capacity of the PPP as it is composed of many reversible reactions and intermediates that participate in the biosynthesis machinery. In the model, the implemented reversible mass action kinetics allow for such a switch from metabolite consumption to metabolite production by the PPP under the lack of alternative sources for glycolysis. However, the flux rates as well as the parameters of the PPP cannot be uniquely identified on the basis of our experimental data (Table C.5). Therefore, we have used the additional constrain that the flux from the PPP into glycolysis is low (section 3.1.2). Although the implemented mechanisms may not definitely be attributed to the PPP, all parameterizations of Table C.5 support the finding that metabolite pools can be maintained (or increased) under limited substrate availability. To this end, the model suggests that the allosteric regulation of PFK and PK as well as the reversibility of GPI and TATK modulate the glycolytic activity in scenarios characterized by limited substrate availability. This is consistent with findings that flux control in glycolysis can rely on a combination of many enzymatic steps [73] and can vary depending on experimental conditions [60]. Counter-intuitively, adenosine-based nucleotides, which are also considered to control the metabolic activity in general [194], are constant during our limitation and pulse experiments (appendix Fig. B.1). Similar

observations were made for yeast and HeLa cells [12, 82]. Therefore, regulation of glycolytic enzymes of MDCK cells by adenosine-based nucleotides seems unlikely under the conditions investigated, which is similarly suggested for rat hepatoma cells by Renner et al. [95]. Furthermore, an activation of glycolysis by a possibly decreasing ATP/ADP ratio stands in contrast to the metabolite pool preservation and renders its influence to be limited (see also discussion section 4.3.11). However, the general purpose of an enzyme-mediated control of the glycolytic activity through PFK, PK, TATK and GPI might lie in the prevention of unnecessary dissipation of valuable biomass precursors and may also guarantee a metabolic status that enables a fast reactivation of glycolysis and other cellular functions when new substrates become available after starvation conditions (Fig. 4.13C, F, I, L, O).

GLUT controls glycolysis during cell cultivation: Over the full course of cultivation cells pass through several growth-phases with varying cell-specific volumes and glucose uptake rates that strongly influence the metabolite pool dynamics. In addition, abundance of enzymes, their covalent modifications as well as the level of allosteric regulators may change over time which can additionally affect metabolite fluxes and pools [65, 310]. However, to our surprise most of the experimental observations were captured by the model under a parameterization that simultaneously explained the perturbation experiments. Obviously, other hierarchical control mechanisms besides the growth regime, for example on the genomic or proteomic level, were not essential for describing the observed metabolite pool dynamics, which is similarly expected by Schaub and Reuss [77]. It seems that the used cultivation conditions and media composition are already tailored to MDCK cells such that an adaptation of the cellular physiology or an influence of other hierarchical control mechanisms is not necessary. Nevertheless, the consideration of other levels of hierarchical control, in addition to the growth regime of this work, may contribute to aspects of the observed dynamics and a greater compliance of the model with the data. However, the enzyme kinetics and the influence by the growth regime through GLUT are in the following considered as the sole source of regulatory principles that control glycolysis during MDCK cell cultivation.

First, the peak in the metabolite pools can be explained with a high GLUT-mediated flux rate in combination with lowered cell-volume-specific enzyme activities, which is caused by an increase in the mean cell-specific volume. Section 4.1.3 already suggested a reduction in enzyme activity to be an explanation for the peak in metabolite pools. However, this effect can only account for smaller metabolite pool changes and, thus,

the GLUT-mediated flux determines the metabolite pool dynamics to a large extent. The purpose of high metabolite pools during growth is, presumably, to induce higher net fluxes into the PPP and other biosynthetic pathways, which is similarly described by Wu et al. [138] for bovine venular endothelial cells after addition of CIT in order to inhibit the PFK activity. In another study, activation of GLUT in rat thymus lymphocytes with concanavalin A resulted in higher fluxes in glycolysis and into the PPP [114]. Eventually, higher fluxes into the PPP enable an enhanced nucleotide, macro-molecule, and lipid synthesis [311], as reviewed by Mazurek et al. [312]. According to our simulations, the maximum net flux is between 13 % and 15 % of the glycolytic flux, which is in the range reported for continuously growing mammalian cells in the exponential growth phase [82, 151]. However, a much lower contribution, e.g. 5.8 % and 3.6 %, can be found in the late intermediate growth phase, which corresponds to findings for other transformed mammalian cells [15, 67, 150]. The lower part of glycolysis is controlled by a feed-forward activation of the PK by F16BP and yields a negative correlation between PEP and upper glycolysis, similarly observed by Schaub and Reuss [77]. Therefore, the regulation of enzymes by substrates, products and allosteric effectors can change concentrations of intracellular metabolite pools, and reorganize the pathway fluxes, especially under limiting conditions (see previous part of the discussion). However, during MDCK cell cultivation the control over the glycolytic activity is exerted by the growth regime through modulation of the GLUT activity. For many mammalian cells, the GLUT is described as the rate limiting step that can control the glycolytic flux [95, 102, 108, 313, 314]. Adenosine-based nucleotides are another source of regulation and reported to play a major role in the control of the glycolytic activity (e.g. HK or PFK) in rat liver cells [194] or *E. coli* [59]. According to our observation of MDCK cell growth in two different media, we already anticipated that the influence of adenosine-based nucleotides on glycolysis is, however, rather low. Furthermore, neither during cell growth nor during substrate perturbation the adenosine-based nucleotides contribute in their role as cofactors to the simulated dynamics (see section 3.1.2). Therefore, we assumed during model construction that the considered glycolytic enzymes are insensitive against changes in the adenosine-based nucleotide levels, which is also anticipated by Soboll et al. [200] for rat liver cells.

Snoep and co-workers hypothesized that GLUT controls cell growth [315]. This, however, raises the question, whether metabolism regulates cell growth or vice versa [21]. In case of adherent MDCK cell growth with sufficient substrate supply, the growth status is changed by internal signaling processes that integrate information on the availability

of free space on the well surface. Eventually, space becomes limiting and cells reduce the glycolytic activity although high extracellular glucose concentrations are present. Therefore, we hypothesize that the growth regime of exponentially growing MDCK cells controls the GLUT activity to realize a higher metabolic activity yielding in turn higher metabolite pools that meet the energy and precursor demands of the biosynthesis machinery. On a lower level of regulation, the properties of the involved enzymes shape metabolism by influencing flux distributions. Under substrate limitation, however, regulation of enzymes has full control over the glycolytic activity since no GLC^x is available for the GLUT-mediated uptake (see previous discussion "Glycolytic activity during cell cultivation"). Thus, the model considers that the regulation of the glycolytic activity changes with the status of the cell [21] and sheds light on the regulatory principles that are essential to simultaneously explain various experimental scenarios. Although regulation of glycolysis can change with the microorganism [59] and the culture condition [103], we are convinced that the derived principles can be applied to other mammalian cell lines relevant for production of biologicals, e.g. the AGE1.HN.AAT (see [283, 303]).

Tuning the ATP and biomass precursors generation: Within a GLUT activity of 0–4 mmol/L/min, the model for glycolysis is validated with cultivation, limitation and pulse experiments. It already shows a good predictive power for an experiment where MDCK cells were grown in DMEM medium with low GLC^x levels, which further strengthens the confidence in the model structure and its parameterization. Although the model prediction for the DMEM cultivation would benefit from a lower enzyme level (E_{level}) to describe all maximum peak-heights, it still confirms the close linkage of GLUT activity and intracellular metabolite dynamics. Based on the finding that the GLUT modulates the glycolytic activity during cell cultivation (under sufficient substrate availability) it seemed desirable to explore the maximum capacity of glycolysis and the corresponding ATP and PPP metabolite production. However, such a maximum capacity clearly depends on the E_{level} and the cell-specific volume (V_S^C). Therefore, we exemplarily analyzed cells from the Cult1 experiment at 24 h of cultivation with an actual uptake of 3.3 mmol/L. For these cells, *in silico* modulation of the GLUT activity revealed that an uptake of up to 3.8 mmol/L/min can be realized until the glycolytic flux saturates the PFK capacity, which slightly enhances the ATP production on average to 105 %, and the PPP metabolite and NADPH production to surprising 153 % for cells of Cult1 at 24 h. According to the model, a further increase in ATP production would require the simultaneous overexpression of the PFK, which illustrates the difficulty in

fast up-regulation of metabolic activity while keeping a certain balance between ATP and PPP metabolite production. Note that Janke et al. [22] measured higher maximum *in vitro* PFK activities than estimated in this study such that glycolysis of MDCK cells may have higher capacities than suggested by the model. However, an increased biomass precursor and ATP production can support higher growth rates as shown for tumor and yeast cells with up-regulation of the GLUT activity [57, 113]. Furthermore, Schmidt et al. [198] described a correlation between the growth of tumor cells and the ATP production rate. Potentially, an increase in the ATP production to 105 % may not or only slightly support higher growth rates for MDCK cells, especially as they are described to have a large overproduction in ATP [15, 16]. But due to the importance of PPP metabolites to pyrimidine production [120, 312] or purine production [302] and NADPH to lipid synthesis, we believe that an increase to 153 % positively affects the growth of cells. A glycolytic activity above 5 mmol/L/min drastically enhances the production of PPP metabolites (433 %) at the expense of the ATP production (77 %) and seems to be an interesting scenario for future experiments. However, also the reduction in the glucose uptake, as done by Liebl et al. [106], poses an interesting strategy to design a more economic breakdown of glucose [87]. For instance, reducing the GLUT activity with a concomitant reduction in PFK may yield lower glycolytic activities but similar biomass precursor production rates. Currently, the reduction of the glucose uptake by interference with the GLUT is also studied as a potential target for cancer treatment [57, 112] and may benefit from the use of mathematical models to evaluate corresponding dynamics in metabolism. Taken together, the model can greatly support the development of strategies that aim either at a faster or a more efficient cell growth, and is also an aid in the design of new experiments.

4.3.6. Glutaminolysis

For glycolysis, we found in the last section that metabolite pool dynamics are to a large degree determined by the facilitated substrate transmembrane transport into the cytoplasm and a few key mechanisms for enzyme regulation. The citric acid cycle of glutaminolysis is, however, located in the mitochondria, which is a separate compartment, is much more complex in its network structure and is influenced by the respiratory chain, ion fluxes and amino acid metabolism. Models for *in vitro* mitochondria are therefore enormously complex and cannot yet be validated with *in vivo* data. The emerging question is whether a straight forward realization of regulation mechanisms discovered for glycolysis is also capable to explain salient features observed for the citric acid cycle or whether additional aspects need to be considered. As before, modeling covers cell cultivation, substrate limitation and substrate pulse experiments and analyzes the predictive power by simulating a cultivation in a second medium (DMEM). The model structure (described in section 3.1.2) focuses on intermediates that were measured experimentally and is composed of a concise set of enzyme kinetics with only few, key regulatory mechanisms. It is coupled to the segregated cell growth model, links glycolysis with the citric acid cycle through modeling of the pyruvate metabolism, and also takes into account the conversion of branched chain amino acids. A schematic overview of the considered enzyme reactions, metabolite pools and maximum *in vitro* enzyme activities of glutaminolysis is given in Fig. 4.19.

Metabolite pool dynamics and fluxes during cell cultivation: For the simulation of the cell cultivation experiments, we already explained that the cells used for inoculation of a new well originate from a preculture that has reached the stationary growth phase (see section 3.2.1 and section 4.3.1). In consequence, we expect the metabolite pools at the beginning and at the end of the cultivation experiment to be identical. However, inspecting the data reveals that metabolite levels of the lower citric acid cycle are already higher or lower in the first measurement time point ($t = 6$ h) compared to the stationary growth phase ($t > 76$ h, Fig. 4.20). Obviously, a change in the citric acid cycle activity took place between inoculation and 6 h of cultivation, which can be attributed to the onset of cell growth. The model suggests a fast drop in α KG and MAL as well as a fast increase in SUC and FUM short after inoculation (around 0 h, Fig. 4.20). The reason for the fast change in metabolite pools lies in the GLN^x uptake, which is not existent in the stationary growth phase (Fig. 4.9E) and, therefore, also not in the preculture. A drop in half of the metabolite pools and a decrease in the

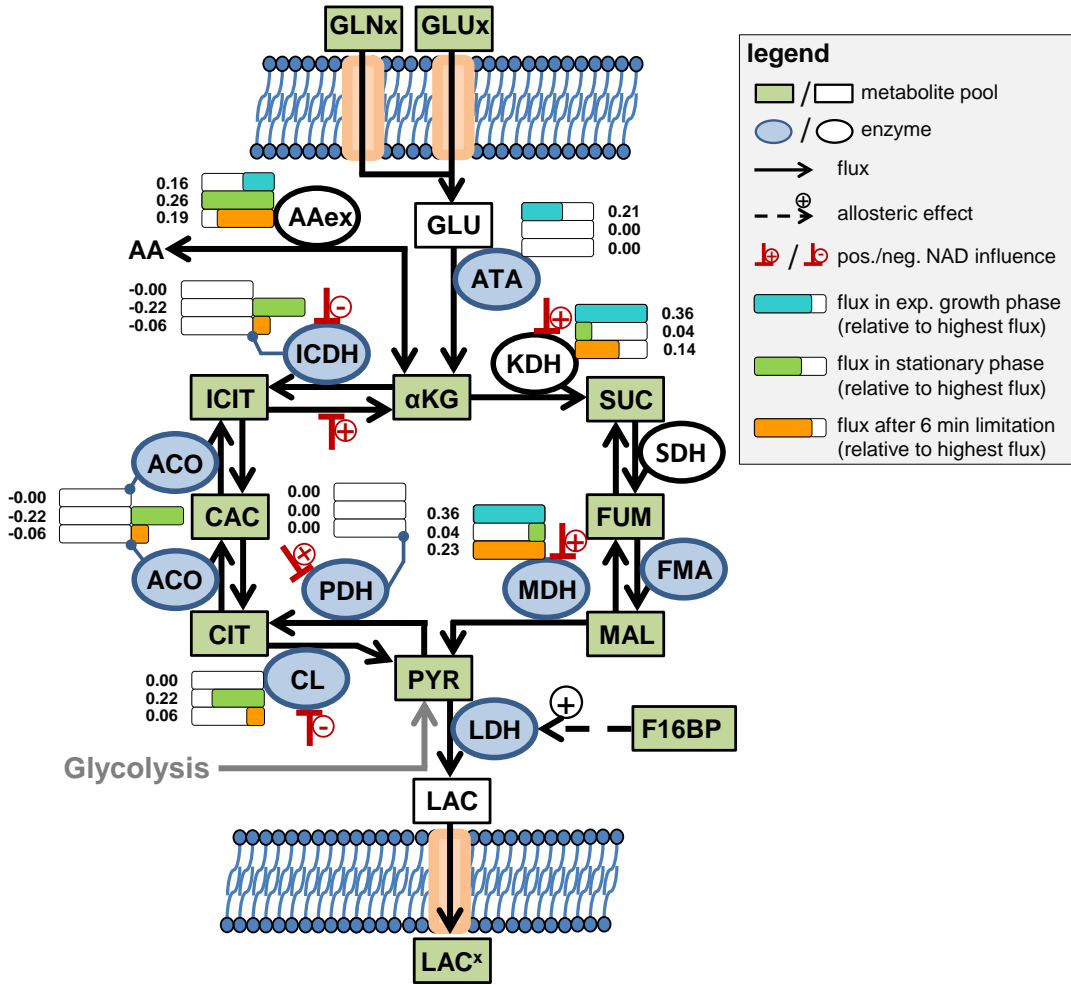


Figure 4.19.: Scheme of glutaminolysis model with calculated fluxes. Green boxes represent metabolite pools that were quantified experimentally, while white ones were not quantified. Enzymes are shown as ellipses with blue background if the maximum enzyme activity was measured *in vitro* and with white background otherwise. Reactions and their directions are shown as arrows. Dashed arrows represent allosteric regulation of enzymes by metabolites. Colored bars are attached to each reaction and express the relative flux compared to the largest flux in glutaminolysis (see legend, blue: cell growth at 24 h of Cult1; green: cell maintenance at 100 h of Cult1; orange: limitation after 6 min). Absolute flux rates (unit: mmol/L/min) are given next to the bars. Fluxes for LDH: 6.03/1.59/0.06 mmol/L/min. Abbreviations are: GLN^x extracellular glutamine; GLU^x extracellular glutamate; GLU glutamate; AA other amino acids; α KG α -ketoglutarate; SUC succinate; FUM fumarate; MAL malate; PYR pyruvate; F16BP fructose 1,6-bisphosphate; LAC lactate; LAC^x extracellular lactate; CIT citrate; CAC cis-aconitate; ICIT isocitrate; ATA aspartate/alanine transaminase; AAex exchange with other amino acids; KDH α -ketoglutarate dehydrogenase; SDH succinate dehydrogenase; FMA fumarase; MDH malate dehydrogenase; LDH lactate dehydrogenase; PDH pyruvate dehydrogenase; CL citrate lyase; ACO aconitase; ICDH isocitrate dehydrogenase.

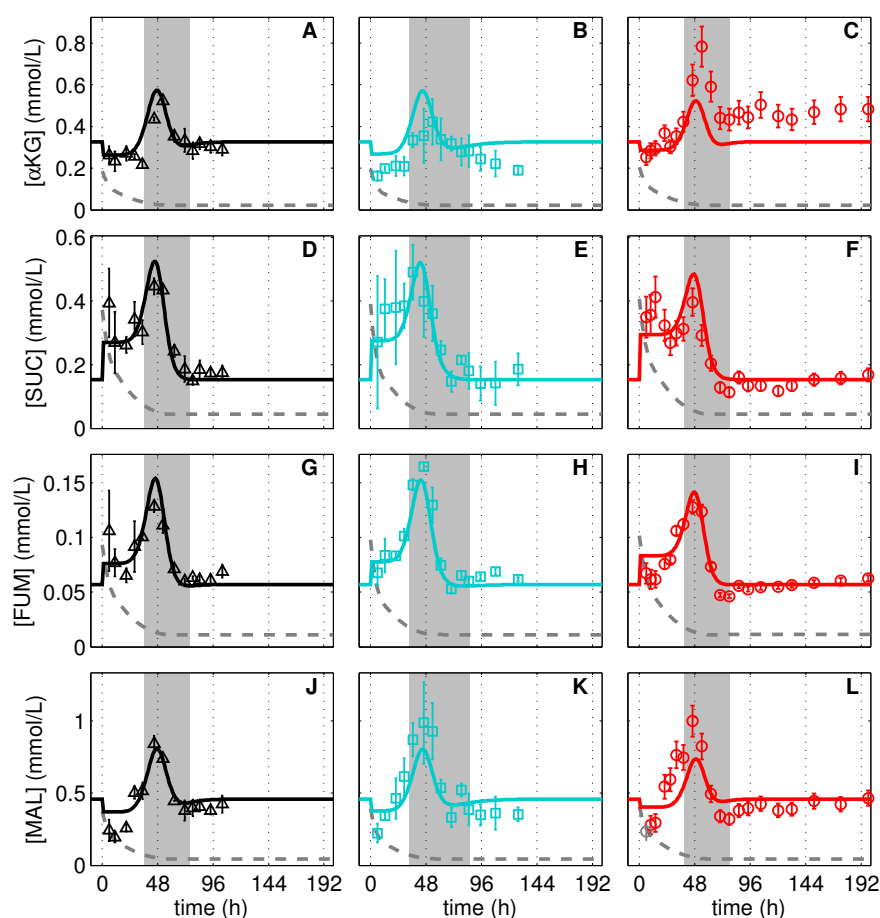


Figure 4.20.: Metabolite pools of lower citric acid cycle during adherent MDCK cell cultivation. α -Ketoglutarate (A – C), succinate (D – F), fumarate (G – I) and malate (J – L) concentrations in three independent MDCK cell cultivations (Δ , \square , \circ) in 6-well plates and GMEM-Z. Data and error bars represent mean and standard deviation of three wells and were taken from Ritter [23]. Dashed lines are the limit of quantification (LOQ; data below LOQ marked in gray). Lines represent the respective simulation result based on the experiment-specific parameters of Table C.1 and parameters of Table C.6. The intermediate growth phase of the cells is indicated as gray bar for the respective cultivation (b_{syn} in Table 4.2). Cells, originating from a cultivation experiment (see Table C.2) were deprived of extracellular nutrients by removal of medium and addition of phosphate buffered saline, shown in the first column (Lim1) and second column (Lim2).

remaining ones indicates two groups of differentially regulated enzymes. However, after one day of cultivation, all four metabolite pools exhibited a peak-like behavior during cell cultivation with a maximum around 48 h of cultivation, which is roughly one day later compared to the peak of glycolytic intermediates. The model suggests the peak to result from the onset of cell growth inhibition and the accompanying uptake of GLU^x

until depletion. The peak in metabolites is, thus, strongly correlated to the uptake rates shown in Fig. 4.9F. Differences in peak height and peak width can be observed among Cult1 – 3 experiments and are largely captured by the model (except for α KG). In the stationary growth phase, all four metabolite pools are constant although the uptake of GLN^x and GLU^x ceases. In the model, degradation of metabolite pools is reduced by inhibition (or lack of activation) of the enzyme group that converts α KG and MAL, which are KDH and MDH. The remaining cataplerotic activity in the lower citric acid cycle is compensated by the consumption of AA, which is representative for any other amino acid such as the branched chain amino acids leucine, isoleucine and valine. For the upper part of the citric acid cycle, Fig. 4.21 shows measured concentration

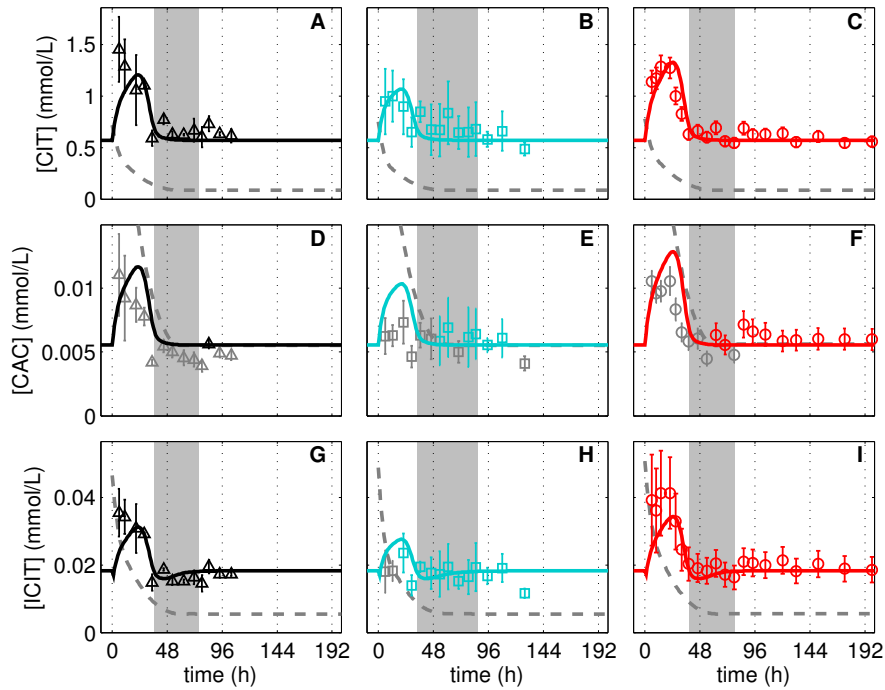


Figure 4.21.: Metabolite pools of upper citric acid cycle during adherent MDCK cell cultivation. Citrate (A – C), cis-aconitate (D – F) and isocitrate (G – I) concentrations in three independent MDCK cell cultivations (Δ , \square , \circ) in 6-well plates and GMEM-Z. Data and error bars represent mean and standard deviation of three wells and were taken from Ritter [23]. Cells, originating from a cultivation experiment (see Table C.2) were deprived of extracellular nutrients by removal of medium and addition of phosphate buffered saline, shown in the first column (Lim1) and second column (Lim2). Dashed lines are the limit of quantification (LOQ; data below LOQ marked in gray). Lines represent the respective simulation result based on the experiment-specific parameters of Table C.1 and parameters of Table C.6. The intermediate growth phase of the cells is indicated as gray bar for the respective cultivation (b_{syn} in Table 4.2).

time courses of CIT, CAC and ICIT that are initially high and increase until 24 h of cultivation (Fig. 4.21). The model suggests an increase in metabolite pools of the upper citric acid cycle until 24 h that largely fits the data. Thus, the upper and lower part of the citric acid cycle show different metabolite dynamics. Afterwards CIT, CAC and ICIT decrease and reach, in the stationary growth phase, the levels that were presumably present at the beginning of cultivation. Among the three cultivations, substantial experiment-specific differences can be observed (especially for experiment Cult2 (\square)). The model suggests that the increase in metabolite levels results from a reversed ICDH activity, which is described as an essential feature of fast proliferating cells to support cytosolic lipid synthesis [174] (Fig. 4.22). Interestingly, only model variants that incorporate a regulation of PDH, CL and ICDH by NAD or NADH were capable to reproduce the observed dynamics. The fact that neither PYR nor α KG, which are the two main substrates for the upper citric acid cycle, show dynamics that correspond to CIT or ICIT further strengthens the idea that this part of the cycle is influenced by other metabolites or cofactors, for example NAD and NADH.

Analysis of the simulated flux rates reveals an activity in the lower citric acid cycle during cell growth of about 0.37 mmol/L/min and in the upper part of 1.10×10^{-3} mmol/L/min (at 48 h, Fig. 4.19). At this stage of cultivation α KG, generated from glutaminolysis (r_{ATA}) and AA (r_{AAex} , Fig. 4.22A), takes mainly the lower citric acid cycle route (Fig. 4.22B). The upper citric acid cycle is, thus, solely fueled by small amounts of PYR (Fig. 4.22C) and its endproduct, CIT, is transferred to the cytosole. With onset of the cell growth inhibition the substrate supply of the citric acid cycle changes. Due to a lacking activation by NAD, the activity of the lower part reduces to 0.06 mmol/L/min and α KG

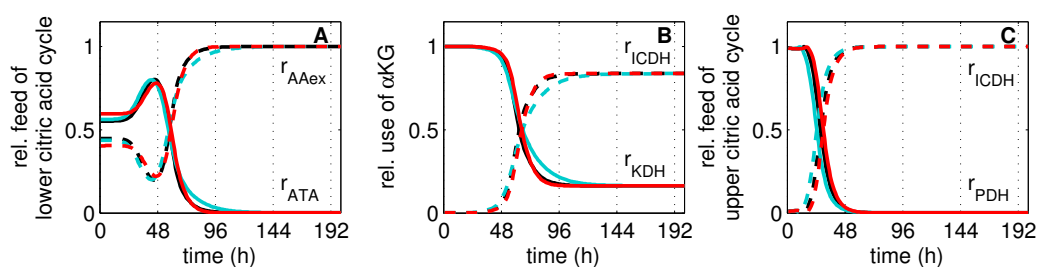


Figure 4.22.: Estimated supply and fluxes of the citric acid cycle during adherent MDCK cell cultivation. (A) Relative supply of citric acid cycle by GLN^x and GLU^x (r_{ATA}) and by other amino acids (r_{AAex}). (B) Relative use of α KG by ICDH and KDH. (C) Relative supply of upper citric acid cycle by ICDH and PDH. Lines are shown in the color code of Fig. 4.21.

generated from AA is transferred to the upper citric acid cycle under a reversed ICDH activity (0.21 mmol/L/min, 4.22B, C). The increasing contribution of α KG (r_{ICDH}) to the upper citric acid cycle exceeds the contribution of PYR (r_{PDH}) very early during cultivation (Fig. 4.22C). Taken together, the model suggests a flexible supply of the citric acid cycle depending on the growth phase and the availability of substrates. Furthermore, its operation is truncated as both parts are mostly independent of each other.

Response of citric acid cycle to substrate limitations and a substrate pulse:

The removal of medium and addition of PBS, which was realized in the model by setting the medium volume to 3×10^{-7} L (section 3.2.2), also limits the cell in GLN^x and GLU^x supply, which affects intermediates of glutaminolysis. We expected the corresponding metabolite pools to decrease over time but in a slower fashion compared to glycolysis. Inspecting the metabolite pool dynamics of the Lim1 experiment indeed shows a moderate overall decrease in metabolite pools but also unravels a peak shortly after the limitation in α KG, FUM and MAL that appears at different time of cultivation (Fig. 4.23A, G, J). In the Lim2 experiment, the peak is not observed and α KG, FUM and MAL simply decrease but more slowly than in the Lim1 experiment (Fig. 4.23B, H, K). The time series of SUC, however, differs from the other three metabolites as its level decreases until 2 min followed by an increase that is only observed for the Lim1 experiment (Fig. 4.23D – E). Furthermore, we again observe differences in the initial metabolite levels for the Lim1 and Lim2 experiment. The experimental data are, thus, to a certain degree unexpected, different between metabolites and specific for the actual experiments. Nonetheless, by considering that cells are taken from a certain time point t^* of cultivation explains most initial conditions. In addition, the model renders the experiment-specific decrease in metabolite pools, which is similarly affected by t^* (see Table C.2) and underlines the importance of considering the preculture of cells for analysis of metabolism. In the model, the supply of the lower citric acid cycle relies during substrate limitation upon the consumption of AA (0.15 mmol/L/min) and the degradation of remaining citric acid cycle intermediates (Fig. 4.19). In the pulse experiments, many data points are below the LOQ but a slow and steady increase in concentrations might be present and is also suggested by the model (Fig. 4.23C, F, I, L). In sum, the derived model may not appropriately resemble all features of the experimental data, especially for Lim1, but describes the main response of the lower citric acid cycle to substrate perturbations adequately, especially with respect to Lim2. The upper part of

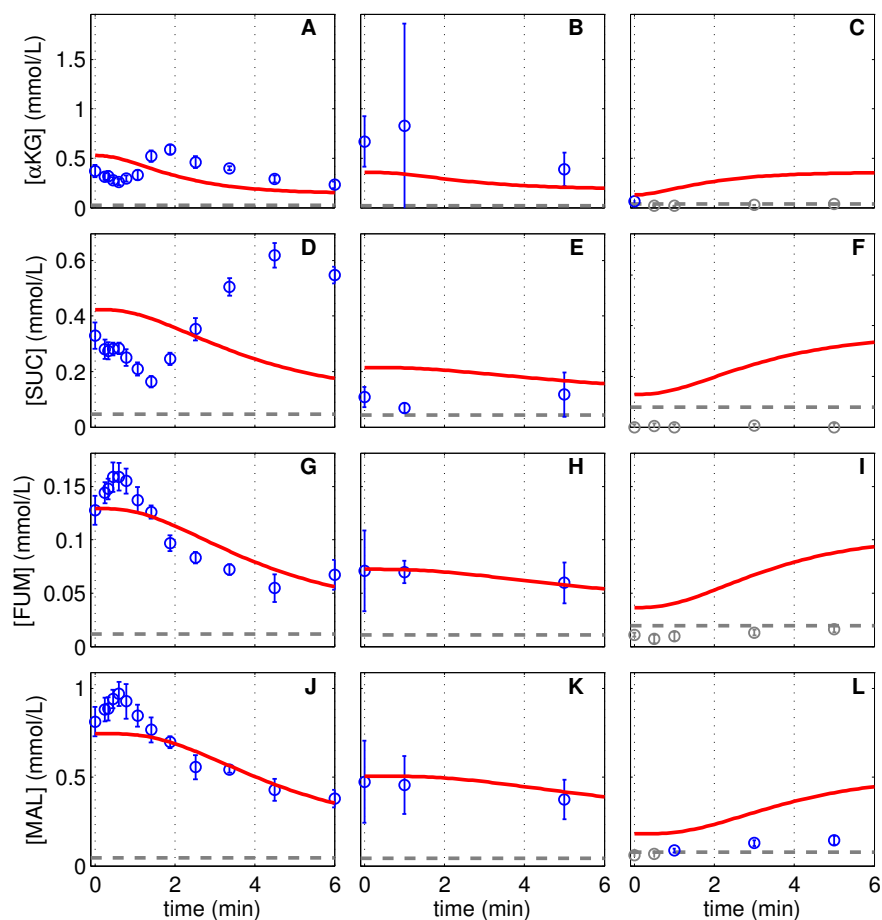


Figure 4.23.: Response of metabolite pools of lower citric acid cycle to substrate limitations and a substrate pulse. α -Ketoglutarate (A – C), succinate (D – F), fumarate (G – I) and malate (J – L) concentrations of three independent perturbation experiments with MDCK cells in 6-well plates. Cells, originating from a cultivation experiment (see Table C.2) were deprived of extracellular nutrients by removal of medium and addition of phosphate buffered saline, shown in the first column (Lim1) and second column (Lim2). In a similar experiment, cells were exposed to a 2 h limitation and afterwards PBS was exchanged by fresh medium, shown in the third column (Pulse). Data (\circ) and error bars represent mean and standard deviation of three wells and were taken from Ritter [23]. Dashed lines are the limit of quantification (LOQ; data below LOQ marked in gray). Lines represent the respective simulation result based on the experiment-specific parameters in Table C.2 and parameters in Table C.6.

the citric acid cycle is not directly dependent on the supply from extracellular substrates and shows a low activity in CL of about 0.06 mmol/L/min at 6 min after onset of the limitation (Fig. 4.19). It is, therefore, not surprising to find the simulation result of the corresponding metabolite pools to be less sensitive against a substrate depletion or

pulse (Fig. 4.24). After 3 min of substrate limitation, the concentrations for CIT, CAC and ICIT of the Lim1 experiment decrease, which is not captured by the model. In the Lim2 experiment, however, this decrease is less obvious and may equally well support a constant behavior if considering the error bars of the data and the LOQ (Fig. 4.24A, B, D, E, G, H). In contrast, a substrate pulse yields a significant increase in intracellular metabolite pools (Fig. 4.24C, F, I), which is also not captured by the model, to levels that are measured during cell cultivation. Taken together, the dynamics of the citric acid cycle are only partly resolved by the model when it comes either to a substrate limitation or a substrate pulse. Under both experimental conditions, the closely related metabolic pathways for conversion of amino acids may have a pronounced influence on the citric

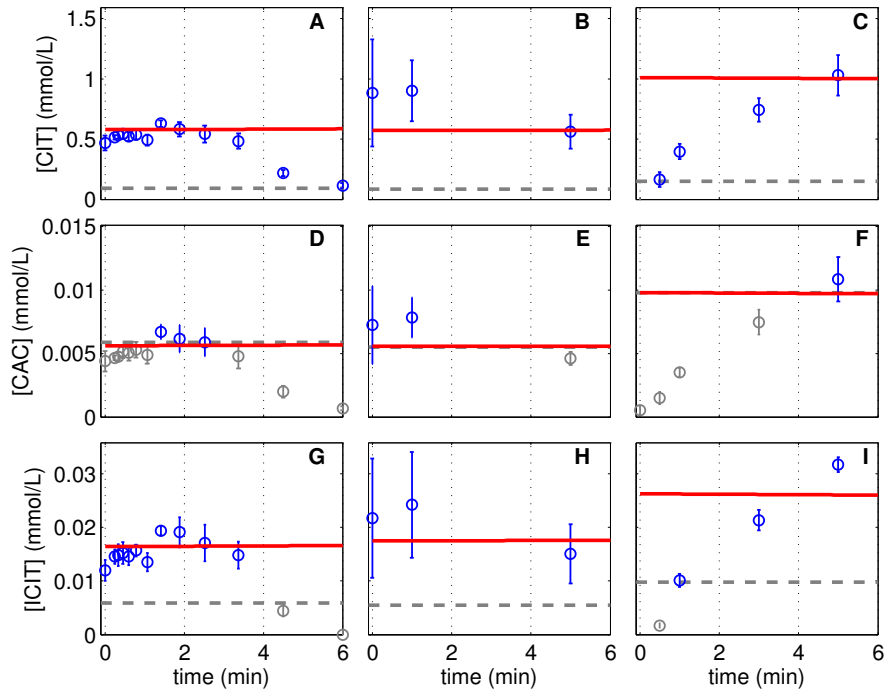


Figure 4.24.: Response of intracellular metabolite pools of upper citric acid cycle to substrate limitations and a substrate pulse. Citrate (A – C), cis-aconitate (D – F) and isocitrate (G – I) concentrations of three independent perturbation experiments with MDCK cells in 6-well plates. Cells, originating from a cultivation experiment (see Table C.2) were deprived of extracellular nutrients by removal of medium and addition of phosphate buffered saline, shown in the first column (Lim1) and second column (Lim2). After a 2 h limitation, PBS was exchanged by fresh medium, shown in the third column (Pulse). Data (\circ) and error bars represent mean and standard deviation of three wells and were taken from Ritter [23]. Dashed lines are the limit of quantification (LOQ; data below LOQ marked in gray). Red lines represent the respective simulation result based on the experiment-specific parameters in Table C.2 and parameters in Table C.6.

acid cycle. Especially the fast increase during the pulse experiment is unexpected.

Prediction for DMEM cultivation: For the prediction of a cultivation in DMEM medium with low initial GLC^x levels, we expected larger discrepancies between model simulation and data as the citric acid cycle is influenced by many source that are not considered by the model, especially, when it comes to a substrate limitation. After adjusting the segregated cell growth model (section A.2), the model prediction suggests generally higher metabolite pools than measured experimentally (Fig 4.25) and, thus, shows a certain error in quantitative aspects. However, the qualitative behavior is surprisingly consistent with the data (except of αKG). It seems that the simulated metabolite pool levels of SUC, FUM and MAL are simply by a factor of two higher than the measurements and than previous simulations for Cult1 – 3. The reason is that cells cultivated in the DMEM medium exhibited a doubled GLN^x consumption compared to the GMEM-Z medium ($Y_{X/\text{GLN}^x} = 5.92 \times 10^{-7}$, section A.2), while the intracellular metabolite pools are similar to Cult1 – 3. Either, the cells respond to the growth on GLU^x with a concerted increase in enzyme levels (e.g. $E_{level} = 2$) or the GLU^x decrease was measured

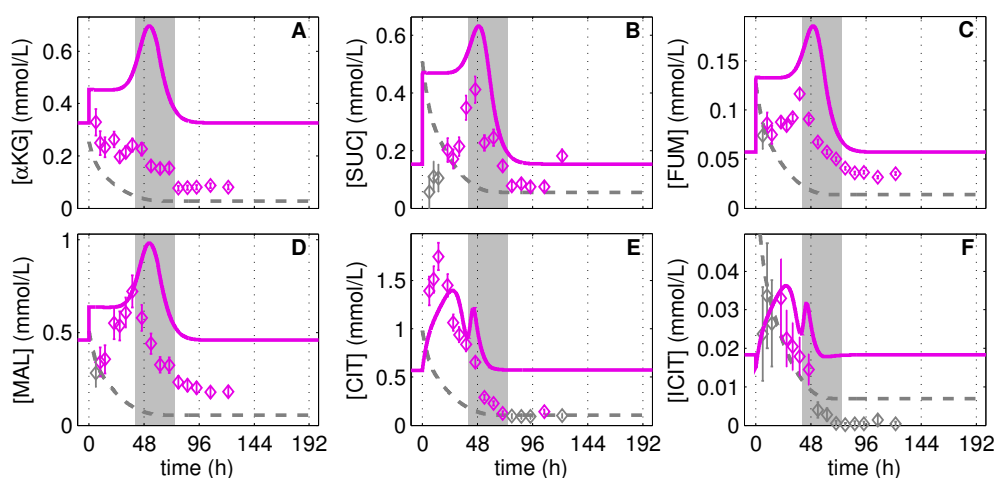


Figure 4.25.: Prediction for metabolite pools of the citric acid cycle during cultivation of adherent MDCK cells in DMEM with 2.5 mmol/L extracellular glucose. Data on α -ketoglutarate (A), succinate (B), fumarate (C), malate (D), citrate (E) and cis-aconitate (F) concentrations (\diamond) is depicted as mean and standard deviation of three wells and were taken from Ritter [23]. Dashed gray line is the limit of quantification (LOQ; data below LOQ marked in gray). Solid lines represent the model prediction based on the modifications of the cell growth model described in the appendix (section A.2) and the parameters in Table C.1 and Table C.6. The intermediate growth phase of the cells is indicated as gray bar for the respective cultivation (b_{syn}).

incorrectly (data inconsistencies). Both adjustments would allow the model to also predict the metabolite pools of the citric acid cycle quantitatively (simulation not shown). CIT and ICIT are predicted to show a two step decrease that partially fits the data although with a broader peak and higher levels during the stationary growth phase.

4.3.7. Pyruvate metabolism

The endproduct of glycolysis and glutaminolysis is PYR. It can also fuel the citric acid cycle and is linked to the amino acid metabolism. Thus, PYR connects these two main metabolic pathways. In the model, however, PYR is mainly degraded by an LDH-mediated reaction and only minor amounts enter the citric acid cycle. The flux through the LDH is activated by F16BP, which is a similar mechanisms as for the PK. Therefore, the substrates of both enzymes PYR and PEP show strong similarities in their dynamics during cell cultivation (Fig. 4.26A – C). During the substrate limitation, however, the measured dynamics in PYR levels decrease and are, thus, different to dynamics in PEP levels although the same regulatory principles are assumed for the

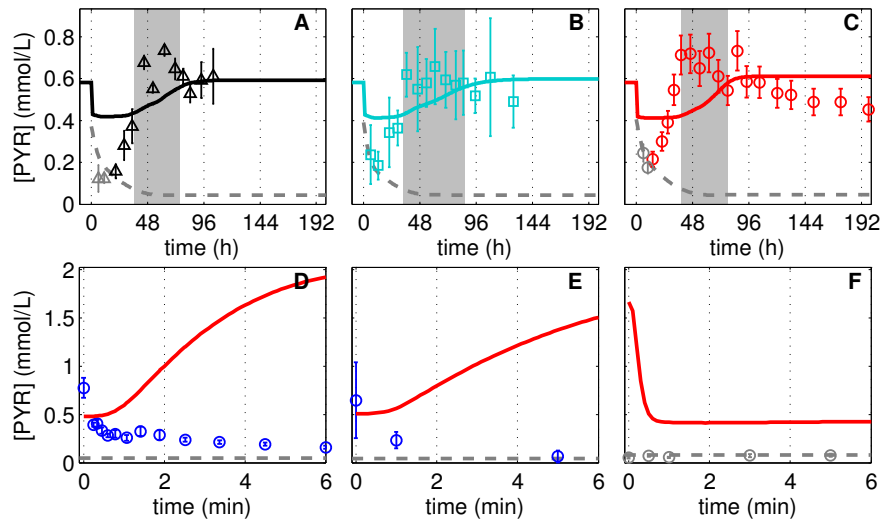


Figure 4.26.: Pyruvate levels during cell cultivation, substrate limitation and substrate pulse. Each single plot illustrates an independent experiment. (A – C) Cultivation of MDCK cells in 6-well plates and GMEM-Z. (D, E) Substrate limitation. (F) Substrate pulse. Data (Δ , \square , \circ , \circ), which are depicted as mean and standard deviation of three wells, were taken from Ritter [23]. Dashed lines are the limit of quantification (LOQ; data below LOQ marked in gray). Lines represent the model simulation based on the parameters in Table C.1, Table C.2, and Table C.6. The intermediate growth phase of the cells in (A – C) is indicated as gray bar for the respective cultivation (b_{syn} in Table 4.2).

model. Thus, the model cannot explain the PYR dynamics during the substrate limitation experiments. During the pulse experiment, the levels of PYR remain below the limit of quantification, which is also different compared to PEP and not captured by the model. It may indicate that PYR is also part of other metabolic pathways that are not considered by the model, for example the amino acid metabolism for which data is not yet available. Nonetheless, the flux through the LDH satisfies the measured LAC^x accumulation (Fig. 4.27A) indicating a basic agreement of the model with the actual flux rate from PYR to LAC. The accumulation fits the data and is also similar to the release inferred from the segregated cell growth model (Fig. 4.8D). Thus, the LDH is the main PYR degrading enzyme. Furthermore, metabolic fluxes from glycolysis into the PPP and glycogenesis are compensated by the production of PYR from glutaminolysis via a truncated citric acid cycle. The resulting, time-dependent Y_{LAC^x/GLC^x} is close to the theoretical maximum of 2.0 during the growth phase and increases to surprising 2.4 for the stationary growth phase (Fig. 4.27B). Note that Y_{LAC^x/GLC^x} is only slightly influenced by changes in the PDH activity (Fig. 4.27C). Thus, the time-dependent Y_{LAC^x/GLC^x} is rather shaped by a flexible use of amino acids in the citric acid cycle and of sugar metabolites in the PPP than by the PDH activity. In consequence, the Y_{LAC^x/GLC^x} may not be an adequate measure for cellular "efficiency" in converting GLC to ATP, although widely used in literature.

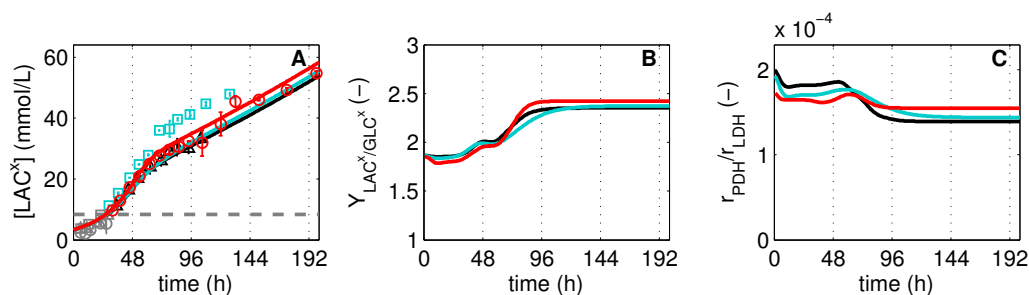


Figure 4.27.: Use of pyruvate during MDCK cell cultivation. (A) Accumulation of extracellular lactate during MDCK cell growth in 6-well plates with cell growth medium (GMEM-Z). Data (Δ , \square , \circ) and error bars, which represent mean and standard deviation of three wells, were taken from Fig. 4.8. Grey dashed line is the limit of quantification (LOQ; data below LOQ marked in gray). (B) Dynamic glucose-specific lactate yield based on the structured central carbon metabolism model. (C) Relative pyruvate dehydrogenase activity. Model simulations (based on parameters of Table C.1, Table C.5 and Table C.6) are shown in the color code of Figure 4.26.

4.3.8. Sensitivity analysis for glutaminolysis

In analogy to glycolysis, we also evaluated the impact of model parameters (Table C.6, C.4) and initial conditions, which take into account culture condition, the growth status, and the metabolic status (Table C.2), on the model behavior. The relative local sensitivity analysis, shown in Fig. 4.28, has many similarities to Fig. 4.18 and its interpretation is, as before, based on the height of values relative to each other and not on absolute numbers. Again, the model behavior during the cultivation experiments is mainly determined by the parameters for growth and metabolism and to a certain extent by the initial growth status of the cells used for inoculation. However, when it comes

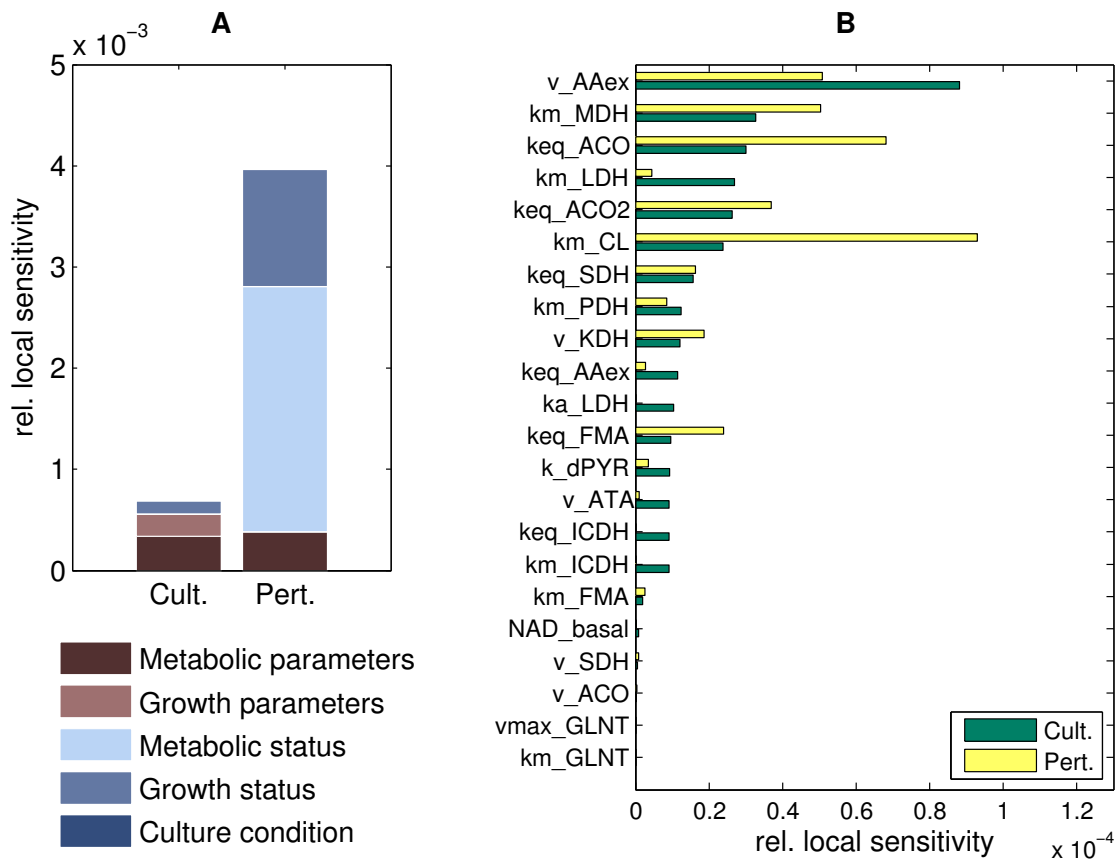


Figure 4.28.: Parameter sensitivity analysis of the structured model of glutaminolysis. (A) Relative local sensitivity of model simulations (for cultivation and perturbation experiments) to a 1% perturbation in glutaminolysis parameters (Table C.6), parameters of the segregated cell growth model (Table C.4), culture conditions, growth status and metabolic status (Table C.2). (B) Relative local sensitivity of model simulations (for cultivation and perturbation experiments) to a 1% perturbation of single glutaminolysis parameter.

to a limitation in substrates the behavior of the model strongly depends on the actual metabolic status and growth status that was present at time of perturbation. The first implication is that the preculture of cells has a large impact on intracellular metabolite pool dynamics. The second is that the sensitivity of glutaminolysis shifts, similarly to glycolysis, with the experimental scenario. Analysis of glutaminolysis parameters reveals that, apart from the GLNT, all enzyme kinetics have a certain influence on the overall network activity. The GLNT is unidentifiable due to multiplication with γ_{GLNT} (Eq. (3.1.89)).

4.3.9. Energy metabolism

Several reaction steps of the central carbon metabolism fulfill the essential function to provide the cell with energy, which is stored as ATP. To our surprise, none of these reactions in the model needed an influence by ADP or ATP. We consequently assumed that the energy state of the cell is rather a result than a regulator of the metabolic activity, at least for the scenarios analyzed in this work. Thus, our modeling implies that biosynthetic processes control the level of ATP, similarly to enzymes that control the level

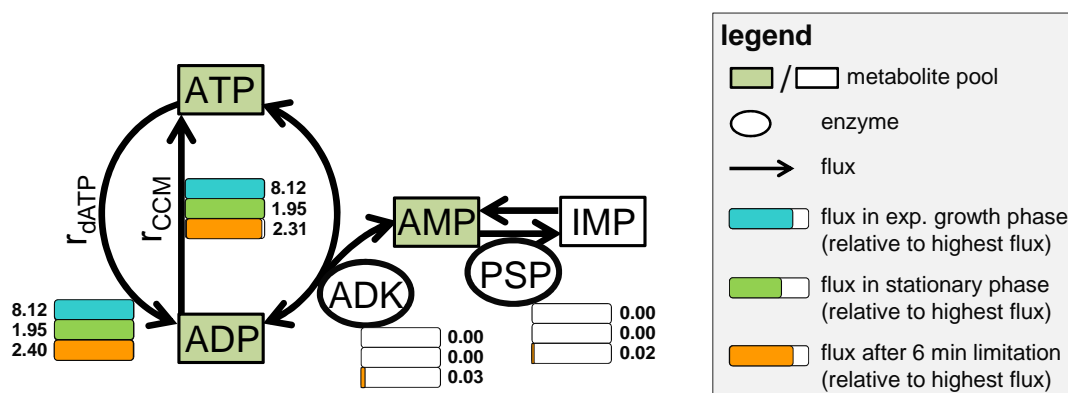


Figure 4.29.: Scheme of energy metabolism model with calculated fluxes. Green boxes represent metabolite pools that were quantified experimentally, while white ones were not measured. Enzymes are shown as ellipses. Reactions and their directions are shown as arrows. Colored bars are attached to each reaction and express the relative flux compared to the largest activity in the energy metabolism (see legend, blue: cell growth at 24 h of Cult1; green: cell maintenance at 100 h of Cult1; orange: limitation after 6 min). Absolute flux rates (unit: mmol/L/min) are given next to the bars. ATP adenosine triphosphate; ADP adenosine diphosphate; AMP adenosine monophosphate; IMP inosine monophosphate; r_{dATP} degradation of ATP by growth and maintenance; r_{CCM} generation of ATP by glycolysis and citric acid cycle; ADK adenylate kinase; PSP purine salvage pathway.

of their substrates [131]. To test whether this hypothesis explains the measured dynamics in adenosine-based nucleotides, we combined the central carbon metabolism model with a macroscopic biosynthetic process that consumes ATP. In the following, we evaluate whether the dynamics of adenosine-based nucleotides can be reproduced during batch cultivation and afterwards conclude on the energy production of the cell. The model also considers the interconversion of the adenosine-based nucleotides as well as the exchange of AMP with the PSP [197]. A schematic overview of considered enzyme reactions, metabolite pools and maximum *in vitro* enzyme activities of the energy metabolism is given in Fig. 4.29.

Nucleotide pool dynamics and fluxes during cell cultivation: As already observed at the beginning of this work (section 4.1), the ATP levels show a negative peak during cell growth and remains constantly high during the stationary growth phase, which is similarly described by the model (Fig. 4.30A – C). In experiment Cult3 (○), a slight overshoot in the intermediate growth phase is observed and also rendered by the model. The pool dynamics of ADP and AMP are negatively correlated to ATP, while the overall decrease in ATP levels exceeds the increase in ADP and AMP levels (the energy charge is depicted in Fig. 4.1I). The model is capable to explain these dynamics by considering that AMP is converted to IMP, which is part of the PSP. For ADP, we observe a rather noisy time course compared to ATP and not all data points are covered by the model (Fig. 4.30D – F). In case of AMP the model shows a reduced peak height compared to the data (Fig. 4.30G – I). The corresponding production rates for ATP by glycolysis and the citric acid cycle are shown in Figure 4.31A. The model suggests, that MDCK cells generate 7 – 10 mmol/L/min ATP during the growth phase with a significantly larger contribution by glycolysis compared to the citric acid cycle. Note that the time course of the ATP generation mainly follows the uptake rate of GLC^x in case of glycolytic ATP production, and of GLN^x and GLU^x in case of mitochondrial ATP production (cf. Fig. 4.9). In the intermediate growth phase, the ATP generation by glycolysis decreases while the generation by the mitochondrion peaks such that both reach an almost equal contribution. In the stationary growth phase, the central carbon metabolism delivers a total ATP production rate of 2 mmol/L/min where glycolysis is again the main source. The consumption of ATP is not separately shown but the model suggests that ATP is mainly consumed by the macroscopic biosynthetic process ($r_{X/ATP}$) and by futile cycles (r_{ATPase}), which is in line with the analysis of Wahl et al. [15]. The generation of ATP from ADP by oxidative phosphorylation is driven by a

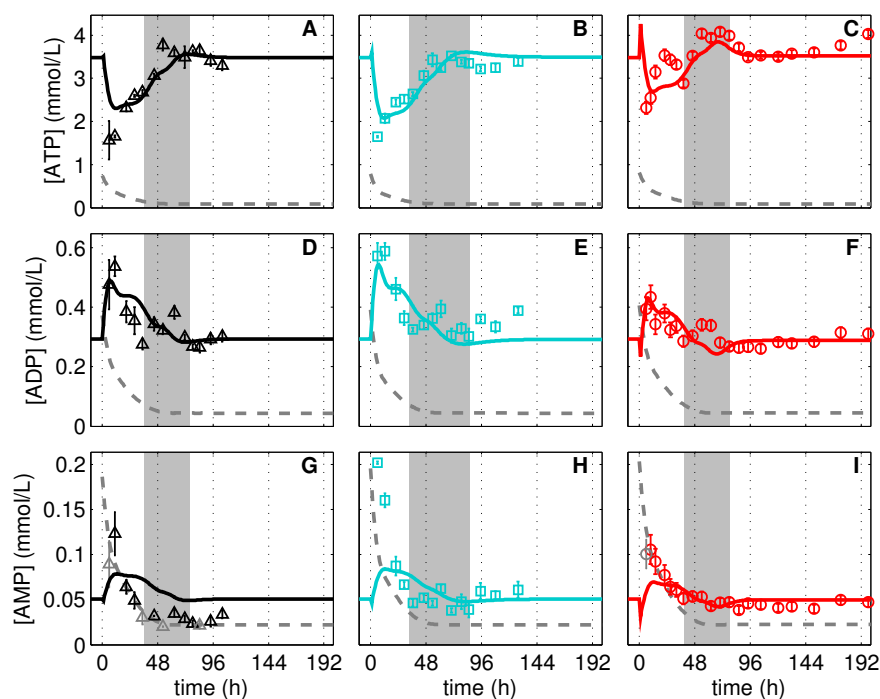


Figure 4.30.: Adenosine-based nucleotide pools during adherent MDCK cell cultivation. ATP (A – C), ADP (D – F) and AMP (G – I) concentrations in three independent MDCK cell cultivations (Cult1 Δ , Cult2 \square , Cult3 \circ) in 6-well plates and GMEM-Z. Data and error bars represent mean and standard deviation of three wells and were taken from Ritter [23]. Dashed lines are the limit of quantification (LOQ; data below LOQ marked in gray). Lines represent the respective simulation result based on the experiment-specific parameters in Table C.2 and parameters in Table C.6. The intermediate growth phase of the cells is indicated as gray bar for the respective cultivation (b_{syn} in Table 4.2).

proton gradient, which is established by oxidation of NADH with O_2 . The resulting mitochondrial consumption of O_2 varies with time (Fig. 4.31B) and follows the time course of the mitochondrial ATP production rate shown in Fig. 4.31A (dashed line). The cell-number-specific consumption of 22 – 168 fmol/cell/h covers the values reported by Wahl et al. [15] (48 fmol/cell/h) and by Bock [316] (70 fmol/cell/h).

4.3.10. Model performance

In the former sections, we comprehensively analyzed simulated and measured metabolite pool dynamics and inferred regulation principles for the central carbon metabolism. Although a systems-level analysis provides valuable insights into the interplay of biological mechanisms, the resulting complexity in data fits may not reveal the actual model performance. Therefore, we analyzed the correlation between simulations and experimental

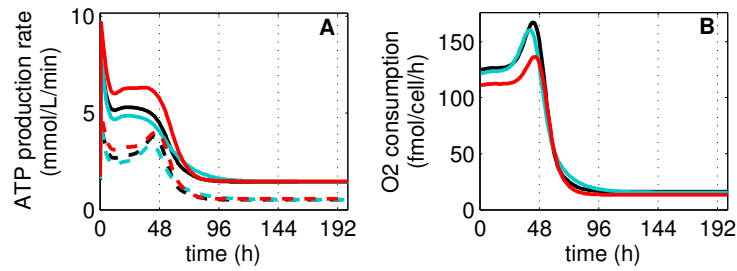


Figure 4.31.: Production of ATP and demand for O_2 during adherent MDCK cell cultivation. (A) Theoretical production rates of ATP by glycolysis (solid lines) and by the citric acid cycle (dashed lines). (B) Theoretical specific oxygen consumption rate (Eq. (3.1.82)). Lines are shown in the color code of Fig. 4.30.

measurements for all model fits (Fig. 4.32A), which is an accepted way to evaluate a model performance [252], and determined a linear correlation coefficient of 0.95 for the glycolysis model and of 0.77 for the glutaminolysis model. For both models, a deviation

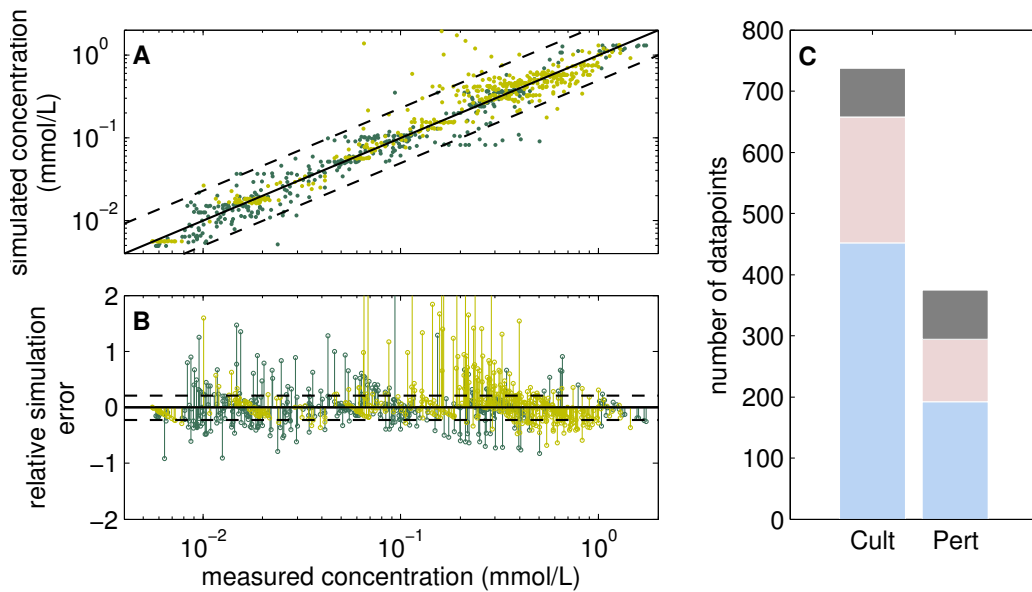


Figure 4.32.: Statistical analysis of structured model performance. (A) Correlation between simulated and measured metabolite concentrations of this chapter. The glycolysis model is marked in green, the glutaminolysis model is marked in yellow. Black line represents ideal correlation and dashed black lines contain 95 % of the dots. (B) Relative distance between simulation and data. Dashed lines show mean relative error. (C) Overview of fitted (light blue, simulation within 95 % confidence interval of data), not fitted (light red, simulation outside 95 % confidence interval of data) and omitted data (gray) for cultivation and perturbation experiments.

of about 0.5-fold to 2.0-fold from the nominal simulation value covers 95 % of the data points (dashed lines Fig. 4.32A; glycolysis: 0.4 – 1.9; glutaminolysis: 0.6 – 2.6). The relative error is homogeneously distributed and in mean ± 21 % between both models and the data (Fig. 4.32B). Under consideration of the data error, which is exceptionally small for many measurements, 70 % of the data is covered by the model when considering two times the standard deviation (Fig. 4.32C). Note that data points below the LOQ were excluded from the analysis.

4.3.11. Discussion part II

Glutaminolysis model structure: Similarly to glycolysis, we coupled the segregated model for cell growth to a kinetic description of glutaminolysis to reflect intracellular metabolite pool dynamics during cell cultivation, medium depletion and medium pulse involving a total of 600 data points. The simulation of the different experiments considers the preculture of cells (already discussed for the structured model of glycolysis) and, thus, initial conditions were not estimated but calculated by the model leading to only 20 unknown parameters (Table C.6). Another feature of the model is the consideration of the relative biosynthesis rate b_{syn} , which reflects the demand of the cell for energy and precursors. In particular, b_{syn} influences the degradation of citric acid cycle intermediates and ATP. Using such macroscopic functions enables the model to consider the influence of complex cellular processes on metabolic pathways. In case of the citric acid cycle, the enzymatic reactions that required regulation by b_{syn} or $(1 - b_{syn})$ use NAD or NADH as cofactors, respectively. Thus, the model implicitly suggests that oxidative phosphorylation has substantial control over the citric acid cycle, which is also proposed by Dalmonte et al. [183] and Rodríguez-Enríquez et al. [182]. However, the coupling to the segregated cell growth model allowed dealing with many more mechanisms that are not explicitly considered such as the control of the glutamate transporter by cell growth inhibition or the NH_4 metabolism (see next section). Furthermore, modeling cell growth and the cell-specific volume V_S^C introduces the option to calculate the dilution of metabolites and enzymes, which can influence the conversion rate within the reaction pathways (see section 3.1.3). For the structured model of glutaminolysis, we chose relatively simple, compartment-unspecific enzyme kinetics to derive a reasonable set of differential equations that focus on key regulatory mechanisms of that pathway. Similarly to the kinetic description of glycolysis, the model for glutaminolysis features the identification of mechanisms that are involved in metabolite pool dynamics and provides a basis for the extension by additional mechanisms, e.g. the oxidative phosphorylation

[251], the influence of cofactors such as GTP and FAD or the compartmentalization of the cell [248], in case further data is available. Models that take into account further, unmeasured metabolites or more complex enzyme reactions than used here may equally well describe the dynamics of the intracellular metabolite pools of this study.

Ammonia release from glutamine and glutamate: The release of NH_4^x was described by a maximum stoichiometric production from GLN^x and GLU^x minus a certain amount that is bound in molecules and used for biosynthesis. We already highlighted that the yield of NH_4^x from GLN^x is roughly 0.8 and that GLU^x does not contribute to the NH_4^x release (section 4.2.2). The metabolic explanation is that GLU is primarily processed via the transamination route without production of free NH_4 . A high transaminase activity is indeed found in MDCK cells [22, 170] and supports our hypothesis. Since accumulation of NH_4^x in the medium can have a negative impact on cell growth and product formation [54], cultivation processes with high NH_4^x levels may benefit from medium adaptation [54, 173] or a modulation of the cellular transporters in favor of GLU^x uptake. However, it requires the cell to have a certain glutaminase activity. For MDCK cells, a sufficient glutaminase activity is indeed present [22] and a switch to GLN^x -free medium was successfully tested as cultivation strategy [14].

Amino acid uptake controls glutaminolysis during cell growth: Since cells from stationary growth phase were used for inoculation of a new well, we hypothesized that initial metabolite levels ($t = 0$) are identical to levels of the stationary growth phase. With the start of cultivation, the model suggests for SUC and FUM a fast increase in concentration that is attributed to the uptake of GLN^x and AA. For MDCK cells, the uptake of branched chain amino acids is commonly observed [15] and a contribution of AA to citric acid cycle intermediates of 40 % (Fig 4.19) is in the range reported for cancer cells [148]. The uptake of GLN^x (perhaps also in AA) yields early ($t > 6$ min) intracellular levels of SUC and FUM that are higher than levels during stationary growth phase. For αKG and MAL the opposite is observed and indicates that the degrading enzymes KDH and MDH are activated between 0 h and 6 h of cultivation. The model suggests that the inhibition of both enzymes by b_{NAD} is released with onset of growth, which may imply a certain influence by NAD. With beginning of the intermediate growth phase, a peak-like behavior is observed for αKG , SUC, FUM and MAL and is, in the model, driven by a high GLU^x uptake. Thus, metabolite pools of the lower citric acid cycle are largely controlled by the growth-dependent uptake of GLN^x , GLU^x , and presumably

AA. To illustrate the link between uptake of extracellular substrates and intracellular metabolite dynamics, which was also found for glycolysis (see section 4.3.5), Fig. 4.33 provides a schematic overview on main central carbon metabolism dynamics, on their linkage and on uptake of substrates (GLC^x , GLN^x , GLU^x) as well as release of byproducts (LAC^x). With onset of the stationary growth phase and a limited supply by GLN^x and GLU^x , the control changes towards mechanisms that maintain intracellular metabolite pools and avoid unnecessary dissipation of biomass precursors. Firstly the

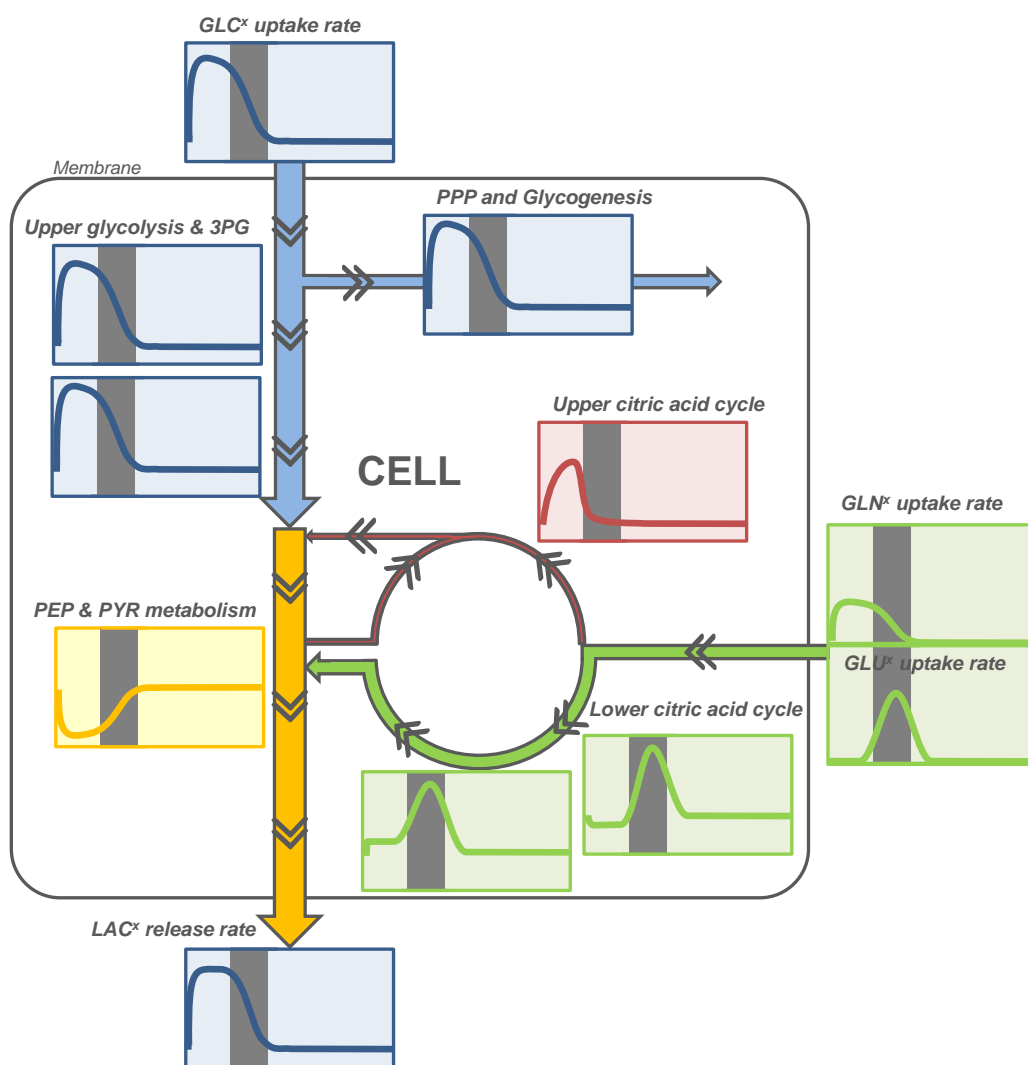


Figure 4.33.: Scheme of central carbon metabolism dynamics during cell cultivation. Arrows and thickness of arrows indicate the relative flux distribution. Metabolite pool dynamics in different parts of the metabolic network are depicted by representative, schematic figures and grouped by color code. Light gray bar illustrates the intermediate growth phase.

inhibition of key enzymes by b_{NAD} becomes significant and, secondly, the breakdown of AA seems to compensate for cataplerotic effects. We, therefore, anticipate that the regulation of enzymes through NAD can reduce the citric acid cycle activity and may pose an intrinsic mechanism to stabilize intracellular concentrations of metabolic intermediates when specific substrates are depleted to critical levels. It seems that seeding of cells into a new well with sufficient growth surface and high substrate levels releases this inhibition to support biosynthesis and cellular energy generation. Yuneva and coworker [300] found a reduction in citric acid cycle intermediates upon limitation in GLN^x , which indicates its role as main substrate, and, most interestingly, reported on MYC-mediated apoptosis if citric acid cycle metabolite drop to low levels. The regulation of the citric acid cycle by NAD is also well documented [182, 183] and an inhibition of the lower citric acid cycle by low NAD levels at late stages of cultivation seems reasonable since ATP levels are at maximum (see section 4.3.9). High ATP levels presumably block oxidative phosphorylation [251] and can yield high intracellular NADH and low NAD levels.

Applying the influence of b_{NAD} consistently to the upper citric acid cycle allowed the model explaining the measured pool dynamics in CIT, CAC and ICIT. A regulation of the upper citric acid cycle is also supported by the observation that metabolite levels differ significantly from PYR and α KG, which are the main substrates for this part of the cycle. However, the actual dynamics show larger variations between the cultivations, which, according to the model, are attributed to differences in cell growth in the presence of low pathway activities. Furthermore, the supply of the upper citric acid cycle seems to change from PYR to α KG with progression in cultivation time indicating a certain flexibility in pathway operation. The products of both citric acid cycle branches eventually fuel the PYR pool under the production of either cytosolic NADPH or cellular energy and, thus, the model reflects a truncation in the cycle [121, 150]. The subsequent degradation of PYR by LDH is activated by F16BP, which yields dynamics that are similar to PEP and that largely suit the cultivation data. We subsequently analyzed whether the activity of glutaminolysis and glycolysis constitute the measured LAC^x production. The simulation is in good agreement for all three cultivations and, thus, strengthens our confidence in the estimated flux distributions. At this point, we can infer the dynamic efficiency in glucose conversion that was previously defined as Y_{LAC^x/GLC^x} . In contrast to the segregated cell growth model, Y_{LAC^x/GLC^x} now varies with cultivation time (also found by Dean and Reddy [13]) between 1.8 and 2.4 and is not a result of a varying contribution of PYR to the citric acid cycle ($< 1\%$) but rather of glutaminolysis to PYR production, which is an aspect that is frequently overseen in

the analysis of mammalian cell cultures.

Glutaminolysis during substrate perturbation: At distinct time points t^* of cultivation, the medium was replaced by PBS and decreasing metabolite pools were measured in the citric acid cycle. For glycolysis, choosing a distinct t^* for each perturbation experiment explains differences in the initial metabolite levels. Using the same t^* as for glycolysis allows the model to also successfully render the starting concentrations of the citric acid cycle (no adjustments necessary). It seems that considering the preculture of cells consistently reproduced the initial metabolic status of glycolysis and glutaminolysis at the beginning of the perturbation experiments.

During the time course of the limitation experiments, however, metabolite pools of the lower part of the cycle show a peak that emerges at different times of cultivation, which cannot be explained with a regulation of the connecting enzymes. Rather, each metabolite is influenced by separate metabolic pathways and by the involved amino acid pools. In line with this hypothesis, the model suggests a significant supply from AA during the substrate limitation scenario. Taken together, the data and the model indicate that the associated metabolism exerts a significant influence on the lower citric acid cycle if its activity is low, which is similarly found for the PPP during the limitation experiments. Nonetheless, the model describes the overall degradation of α KG, SUC, FUM, and MAL sufficiently well, especially for the Lim2 experiment. Further measurements on the closely related metabolic pathways may help to also clarify the reason for the measured peaks. With the addition of fresh medium, a pulse in GLN^x and GLU^x is applied that leads in the model to slow but steady reactivation of the lower citric acid cycle. The data, however, shows very low levels for all four metabolites at all time points. Since cells are capable of growth after the limitation and pulse experiments, the citric acid cycle might be activated at later times or in a different mode, which the model cannot yet explain. Currently, the model simply suggests that the citric acid cycle returns to the metabolic status that was present before the perturbation experiments.

In the upper part of the cycle, the measured metabolite pools are mainly constant during the limitation experiments, perhaps with a slight decrease towards later time points. The model suggests very low activities and the resulting straight line captures most of the data. During the pulse experiment, the concentrations for the metabolite pools increase significantly from these low levels, which is in contrast to the lower part of the cycle. Obviously, a substrate pulse to the citric acid cycle offers a puzzle that cannot yet be solved by the developed model. The discrepancy to the data is perhaps linked

to the difficulties in fitting PYR during the pulse experiments. We defined the LDH to be the main degrading enzyme for PYR, which is activated by F16BP. Instead of an increase in concentration due to decreasing F16BP levels, PYR drops fast to low levels, which the model cannot explain. It may indicate that the closely related metabolic pathways have a certain influence on PYR under these experimental conditions. Taken together, during the pulse experiment and especially when the pathway activities are low, parts of the metabolism, which are not considered in this work, play a pronounced role, such as metabolism of amino acids, compartmentalization and ion fluxes across the compartment membrane. When the citric acid cycle is operated with higher flux rates, the metabolite pools are robustly controlled by a few key mechanisms [122] and can, thus, be described with a facilitated amino acid uptake and an NAD-based regulation of enzymes.

Estimations and predictions for the operation of glutaminolysis: Since the functioning of glutaminolysis is only partly understood when it comes to short term responses upon substrate perturbations, the model-based estimations of this work focus only on standard cell cultivation conditions. The predictive power of the model for these conditions is appreciable considering that the two-fold higher levels in citric acid cycle metabolites may result from data inconsistencies or changes in the enzyme level. For bioprocessing, we anticipate that increasing the GLU^x uptake may enhance ATP production but, more importantly, may also enhance the lipid-synthesis from MAL-derived NADPH, which might effect μ_{max} in a positive way. Furthermore, a shift towards higher lipid synthesis might be important for the production of enveloped viruses [297]. Measurements for the maximum *in vitro* enzyme activities of FMA and MDH indicate a significant additional capacity for metabolite conversion [22] such that an enhanced glutaminolysis activity is not limited by these enzymes.

The control of the energy metabolism: The kinetic description for the citric acid cycle uses a combination of enzyme metabolite interactions and growth-dependent functions to describe the degradation of metabolite pools. Such macroscopic functions represent hierarchical regulation mechanisms and can influence the metabolic activity independent from the abundance of intracellular metabolites. For modeling the energy metabolism, we again used growth-dependent functions to account for the use of ATP in biosynthetic reactions. Together with enzyme metabolite interactions, the model successfully describes the pool dynamics in ATP, ADP, and AMP during cell cultivation

using 10 parameters and 3 initial conditions. Since the model for glutaminolysis struggled with describing all dynamics observed during the perturbation experiments, the model for the energy metabolism is not fitted to corresponding data and not used for predictions. Nonetheless, it contributes to the analysis of *in vivo* nucleotide pool dynamics of mammalian cells and offers a fit that is similar or better than for yeast cells [199]. The estimated flux rates through glycolysis and the citric acid cycle constitute a maximum production rate of 10 mmol/L/min. The model suggests that glycolysis provides the majority of ATP in adherent MDCK cells, which fits to our observations of a partial oxidation of glutamine and high lactate secretion rates, and is also reported in literature [58, 89, 121, 150]. A higher ATP production by glycolysis compared to the citric acid cycle is also proposed by Wahl et al. [15] using metabolic flux analysis. Another question is how metabolism, biosynthesis and the energy level influence each other. Since the energy producing steps are found in the last sections to be independent of the actual energy level, hypotheses on a demand-driven energy metabolism [193] or on the control of enzymes by ATP levels [194, 195] are not supported by the model. The explanation is that a control of enzymes by ATP on the one hand interrupts concerted changes in metabolite pools, e.g. upper glycolysis, and on the other yields a constant time course for ATP, which both is not observed in our data (Fig. 4.34A). In a demand-driven control, intracellular metabolite pools decrease in response to cell growth and eventually induce the uptake of substrates. However, decreasing metabolite pools for the cell growth phase are neither observed for glycolysis nor for the citric acid cycle (Fig. 4.34B). Also a control by extracellular nutrient levels, which is suggested by Dean and Reddy [13] and Barnabé and Butler [78], is not observed during cell cultivation and may only occur under substrate limiting conditions. Furthermore, the ATP levels can sustain a substrate limitation for at least 2 h of medium depletion (see Appendix B.2 Fig. B.1 and [23]). Thus, the only hypothesis remaining and supported by the model is that metabolism generates ATP irrespective of its actual level, which is also suggested by Soboll et al. [200], while the level of ATP is shaped by the biosynthesis activity. Note that continuously proliferating cells may never be limited in the ATP supply, which is implicitly found for tumor cells by Schmidt et al. [198] and reviewed by Vander Heiden et al. [61]. Furthermore, the observation of a decreasing ATP level in the presence of increasing metabolite pools indicates that biosynthesis is rather driven by the precursor supply, which may initially consume more ATP than provided by metabolism. At later stages of cultivation, cells are more and more inhibited in cell growth and the overproduction in ATP by metabolism slowly restores the pool. Taken together, our hypothesis

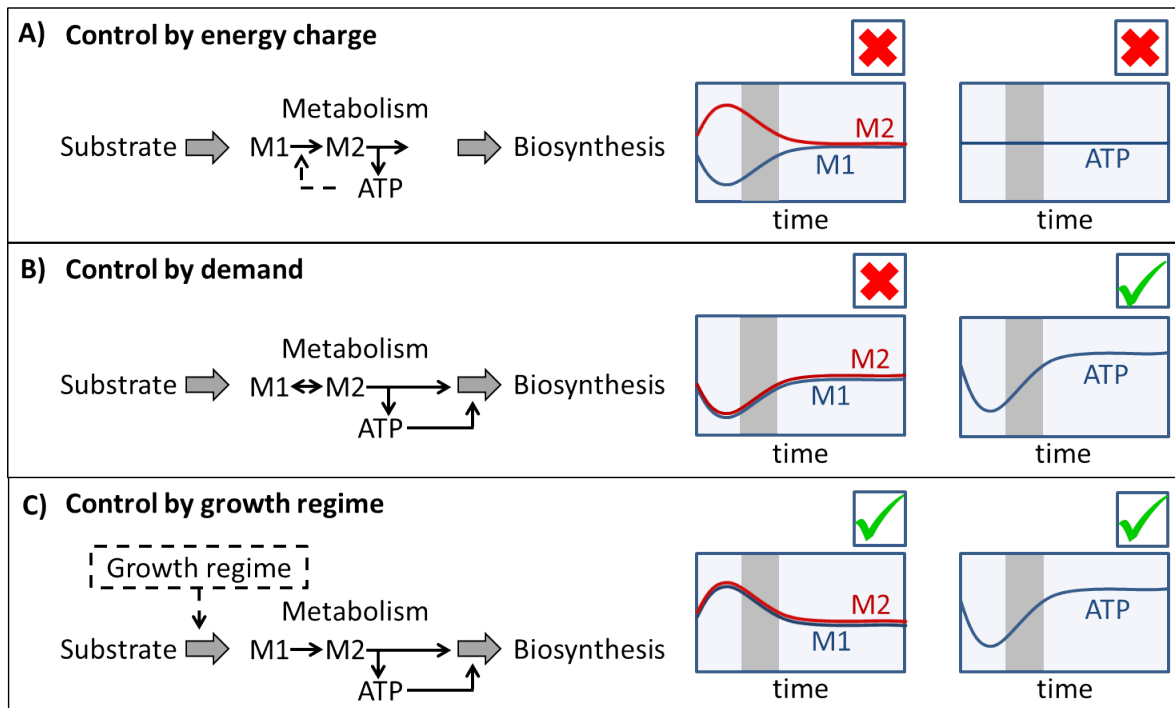


Figure 4.34.: Role of ATP in the control of the central carbon metabolism and observations of this study. Light arrows indicate reactions for metabolite M, which may stand for e.g. M1: F6P and M2:F16BP, large arrows indicate a supply and dashed arrows indicate regulation.

is that biosynthesis is induced by high precursor levels and, because of the increasing demand, simultaneously reduces ATP levels (Fig. 4.34C).

Model performance: Current models for yeast and bacteria metabolism that consider *in vivo* dynamics in metabolite pools focus mainly on glucose pulse experiments [20, 237, 242, 317]. The model of this work describes data of pulse experiments equally well (or even better) and captures additional measurements from two independent limitation experiments. Although perturbation experiments are ideal to study pathway dynamics they depict extreme scenarios in which the substrate levels have a pronounced influence. The advantage of our model is that it explains metabolite pool dynamics of several perturbation experiments and, at the same time, for cell cultivation experiments, while using the same parameterization. Differences between replicate experiments are reflected by considering the preculture of cells and also circumvents the estimation of individual initial conditions. Based on the comprehensive validation with data from a broad operation range of metabolism, the model is capable to predict the metabolism

for a cultivation in a second medium. In sum, the model describes about 70 % of the 1200 data points from a variety of experiments and time scale (Cult1 – 3, Lim1, Lim2, Pulse), while being relatively simple, biologically relevant and predictive.

4.3.12. Summary

In this part, we coupled the segregated cell growth model to a structured model that incorporates the two main metabolic pathways, glycolysis and glutaminolysis, as well as their links to the associated metabolism of PPP, glycogenesis, pyruvate metabolism and to the energy metabolism. To unravel mechanisms that are involved in the metabolite pool dynamics, the model structure is composed of relatively simple enzyme kinetics that focus on a few well-known enzyme metabolite interactions. By using macroscopic growth functions, the model can realize growth-dependent substrate transports as well as consumption of metabolites and cellular energy for biosynthesis. Furthermore, the model considers the preculture of cells as well as different intracellular enzyme levels and explains most experimental observations for cultivation, limitation and pulse experiments under a single parameterization. Thus, the model not only provides a good performance in describing the experimental data but also delivers a systems level understanding of the metabolic regulation for a variety of experimental conditions and time scales. In particular, the model suggests that the metabolic activity is regulated by growth-dependent transports of GLC^x , GLN^x and GLU^x , while the resulting production rates of biomass precursors and cellular energy are influenced by intrinsic pathway properties. When limited in substrates, the control over the metabolic activity shifts from the growth regime towards an inherent one that is shared by several enzyme metabolite interactions. Furthermore, the model suggests that oxidative phosphorylation has a pronounced control over the activity of the citric acid cycle that prevents the dissipation of valuable biomass precursors and eventually apoptosis. We also successfully tested the predictive power of the model for the glycolysis and glutaminolysis pathways by simulating a cultivation in a second medium (DMEM), which strengthened our confidence in the model structure and its parameterization. Based on the model, we hypothesize that a faster or a more efficient cell growth can be achieved by tuning the substrate uptake rates of the cell, which has great relevance to the design of bioprocesses and of new experiments.

5 Chapter

Conclusion

When this work was conceptually formulated, it was not clear whether the overall dynamics in the central carbon metabolism of adherent MDCK cells can be explained by mathematical models. Existing models for metabolism largely focus on yeast and *E. coli* or on isolated mitochondria. Furthermore, these models often focus on rather special scenarios, such as pulse experiments, than on basic metabolic functions relevant for cell cultivation and production of biologicals. Fortunately, numerous concepts for the regulation of the cellular metabolism are available and cover the influence by extracellular substances, transport mechanisms, hierarchical control and intrinsic pathway properties. The contribution of this work to the field of metabolic research is, thus, the reasonable combination of the most promising theories such that a mathematical model is derived that consistently explains intracellular metabolite pool dynamics found for adherent MDCK cells under various experimental conditions.

The first challenge was to identify regulatory principles that are likely involved in the control of the MDCK cell metabolism. Although it is clear that the metabolic activity correlates with cell growth, studies on the interplay of metabolic regulation mechanisms through analysis of metabolite pools under different growth conditions are barely available, especially not for a broader systems-level analysis. The first part of this work, therefore, analyzes growth and metabolism of MDCK cells that were cultivated in two different media using biological and technical replicate measurements for both media. Surprisingly, the metabolic behavior is quite the same and fundamental changes in metabolite pools are highly correlated to changes in the growth behavior. These observations not only imply that the influence of extracellular substrates is limited but also unravel a robust regulation of the metabolic activity by simple cellular mechanisms, such as key enzyme-metabolite interactions and transport reactions.

Based on the recognition of these first principles, we aimed for an analysis of metabolite pool dynamics that specifically takes into account the growth rate, nutrient uptake and size change of cells. Conventional cell growth models, however, can often not distinguish between cell size and cell number increase, while mass population-based models

are difficult to calibrate with experimental data. Therefore, we developed a segregated cell growth model where cells pass through different cell diameter classes, thereby consuming substrates and releasing byproducts, until a critical size is reached and the cells divide. Cell volume-dependent growth inhibition occurs at the first transition and allows the model to recapitulate the observed mean cell diameter dynamics. When applied to three independent cultivations, the model shows a convincing performance in capturing cell growth in numbers and volume while it also precisely explains the cellular uptake of substrates and the release of byproducts. Furthermore, it possesses a simple structure and is easy to compute. In comparison to conventional approaches, the model proved advantageous for the simultaneous description of different cultivations with a single parameterization and is, thus, particularly suited for coupling with structured models of metabolism. The successful prediction of cultivation experiments as well as the analysis of other cell lines and cultivation conditions indicate applicability and generality. Hence, the model fills the gap between existent approaches and represents a promising alternative to mammalian cell growth models that are typically used to design and optimize bioprocesses.

The second challenge in the analysis of metabolism lied in its enormous variability, even for experiments that were seemingly performed as replicates. It is hypothesized by other groups that variations in the metabolic state can be a result of the cultivation history of cells. Changes in the cell size as well as in genomic, transcriptomic or proteomic properties are typically found. Following this idea, we designed a simulation scheme that links the initial cell status of the actual experiments with the preculture of cells, which differ in cell diameters and the intracellular enzyme level. For example, simulating the dynamics during cell cultivation delivered all aspects of cell growth, metabolism and culture condition for the simulation of substrate limitations and finally pulse experiments. Another benefit of this concept is that it enables the model to explain experiment-specific variations in metabolite pool dynamics with differences in the preculture, which otherwise introduce large uncertainties to the analysis of metabolism.

With a solution for both challenges, we finally developed a structured model for the central carbon metabolism and its associated pathways. To illuminate central regulatory principles, the model focuses on simple, yet biologically relevant descriptions that feature the identification of mechanisms that are involved in main intracellular metabolite dynamics. Interestingly, a few key enzyme-metabolite interactions together with macroscopic growth functions already explain metabolite pool changes from a comprehensive data set that covers a variety of experiments and time scales. The quality and relia-

bility of the model is further emphasized by the successful prediction of a cultivation in second medium (DMEM) and allows us to infer with greater confidence how different regulatory mechanisms interact to realize a broad range of pathway operations. In particular, the model suggests that glycolysis and glutaminolysis are both controlled by a cellular growth regime through modulation of the glucose, glutamine and glutamate transporter activity. On a lower regulatory layer, enzyme-metabolite interactions influence the flux distribution to suit the cellular demand for energy and biomass precursors. In extreme cases, where cells are limited in their substrates, the control shifts from the transporter through the limiting substrates to a control that is shared by key enzymes. The frequent expectation, however, that enzyme-metabolite interactions constitute a demand-driven control that shapes metabolism for various growth conditions fails in explaining metabolite pool dynamics observed for MDCK cells. Therefore, the shift in control is an essential property of the cellular metabolism that is unraveled in this work by the systematic integration of various experimental conditions into a coherent modeling framework. Furthermore, the substrate transport is an often overseen element that can exert significant control over metabolism but might not become obvious from substrate pulse experiments or steady state data. Since the transport is regulated by macroscopic growth functions, it seems that the growth regime ultimately controls the generation of biomass precursors and cellular energy with rates that are encoded in the network architecture. Nonetheless, the influence of extracellular substrate concentrations and intracellular enzyme levels (proteomic level) are a necessary part of the model and contribute already to the metabolite pool dynamics. Furthermore, other hierarchical aspects, such as enzyme phosphorylation and transcriptional regulation may improve the current interpretations and can, thus, not be excluded as sources of regulation. Interestingly, the hypothesis of a control by energy charge is neither supported by the model nor by the experimental data. Although the contribution of all of these additional mechanisms is not essential for describing the metabolite pool data of this work, they may play a role in very specific and stressful situations, for example when cells are adapted to a new medium. For the understanding of the cellular metabolism, however, it seems intuitive that the driving force of cellular life relies on simple mechanisms, i.e. ordinary enzyme-metabolite interactions and the rate limiting activity of transporters, as they facilitate a robust functioning in a changing environment.

Overall, we successfully combined the analysis of cell growth dynamics with relatively simple enzyme-metabolite interactions to study the capacity and regulation of the mammalian cell metabolism. Based on a mathematical model, we inferred principles of

5. Conclusion

metabolic regulation and their interplay by describing dynamics in metabolism for a variety of experiments. The insights into metabolism and the predictions for the cell significantly contribute to the field of metabolic research and support the design of more efficient cell cultivations.

6 Chapter Outlook

With the successful development of a mathematical model that consistently explains data of a complex metabolic network, a promising systems biotechnology framework is created that supports the analysis of further metabolic phenomena. Within the vision of an iterative cycle of model development and data generation, we here draw an outlook on experiments that possess the greatest potential for improvement of the model and for discoveries in the fields of metabolic research and bioprocessing.

Importance of labeling experiments: For the central carbon metabolism of MDCK cells, the exchange of metabolites with associated pathways is only partially validated by substrate uptake and byproduct release rates. Flux data from labeling experiments can provide insights into the metabolic flux distribution and reduce the degree of freedom in the current interpretation of the metabolic activity. The citric acid cycle, for example, showed a peak-like response in metabolite levels when it comes to a substrate limitation. Application of labeling experiments may address the source of these peaks as well as the surprising observations of constant ATP levels during these experiments. Currently, the model suggests that AA are converted by the citric acid cycle under the production of ATP but cannot explain constant ATP levels or peaks in metabolite pools. Furthermore, it remains to be elucidated for how long the cell can sustain limiting conditions and how active the different parts of metabolism are. In principle, labeling experiments are an important element in the analysis of metabolism, even though the method is time and cost expensive.

Complement existing data sets: Experiments in which single substrates are removed from the medium represent a reasonable strategy to further validate the exchange of metabolites among pathways with the convenient side effect that current measurement methods are exploited in an economic fashion. Since the model already showed a good performance in predicting a cultivation with reduced GLC^x levels, additional cultivations with limitations in GLN^x and GLU^x not only complement the set of experiments

and simulations but can also illuminate the conversion routes in glutaminolysis and the citric acid cycle. Currently, the model suggests a relatively low supply of the citric acid cycle with PYR and a substantial contribution from GLN and AA. In addition, the quantification of extracellular amino acid concentrations may clarify the dynamics in the substrate supply of the citric acid cycle. Another open question is the role of NADH in the regulation of the citric acid cycle activity. Methods for the quantification of intracellular NAD and NADH can be adopted for MDCK cells to prove or reject the hypothesis that high NADH levels limit the activity of the citric acid cycle.

Enzyme activity and content: For the cultivation experiments, we observed that cells with different cultivation histories varied in d_m and d_c and anticipated a concomitant change in the E_{level} . The assumption readily explains experiment-specific variations in metabolite pool dynamics. However, it remains to be shown whether and, if so, to which extent the enzyme content changes with the cell size. The use of a proteomic approach, in addition to enzyme activity measurements, provides independent data on protein level and specific activity. Corresponding studies may unravel principles for the link between enzyme content and cell diameter, which can potentially refine the current model. In a preliminary study, S. Kluge analyzed the adaptation of MDCK cells to suspension growth and we found a reduction in the glycolytic activity equal to the reduction in enzyme activity. The use of enzyme activity measurements and relative protein quantifications indicated that changes in the enzymes activity are correlated with the reduction in protein content. As suspension cells are much smaller than adherent cells, this finding may support the idea that the enzyme level correlates in general with the size of cells.

Perturbation of intrinsic pathway properties: Next to the acquisition of data on further metabolic components, it seems worth to also perturb cellular components and track the metabolic response. Based on the model, the modulation of the GLUT has a certain potential for enhancing or decreasing the biomass precursor production rates. Also an increase of the NADPH production rate by the PPP seems possible and may support lipid synthesis, which may have great relevance for the cell-based production of viruses. Therefore, experiments dealing with the overexpression or inhibition of GLUT can be used to validate its control over glycolysis and to clarify effects on the biosynthesis activity. Alternatively, GLUT and many enzymes of the glycolytic pathway can be perturbed by activation or suppression of HIF-1, which is currently tested as a strategy

to interfere with the Crabtree effect by a member of the BPT group.

Extension of the model: In its current version, the model neglects any compartmentalization of the cell as it is designed to comply with the data. In addition, extending the model by distinct reactions for mitochondria and cytosol will cause identifiability problems unless compartment-specific data are taken into account. Methods for gathering compartment-specific data are currently available but an even distribution of metabolites within the compartments cannot be expected. It seems that metabolites are converted in enzyme complexes [318] and resolving these metabolic processes may introduce enormous challenges for both experimental methods and modeling. Nonetheless, metabolism is linked to most cellular processes and, thus, many more cellular functions can be addressed by model extensions such as the osmotic stress, hypoxia or glycosylation of proteins. Also the lipid metabolism, as mentioned above, poses a promising extension to the model if corresponding data becomes available.

Transfer of model to other cell lines: Preliminary studies by Klassen [303] indicate that central principles for the regulation of metabolism in adherent MDCK cell also apply to suspension AGE1.HN.AAT cells. Although some mechanisms may require adjustments, i.e. influence of growth inhibitors and the kinetics for enzyme-mediated reactions, a direct comparison to MDCK cells seems interesting and would contribute to a more general understanding of the mammalian cell metabolism. Also, CHO cells, which are the best studied mammalian cells and widely used for the production of recombinant proteins, can be considered as field of application for the presented modeling approach if data on intracellular metabolites and enzyme activities become available. Both cell lines can also be used to study the link between glycolytic activity and protein glycosylation and are, thus, highly attractive research objects with great relevance for a larger biotechnological community. In the field of virus production, the design of highly productive cells can be supported by the presented modeling approach through identification of metabolic bottlenecks and of optimal cultivation strategies.

List of figures

2.1. Madin Darby canine kidney cells	5
2.2. Growth phases during cell cultivation	7
2.3. Mutual influence of cell growth, metabolism and environment	9
2.4. Central carbon metabolism of MDCK cells	13
3.1. Coupling of cell growth and metabolism model	49
3.2. Flow of information and link to experimental data	52
3.3. A priori estimations for the substrate limitation experiments	53
3.4. Hierarchy of model parts	54
4.1. Growth of adherent MDCK cells in two media	58
4.2. Glycolysis dynamics for growth in two different media	60
4.3. Closely related metabolism dynamics for growth in two different media	61
4.4. Citric acid cycle dynamics for growth in two different media	62
4.5. Purine dynamics for growth in two different media	63
4.6. Scheme of segregated cell growth model	70
4.7. Cell growth in 6-well plates	71
4.8. Extracellular metabolite levels during cell cultivation	73
4.9. Simulated uptake rates during cell cultivation	76
4.10. Scheme of glycolysis model	82
4.11. Glycolysis during cell cultivation	84
4.12. Fluxes from glycolysis into associated pathways	85
4.13. Response of glycolysis to substrate perturbations	87
4.14. <i>In silico</i> GLUT modulation	89
4.15. Predicting the glycolytic response to cell cultivation in DMEM medium	90
4.16. Ribose 5-phosphate during cell cultivation and substrate perturbations	91
4.17. UDP-glucose during cell cultivation and substrate perturbations	92
4.18. Parameter sensitivity analysis of structured glycolysis model	94

4.19. Scheme of glutaminolysis model	103
4.20. Lower citric acid cycle during cell cultivation	104
4.21. Upper citric acid cycle during cell cultivation	105
4.22. Fluxes in citric acid cycle	106
4.23. Response of lower citric acid cycle to substrate perturbations	108
4.24. Response of upper citric acid cycle to substrate perturbations	109
4.25. Predicting the TCA response to cell cultivation in DMEM medium	110
4.26. Pyruvate during cell cultivation and perturbation	111
4.27. Use of pyruvate in MDCK cells	112
4.28. Parameter sensitivity analysis of structured glutaminolysis model	113
4.29. Scheme of energy metabolism model	114
4.30. Adenosine-based nucleotide pools during cell cultivation	116
4.31. Production of ATP and demand for oxygen during cultivation	117
4.32. Statistical analysis of structured model performance	117
4.33. Scheme of central carbon metabolism dynamics during cell cultivation	120
4.34. Role of ATP in the control of the central carbon metabolism	125
A.1. Attachment cells to 6-well plate surface	173
A.2. Cell growth in 6-well plates with DMEM medium	175
A.3. Extracellular metabolite levels during cell cultivation in DMEM medium	176
A.4. MDCK.SUS growth with MEDIUM in BIOREACTOR	177
A.5. Extracellular metabolites during MDCK.SUS growth	177
A.6. Correlation analysis of glycolysis model	178
A.7. Correlation analysis of glutaminolysis model	179
B.1. Adenosine-based nucleotide pools during substrate perturbation	181

List of tables

4.1. Measured uptake and release rates of metabolites	59
4.2. Calculated growth phases in the cell cultivation experiments	72
4.3. Parameters of adherent MDCK cell growth	75
B.1. Limit of quantification	180
C.1. Local parameters for central carbon metabolism model I	182
C.2. Local parameters for central carbon metabolism model II	183
C.3. Local parameters for segregated cell growth model	185
C.4. Global parameters for segregated cell growth model	186
C.5. Global parameters for central carbon metabolism model I	187
C.6. Global parameters for central carbon metabolism model II	188

List of publications

Parts of the following publications and supervised theses were included in this work

Journal articles

Rehberg M., Ritter J.B., Reichl U., Glycolysis Is Governed by Growth Regime and Simple Enzyme Regulation in Adherent MDCK Cells, *PLoS Computational Biology*, 10/2014, 10(10):e1003885

Rath A., **Rehberg M.**, Janke R., Genzel Y., Scholz S., Noll T., Rose T., Sandig V., Reichl U., The influence of cell growth and enzyme activity changes on intracellular metabolite dynamics in AGE1.HN.aat cells, *J. of Biotechnol.*, 2014, 178: 43–53

Rehberg M., Rath A., Genzel Y., Ritter J.B., Reichl U., Changes in intracellular metabolite pools during growth of adherent MDCK cells in two different media, *Appl. Microbiol. Biotechnol.*, 2014, 98(1): 385–397

Rehberg M., Wetzel M., Ritter J.B., Reichl U., The regulation of glutaminolysis and citric acid cycle activity during mammalian cell cultivation, *IFAC proceedings*, 2013, 12(1): 48–53

Rodriguez-Fernandez M., **Rehberg M.**, Kremling A., Banga J.R., Simultaneous model discrimination and parameter estimation in dynamic models of cellular systems, *BMC Systems Biology*, 2013, 7(1): 76

Rehberg M., Ritter J.B., Genzel Y., Flockerzi D., Reichl U., The relation between growth phases, cell volume changes and metabolism of adherent cells during cultivation, *J. Biotechnol.*, 2013, 164: 498–499

Supervised theses

Maria Wetzel, Modeling of glutaminolysis and citric acid cycle to analyze energy and biomass generation in MDCK cells, 2013, Group of Bioprocess Engineering, Max Planck Institute for Dynamics of Complex Technical Systems, Magdeburg, Germany

Jan Mares Klassen, Modeling growth and metabolism of continuously growing AGE1.HN.AAT cells, 2015, Group of Bioprocess Engineering, Max Planck Institute for Dynamics of Complex Technical Systems, Magdeburg, Germany

Talks

Rehberg M., Wetzel M., Ritter J.B., Reichl U., The regulation of glutaminolysis and citric acid cycle activity during mammalian cell cultivation, *Computer Applications in Biotechnology*, 2013, Mumbai, India

Rehberg M., Wetzel M., Genzel Y., Ritter J.B., Reichl U., The modulation of central carbon metabolism during adherent MDCK cell growth, *International Conference on Systems Biology*, 2013, Copenhagen, Denmark

Rehberg M., Ritter J.B., Reichl U., Glycolysis of adherently growing mammalian cells - dynamics during cell growth and glucose limitation, 2012, *guest presentation at the Institute for Experimental Physics*, Otto-von-Guericke University, Magdeburg, Germany

Rehberg M., Ritter J.B., Reichl U., Inherent Dynamics of Glycolysis in MDCK Cells, *guest presentation at the Institute for Complex Systems and Mathematical Biology*, 2010, University of Aberdeen, Scotland

Poster

Rehberg M., Ritter J.B., Reichl U., Glycolysis of adherently growing MDCK cells - influence of cell growth and glucose limitation, 2014, *Systems Biology of Mammalian Cells*, Berlin, Germany

Rehberg M., Genzel Y., Ritter J.B., Reichl U., Quantitative analysis of glycolysis in MDCK cells during cell growth, medium removal and medium addition, 2013, *ESACT meeting*, Lille, France

Rehberg M., Genzel Y., Ritter J.B., Reichl U., Funktionsweise der Glykolyse von MDCK Zellen bei Zellwachstum, Mediumentzug und Mediumzugabe, 2013, *DECHEMA Himmelfahrtstagung*, Bad-Wildungen, Germany

Rehberg M., Genzel Y., Ritter J.B., Reichl U., Glycolysis of adherently growing MDCK cells - influence of cell growth and glucose limitation, 2012, *Systems Biology of Mammalian Cells*, Leipzig, Germany

Rehberg M., Ritter J.B., Reichl U., The influence of growth phases on glycolysis - combining two models for adherent MDCK cells, 2011, *International Conference on Systems Biology*, Mannheim/Heidelberg, Germany

Rehberg M., Ritter J.B., Genzel Y., Reichl U., Inherent Dynamics of Glycolysis in MDCK Cells, 2010, *International Conference on Systems Biology*, Edinburgh, Scotland

Rehberg M., Ritter J.B., Genzel Y., Reichl U., Dynamics of central metabolism in MDCK cells: modeling approach on 30 intracellular metabolites, 2010, *Systems Biology of Mammalian Cells*, Freiburg, Germany

Bibliography

- [1] J. R. Swartz. Advances in escherichia coli production of therapeutic proteins. *Curr Opin Biotechnol*, 12(2):195–201, Apr 2001. URL [http://dx.doi.org/10.1016/S0958-1669\(00\)00199-3](http://dx.doi.org/10.1016/S0958-1669(00)00199-3).
- [2] Neil Templeton, Jason Dean, Pranhitha Reddy, and Jamey D. Young. Peak antibody production is associated with increased oxidative metabolism in an industrially relevant fed-batch cho cell culture. *Biotechnol Bioeng*, 110(7):2013–2024, Jul 2013. URL <http://dx.doi.org/10.1002/bit.24858>.
- [3] S. Dhir, K. J. Morrow, R. R. Rhinehart, and T. Wiesner. Dynamic optimization of hybridoma growth in a fed-batch bioreactor. *Biotechnol Bioeng*, 67(2):197–205, Jan 2000. URL [http://dx.doi.org/10.1002/\(SICI\)1097-0290\(2000120\)67:2<197::AID-BIT9>3.0.CO;2-W](http://dx.doi.org/10.1002/(SICI)1097-0290(2000120)67:2<197::AID-BIT9>3.0.CO;2-W).
- [4] Héla Kallel, Ahlem Jouini, Samy Majoul, and Samia Rourou. Evaluation of various serum and animal protein free media for the production of a veterinary rabies vaccine in bhk-21 cells. *J Biotechnol*, 95(3):195–204, May 2002. URL [http://dx.doi.org/10.1016/S0168-1656\(02\)00009-3](http://dx.doi.org/10.1016/S0168-1656(02)00009-3).
- [5] Y. Genzel, I. Behrendt, S. König, H. Sann, and U. Reichl. Metabolism of mdck cells during cell growth and influenza virus production in large-scale microcarrier culture. *Vaccine*, 22(17-18):2202–2208, Jun 2004. URL <http://dx.doi.org/10.1016/j.vaccine.2003.11.041>.
- [6] J. G. Salway. *Metabolism at a Glance*. Blackwell Publishing, Oxford, 2004.
- [7] Alberts, Johnson, Lewis, Raff, Roberts, and Walter. *Molekularbiologie der Zelle*, volume 4. ed. Wiley-VCH, Weinheim, Germany, 2004.
- [8] G. Avigad. Stimulation of yeast phosphofructokinase activity by fructose 2,6-bisphosphate. *Biochem Biophys Res Commun*, 102(3):985–991, Oct 1981. URL [http://dx.doi.org/10.1016/0006-291X\(81\)91635-1](http://dx.doi.org/10.1016/0006-291X(81)91635-1).
- [9] A. M. Reynard, L. F. Hass, D. D. Jacobsen, and P. D. Boyer. The correlation of reaction kinetics and substrate binding with the mechanism of pyruvate kinase. *J Biol Chem*, 236:2277–2283, Aug 1961. URL <http://www.jbc.org/content/236/8/2277.short>.

-
- [10] H. J. Fromm and V. Zewe. Kinetic studies of yeast hexokinase. *J Biol Chem*, 237: 3027–3032, Oct 1962. URL <http://www.jbc.org/content/237/10/3027.short>.
- [11] Karen van Eunen, Jildau Bouwman, Pascale Daran-Lapujade, Jarne Postmus, André B Canelas, Femke I C Mensonides, Rick Orij, Isil Tuzun, Joost van den Brink, Gertien J Smits, Walter M van Gulik, Stanley Brul, Joseph J Heijnen, Johannes H de Winde, M. Joost Teixeira de Mattos, Carsten Kettner, Jens Nielsen, Hans V Westerhoff, and Barbara M Bakker. Measuring enzyme activities under standardized in vivo-like conditions for systems biology. *FEBS J*, 277(3):749–760, Feb 2010. URL <http://dx.doi.org/10.1111/j.1742-4658.2009.07524.x>.
- [12] Hannes Link, Karl Kochanowski, and Uwe Sauer. Systematic identification of allosteric protein-metabolite interactions that control enzyme activity in vivo. *Nat Biotechnol*, 31(4):357–361, Apr 2013. URL <http://dx.doi.org/10.1038/nbt.2489>.
- [13] Jason Dean and Pranhitha Reddy. Metabolic analysis of antibody producing cho cells in fed-batch production. *Biotechnol Bioeng*, 110(6):1735–1747, Jun 2013. URL <http://dx.doi.org/10.1002/bit.24826>.
- [14] Yvonne Genzel, Joachim B Ritter, Susanne König, Rüdiger Alt, and Udo Reichl. Substitution of glutamine by pyruvate to reduce ammonia formation and growth inhibition of mammalian cells. *Biotechnol Prog*, 21(1):58–69, 2005. URL <http://dx.doi.org/10.1021/bp049827d>.
- [15] Aljoscha Wahl, Yury Sidorenko, Michael Dauner, Yvonne Genzel, and Udo Reichl. Metabolic flux model for an anchorage-dependent MDCK cell line: characteristic growth phases and minimum substrate consumption flux distribution. *Biotechnol Bioeng*, 101(1):135–52, Sep 2008. URL <http://dx.doi.org/10.1002/bit.21873>.
- [16] Yury Sidorenko, Aljoscha Wahl, Michael Dauner, Yvonne Genzel, and Udo Reichl. Comparison of metabolic flux distributions for MDCK cell growth in glutamine- and pyruvate-containing media. *Biotechnol Prog*, 24(2):311–20, 2008. URL <http://dx.doi.org/10.1021/bp0702673>.
- [17] Uwe Sauer. Metabolic networks in motion: 13c-based flux analysis. *Mol Syst Biol*, 2:62, 2006. URL <http://dx.doi.org/10.1038/msb4100109>.
- [18] Alan J. Dickson. Enhancement of production of protein biopharmaceuticals by mammalian cell cultures: the metabolomics perspective. *Curr Opin Biotechnol*, 30C:73–79, Jul 2014. URL <http://dx.doi.org/10.1016/j.copbio.2014.06.004>.
- [19] E. Tziampazis and A. Sambanis. Modeling of cell culture processes. *Cytotechnology*, 14(3):191–204, 1994. URL <http://dx.doi.org/10.1007/BF00749616>.

- [20] Karen van Eunen, José A L Kiewiet, Hans V Westerhoff, and Barbara M Bakker. Testing biochemistry revisited: how in vivo metabolism can be understood from in vitro enzyme kinetics. *PLoS Comput Biol*, 8(4):e1002483, 2012. URL <http://dx.doi.org/10.1371/journal.pcbi.1002483>.
- [21] Raul K Suarez and Christopher D Moyes. Metabolism in the age of 'omes'. *J Exp Biol*, 215(Pt 14):2351–2357, Jul 2012. URL <http://dx.doi.org/10.1242/jeb.059725>.
- [22] R. Janke, Y. Genzel, N. nd A. Wahl, and U. Reichl. Metabolic adaptation of mdck cells to different growth conditions: effects on catalytic activities of central metabolic enzymes. *Biotechnol Bioeng*, 108(11):2691–2704, Nov 2011. URL <http://dx.doi.org/10.1002/bit.23215>.
- [23] Joachim Ritter. *Charakterisierung tierischer Zellkulturen anhand einer Quantifizierung intrazellulärer Metaboliten aus dem Zentralstoffwechsel*. PhD thesis, Otto-von-Guericke Universitaet Magdeburg, 2010.
- [24] S. H. Madin and NB Darby, Jr. Established kidney cell lines of normal adult bovine and ovine origin. *Proc Soc Exp Biol Med*, 98(3):574–576, Jul 1958. URL <http://dx.doi.org/10.3181/00379727-98-24111>.
- [25] B. Rothen-Rutishauser, S. D. Krämer, A. Braun, M. Günthert, and H. Wunderli-Allenspach. Mdkc cell cultures as an epithelial in vitro model: cytoskeleton and tight junctions as indicators for the definition of age-related stages by confocal microscopy. *Pharm Res*, 15(7):964–971, Jul 1998. URL <http://dx.doi.org/10.1023/A:1011953405272>.
- [26] K. Takaishi, T. Sasaki, H. Kotani, H. Nishioka, and Y. Takai. Regulation of cell-cell adhesion by rac and rho small g proteins in mdck cells. *Journal of Cell Biology*, 139(4):1047–1059, November 1997. URL <http://dx.doi.org/10.1083/jcb.139.4.1047>.
- [27] J. Balcarovastander, S. E. Pfeiffer, S. D. Fuller, and K. Simons. Development of cell-surface polarity in the epithelial madin-darby canine kidney (mdck) cell-line. *Embo Journal*, 3(11):2687–2694, 1984. URL <http://www.ncbi.nlm.nih.gov/pmc/articles/PMC557750/pdf/emboj00315-0230.pdf>.
- [28] K Takata, A Iizuka, T Suzuki, T Matsuzaki, M Sugawara, BC Shin, T Nomingere, and Y Shinoda. Sugar transporters in polarized epithelial cells. *ACTA HISTOCHEMICA ET CYTOCHEMICA*, 32(1):53–58, 1999. ISSN 0044-5991. URL <http://dx.doi.org/10.1267/ahc.32.53>. 5th Joint Meeting of the Japan-Society-of-Histochemistry-and-Cytochemistry / Histochemical-Society, SAN DIEGO, CALIFORNIA, JUL 23-26, 1998.
- [29] H Chmiel. *Bioprozesstechnik*. 2. Auflage. Spectrum Akademischer Verlag, Elsevier GmbH, 2005.

-
- [30] Yvonne Genzel and Udo Reichl. Continuous cell lines as a production system for influenza vaccines. *Expert Rev Vaccines*, 8(12):1681–1692, Dec 2009. URL <http://dx.doi.org/10.1586/erv.09.128>.
- [31] Michael L. Perdue, Frank Arnold, Sheng Li, Armen Donabedian, Vittoria Cioce, Thomas Warf, and Robert Huebner. The future of cell culture-based influenza vaccine production. *Expert Rev Vaccines*, 10(8):1183–1194, Aug 2011. URL <http://dx.doi.org/10.1586/erv.11.82>.
- [32] Christopher A Sellick, Alexandra S Croxford, Arfa R Maqsood, Gill Stephens, Hans V Westerhoff, Royston Goodacre, and Alan J Dickson. Metabolite profiling of recombinant cho cells: designing tailored feeding regimes that enhance recombinant antibody production. *Biotechnol Bioeng*, 108(12):3025–3031, Dec 2011. URL <http://dx.doi.org/10.1002/bit.23269>.
- [33] Stefanie Dietmair, Mark P Hodson, Lake-Ee Quek, Nicholas E Timmins, Panagiotis Chrysanthopoulos, Shana S John, Peter Gray, and Lars K Nielsen. Metabolite profiling of cho cells with different growth characteristics. *Biotechnol Bioeng*, Mar 2012. URL <http://dx.doi.org/10.1002/bit.24496>.
- [34] J. B. Ritter, Y. Genzel, and U. Reichl. Simultaneous extraction of several metabolites of energy metabolism and related substances in mammalian cells: optimization using experimental design. *Anal Biochem*, 373(2):349–69, Feb 2008. URL <http://dx.doi.org/10.1016/j.ab.2007.10.037>.
- [35] Joachim B Ritter, Yvonne Genzel, and Udo Reichl. High-performance anion-exchange chromatography using on-line electrolytic eluent generation for the determination of more than 25 intermediates from energy metabolism of mammalian cells in culture. *J Chromatogr B Analyt Technol Biomed Life Sci*, 843(2):216–26, Nov 2006. URL <http://dx.doi.org/10.1016/j.jchromb.2006.06.004>.
- [36] Joachim B Ritter, Aljoscha S Wahl, Susann Freund, Yvonne Genzel, and Udo Reichl. Metabolic effects of influenza virus infection in cultured animal cells: Intra- and extracellular metabolite profiling. *BMC Syst Biol*, 4:61, 2010. URL <http://dx.doi.org/10.1186/1752-0509-4-61>.
- [37] R. Janke, Y. Genzel, A. Wahl, and U. Reichl. Measurement of key metabolic enzyme activities in mammalian cells using rapid and sensitive microplate-based assays. *Biotechnol Bioeng*, 107(3):566–581, Oct 2010. URL <http://dx.doi.org/10.1002/bit.22817>.
- [38] J. J. Ramsden, S. Y. Li, J. E. Prenosil, and E. Heinzle. Kinetics of adhesion and spreading of animal cells. *Biotechnol Bioeng*, 43(10):939–945, Apr 1994. URL <http://dx.doi.org/10.1002/bit.260431007>.

- [39] K. K. Frame and W. S. Hu. Kinetic study of hybridoma cell growth in continuous culture. i. a model for non-producing cells. *Biotechnol Bioeng*, 37(1):55–64, Jan 1991. URL <http://dx.doi.org/10.1002/bit.260370109>.
- [40] R. L. Adams. The effect of endogenous pools of thymidylate on the apparent rate of dna synthesis. *Exp Cell Res*, 56(1):55–58, Jul 1969. URL [http://dx.doi.org/10.1016/0014-4827\(69\)90393-0](http://dx.doi.org/10.1016/0014-4827(69)90393-0).
- [41] M.W. Glacken, R.J. Fleischaker, and Sinskey A.J. Reduction of waste product excretion via nutrient control - possible strategies for maximizing product and cell yields on serum in cultures of mammalian-cells. *Biotechnology And Bioengineering*, 28:1376–1389, 1986. URL <http://dx.doi.org/10.1002/bit.260280912>.
- [42] L. K. Nielsen, S. Reid, and P. F. Greenfield. Cell cycle model to describe animal cell size variation and lag between cell number and biomass dynamics. *Biotechnol Bioeng*, 56(4):372–379, Nov 1997. URL <http://dx.doi.org/3.0.CO;2-L>.
- [43] K. K. Frame and W. S. Hu. Cell volume measurement as an estimation of mammalian cell biomass. *Biotechnol Bioeng*, 36(2):191–197, Jun 1990. URL <http://dx.doi.org/10.1002/bit.260360211>.
- [44] S. U. Erlinger and M. H. Saier. Decrease in protein content and cell volume of cultured dog kidney epithelial cells during growth. *In Vitro*, 18(3 Pt 1):196–202, Mar 1982. URL <http://dx.doi.org/10.1007/BF02618571>.
- [45] Octavio T. Ramirez and R. Mutharasan. Cell cycle- and growth phase-dependent variations in size distribution, antibody productivity, and oxygen demand in hybridoma cultures. *Biotechnology and Bioengineering*, 36:839 – 848, 1990. URL <http://dx.doi.org/10.1002/bit.260360814>.
- [46] Emmanuel Boucrot and Tomas Kirchhausen. Mammalian cells change volume during mitosis. *PLoS One*, 3(1):e1477, 2008. URL <http://dx.doi.org/10.1371/journal.pone.0001477>.
- [47] Kidong Park, Larry J Millet, Namjung Kim, Huan Li, Xiaozhong Jin, Gabriel Popescu, N. R. Aluru, K. Jimmy Hsia, and Rashid Bashir. Measurement of adherent cell mass and growth. *Proc Natl Acad Sci U S A*, 107(48):20691–20696, Nov 2010. URL <http://dx.doi.org/10.1073/pnas.1011365107>.
- [48] Amit Tzur, Ran Kafri, Valerie S LeBleu, Galit Lahav, and Marc W Kirschner. Cell growth and size homeostasis in proliferating animal cells. *Science*, 325(5937):167–171, Jul 2009. URL <http://dx.doi.org/10.1126/science.1174294>.
- [49] M. G. Stoker and H. Rubin. Density dependent inhibition of cell growth in culture. *Nature*, 215(5097):171–172, Jul 1967. URL <http://dx.doi.org/10.1038/215171a0>.

-
- [50] L. G. Baggetto. Deviant energetic metabolism of glycolytic cancer cells. *Biochimie*, 74(11):959–974, Nov 1992. URL [http://dx.doi.org/10.1016/0300-9084\(92\)90016-8](http://dx.doi.org/10.1016/0300-9084(92)90016-8).
- [51] M. W. Glacken, E. Adema, and A. J. Sinskey. Mathematical descriptions of hybridoma culture kinetics: I. initial metabolic rates. *Biotechnol Bioeng*, 32(4):491–506, Aug 1988. URL <http://dx.doi.org/10.1002/bit.260320412>.
- [52] T. Hassell, S. Gleave, and M. Butler. Growth inhibition in animal cell culture. the effect of lactate and ammonia. *Appl Biochem Biotechnol*, 30(1):29–41, Jul 1991. URL <http://dx.doi.org/10.1007/BF02922022>.
- [53] S. S. Ozturk and B. O. Palsson. Chemical decomposition of glutamine in cell culture media: effect of media type, ph, and serum concentration. *Biotechnol Prog*, 6(2):121–128, 1990. URL <http://dx.doi.org/10.1021/bp00002a005>.
- [54] M. Butler, T. Imamura, J. Thomas, and W. G. Thilly. High yields from microcarrier cultures by medium perfusion. *J Cell Sci*, 61:351–363, May 1983.
- [55] M. Schneider, I. W. Marison, and U. von Stockar. The importance of ammonia in mammalian cell culture. *J Biotechnol*, 46(3):161–185, May 1996. URL [http://dx.doi.org/10.1016/0168-1656\(95\)00196-4](http://dx.doi.org/10.1016/0168-1656(95)00196-4).
- [56] O. Warburg, F. Wind, and E. Negelein. The metabolism of tumors in the body. *J Gen Physiol*, 8(6):519–530, Mar 1927.
- [57] M. Johnston and J-H. Kim. Glucose as a hormone: receptor-mediated glucose sensing in the yeast *saccharomyces cerevisiae*. *Biochem Soc Trans*, 33(Pt 1):247–252, Feb 2005. URL <http://dx.doi.org/10.1042/BST0330247>.
- [58] Rafael Moreno-Sanchez, Sara Rodriguez-Enriquez, Alvaro Marin-Hernandez, and Emma Saavedra. Energy metabolism in tumor cells. *FEBS J*, 274(6):1393–1418, Mar 2007. URL <http://dx.doi.org/10.1111/j.1742-4658.2007.05686.x>.
- [59] Brian J Koebmann, Hans V Westerhoff, Jacky L Snoep, Christian Solem, Martin B Pedersen, Dan Nilsson, Ole Michelsen, and Peter R Jensen. The extent to which atp demand controls the glycolytic flux depends strongly on the organism and conditions for growth. *Mol Biol Rep*, 29(1-2):41–45, 2002. URL <http://dx.doi.org/10.1023/A:1020398117281>.
- [60] Y. Kashiwaya, K. Sato, N. Tsuchiya, S. Thomas, D. A. Fell, R. L. Veech, and J. V. Passonneau. Control of glucose utilization in working perfused rat heart. *J Biol Chem*, 269(41):25502–25514, Oct 1994. URL <http://www.jbc.org/content/269/41/25502.short>.
- [61] Matthew G. Vander Heiden, Lewis C. Cantley, and Craig B. Thompson. Understanding the warburg effect: the metabolic requirements of cell proliferation.

- Science*, 324(5930):1029–1033, May 2009. URL <http://dx.doi.org/10.1126/science.1160809>.
- [62] Neelanjan Sengupta, Steven T. Rose, and John A. Morgan. Metabolic flux analysis of cho cell metabolism in the late non-growth phase. *Biotechnol Bioeng*, 108(1): 82–92, Jan 2011. URL <http://dx.doi.org/10.1002/bit.22890>.
- [63] Michael C Archer. Role of sp transcription factors in the regulation of cancer cell metabolism. *Genes Cancer*, 2(7):712–719, Jul 2011. URL <http://dx.doi.org/10.1177/1947601911423029>.
- [64] Juan P Bolaños, Angeles Almeida, and Salvador Moncada. Glycolysis: a bioenergetic or a survival pathway? *Trends Biochem Sci*, 35(3):145–149, Mar 2010. URL <http://dx.doi.org/10.1016/j.tibs.2009.10.006>.
- [65] Ana Paula Oliveira, Christina Ludwig, Paola Picotti, Maria Kogadeeva, Ruedi Aebersold, and Uwe Sauer. Regulation of yeast central metabolism by enzyme phosphorylation. *Mol Syst Biol*, 8:623, 2012. URL <http://dx.doi.org/10.1038/msb.2012.55>.
- [66] Denise R. Minton, Leiping Fu, Qiuying Chen, Brian D. Robinson, Steven S. Gross, David M. Nanus, and Lorraine J. Gudas. Analyses of the transcriptome and metabolome demonstrate that hif1alpha mediates altered tumor metabolism in clear cell renal cell carcinoma. *PLoS One*, 10(4):e0120649, 2015. URL <http://dx.doi.org/10.1371/journal.pone.0120649>.
- [67] Ralph J. DeBerardinis, Julian J. Lum, Georgia Hatzivassiliou, and Craig B. Thompson. The biology of cancer: metabolic reprogramming fuels cell growth and proliferation. *Cell Metab*, 7(1):11–20, Jan 2008. URL <http://dx.doi.org/10.1016/j.cmet.2007.10.002>.
- [68] Rafael Moreno-Sánchez, Alvaro Marín-Hernández, Emma Saavedra, Juan P. Pardo, Stephen J. Ralph, and Sara Rodríguez-Enríquez. Who controls the atp supply in cancer cells? biochemistry lessons to understand cancer energy metabolism. *Int J Biochem Cell Biol*, 50:10–23, May 2014. URL <http://dx.doi.org/10.1016/j.biocel.2014.01.025>.
- [69] Arnold J Levine and Anna M Puzio-Kuter. The control of the metabolic switch in cancers by oncogenes and tumor suppressor genes. *Science*, 330(6009):1340–1344, Dec 2010. URL <http://dx.doi.org/10.1126/science.1193494>.
- [70] Fabiana Schwartzenberg-Bar-Yoseph, Michal Armoni, and Eddy Karnieli. The tumor suppressor p53 down-regulates glucose transporters glut1 and glut4 gene expression. *Cancer Res*, 64(7):2627–2633, Apr 2004. URL <http://dx.doi.org/10.1158/0008-5472.CAN-03-0846>.

-
- [71] Rei Noguchi, Hiroyuki Kubota, Katsuyuki Yugi, Yu Toyoshima, Yasunori Komori, Tomoyoshi Soga, and Shinya Kuroda. The selective control of glycolysis, gluconeogenesis and glycogenesis by temporal insulin patterns. *Mol Syst Biol*, 9:664, 2013. URL <http://dx.doi.org/10.1038/msb.2013.19>.
- [72] G. Bandyopadhyay, M. P. Sajan, Y. Kanoh, M. L. Standaert, T. R. Burke, M. J. Quon, B. C. Reed, I. Dikic, L. E. Noel, C. B. Newgard, and R. Farese. Glucose activates mitogen-activated protein kinase (extracellular signal-regulated kinase) through proline-rich tyrosine kinase-2 and the glut1 glucose transporter. *J Biol Chem*, 275(52):40817–40826, Dec 2000. URL <http://dx.doi.org/10.1074/jbc.M007920200>.
- [73] Klaus Maier, Ute Hofmann, Matthias Reuss, and Klaus Mauch. Dynamics and control of the central carbon metabolism in hepatoma cells. *BMC Syst Biol*, 4(1): 54, Apr 2010. URL <http://dx.doi.org/10.1186/1752-0509-4-54>.
- [74] Karl Kochanowski, Benjamin Volkmer, Luca Gerosa, Bart R. Haverkorn van Rijsewijk, Alexander Schmidt, and Matthias Heinemann. Functioning of a metabolic flux sensor in escherichia coli. *Proceedings of the National Academy of Sciences*, 2012. URL <http://www.pnas.org/content/early/2012/12/28/1202582110.abstract>.
- [75] D. E. Atkinson. Biological feedback control at the molecular level. *Science*, 150(3698):851–857, Nov 1965. URL <http://dx.doi.org/10.1126/science.150.3698.851>.
- [76] Nana-Maria Grüning, Hans Lehrach, and Markus Ralser. Regulatory crosstalk of the metabolic network. *Trends Biochem Sci*, 35(4):220–227, Apr 2010. URL <http://dx.doi.org/10.1016/j.tibs.2009.12.001>.
- [77] Jochen Schaub and Matthias Reuss. In vivo dynamics of glycolysis in escherichia coli shows need for growth-rate dependent metabolome analysis. *Biotechnol Prog*, 24(6):1402–1407, 2008. URL <http://dx.doi.org/10.1002/btpr.59>.
- [78] N. Barnabé and M. Butler. The effect of glucose and glutamine on the intracellular nucleotide pool and oxygen uptake rate of a murine hybridoma. *Cytotechnology*, 34(1-2):47–57, Oct 2000. URL <http://dx.doi.org/10.1023/A:1008154615643>.
- [79] M. Newland, P. F. Greenfield, and S. Reid. Hybridoma growth limitations: the roles of energy metabolism and ammonia production. *Cytotechnology*, 3(3):215–229, May 1990. URL <http://dx.doi.org/10.1007/BF00365485>.
- [80] Ralph J DeBerardinis, Anthony Mancuso, Evgueni Daikhin, Ilana Nissim, Marc Yudkoff, Suzanne Wehrli, and Craig B Thompson. Beyond aerobic glycolysis: transformed cells can engage in glutamine metabolism that exceeds the requirement for protein and nucleotide synthesis. *Proc Natl Acad Sci U S A*, 104(49): 19345–19350, Dec 2007. URL <http://dx.doi.org/10.1073/pnas.0709747104>.

- [81] D. A. Hume, J. L. Radik, E. Ferber, and M. J. Weidemann. Aerobic glycolysis and lymphocyte transformation. *Biochem J*, 174(3):703–709, Sep 1978. URL <http://www.biochemj.org/bj/174/bj1740703.htm>.
- [82] L. J. Reitzer, B. M. Wice, and D. Kennell. Evidence that glutamine, not sugar, is the major energy source for cultured hela cells. *J Biol Chem*, 254(8):2669–2676, Apr 1979. URL <http://www.jbc.org/cgi/pmidlookup?view=long&pmid=429309>.
- [83] Jing Fan, Jurre J. Kamphorst, Robin Mathew, Michelle K. Chung, Eileen White, Tomer Shlomi, and Joshua D. Rabinowitz. Glutamine-driven oxidative phosphorylation is a major atp source in transformed mammalian cells in both normoxia and hypoxia. *Molecular Systems Biology*, 9:712, December 2013. URL <http://dx.doi.org/10.1038/msb.2013.65>.
- [84] L. Häggström. *Energetics of glutaminolysis - a theoretical evaluation*. In *Production of Biologicals from Animal Cells in Culture.*, volume Eds.: 79-81. Butterworth-Heinemann Ltd. Oxford ., 1991. URL http://dx.doi.org/10.1007/1-4020-3363-X_24.
- [85] T. Ryll, U. Valley, and R. Wagner. Biochemistry of growth inhibition by ammonium ions in mammalian cells. *Biotechnol Bioeng*, 44(2):184–193, Jun 1994. URL <http://dx.doi.org/10.1002/bit.260440207>.
- [86] J. Neermann and R. Wagner. Comparative analysis of glucose and glutamine metabolism in transformed mammalian cell lines, insect and primary liver cells. *J Cell Physiol*, 166(1):152–169, Jan 1996. URL <http://dx.doi.org/3.0.CO;2-H>.
- [87] H. J. Cruz, A. S. Ferreira, C. M. Freitas, J. L. Moreira, and M. J. Carrondo. Metabolic responses to different glucose and glutamine levels in baby hamster kidney cell culture. *Appl Microbiol Biotechnol*, 51(5):579–585, May 1999. URL <http://dx.doi.org/10.1007/s002530051435>.
- [88] R. M. Lynch and R. S. Balaban. Energy metabolism of renal cell lines, a6 and mdck: regulation by na-k-atpase. *Am J Physiol*, 252(2 Pt 1):C225–C231, Feb 1987. URL <http://ajpcell.physiology.org/content/252/2/C225>.
- [89] WL McKeehan. Glycolysis, glutaminolysis and cell-proliferation. *Cell Biology International Reports*, 6(7):635–650, 1982. URL [http://dx.doi.org/10.1016/0309-1651\(82\)90125-4](http://dx.doi.org/10.1016/0309-1651(82)90125-4).
- [90] Y. Genzel, M. Fischer, and U. Reichl. Serum-free influenza virus production avoiding washing steps and medium exchange in large-scale microcarrier culture. *Vaccine*, 24(16):3261–3272, Apr 2006. URL <http://dx.doi.org/10.1016/j.vaccine.2006.01.019>.

-
- [91] G. Schmid and H. W. Blanch. Extra- and intracellular metabolite concentrations for murine hybridoma cells. *Appl Microbiol Biotechnol*, 36(5):621–625, Feb 1992. URL <http://dx.doi.org/10.1007/BF00183239>.
- [92] L. Häggström, J. Ljunggren, and L. Ohman. Metabolic engineering of animal cells. *Ann N Y Acad Sci*, 782:40–52, May 1996. URL <http://dx.doi.org/10.1111/j.1749-6632.1996.tb40545.x>.
- [93] J. Ljunggren and L. Häggström. Catabolic control of hybridoma cells by glucose and glutamine limited fed batch cultures. *Biotechnol Bioeng*, 44(7):808–818, Sep 1994. URL <http://dx.doi.org/10.1002/bit.260440706>.
- [94] I. Sussman, M. Erecinska, and D. F. Wilson. Regulation of cellular energy metabolism: the crabtree effect. *Biochim Biophys Acta*, 591(2):209–223, Jul 1980. URL [http://dx.doi.org/10.1016/0005-2728\(80\)90153-X](http://dx.doi.org/10.1016/0005-2728(80)90153-X).
- [95] E. D. Renner, P. G. Plagemann, and R. W. Bernlohr. Permeation of glucose by simple and facilitated diffusion by novikoff rat hepatoma cells in suspension culture and its relationship to glucose metabolism. *J Biol Chem*, 247(18):5765–5776, Sep 1972. URL <http://www.jbc.org/content/247/18/5765.abstract>.
- [96] B. Thorens. Facilitated glucose transporters in epithelial cells. *Annu Rev Physiol*, 55:591–608, 1993. URL <http://dx.doi.org/10.1146/annurev.ph.55.030193.003111>.
- [97] J. Z. Zhang, A. Behrooz, and F. Ismail-Beigi. Regulation of glucose transport by hypoxia. *Am J Kidney Dis*, 34(1):189–202, Jul 1999. URL [http://dx.doi.org/10.1016/S0272-6386\(99\)70131-9](http://dx.doi.org/10.1016/S0272-6386(99)70131-9).
- [98] Merav Cohen, Daniel Kitsberg, Sabina Tsytkin, Maria Shulman, Benjamin Aroeti, and Yaakov Nahmias. Live imaging of glut2 glucose-dependent trafficking and its inhibition in polarized epithelial cysts. *Open Biol*, 4(7), Jul 2014. URL <http://dx.doi.org/10.1098/rsob.140091>.
- [99] R. F. Kletzien and J. F. Perdue. Sugar transport in chick embryo fibroblasts. i. a functional change in the plasma membrane associated with the rate of cell growth. *J Biol Chem*, 249(11):3366–3374, Jun 1974. URL <http://www.jbc.org/content/249/11/3366>.
- [100] Kara B Levine, Erin K Cloherty, Stephanie Hamill, and Anthony Carruthers. Molecular determinants of sugar transport regulation by atp. *Biochemistry*, 41(42):12629–12638, Oct 2002. URL <http://dx.doi.org/10.1021/bi0258997>.
- [101] J. S. Flier, M. M. Mueckler, P. Usher, and H. F. Lodish. Elevated levels of glucose transport and transporter messenger rna are induced by ras or src oncogenes. *Science*, 235(4795):1492–1495, Mar 1987. URL <http://dx.doi.org/10.1126/science.3103217>.

- [102] K. A. Reijenga, J. L. Snoep, J. A. Diderich, H. W. van Verseveld, H. V. Westerhoff, and B. Teusink. Control of glycolytic dynamics by hexose transport in *saccharomyces cerevisiae*. *Biophys J*, 80(2):626–634, Feb 2001. URL [http://dx.doi.org/10.1016/S0006-3495\(01\)76043-2](http://dx.doi.org/10.1016/S0006-3495(01)76043-2).
- [103] Jorge L. Galazzo and James E. Bailey. Fermentation pathway kinetics and metabolic flux control in suspended and immobilized *saccharomyces cerevisiae*. *Enzyme and Microbial Technology*, 12(3):162 – 172, 1990. ISSN 0141-0229. URL <http://www.sciencedirect.com/science/article/B6TG1-47GMG9P-4C/2/68eb4146ee871947386460abe7135b3c>.
- [104] L. Fitzpatrick, H. A. Jenkins, and M. Butler. Glucose and glutamine metabolism of a murine b-lymphocyte hybridoma grown in batch culture. *Appl Biochem Biotechnol*, 43(2):93–116, Nov 1993. URL <http://dx.doi.org/10.1007/BF02916435>.
- [105] Katie F. Wlaschin and Wei-Shou Hu. Engineering cell metabolism for high-density cell culture via manipulation of sugar transport. *J Biotechnol*, 131(2):168–176, Aug 2007. URL <http://dx.doi.org/10.1016/j.jbiotec.2007.06.006>.
- [106] B. Liebl, H. Mückter, E. Doklea, B. Fichtl, and W. Forth. Influence of 2,3-dimercaptopropanol and other sulfur compounds on oxophenylarsine-mediated inhibition of glucose uptake in mdck cells. *Analyst*, 120(3):771–774, Mar 1995. URL <http://dx.doi.org/10.1039/AN9952000771>.
- [107] D. Rivenzon-Segal, E. Rushkin, S. Polak-Charcon, and H. Degani. Glucose transporters and transport kinetics in retinoic acid-differentiated t47d human breast cancer cells. *Am J Physiol Endocrinol Metab*, 279(3):E508–E519, Sep 2000. URL <http://ajpendo.physiology.org/content/279/3/E508.short>.
- [108] Alvaro Marín-Hernández, Sara Rodríguez-Enríquez, Paola A. Vital-González, Fanny L. Flores-Rodríguez, Marina Macías-Silva, Marcela Sosa-Garrocho, and Rafael Moreno-Sánchez. Determining and understanding the control of glycolysis in fast-growth tumor cells. flux control by an over-expressed but strongly product-inhibited hexokinase. *FEBS J*, 273(9):1975–1988, May 2006. URL <http://dx.doi.org/10.1111/j.1742-4658.2006.05214.x>.
- [109] Adhiraj Roy, Yong Jae Shin, and Jeong-Ho Kim. Construction of yeast strains useful for screening drugs that inhibit glucose uptake and glycolysis. *Anal Biochem*, 436(1):53–54, May 2013. URL <http://dx.doi.org/10.1016/j.ab.2013.01.013>.
- [110] T. Ohta, K. J. Isselbacher, and D. B. Rhoads. Regulation of glucose transporters in llc-pk1 cells: effects of d-glucose and monosaccharides. *Mol Cell Biol*, 10(12):6491–6499, Dec 1990. URL <http://mcb.asm.org/content/10/12/6491.short>.
- [111] C. A. Nelson, J. Q. Wang, I. Leav, and P. D. Crane. The interaction among glucose transport, hexokinase, and glucose-6-phosphatase with respect to 3h-2-

-
- deoxyglucose retention in murine tumor models. *Nucl Med Biol*, 23(4):533–541, May 1996. URL [http://dx.doi.org/10.1016/0969-8051\(96\)00037-6](http://dx.doi.org/10.1016/0969-8051(96)00037-6).
- [112] Kohei Matsushita, Keiichi Uchida, Susumu Saigusa, Shozo Ide, Kiyoshi Hashimoto, Yuki Koike, Kohei Otake, Mikihiro Inoue, Koji Tanaka, and Masato Kusunoki. Glycolysis inhibitors as a potential therapeutic option to treat aggressive neuroblastoma expressing glut1. *J Pediatr Surg*, 47(7):1323–1330, Jul 2012. URL <http://dx.doi.org/10.1016/j.jpedsurg.2011.12.007>.
- [113] Christian D Young, Andrew S Lewis, Michael C Rudolph, Marisa D Ruehle, Matthew R Jackman, Ui J Yun, Olesya Ilkun, Renata Pereira, E. Dale Abel, and Steven M Anderson. Modulation of glucose transporter 1 (glut1) expression levels alters mouse mammary tumor cell growth in vitro and in vivo. *PLoS One*, 6(8):e23205, 2011. URL <http://dx.doi.org/10.1371/journal.pone.0023205>.
- [114] D. Yasmeen, A. J. Laird, D. A. Hume, and M. J. Weidemann. Activation of 3-o-methyl-glucose transport in rat thymus lymphocytes by concanavalin a. temperature and calcium ion dependence and sensitivity to puromycin but to cycloheximide. *Biochim Biophys Acta*, 500(1):89–102, Nov 1977. URL [http://dx.doi.org/10.1016/0304-4165\(77\)90049-6](http://dx.doi.org/10.1016/0304-4165(77)90049-6).
- [115] T. Liu, R. J. Kishton, A. N. Macintyre, V. A. Gerriets, H. Xiang, X. Liu, E. Dale Abel, D. Rizzieri, J. W. Locasale, and J. C. Rathmell. Glucose transporter 1-mediated glucose uptake is limiting for b-cell acute lymphoblastic leukemia anabolic metabolism and resistance to apoptosis. *Cell Death Dis*, 5:e1470, 2014. URL <http://dx.doi.org/10.1038/cddis.2014.431>.
- [116] Camilla Luni, Jamey D Marth, and Francis J Doyle. Computational modeling of glucose transport in pancreatic beta-cells identifies metabolic thresholds and therapeutic targets in diabetes. *PLoS One*, 7(12):e53130, 2012. URL <http://dx.doi.org/10.1371/journal.pone.0053130>.
- [117] John D. McGivan and Claire I. Bungard. The transport of glutamine into mammalian cells. *Front Biosci*, 12:874–882, 2007. URL <http://dx.doi.org/10.2741/2109>.
- [118] David R. Wise, Ralph J. DeBerardinis, Anthony Mancuso, Nabil Sayed, Xiao-Yong Zhang, Harla K. Pfeiffer, Ilana Nissim, Evgueni Daikhin, Marc Yudkoff, Steven B. McMahon, and Craig B. Thompson. Myc regulates a transcriptional program that stimulates mitochondrial glutaminolysis and leads to glutamine addiction. *Proc Natl Acad Sci U S A*, 105(48):18782–18787, Dec 2008. URL <http://dx.doi.org/10.1073/pnas.0810199105>.
- [119] R. H. McDermott and M. Butler. Uptake of glutamate, not glutamine synthetase, regulates adaptation of mammalian cells to glutamine-free medium. *J Cell Sci*, 104 (Pt 1):51–58, Jan 1993. URL <http://jcs.biologists.org/content/104/1/51.short>.

- [120] E Eigenbrodt and H Glossmann. Glycolysis - one of the keys to cancer. *Trends in Pharmacological Sciences*, 1(9):240–245, 1980. ISSN 0165-6147. URL [http://dx.doi.org/10.1016/0165-6147\(80\)90009-7](http://dx.doi.org/10.1016/0165-6147(80)90009-7).
- [121] M. Watford. Glutamine metabolism in rat small intestine: synthesis of three-carbon products in isolated enterocytes. *Biochim Biophys Acta*, 1200(1):73–78, May 1994. URL [http://dx.doi.org/10.1016/0304-4165\(94\)90029-9](http://dx.doi.org/10.1016/0304-4165(94)90029-9).
- [122] E. A. Newsholme, B. Crabtree, and M. S. Ardawi. The role of high rates of glycolysis and glutamine utilization in rapidly dividing cells. *Biosci Rep*, 5(5):393–400, May 1985. URL <http://www.bioscirep.org/bsr/005/bsr0050393.htm>.
- [123] R. Curi, P. Newsholme, and E. A. Newsholme. Metabolism of pyruvate by isolated rat mesenteric lymphocytes, lymphocyte mitochondria and isolated mouse macrophages. *Biochem J*, 250(2):383–388, Mar 1988. URL <http://www.biochemj.org/bj/250/bj2500383.htm>.
- [124] G. Gstraunthaler, T. Seppi, and W. Pfaller. Impact of culture conditions, culture media volumes, and glucose content on metabolic properties of renal epithelial cell cultures. are renal cells in tissue culture hypoxic? *Cell Physiol Biochem*, 9(3):150–172, 1999. URL <http://dx.doi.org/16312>.
- [125] M. Board, S. Humm, and E. A. Newsholme. Maximum activities of key enzymes of glycolysis, glutaminolysis, pentose phosphate pathway and tricarboxylic acid cycle in normal, neoplastic and suppressed cells. *Biochem J*, 265(2):503–509, Jan 1990. URL <http://www.biochemj.org/bj/265/0503/2650503.pdf>.
- [126] Sybille Mazurek. Pyruvate kinase type m2: a key regulator of the metabolic budget system in tumor cells. *Int J Biochem Cell Biol*, 43(7):969–980, Jul 2011. URL <http://dx.doi.org/10.1016/j.biocel.2010.02.005>.
- [127] Anique Herling, Matthias König, Sascha Bulik, and Hermann-Georg Holzhütter. Enzymatic features of the glucose metabolism in tumor cells. *FEBS J*, 278(14):2436–2459, Jul 2011. URL <http://dx.doi.org/10.1111/j.1742-4658.2011.08174.x>.
- [128] G. Weber. Enzymology of cancer cells (first of two parts). *N Engl J Med*, 296(9):486–492, Mar 1977. URL <http://dx.doi.org/10.1056/NEJM197703032960905>.
- [129] N. Vriezen and J. P. van Dijken. Fluxes and enzyme activities in central metabolism of myeloma cells grown in chemostat culture. *Biotechnol Bioeng*, 59(1):28–39, Jul 1998. URL [http://dx.doi.org/10.1002/\(SICI\)1097-0290\(19980705\)59:1<28::AID-BIT5>3.0.CO;2-V](http://dx.doi.org/10.1002/(SICI)1097-0290(19980705)59:1<28::AID-BIT5>3.0.CO;2-V).
- [130] P. Niederberger, R. Prasad, G. Miozzari, and H. Kacser. A strategy for increasing an in vivo flux by genetic manipulations. the tryptophan system of yeast. *Biochem J*, 287 (Pt 2):473–479, Oct 1992. URL <http://www.biochemj.org/bj/287/bj2870473.htm>.

-
- [131] B. Teusink and H. V. Westerhoff. 'slave' metabolites and enzymes. a rapid way of delineating metabolic control. *Eur J Biochem*, 267(7):1889–1893, Apr 2000. URL <http://dx.doi.org/10.1046/j.1432-1327.2000.01220.x>.
- [132] E. Bustamante, H. P. Morris, and P. L. Pedersen. Energy metabolism of tumor cells. requirement for a form of hexokinase with a propensity for mitochondrial binding. *J Biol Chem*, 256(16):8699–8704, Aug 1981. URL <http://www.jbc.org/content/256/16/8699.short>.
- [133] Sara Rodríguez-Enríquez, Alvaro Marín-Hernández, Juan Carlos Gallardo-Pérez, and Rafael Moreno-Sánchez. Kinetics of transport and phosphorylation of glucose in cancer cells. *J Cell Physiol*, 221(3):552–559, Dec 2009. URL <http://dx.doi.org/10.1002/jcp.21885>.
- [134] C. Sánchez-Martínez and J. J. Aragón. Analysis of phosphofructokinase subunits and isozymes in ascites tumor cells and its original tissue, murine mammary gland. *FEBS Lett*, 409(1):86–90, Jun 1997. URL [http://dx.doi.org/10.1016/S0014-5793\(97\)00496-1](http://dx.doi.org/10.1016/S0014-5793(97)00496-1).
- [135] Abdullah Yalcin, Sucheta Telang, Brian Clem, and Jason Chesney. Regulation of glucose metabolism by 6-phosphofructo-2-kinase/fructose-2,6-bisphosphatases in cancer. *Exp Mol Pathol*, 86(3):174–179, Jun 2009. URL <http://dx.doi.org/10.1016/j.yexmp.2009.01.003>.
- [136] E. Van Schaftingen, M. F. Jett, L. Hue, and H. G. Hers. Control of liver 6-phosphofructokinase by fructose 2,6-bisphosphate and other effectors. *Proc Natl Acad Sci U S A*, 78(6):3483–3486, Jun 1981. URL <http://www.pnas.org/content/78/6/3483.abstract>.
- [137] G. A. Dunaway. A review of animal phosphofructokinase isozymes with an emphasis on their physiological role. *Mol Cell Biochem*, 52(1):75–91, 1983. URL <http://dx.doi.org/10.1007/BF00230589>.
- [138] G. Wu, T. E. Haynes, H. Li, W. Yan, and C. J. Meininger. Glutamine metabolism to glucosamine is necessary for glutamine inhibition of endothelial nitric oxide synthesis. *Biochem J*, 353(Pt 2):245–252, Jan 2001. URL <http://www.biochemj.org/bj/353/bj3530245.htm>.
- [139] Alvaro Marín-Hernández, Juan Carlos Gallardo-Pérez, Sara Rodríguez-Enríquez, Rusely Encalada, Rafael Moreno-Sánchez, and Emma Saavedra. Modeling cancer glycolysis. *Biochim Biophys Acta*, 1807(6):755–767, Jun 2011. URL <http://dx.doi.org/10.1016/j.bbabi.2010.11.006>.
- [140] Taro Hitosugi, Lu Zhou, Shannon Elf, Jun Fan, Hee-Bum Kang, Jae Ho Seo, Changliang Shan, Qing Dai, Liang Zhang, Jianxin Xie, Ting-Lei Gu, Peng Jin, Masa Aleckovic, Gary LeRoy, Yibin Kang, Jessica A. Sudderth, Ralph J. DeBerardinis, Chi-Hao Luan, Georgia Z. Chen, Susan Muller, Dong M. Shin, Taofeek K.

- Owonikoko, Sagar Lonial, Martha L. Arellano, Hanna J. Khoury, Fadlo R. Khuri, Benjamin H. Lee, Keqiang Ye, Titus J. Boggon, Sumin Kang, Chuan He, and Jing Chen. Phosphoglycerate mutase 1 coordinates glycolysis and biosynthesis to promote tumor growth. *Cancer Cell*, 22(5):585–600, Nov 2012. URL <http://dx.doi.org/10.1016/j.ccr.2012.09.020>.
- [141] Matthias Engel, Sybille Mazurek, Erich Eigenbrodt, and Cornelius Welter. Phosphoglycerate mutase-derived polypeptide inhibits glycolytic flux and induces cell growth arrest in tumor cell lines. *J Biol Chem*, 279(34):35803–35812, Aug 2004. URL <http://dx.doi.org/10.1074/jbc.M402768200>.
- [142] E. Eigenbrodt, M. Reinacher, U. Scheefers-Borchel, H. Scheefers, and R. Friis. Double role for pyruvate kinase type m2 in the expansion of phosphometabolite pools found in tumor cells. *Crit Rev Oncog*, 3(1-2):91–115, 1992.
- [143] K. Ashizawa, M. C. Willingham, C. M. Liang, and S. Y. Cheng. In vivo regulation of monomer-tetramer conversion of pyruvate kinase subtype m2 by glucose is mediated via fructose 1,6-bisphosphate. *J Biol Chem*, 266(25):16842–16846, Sep 1991. URL <http://www.jbc.org/content/266/25/16842.full.pdf>.
- [144] Matthew J. Rogatzki, Brian S. Ferguson, Matthew L. Goodwin, and L Bruce Gladden. Lactate is always the end product of glycolysis. *Front Neurosci*, 9:22, 2015. URL <http://dx.doi.org/10.3389/fnins.2015.00022>.
- [145] T. Imamura, C. L. Crespi, W. G. Thilly, and H. Brunengraber. Fructose as a carbohydrate source yields stable ph and redox parameters in microcarrier cell culture. *Anal Biochem*, 124(2):353–358, Aug 1982. URL [http://dx.doi.org/10.1016/0003-2697\(82\)90051-3](http://dx.doi.org/10.1016/0003-2697(82)90051-3).
- [146] Matthias König, Sascha Bulik, and Hermann-Georg Holzhütter. Quantifying the contribution of the liver to glucose homeostasis: a detailed kinetic model of human hepatic glucose metabolism. *PLoS Comput Biol*, 8(6):e1002577, Jun 2012. URL <http://dx.doi.org/10.1371/journal.pcbi.1002577>.
- [147] M. J. Tang, K. R. Suresh, and R. L. Tannen. Carbohydrate metabolism by primary cultures of rabbit proximal tubules. *Am J Physiol*, 256(3 Pt 1):C532–C539, Mar 1989. URL <http://ajpcell.physiology.org/content/256/3/C532.short>.
- [148] David A. Scott, Adam D. Richardson, Fabian V. Filipp, Christine A. Knutzen, Gary G. Chiang, Ze'ev A. Ronai, Andrei L. Osterman, and Jeffrey W. Smith. Comparative metabolic flux profiling of melanoma cell lines: beyond the warburg effect. *J Biol Chem*, 286(49):42626–42634, Dec 2011. URL <http://dx.doi.org/10.1074/jbc.M111.282046>.
- [149] H. A. Krebs, D. A. H. Bennett, P. De Gasquet, T. Gascoyne, and T. Yoshida. Renal gluconeogenesis. the effect of diet on the gluconeogenic capacity of rat-

-
- kidney-cortex slices. *Biochem J*, 86:22–27, Jan 1963. URL <http://www.ncbi.nlm.nih.gov/pmc/articles/PMC1201705/>.
- [150] D. Petch and M. Butler. Profile of energy metabolism in a murine hybridoma: glucose and glutamine utilization. *J Cell Physiol*, 161(1):71–76, Oct 1994. URL <http://dx.doi.org/10.1002/jcp.1041610110>.
- [151] H. P. Bonarius, A. Ozemre, B. Timmerarends, P. Skrabal, J. Tramper, G. Schmid, and E. Heinzle. Metabolic-flux analysis of continuously cultured hybridoma cells using $(^{13}\text{C})_2$ mass spectrometry in combination with (^{13}C) -lactate nuclear magnetic resonance spectroscopy and metabolite balancing. *Biotechnol Bioeng*, 74(6): 528–538, Sep 2001. URL <http://dx.doi.org/10.1002/bit.1145>.
- [152] Chetan Goudar, Richard Biener, C. Boisart, Rüdiger Heidemann, James Piret, Albert de Graaf, and Konstantin Konstantinov. Metabolic flux analysis of CHO cells in perfusion culture by metabolite balancing and 2d $[^{13}\text{C}, ^1\text{H}]$ cosy nmr spectroscopy. *Metab Eng*, 12(2):138–149, Mar 2010. URL <http://dx.doi.org/10.1016/j.ymben.2009.10.007>.
- [153] Averina Nicolae, Judith Wahrheit, Janina Bahnemann, An-Ping Zeng, and Elmar Heinzle. Non-stationary ^{13}C metabolic flux analysis of chinese hamster ovary cells in batch culture using extracellular labeling highlights metabolic reversibility and compartmentation. *BMC Syst Biol*, 8:50, 2014. URL <http://dx.doi.org/10.1186/1752-0509-8-50>.
- [154] Jing Fan, Jiangbin Ye, Jurre J. Kamphorst, Tomer Shlomi, Craig B. Thompson, and Joshua D. Rabinowitz. Quantitative flux analysis reveals folate-dependent nadph production. *Nature*, 510(7504):298–302, Jun 2014. URL <http://dx.doi.org/10.1038/nature13236>.
- [155] U. Valley, M. Nimtz, H. S. Conradt, and R. Wagner. Incorporation of ammonium into intracellular udp-activated n-acetylhexosamines and into carbohydrate structures in glycoproteins. *Biotechnol Bioeng*, 64(4):401–417, Aug 1999. URL [http://dx.doi.org/10.1002/\(SICI\)1097-0290\(19990820\)64:4<401::AID-BIT3>3.0.CO;2-M](http://dx.doi.org/10.1002/(SICI)1097-0290(19990820)64:4<401::AID-BIT3>3.0.CO;2-M).
- [156] Ana C. Donadio, Carolina Lobo, Marta Tosina, Vanessa de la Rosa, Mercedes Martín-Rufián, José A. Campos-Sandoval, José M. Matés, Javier Márquez, Francisco J. Alonso, and Juan A. Segura. Antisense glutaminase inhibition modifies the o-glcnae pattern and flux through the hexosamine pathway in breast cancer cells. *J Cell Biochem*, 103(3):800–811, Feb 2008. URL <http://dx.doi.org/10.1002/jcb.21449>.
- [157] Kathryn E. Wellen, Chao Lu, Anthony Mancuso, Johanna M S. Lemons, Michael Ryczko, James W. Dennis, Joshua D. Rabinowitz, Hilary A. Collier, and Craig B. Thompson. The hexosamine biosynthetic pathway couples growth factor-induced

- glutamine uptake to glucose metabolism. *Genes Dev*, 24(24):2784–2799, Dec 2010. URL <http://dx.doi.org/10.1101/gad.1985910>.
- [158] Susan C. Burleigh, Teun van de Laar, Corné J M. Stroop, Wout M J. van Grunsven, Niaobh O’Donoghue, Pauline M. Rudd, and Gavin P. Davey. Synergizing metabolic flux analysis and nucleotide sugar metabolism to understand the control of glycosylation of recombinant protein in cho cells. *BMC Biotechnol*, 11:95, 2011. URL <http://dx.doi.org/10.1186/1472-6750-11-95>.
- [159] Jason W. Locasale, Alexandra R. Grassian, Tamar Melman, Costas A. Lyssiotis, Katherine R. Mattaini, Adam J. Bass, Gregory Heffron, Christian M. Metallo, Taru Muranen, Hadar Sharfi, Atsuo T. Sasaki, Dimitrios Anastasiou, Edouard Mullarky, Natalie I. Vokes, Mika Sasaki, Rameen Beroukhim, Gregory Stephanopoulos, Azra H. Ligon, Matthew Meyerson, Andrea L. Richardson, Lynda Chin, Gerhard Wagner, John M. Asara, Joan S. Brugge, Lewis C. Cantley, and Matthew G. Vander Heiden. Phosphoglycerate dehydrogenase diverts glycolytic flux and contributes to oncogenesis. *Nat Genet*, 43(9):869–874, Sep 2011. URL <http://dx.doi.org/10.1038/ng.890>.
- [160] Elzbieta Petelencz-Kurdziel, Clemens Kuehn, Bodil Nordlander, Dagmara Klein, Kuk-Ki Hong, Therese Jacobson, Peter Dahl, Jörg Schaber, Jens Nielsen, Stefan Hohmann, and Edda Klipp. Quantitative analysis of glycerol accumulation, glycolysis and growth under hyper osmotic stress. *PLoS Comput Biol*, 9(6):e1003084, 2013. URL <http://dx.doi.org/10.1371/journal.pcbi.1003084>.
- [161] P. L. Pedersen. Tumor mitochondria and the bioenergetics of cancer cells. *Prog Exp Tumor Res*, 22:190–274, 1978.
- [162] D. A. Briscoe, G. Fiskum, A. L. Holleran, and J. K. Kelleher. Acetoacetate metabolism in as-30d hepatoma cells. *Mol Cell Biochem*, 136(2):131–137, Jul 1994. URL <http://dx.doi.org/10.1007/BF00926073>.
- [163] Tomer Shlomi, Tomer Benyamini, Eyal Gottlieb, Roded Sharan, and Eytan Ruppin. Genome-scale metabolic modeling elucidates the role of proliferative adaptation in causing the warburg effect. *PLoS Comput Biol*, 7(3):e1002018, Mar 2011. URL <http://dx.doi.org/10.1371/journal.pcbi.1002018>.
- [164] Jens Niklas, Volker Sandig, and Elmar Heinzle. Metabolite channeling and compartmentation in the human cell line age1.hn determined by 13c labeling experiments and 13c metabolic flux analysis. *J Biosci Bioeng*, 112(6):616–623, Dec 2011. URL <http://dx.doi.org/10.1016/j.jbiosc.2011.07.021>.
- [165] Christian Frezza, Liang Zheng, Ori Folger, Kartik N. Rajagopalan, Elaine D. MacKenzie, Livnat Jerby, Massimo Micaroni, Barbara Chaneton, Julie Adam, Ann Hedley, Gabriela Kalna, Ian P M. Tomlinson, Patrick J. Pollard, Dave G. Watson, Ralph J. Deberardinis, Tomer Shlomi, Eytan Ruppin, and Eyal Gottlieb.

-
- Haem oxygenase is synthetically lethal with the tumour suppressor fumarate hydratase. *Nature*, 477(7363):225–228, Sep 2011. URL <http://dx.doi.org/10.1038/nature10363>.
- [166] M. F. Chauvin, F. Megnin-Chanet, G. Martin, J. Mispelter, and G. Baverel. The rabbit kidney tubule simultaneously degrades and synthesizes glutamate. a ^{13}C nmr study. *J Biol Chem*, 272(8):4705–4716, Feb 1997. URL <http://www.jbc.org/content/272/8/4705.long>.
- [167] Fan Wu, Feng Yang, Kalyan C. Vinnakota, and Daniel A. Beard. Computer modeling of mitochondrial tricarboxylic acid cycle, oxidative phosphorylation, metabolite transport, and electrophysiology. *J Biol Chem*, 282(34):24525–24537, Aug 2007. URL <http://dx.doi.org/10.1074/jbc.M701024200>.
- [168] Jens Niklas, Eva Schröder, Volker Sandig, Thomas Noll, and Elmar Heinzle. Quantitative characterization of metabolism and metabolic shifts during growth of the new human cell line age1.hn using time resolved metabolic flux analysis. *Bioprocess Biosyst Eng*, 34(5):533–545, Jun 2011. URL <http://dx.doi.org/10.1007/s00449-010-0502-y>.
- [169] R. W. Moreadith and A. L. Lehninger. The pathways of glutamate and glutamine oxidation by tumor cell mitochondria. role of mitochondrial nad(p)+-dependent malic enzyme. *J Biol Chem*, 259(10):6215–6221, May 1984. URL <http://www.jbc.org/content/259/10/6215.short>.
- [170] G. Gstraunthaler, W. Pfaller, and P. Kotanko. Biochemical characterization of renal epithelial cell cultures (llc-pk1 and mdck). *Am J Physiol*, 248(4 Pt 2):F536–F544, Apr 1985. URL <http://ajprenal.physiology.org/content/248/4/F536>.
- [171] J. C. Street, A. M. Delort, P. S. Braddock, and K. M. Brindle. A $^1\text{H}/^{15}\text{N}$ n.m.r. study of nitrogen metabolism in cultured mammalian cells. *Biochem J*, 291 (Pt 2):485–492, Apr 1993. URL <http://www.biochemj.org/bj/291/bj2910485.htm>.
- [172] AL Lehninger. *Biochemistry, the molecular basis of cell structure and function*. 2nd ed. Worth Publishers, Inc, 1975.
- [173] H. Eagle, V. I. Oyama, M. Levy, C. L. Horton, and R. Fleischmann. The growth response of mammalian cells in tissue culture to l-glutamine and l-glutamic acid. *J Biol Chem*, 218(2):607–616, Feb 1956. URL <http://www.jbc.org/content/218/2/607.full.pdf>.
- [174] Fabian V. Filipp, David A. Scott, Ze’ev A. Ronai, Andrei L. Osterman, and Jeffrey W. Smith. Reverse tca cycle flux through isocitrate dehydrogenases 1 and 2 is required for lipogenesis in hypoxic melanoma cells. *Pigment Cell Melanoma Res*, 25 (3):375–383, May 2012. URL <http://dx.doi.org/10.1111/j.1755-148X.2012.00989.x>.

- [175] Christian M. Metallo, Paulo A. Gameiro, Eric L. Bell, Katherine R. Mattaini, Juanjuan Yang, Karsten Hiller, Christopher M. Jewell, Zachary R. Johnson, Darrell J. Irvine, Leonard Guarente, Joanne K. Kelleher, Matthew G. Vander Heiden, Othon Iliopoulos, and Gregory Stephanopoulos. Reductive glutamine metabolism by *idh1* mediates lipogenesis under hypoxia. *Nature*, 481(7381):380–384, Jan 2012. URL <http://dx.doi.org/10.1038/nature10602>.
- [176] Andrew R. Mullen, Zeping Hu, Xiaolei Shi, Lei Jiang, Lindsey K. Borouhgs, Zoltan Kovacs, Richard Boriack, Dinesh Rakheja, Lucas B. Sullivan, W Marston Linehan, Navdeep S. Chandel, and Ralph J. DeBerardinis. Oxidation of alpha-ketoglutarate is required for reductive carboxylation in cancer cells with mitochondrial defects. *Cell Rep*, 7(5):1679–1690, Jun 2014. URL <http://dx.doi.org/10.1016/j.celrep.2014.04.037>.
- [177] Hai Yan, D Williams Parsons, Genglin Jin, Roger McLendon, B Ahmed Rasheed, Weishi Yuan, Ivan Kos, Ines Batinic-Haberle, Siân Jones, Gregory J. Riggins, Henry Friedman, Allan Friedman, David Reardon, James Herndon, Kenneth W. Kinzler, Victor E. Velculescu, Bert Vogelstein, and Darell D. Bigner. *Idh1* and *idh2* mutations in gliomas. *N Engl J Med*, 360(8):765–773, Feb 2009. URL <http://dx.doi.org/10.1056/NEJMoa0808710>.
- [178] V. B. Lawlis and T. E. Roche. Inhibition of bovine kidney alpha-ketoglutarate dehydrogenase complex by reduced nicotinamide adenine dinucleotide in the presence or absence of calcium ion and effect of adenosine 5'-diphosphate on reduced nicotinamide adenine dinucleotide inhibition. *Biochemistry*, 20(9):2519–2524, Apr 1981. URL <http://dx.doi.org/10.1021/bi00512a024>.
- [179] J. S. Rodríguez-Zavala, J. P. Pardo, and R. Moreno-Sánchez. Modulation of 2-oxoglutarate dehydrogenase complex by inorganic phosphate, $mg(2+)$, and other effectors. *Arch Biochem Biophys*, 379(1):78–84, Jul 2000. URL <http://dx.doi.org/10.1006/abbi.2000.1856>.
- [180] D. L. Nelson and M. M. Cox. *Lehninger Principles of Biochemistry*. 3rd. ed. Worth Publishers, 41 Madison Avenue, New York, NY 10010, 2000.
- [181] R. Moreno-Sánchez, B. A. Hogue, and R. G. Hansford. Influence of nad-linked dehydrogenase activity on flux through oxidative phosphorylation. *Biochem J*, 268(2):421–428, Jun 1990. URL <http://www.biochemj.org/bj/268/bj2680421.htm>.
- [182] S. Rodríguez-Enríquez, M. E. Torres-Márquez, and R. Moreno-Sánchez. Substrate oxidation and atp supply in as-30d hepatoma cells. *Arch Biochem Biophys*, 375(1):21–30, Mar 2000. URL <http://dx.doi.org/10.1006/abbi.1999.1582>.
- [183] Maria Elena Dalmonte, Elena Forte, Maria Luisa Genova, Alessandro Giuffrè, Paolo Sarti, and Giorgio Lenaz. Control of respiration by cytochrome c oxidase in

intact cells: role of the membrane potential. *J Biol Chem*, 284(47):32331–32335, Nov 2009. URL <http://dx.doi.org/10.1074/jbc.M109.050146>.

- [184] Sara Rodríguez-Enríquez, Paola A. Vital-González, Fanny L. Flores-Rodríguez, Alvaro Marín-Hernández, Lena Ruiz-Azuara, and Rafael Moreno-Sánchez. Control of cellular proliferation by modulation of oxidative phosphorylation in human and rodent fast-growing tumor cells. *Toxicol Appl Pharmacol*, 215(2):208–217, Sep 2006. URL <http://dx.doi.org/10.1016/j.taap.2006.02.005>.
- [185] Katherine A. Janeway, Su Young Kim, Maya Lodish, Vânia Nosé, Pierre Rustin, José Gaal, Patricia L M. Dahia, Bernadette Liegl, Evan R. Ball, Margarita Raygada, Angela H. Lai, Lorna Kelly, Jason L. Hornick, N. I. H Pediatric , Wild-Type GIST Clinic, Maureen O’Sullivan, Ronald R. de Krijger, Winand N M. Dinjens, George D. Demetri, Cristina R. Antonescu, Jonathan A. Fletcher, Lee Helman, and Constantine A. Stratakis. Defects in succinate dehydrogenase in gastrointestinal stromal tumors lacking kit and pdgfra mutations. *Proc Natl Acad Sci U S A*, 108(1):314–318, Jan 2011. URL <http://dx.doi.org/10.1073/pnas.1009199108>.
- [186] M. Hillar, V. Lott, and B. Lennox. Correlation of the effects of citric acid cycle metabolites on succinate oxidation by rat liver mitochondria and submitochondrial particles. *J Bioenerg*, 7(1):1–16, Mar 1975. URL <http://dx.doi.org/10.1007/BF01558459>.
- [187] Philippe Icard, Laurent Poulain, and Hubert Lincet. Understanding the central role of citrate in the metabolism of cancer cells. *Biochim Biophys Acta*, 1825(1):111–116, Jan 2012. URL <http://dx.doi.org/10.1016/j.bbcan.2011.10.007>.
- [188] R. A. Parlo and P. S. Coleman. Enhanced rate of citrate export from cholesterol-rich hepatoma mitochondria. the truncated krebs cycle and other metabolic ramifications of mitochondrial membrane cholesterol. *J Biol Chem*, 259(16):9997–10003, Aug 1984. URL <http://www.jbc.org/content/259/16/9997.long>.
- [189] Georgia Hatzivassiliou, Fangping Zhao, Daniel E. Bauer, Charalambos Andreadis, Anthony N. Shaw, Dashyant Dhanak, Sunil R. Hingorani, David A. Tuveson, and Craig B. Thompson. Atp citrate lyase inhibition can suppress tumor cell growth. *Cancer Cell*, 8(4):311–321, Oct 2005. URL <http://dx.doi.org/10.1016/j.ccr.2005.09.008>.
- [190] John C. Schell, Kristofor A. Olson, Lei Jiang, Amy J. Hawkins, Jonathan G. Van Vranken, Jianxin Xie, Robert A. Egnatchik, Espen G. Earl, Ralph J. DeBerardinis, and Jared Rutter. A role for the mitochondrial pyruvate carrier as a repressor of the warburg effect and colon cancer cell growth. *Mol Cell*, 56(3):400–413, Nov 2014. URL <http://dx.doi.org/10.1016/j.molcel.2014.09.026>.

- [191] Jung-whan Kim, Irina Tchernyshyov, Gregg L. Semenza, and Chi V. Dang. Hif-1-mediated expression of pyruvate dehydrogenase kinase: a metabolic switch required for cellular adaptation to hypoxia. *Cell Metab*, 3(3):177–185, Mar 2006. URL <http://dx.doi.org/10.1016/j.cmet.2006.02.002>.
- [192] F. J. Ballard. Adenine nucleotides and the adenylate kinase equilibrium in livers of foetal and newborn rats. *Biochem J*, 117(2):231–235, Apr 1970. URL <http://www.biochemj.org/bj/117/bj1170231.htm>.
- [193] J. S. Hofmeyr and A. Cornish-Bowden. Regulating the cellular economy of supply and demand. *FEBS Lett*, 476(1-2):47–51, Jun 2000. URL [http://dx.doi.org/10.1016/S0014-5793\(00\)01668-9](http://dx.doi.org/10.1016/S0014-5793(00)01668-9).
- [194] D. E. Atkinson and G. M. Walton. Adenosine triphosphate conservation in metabolic regulation. rat liver citrate cleavage enzyme. *J Biol Chem*, 242(13):3239–3241, Jul 1967. URL <http://www.jbc.org/content/242/13/3239.short>.
- [195] D. E. Atkinson. Regulation of enzyme function. *Annu Rev Microbiol*, 23:47–68, 1969. URL <http://dx.doi.org/10.1146/annurev.mi.23.100169.000403>.
- [196] A. G. Chapman, L. Fall, and D. E. Atkinson. Adenylate energy charge in escherichia coli during growth and starvation. *J Bacteriol*, 108(3):1072–1086, Dec 1971. URL <http://jlb.asm.org/content/108/3/1072.short>.
- [197] Thomas Walther, Maite Novo, Katrin Rössger, Fabien Létisse, Marie-Odile Loret, Jean-Charles Portais, and Jean-Marie François. Control of atp homeostasis during the respiro-fermentative transition in yeast. *Mol Syst Biol*, 6:344, 2010. URL <http://dx.doi.org/10.1038/msb.2009.100>.
- [198] H. Schmidt, W. Siems, M. Müller, R. Dumdey, and S. M. Rapoport. Atp-producing and consuming processes of ehrlich mouse ascites tumor cells in proliferating and resting phases. *Exp Cell Res*, 194(1):122–127, May 1991. URL [http://dx.doi.org/10.1016/0014-4827\(91\)90140-P](http://dx.doi.org/10.1016/0014-4827(91)90140-P).
- [199] Malkhey Verma, Maksim Zakhartsev, Matthias Reuss, and Hans V Westerhoff. 'domino' systems biology and the 'a' of atp. *Biochim Biophys Acta*, 1827(1):19–29, Jan 2013. URL <http://dx.doi.org/10.1016/j.bbabi.2012.09.014>.
- [200] S. Soboll, R. Scholz, and H. W. Heldt. Subcellular metabolite concentrations. dependence of mitochondrial and cytosolic atp systems on the metabolic state of perfused rat liver. *Eur J Biochem*, 87(2):377–390, Jun 1978. URL <http://dx.doi.org/10.1111/j.1432-1033.1978.tb12387.x>.
- [201] Hiroaki Kitano. Computational systems biology. *Nature*, 420(6912):206–210, Nov 2002. URL <http://dx.doi.org/10.1038/nature01254>.

-
- [202] Frank J. Bruggeman and Hans V. Westerhoff. The nature of systems biology. *Trends Microbiol*, 15(1):45–50, Jan 2007. URL <http://dx.doi.org/10.1016/j.tim.2006.11.003>.
- [203] Natal A W van Riel. Dynamic modelling and analysis of biochemical networks: mechanism-based models and model-based experiments. *Brief Bioinform*, 7(4): 364–374, Dec 2006. URL <http://dx.doi.org/10.1093/bib/bb1040>.
- [204] M. Rodriguez-Fernandez, E. Balsa-Canto, J.A. Egea, and J.R. Banga. Identifiability and robust parameter estimation in food process modeling: Application to a drying model. *Journal of Food Engineering*, 83:374–383, 2007. URL <http://dx.doi.org/10.1016/j.jfoodeng.2007.03.023>.
- [205] Markus Krauss, Rolf Burghaus, Jörg Lippert, Mikko Niemi, Pertti Neuvonen, Andreas Schuppert, Stefan Willmann, Lars Kuepfer, and Linus Görlitz. Using bayesian-pbpc modeling for assessment of inter-individual variability and subgroup stratification. *In Silico Pharmacol*, 1:6, 2013. URL <http://dx.doi.org/10.1186/2193-9616-1-6>.
- [206] H.M. Tsuchiya, A.G. Fredrickson, and R. Aris. Dynamics of microbial cell populations. volume 6 of *Advances in Chemical Engineering*, pages 125 – 206. Academic Press, 1966. URL <http://www.sciencedirect.com/science/article/pii/S0065237708602756>.
- [207] Ana P Teixeira, Nuno Carinhas, João M L Dias, Pedro Cruz, Paula M Alves, Manuel J T Carrondo, and Rui Oliveira. Hybrid semi-parametric mathematical systems: bridging the gap between systems biology and process engineering. *J Biotechnol*, 132(4):418–425, Dec 2007. URL <http://dx.doi.org/10.1016/j.jbiotec.2007.08.020>.
- [208] W. M. Miller, H. W. Blanch, and C. R. Wilke. A kinetic analysis of hybridoma growth and metabolism in batch and continuous suspension culture: effect of nutrient concentration, dilution rate, and ph. *Biotechnol Bioeng*, 67(6):853–871, Mar 2000. URL <http://dx.doi.org/10.1002/bit.260320803>.
- [209] Chetan T Goudar, Klaus Joeris, Konstantin B Konstantinov, and James M Piret. Logistic equations effectively model mammalian cell batch and fed-batch kinetics by logically constraining the fit. *Biotechnol Prog*, 21(4):1109–1118, 2005. URL <http://dx.doi.org/10.1021/bp050018j>.
- [210] R. Poertner and T. Schaefer. Modelling hybridoma cell growth and metabolism—a comparison of selected models and data. *J Biotechnol*, 49(1-3):119–135, Aug 1996. URL [http://dx.doi.org/10.1016/0168-1656\(96\)01535-0](http://dx.doi.org/10.1016/0168-1656(96)01535-0).
- [211] Lars Möhler, Andreas Bock, and Udo Reichl. Segregated mathematical model for growth of anchorage-dependent mdck cells in microcarrier culture. *Biotechnol Prog*, 24(1):110–119, 2008. URL <http://dx.doi.org/10.1021/bp0701923>.

- [212] Andreas Bock, Heiner Sann, Josef Schulze-Horsel, Yvonne Genzel, Udo Reichl, and Lars Möhler. Growth behavior of number distributed adherent mdck cells for optimization in microcarrier cultures. *Biotechnol Prog*, 25(6):1717–1731, 2009. URL <http://dx.doi.org/10.1002/btpr.262>.
- [213] R. S. Cherry and E. T. Papoutsakis. Modeling of contact-inhibited animal cell growth on flat surfaces and spheres. *Biotechnol Bioeng*, 33(3):300–305, Jan 1989. URL <http://dx.doi.org/10.1002/bit.260330308>.
- [214] J. H. Lim and G. A. Davies. A stochastic model to simulate the growth of anchorage dependent cells on flat surfaces. *Biotechnol Bioeng*, 36(6):547–562, Sep 1990. URL <http://dx.doi.org/10.1002/bit.260360602>.
- [215] K. Zygourakis, R. Bizios, and P. Markenscoff. Proliferation of anchorage-dependent contact-inhibited cells: I. development of theoretical models based on cellular automata. *Biotechnol Bioeng*, 38(5):459–470, Aug 1991. URL <http://dx.doi.org/10.1002/bit.260380504>.
- [216] M. Rehberg, J. B. Ritter, Y. Genzel, D. Flockerzi, and U. Reichl. The relation between growth phases, cell volume changes and metabolism of adherent cells during cultivation. *J Biotechnol*, Feb 2013. URL <http://dx.doi.org/10.1016/j.jbiotec.2013.01.018>.
- [217] M Baltes, R Schneider, C Sturm, and M Reuss. Optimal experimental-design for parameter-estimation in unstructured growth-models. *Biotechnology Progress*, 10(5):480–488, SEP-OCT 1994. ISSN 8756-7938. URL <http://dx.doi.org/10.1021/bp00029a005>.
- [218] AG Fredrickson and NV Mantzaris. A new set of population balance equations for microbial and cell cultures. *Chemical Engineering Science*, 57(12):2265–2278, JUN 2002. ISSN 0009-2509. URL [http://dx.doi.org/10.1016/S0009-2509\(02\)00116-1](http://dx.doi.org/10.1016/S0009-2509(02)00116-1).
- [219] A. G. Fredrickson. Population balance equations for cell and microbial cultures revisited. *Aiche Journal*, 49(4):1050–1059, April 2003. URL <http://dx.doi.org/10.1002/aic.690490422>.
- [220] E. C. Anderson, G. I. Bell, D. F. Petersen, and R. A. Tobey. Cell growth and division. iv. determination of volume growth rate and division probability. *Biophys J*, 9(2):246–263, Feb 1969. URL [http://dx.doi.org/10.1016/S0006-3495\(69\)86383-6](http://dx.doi.org/10.1016/S0006-3495(69)86383-6).
- [221] J. M. Eakman, A. G. Fredickson, and Tsuchiya H. M. Statistics and dynamics of microbial cell populations. *Chem Eng Prog Symp Ser*, 62((69)):37–49, 1966.

-
- [222] Sarah Fadda, Alberto Cincotti, and Giacomo Cao. A novel population balance model to investigate the kinetics of in vitro cell proliferation: part i. model development. *Biotechnol Bioeng*, 109(3):772–781, Mar 2012. URL <http://dx.doi.org/10.1002/bit.24351>.
- [223] G. Subramanian, D. Ramkrishna, A. G. Fredrickson, and H. M. Tsuchiya. On the mass distribution model for microbial cell populations. *Bull Math Biophys*, 32(4):521–537, Dec 1970. URL <http://dx.doi.org/10.1007/BF02476769>.
- [224] J. J. Liou, F. Sreenc, and A. G. Fredrickson. Solutions of population balance models based on a successive generations approach. *Chemical Engineering Science*, 52(9):1529–1540, May 1997. URL [http://dx.doi.org/10.1016/S0009-2509\(96\)00510-6](http://dx.doi.org/10.1016/S0009-2509(96)00510-6).
- [225] N. V. Mantzaris, P. Daoutidis, and F. Sreenc. Numerical solution of multi-variable cell population balance models: I. finite difference methods. *Computers & Chemical Engineering*, 25(11-12):1411–1440, November 2001. URL [http://dx.doi.org/10.1016/S0098-1354\(01\)00709-8](http://dx.doi.org/10.1016/S0098-1354(01)00709-8).
- [226] B. Chance, D. Garfinkel, J. Higgins, and B. Hess. Metabolic control mechanisms. 5. a solution for the equations representing interaction between glycolysis and respiration in ascites tumor cells. *J Biol Chem*, 235:2426–2439, Aug 1960. URL <http://www.jbc.org/content/235/8/2426.long>.
- [227] T. A. Rapoport, R. Heinrich, G. Jacobasch, and S. Rapoport. A linear steady-state treatment of enzymatic chains. a mathematical model of glycolysis of human erythrocytes. *Eur J Biochem*, 42(1):107–120, Feb 1974. URL <http://dx.doi.org/10.1111/j.1432-1033.1974.tb03320.x>.
- [228] M. Otto, R. Heinrich, G. Jacobasch, and S. Rapoport. A mathematical model for the influence of anionic effectors on the phosphofructokinase from rat erythrocytes. *Eur J Biochem*, 74(2):413–420, Apr 1977. URL <http://dx.doi.org/10.1111/j.1432-1033.1977.tb11406.x>.
- [229] M. Otto, R. Heinrich, B. Kuhn, and G. Jacobasch. A mathematical model for the influence of fructose 6-phosphate, atp, potassium, ammonium and magnesium on the phosphofructokinase from rat erythrocytes;. *Eur J Biochem*, 49(1):169–178, Nov 1974. URL <http://dx.doi.org/10.1111/j.1432-1033.1974.tb03822.x>.
- [230] M. Schauer, R. Heinrich, and S. M. Rapoport. Mathematical modelling of glycolysis and adenine nucleotide metabolism of human erythrocytes. i. reaction-kinetic statements, analysis of in vivo state and determination of starting conditions for in vitro experiments. *Acta Biol Med Ger*, 40(12):1659–1682, 1981.
- [231] M. Schauer, R. Heinrich, and S. M. Rapoport. Mathematical modelling of glycolysis and of adenine nucleotide metabolism of human erythrocytes. ii. simulation

- of adenine nucleotide breakdown following glucose depletion. *Acta Biol Med Ger*, 40(12):1683–1697, 1981.
- [232] R. Heinrich, S. M. Rapoport, and T. A. Rapoport. Metabolic regulation and mathematical models. *Prog Biophys Mol Biol*, 32(1):1–82, 1977. URL [http://dx.doi.org/10.1016/0079-6107\(78\)90017-2](http://dx.doi.org/10.1016/0079-6107(78)90017-2).
- [233] R. Schuster, G. Jacobasch, and H. G. Holzhütter. Mathematical modelling of metabolic pathways affected by an enzyme deficiency. energy and redox metabolism of glucose-6-phosphate-dehydrogenase-deficient erythrocytes. *Eur J Biochem*, 182(3):605–612, Jul 1989. URL <http://dx.doi.org/10.1111/j.1432-1033.1989.tb14869.x>.
- [234] H. G. Holzhütter, G. Jacobasch, and A. Bisdorff. Mathematical modelling of metabolic pathways affected by an enzyme deficiency. a mathematical model of glycolysis in normal and pyruvate-kinase-deficient red blood cells. *Eur J Biochem*, 149(1):101–111, May 1985. URL <http://dx.doi.org/10.1111/j.1432-1033.1985.tb08899.x>.
- [235] Melissa J Lambeth and Martin J Kushmerick. A computational model for glycogenolysis in skeletal muscle. *Ann Biomed Eng*, 30(6):808–827, Jun 2002. URL <http://dx.doi.org/10.1114/1.1492813>.
- [236] D. Visser, R. van der Heijden, K. Mauch, M. Reuss, and S. Heijnen. Tendency modeling: a new approach to obtain simplified kinetic models of metabolism applied to *saccharomyces cerevisiae*. *Metab Eng*, 2(3):252–275, Jul 2000. URL <http://dx.doi.org/10.1006/mben.2000.0150>.
- [237] M. Rizzi, M. Baltes, U. Theobald, and M. Reuss. In vivo analysis of metabolic dynamics in *saccharomyces cerevisiae*: Ii. mathematical model. *Biotechnol Bioeng*, 55(4):592–608, Aug 1997. URL <http://dx.doi.org/3.0.C0;2-C>.
- [238] Oliver Kotte, Judith B. Zaugg, and Matthias Heinemann. Bacterial adaptation through distributed sensing of metabolic fluxes. *Mol Syst Biol*, 6:355, 2010. URL <http://dx.doi.org/10.1038/msb.2010.10>.
- [239] A. Kremling, K. Bettenbrock, B. Laube, K. Jahreis, J. W. Lengeler, and E. D. Gilles. The organization of metabolic reaction networks. iii. application for diauxic growth on glucose and lactose. *Metab Eng*, 3(4):362–379, Oct 2001. URL <http://dx.doi.org/10.1006/mben.2001.0199>.
- [240] F. Hynne, S. Danø, and P. G. Sørensen. Full-scale model of glycolysis in *saccharomyces cerevisiae*. *Biophys Chem*, 94(1-2):121–163, Dec 2001. URL [http://dx.doi.org/10.1016/S0301-4622\(01\)00229-0](http://dx.doi.org/10.1016/S0301-4622(01)00229-0).
- [241] O. Richter, A. Betz, and C. Giersch. The response of oscillating glycolysis to perturbations in the nadh/nad system: a comparison between experiments and a computer model. *Biosystems*, 7(1):137–146, Jul 1975.

-
- [242] B. Teusink, J. Passarge, C. A. Reijenga, E. Esgalhado, C. C. van der Weijden, M. Schepper, M. C. Walsh, B. M. Bakker, K. van Dam, H. V. Westerhoff, and J. L. Snoep. Can yeast glycolysis be understood in terms of in vitro kinetics of the constituent enzymes? testing biochemistry. *Eur J Biochem*, 267(17):5313–5329, Sep 2000.
- [243] Arren Bar-Even, Avi Flamholz, Elad Noor, and Ron Milo. Rethinking glycolysis: on the biochemical logic of metabolic pathways. *Nat Chem Biol*, 8(6):509–517, Jun 2012. URL <http://dx.doi.org/10.1038/nchembio.971>.
- [244] D. Garfinkel. Simulation of the krebs cycle and closely related metabolism in perfused rat liver. i. construction of a model. *Comput Biomed Res*, 4(1):1–17, Apr 1971. URL [http://dx.doi.org/10.1016/0010-4809\(71\)90044-9](http://dx.doi.org/10.1016/0010-4809(71)90044-9).
- [245] E. M. Chance, S. H. Seeholzer, K. Kobayashi, and J. R. Williamson. Mathematical analysis of isotope labeling in the citric acid cycle with applications to ^{13}C nmr studies in perfused rat hearts. *J Biol Chem*, 258(22):13785–13794, Nov 1983. URL <http://www.jbc.org/content/258/22/13785.full.pdf>.
- [246] R. G. Weiss, S. T. Gloth, R. Kalil-Filho, V. P. Chacko, M. D. Stern, and G. Gerstenblith. Indexing tricarboxylic acid cycle flux in intact hearts by carbon-13 nuclear magnetic resonance. *Circ Res*, 70(2):392–408, Feb 1992. URL <http://circres.ahajournals.org/content/70/2/392.short>.
- [247] My-Hanh T. Nguyen, S. J. Dudycha, and M Saleet Jafri. Effect of Ca^{2+} on cardiac mitochondrial energy production is modulated by Na^{+} and H^{+} dynamics. *Am J Physiol Cell Physiol*, 292(6):C2004–C2020, Jun 2007. URL <http://dx.doi.org/10.1152/ajpcell.00271.2006>.
- [248] J. N. Bazil, G. T. Buzzard, and A. E. Rundell. Modeling mitochondrial bioenergetics with integrated volume dynamics. *Plos Computational Biology*, 6(1):e1000632, January 2010. URL <http://dx.doi.org/10.1371/journal.pcbi.1000632>.
- [249] Sonia Cortassa, Miguel A. Aon, Brian O’Rourke, Robert Jacques, Hsiang-Jer Tseng, Eduardo Marbán, and Raimond L. Winslow. A computational model integrating electrophysiology, contraction, and mitochondrial bioenergetics in the ventricular myocyte. *Biophys J*, 91(4):1564–1589, Aug 2006. URL <http://dx.doi.org/10.1529/biophysj.105.076174>.
- [250] K Mauch, S Vaseghi, and M Reuss. *Bioreaction engineering. Modeling and Control*. Springer, 2000.
- [251] Christine Nazaret, Margit Heiske, Kevin Thurley, and Jean-Pierre Mazat. Mitochondrial energetic metabolism: a simplified model of tca cycle with atp production. *J Theor Biol*, 258(3):455–464, Jun 2009. URL <http://dx.doi.org/10.1016/j.jtbi.2008.09.037>.

- [252] Ali Khodayari, Ali R. Zomorodi, James C. Liao, and Costas D. Maranas. A kinetic model of escherichia coli core metabolism satisfying multiple sets of mutant flux data. *Metab Eng*, Jun 2014. URL <http://dx.doi.org/10.1016/j.ymben.2014.05.014>.
- [253] C. Chassagnole, N. Noisommit-Rizzi, J. W. Schmid, K. Mauch, and M. Reuss. Dynamic modeling of the central carbon metabolism of escherichia coli. *Biotechnology and Bioengineering*, 79(1):53–73, July 2002. URL <http://dx.doi.org/10.1002/bit.10288>.
- [254] Atefeh Ghorbaniaghdam, Olivier Henry, and Mario Jolicoeur. A kinetic-metabolic model based on cell energetic state: study of cho cell behavior under na-butyrate stimulation. *Bioprocess Biosyst Eng*, 36(4):469–487, Apr 2013. URL <http://dx.doi.org/10.1007/s00449-012-0804-3>.
- [255] Z. Amribt, L. Dewasme, A. Vande Wouwer, and Ph Bogaerts. Optimization and robustness analysis of hybridoma cell fed-batch cultures using the overflow metabolism model. *Bioprocess Biosyst Eng*, 37(8):1637–1652, Aug 2014. URL <http://dx.doi.org/10.1007/s00449-014-1136-2>.
- [256] B. C. Batt and D. S. Kompala. A structured kinetic modeling framework for the dynamics of hybridoma growth and monoclonal antibody production in continuous suspension cultures. *Biotechnol Bioeng*, 34(4):515–531, Aug 1989. URL <http://dx.doi.org/10.1002/bit.260340412>.
- [257] W. W. Cleland. The kinetics of enzyme-catalyzed reactions with two or more substrates or products. i. nomenclature and rate equations. 1963. *Biochim Biophys Acta*, 1000:213–220, 1989. URL [http://dx.doi.org/10.1016/0926-6569\(63\)90211-6](http://dx.doi.org/10.1016/0926-6569(63)90211-6).
- [258] W. W. Cleland. The kinetics of enzyme-catalyzed reactions with two or more substrates or products. ii. inhibition: nomenclature and theory. *Biochim Biophys Acta*, 67:173–187, Feb 1963. URL [http://dx.doi.org/10.1016/0926-6569\(63\)90226-8](http://dx.doi.org/10.1016/0926-6569(63)90226-8).
- [259] W. W. Cleland. The kinetics of enzyme-catalyzed reactions with two or more substrates or products : Iii. prediction of initial velocity and inhibition patterns by inspection. *Biochimica et Biophysica Acta (BBA) - Specialized Section on Enzymological Subjects*, 67:188 – 196, 1963. ISSN 0926-6569. URL <http://www.sciencedirect.com/science/article/B73GF-49518TS-Y/2/67d6f85eca623509bb462aad087c6e3f>.
- [260] EL King and C Altman. A schematic method of deriving the rate laws for enzyme-catalyzed reactions. *Journal of physical chemistry*, 60(10):1375–1378, 1956. ISSN 0022-3654. URL <http://dx.doi.org/10.1021/j150544a010>.

-
- [261] A. V. Hill. The possible effects of the aggregation of the molecules of haemoglobin on its dissociation curves. *The Journal of Physiology*, 40:iv–vii, 1910. URL <http://jp.physoc.org/content/40/supplement/i.short>.
- [262] J Monod, J Wyman, and P Changeux. On the nature of allosteric transitions: a plausible model. *J Mol Biol*, 12:88–118, May 1965. URL [http://dx.doi.org/10.1016/S0022-2836\(65\)80285-6](http://dx.doi.org/10.1016/S0022-2836(65)80285-6).
- [263] H Bisswanger. *Enzymkinetik. Theorie und Methoden*. 3. Auflage. WILEY-VHC Verlag GmbH, Weinheim, Germany, 2000.
- [264] R. Bellman and K.J. Åström. On structural identifiability. *Mathematical Biosciences*, 7(3-4):329 – 339, 1970. ISSN 0025-5564. URL <http://www.sciencedirect.com/science/article/pii/002555647090132X>.
- [265] C.G. Moles, P. Mendes, and J.R. Banga. Parameter estimation in biochemical pathways: a comparison of global optimization methods. *Genome Research.*, 13: 2467–2474, 2003b. URL <http://dx.doi.org/10.1101/gr.1262503>.
- [266] JA Jacquez and P Greif. Numerical parameter identifiability and estimability - integrating identifiability, estimability, and optimal sampling design. *Mathematical Biosciences*, 77(1-2):201–227, DEC 1985. ISSN 0025-5564. URL [http://dx.doi.org/10.1016/0025-5564\(85\)90098-7](http://dx.doi.org/10.1016/0025-5564(85)90098-7).
- [267] A. Raue, C. Kreutz, T. Maiwald, J. Bachmann, M. Schilling, U. Klingmüller, and J. Timmer. Structural and practical identifiability analysis of partially observed dynamical models by exploiting the profile likelihood. *Bioinformatics*, 25(15): 1923–9, Aug 2009. URL <http://dx.doi.org/10.1093/bioinformatics/btp358>.
- [268] E. D. Sontag. For differential equations with r parameters, $2r+1$ experiments are enough for identification. *Nonlinear Science*, 12:553–583, 2002. URL <http://arxiv.org/pdf/math/0111135.pdf>.
- [269] Ryan N. Gutenkunst, Joshua J. Waterfall, Fergal P. Casey, Kevin S. Brown, Christopher R. Myers, and James P. Sethna. Universally sloppy parameter sensitivities in systems biology models. *PLoS Comput Biol*, 3(10):1871–1878, Oct 2007. URL <http://dx.doi.org/10.1371/journal.pcbi.0030189>.
- [270] E. Balsa-Canto, A. A. Alonso, and J. R. Banga. Computational procedures for optimal experimental design in biological systems. *IET Syst Biol*, 2(4):163–172, Jul 2008. URL <http://dx.doi.org/10.1049/iet-syb:20070069>.
- [271] B. Efron and R. Tibshirani. Bootstrap methods for standard errors, confidence intervals, and other measures of statistical accuracy. *Statistical Science*, 1(1):54–77, 1986. URL <http://dx.doi.org/10.1214/ss/1177013815>.

- [272] M. C. Neale and M. B. Miller. The use of likelihood-based confidence intervals in genetic models. *Behav Genet*, 27(2):113–120, Mar 1997. URL <http://dx.doi.org/10.1023/A%3A1025681223921>.
- [273] M. Girolami. Bayesian inference for differential equations. *Theoretical Computer Science*, 408(1):4–16, November 2008. URL <http://dx.doi.org/10.1016/j.tcs.2008.07.005>.
- [274] K. S. Brown, C. C. Hill, G. A. Calero, C. R. Myers, K. H. Lee, J. P. Sethna, and R. A. Cerione. The statistical mechanics of complex signaling networks: nerve growth factor signaling. *Phys Biol*, 1(3-4):184–195, Dec 2004. URL <http://dx.doi.org/10.1088/1478-3967/1/3/006>.
- [275] J. M. Carlson and John Doyle. Complexity and robustness. *Proc Natl Acad Sci U S A*, 99 Suppl 1:2538–2545, Feb 2002. URL <http://dx.doi.org/10.1073/pnas.012582499>.
- [276] J Monod. The growth of bacterial cultures. *ANNUAL REVIEW OF MICROBIOLOGY*, 3:371–394, 1949. ISSN 0066-4227.
- [277] Suh-Chin Wu. Influence of hydrodynamic shear stress on microcarrier-attached cell growth: Cell line dependency and surfactant protection. *Bioprocess Engineering*, 21(3):201–206, 1999. ISSN 0178-515X. URL <http://dx.doi.org/10.1007/s004490050663>.
- [278] K. K. Frame and W. S. Hu. A model for density-dependent growth of anchorage-dependent mammalian cells. *Biotechnol Bioeng*, 32(8):1061–1066, Oct 1988. URL <http://dx.doi.org/10.1002/bit.260320813>.
- [279] K. K. Frame and W. S. Hu. Kinetic study of hybridoma cell growth in continuous culture: Ii. behavior of producers and comparison to nonproducers. *Biotechnol Bioeng*, 38(9):1020–1028, Nov 1991. URL <http://dx.doi.org/10.1002/bit.260380910>.
- [280] Maria Wetzel. Modellierung von glutaminolyse und citratzyklus zur analyse von energiegewinnung und biosynthese in mdck zellen. Master’s thesis, Otto von Guericke University Magdeburg, 2013.
- [281] D. L. Purich and H. J. Fromm. Studies on factors influencing enzyme responses to adenylate energy charge. *Journal of Biological Chemistry*, 247(1):249–&, 1972.
- [282] M. Rizzi, U. Theobald, E. Querfurth, T. Rohrhirsch, M. Baltes, and M. Reuss. In vivo investigations of glucose transport in *saccharomyces cerevisiae*. *Biotechnol Bioeng*, 49(3):316–327, Feb 1996. URL <http://dx.doi.org/3.0.CO;2-C>.
- [283] Alexander G. Rath, Markus Rehberg, Robert Janke, Yvonne Genzel, Sebastian Scholz, Thomas Noll, Thomas Rose, Volker Sandig, and Udo Reichl. The influence

of cell growth and enzyme activity changes on intracellular metabolite dynamics in *age1.hn.aat* cells. *Journal of Biotechnology*, (0):–, 2014. ISSN 0168-1656. URL <http://www.sciencedirect.com/science/article/pii/S0168165614001151>.

- [284] A. Boiteux and B. Hess. Design of glycolysis. *Philos Trans R Soc Lond B Biol Sci*, 293(1063):5–22, Jun 1981. URL <http://dx.doi.org/10.1098/rstb.1981.0056>.
- [285] B. P. Bode, D. L. Kaminski, W. W. Souba, and A. P. Li. Glutamine transport in isolated human hepatocytes and transformed liver cells. *Hepatology*, 21(2):511–520, Feb 1995. URL <http://dx.doi.org/10.1002/hep.1840210236>.
- [286] Fabian V. Filipp, Boris Ratnikov, Jessica De Ingeniis, Jeffrey W. Smith, Andrei L. Osterman, and David A. Scott. Glutamine-fueled mitochondrial metabolism is decoupled from glycolysis in melanoma. *Pigment Cell Melanoma Res*, 25(6):732–739, Nov 2012. URL <http://dx.doi.org/10.1111/pcmr.12000>.
- [287] R. F. Chen and G. W. Plaut. Studies on the hydrogen transfer mediated by the dpn-linked isocitric dehydrogenase of heart. *Biochemistry*, 2:752–756, 1963. URL <http://dx.doi.org/10.1021/bi00904a022>.
- [288] G. W. Plaut, C. P. Cheung, R. J. Suhadolnik, and T. Aogaichi. Cosubstrate and allosteric modifier activities of structural analogues of nad and adp for nad-specific isocitrate dehydrogenase from bovine heart. *Biochemistry*, 18(15):3430–3438, Jul 1979. URL <http://dx.doi.org/10.1021/bi00582a034>.
- [289] U. Theobald, W. Mailinger, M. Baltés, M. Rizzi, and M. Reuss. In vivo analysis of metabolic dynamics in *saccharomyces cerevisiae* : I. experimental observations. *Biotechnol Bioeng*, 55(2):305–316, Jul 1997. URL <http://dx.doi.org/3.0.CO;2-M>.
- [290] H. J. Cruz, J. L. Moreira, and M. J. Carrondo. Metabolic shifts by nutrient manipulation in continuous cultures of *bhk* cells. *Biotechnol Bioeng*, 66(2):104–113, 1999. URL [http://dx.doi.org/10.1002/\(SICI\)1097-0290\(1999\)66:2<104::AID-BIT3>3.0.CO;2-#](http://dx.doi.org/10.1002/(SICI)1097-0290(1999)66:2<104::AID-BIT3>3.0.CO;2-#).
- [291] Henning Schmidt and Mats Jirstrand. Systems biology toolbox for matlab: a computational platform for research in systems biology. *Bioinformatics*, 22(4):514–515, Feb 2006. URL <http://dx.doi.org/10.1093/bioinformatics/bti799>.
- [292] S.D. Cohen and A.C. Hindmarsh. Cvode, a stiff/nonstiff ode solver in c. *Computers in Physics*, 10(2):138–43, March-April 1996. ISSN 0894-1866. URL <https://computation.llnl.gov/casc/nsde/pubs/u121014.pdf>.
- [293] J. A. Egea, M. Rodriguez-Fernandez, J. R. Banga, and R. Marti. Scatter search for chemical and bio-process optimization. *Journal of Global Optimization*, 37 (3): 481–503, 2007. URL <http://dx.doi.org/10.1007/s10898-006-9075-3>.

- [294] M. Joshi, A. Seidel-Morgenstern, and A. Kremling. Exploiting the bootstrap method for quantifying parameter confidence intervals in dynamical systems. *Metab Eng*, 8(5):447–455, Sep 2006. URL <http://dx.doi.org/10.1016/j.ymben.2006.04.003>.
- [295] M. Rehberg, A. Rath, J. B. Ritter, Y. Genzel, and U. Reichl. Changes in intracellular metabolite pools during growth of adherent mdck cells in two different media. *Appl Microbiol Biotechnol*, 98(1):385–397, Jan 2014. URL <http://dx.doi.org/10.1007/s00253-013-5329-4>.
- [296] R. Wu and E. Racker. Regulatory mechanisms in carbohydrate metabolism. iii. limiting factors in glycolysis of ascites tumor cells. *J Biol Chem*, 234(5):1029–1035, May 1959. URL <http://www.jbc.org/content/234/5/1029.full.pdf>.
- [297] Joshua Munger, Bryson D Bennett, Anuraag Parikh, Xiao-Jiang Feng, Jessica McArdle, Herschel A Rabitz, Thomas Shenk, and Joshua D Rabinowitz. Systems-level metabolic flux profiling identifies fatty acid synthesis as a target for antiviral therapy. *Nat Biotechnol*, 26(10):1179–1186, Oct 2008. URL <http://dx.doi.org/10.1038/nbt.1500>.
- [298] Maria L Macheda, Suzanne Rogers, and James D Best. Molecular and cellular regulation of glucose transporter (glut) proteins in cancer. *J Cell Physiol*, 202(3):654–662, Mar 2005. URL <http://dx.doi.org/10.1002/jcp.20166>.
- [299] Yvonne Genzel, Christian Dietzsch, Erdmann Rapp, Jana Schwarzer, and Udo Reichl. Mdck and vero cells for influenza virus vaccine production: a one-to-one comparison up to lab-scale bioreactor cultivation. *Appl Microbiol Biotechnol*, 88(2):461–475, Sep 2010. URL <http://dx.doi.org/10.1007/s00253-010-2742-9>.
- [300] Mariia Yuneva, Nicola Zamboni, Peter Oefner, Ravi Sachidanandam, and Yuri Lazebnik. Deficiency in glutamine but not glucose induces myc-dependent apoptosis in human cells. *The Journal of Cell Biology*, 178(1):93–105, 2007. URL <http://jcb.rupress.org/content/178/1/93.abstract>.
- [301] Marie Odile Loret, Lene Pedersen, and Jean François. Revised procedures for yeast metabolites extraction: application to a glucose pulse to carbon-limited yeast cultures, which reveals a transient activation of the purine salvage pathway. *Yeast*, 24(1):47–60, Jan 2007. URL <http://dx.doi.org/10.1002/yea.1435>.
- [302] T. W. Traut. Physiological concentrations of purines and pyrimidines. *Mol Cell Biochem*, 140(1):1–22, Nov 1994. URL <http://dx.doi.org/10.1007/BF00928361>.
- [303] J. M. Klassen. Modeling growth and metabolism of continuously growing age1.hn.aat cells. Master’s thesis, Otto von Guericke University Magdeburg, 2015.

-
- [304] Markus Rehberg, Joachim B. Ritter, and Udo Reichl. Glycolysis is governed by growth regime and simple enzyme regulation in adherent mdck cells. *PLoS Comput Biol*, 10(10):e1003885, Oct 2014. URL <http://dx.doi.org/10.1371/journal.pcbi.1003885>.
- [305] Markus Rehberg, Maria Wetzels, Joachim B. Ritter, and Udo Reichl. The regulation of glutaminolysis and citric acid cycle activity during mammalian cell cultivation. In *Proc. 12th IFAC Symposium on Computer Applications in Biotechnology (CAB), Mumbai*, 12(48-53):48–53, 2013.
- [306] Gregg L. Semenza. Hif-1 mediates the warburg effect in clear cell renal carcinoma. *J Bioenerg Biomembr*, 39(3):231–234, Jun 2007. URL <http://dx.doi.org/10.1007/s10863-007-9081-2>.
- [307] R. W. Nash, B. S. McKay, and J. M. Burke. The response of cultured human retinal pigment epithelium to hypoxia: a comparison to other cell types. *Invest Ophthalmol Vis Sci*, 35(6):2850–2856, May 1994. URL <http://www.iovs.org/content/35/6/2850.short>.
- [308] Patrick Hossler, Bhanu Chandra Mulukutla, and Wei-Shou Hu. Systems analysis of n-glycan processing in mammalian cells. *PLoS One*, 2(8):e713, 2007. URL <http://dx.doi.org/10.1371/journal.pone.0000713>.
- [309] K. van Eunen, P. Dool, A. B. Canelas, J. Kiewiet, J. Bouwman, W. M. van Gulik, H. V. Westerhoff, and B. M. Bakker. Time-dependent regulation of yeast glycolysis upon nitrogen starvation depends on cell history. *IET SYSTEMS BIOLOGY*, 4(2):157–168, MAR 2010. ISSN 1751-8849. URL <http://dx.doi.org/10.1049/iet-syb.2009.0025>.
- [310] Sergio Grimbs, Joachim Selbig, Sascha Bulik, Hermann-Georg Holzhütter, and Ralf Steuer. The stability and robustness of metabolic states: identifying stabilizing sites in metabolic networks. *Mol Syst Biol*, 3:146, 2007. URL <http://dx.doi.org/10.1038/msb4100186>. [msb4100186-s1.pdf](#).
- [311] Morgan Stathem, Subathra Marimuthu, Julie O’Neal, Jeffrey C. Rathmell, Jason A. Chesney, Levi J. Beverly, and Leah J. Siskind. Glucose availability and glycolytic metabolism dictate glycosphingolipid levels. *J Cell Biochem*, 116(1):67–80, Jan 2015. URL <http://dx.doi.org/10.1002/jcb.24943>.
- [312] S Mazurek, CB Boschek, and E Eigenbrodt. The role of phosphometabolites in cell proliferation, energy metabolism, and tumor therapy. *J Bioenerg Biomembr*, 29(4):315–330, 1997. URL <http://dx.doi.org/10.1023/A%3A1022490512705>.
- [313] Rafael Moreno-Sanchez, Sara Rodriguez-Enriquez, Emma Saavedra, Alvaro Marin-Hernandez, and Juan Carlos Gallardo-Perez. The bioenergetics of cancer: is glycolysis the main atp supplier in all tumor cells? *Biofactors*, 35(2):209–225, 2009. URL <http://dx.doi.org/10.1002/biof.31>.

- [314] M. Hatanaka. Transport of sugars in tumor cell membranes. *Biochim Biophys Acta*, 355(1):77–104, Apr 1974. URL [http://dx.doi.org/10.1016/0304-419X\(74\)90008-0](http://dx.doi.org/10.1016/0304-419X(74)90008-0).
- [315] J. L. Snoep, M. Mrwebi, J. M. Schuurmans, J. M. Rohwer, and M. J. Teixeira de Mattos. Control of specific growth rate in *saccharomyces cerevisiae*. *Microbiology*, 155(Pt 5):1699–1707, May 2009. URL <http://dx.doi.org/10.1099/mic.0.023119-0>.
- [316] A. Bock. *Überwachung und Regelung von Hochzelldichtekultivierungen in der Influenza-Impfstoffproduktion*. Shaker Verlag, Aachen, Germany, Jun 2012. URL <http://dx.doi.org/10.2370/9783844010404>.
- [317] Jennifer Levering, Mark W J M. Musters, Martijn Bekker, Domenico Bellomo, Tomas Fiedler, Willem M. de Vos, Jeroen Hugenholtz, Bernd Kreikemeyer, Ursula Kummer, and Bas Teusink. Role of phosphate in the central metabolism of two lactic acid bacteria—a comparative systems biology approach. *FEBS J*, 279(7):1274–1290, Apr 2012. URL <http://dx.doi.org/10.1111/j.1742-4658.2012.08523.x>.
- [318] J. Ovádi and P. A. Srere. Macromolecular compartmentation and channeling. *Int Rev Cytol*, 192:255–280, 2000. URL [http://dx.doi.org/10.1016/S0074-7696\(08\)60529-X](http://dx.doi.org/10.1016/S0074-7696(08)60529-X).
- [319] Qiaoling Huang, Alice Cheng, Martin Antensteiner, Changjian Lin, and Erwin A. Vogler. Mammalian cell-adhesion kinetics measured by suspension depletion. *Biomaterials*, 34(2):434–441, Jan 2013. URL <http://dx.doi.org/10.1016/j.biomaterials.2012.09.073>.
- [320] S. J. Pirt. *Principles of microbe and cell cultivation*. Wiley, New York, 1975. URL <http://dx.doi.org/10.1002/aic.690220342>.
- [321] H. J. Tsai and J. E. Wilson. Functional organization of mammalian hexokinases: characterization of the rat type iii isozyme and its chimeric forms, constructed with the n- and c-terminal halves of the type i and type ii isozymes. *Arch Biochem Biophys*, 338(2):183–192, Feb 1997. URL <http://dx.doi.org/10.1006/abbi.1996.9850>.

A Appendix

Supplementary studies

A.1. Sedimentation and attachment of MDCK cells to 6-well plate surface

The lag phase in cell growth can be decomposed in case of adherent MDCK cells into sedimentation, attachment and increase in cell size until first division. To further clarify the first two steps, i.e. speed of sedimentation and attachment, we inoculated cells in 6-well plates with GMEM-Z medium and quantified the cell concentration in suspension (Fig. A.1A), known as suspension depletion [319], and of cells attached to the well surface (Fig. A.1B, we thank C. Best from the Max Planck Institute for Dynamics of Complex Technical Systems Magdeburg for conducting the experiments and for measurement of the cell numbers). Polynomial regression of the supernatant cell number with exponential functions yielded a cell number decrease of $k_{sett} = 0.28 \pm 0.02 \text{ h}^{-1}$ (\circ : 0.27 h^{-1} ; Δ : 0.27 h^{-1} ; \square : 0.31 h^{-1}). Afterwards we used a simple first order kinetic with

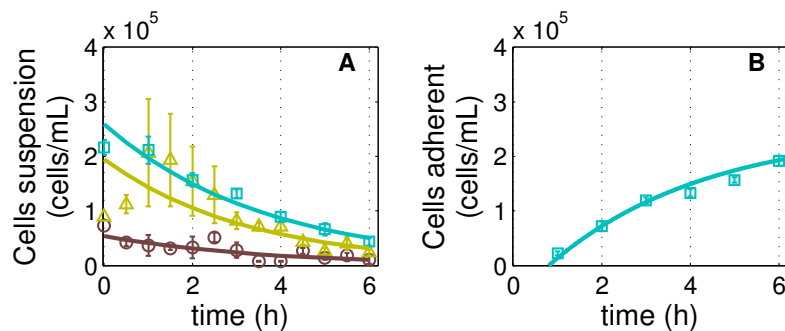


Figure A.1.: Attachment of MDCK cells to the surface of a 6-well plate. (A) Concentration of cells in suspension determined in three technical replicates (\circ , Δ , \square). Experiments Δ , \square were shaken before sampling. Lines represent regression of an exponential function (see text). (B) Concentration of adherent cells in experiment \square . Line represents prediction for adherent cell concentration based on a specific attachment rate of 0.28 h^{-1} and an initial cell concentration in the supernatant of 2.5×10^5 and was shifted by 0.8 h. Data was taken by Claudia Best and is shown as mean and standard deviation of three wells.

an initial suspension cell concentration of 2.5×10^5 cells/mL and compared the time integral of the sedimentation rate with the increase in adherent cell number (model not shown, Fig. A.1B). The integral in Fig. A.1B recapitulates the data as long as the onset of the cell attachment is shifted towards later times by about 0.8 h. Therefore, we anticipate that cells require 0.8 h for the actual attachment process while the sedimentation requires 2.4 h for half of the cells according to k_{sett} . The sum of both renders the mean cell to potentially start growing in size as early as 3.2 h after inoculation.

A.2. Adjusting the segregated cell growth model to growth in DMEM medium

The model for cell growth was comprehensively validated with data from three independent cultivations in GMEM-Z medium. The well-surface was identified as the main limiting factor of growth. However, for MDCK cell growth in DMEM medium, the model of section 3.1.1 requires modifications such that it reflects cell growth under low GLC^x levels.

Changes to the model structure

By fitting the model to the experimental data, we found that the total cell volume reached by the cells is lower at the end of cultivation ($V_*^C = 5.20$ μ L) than for GMEM-Z cultivations. Furthermore, the specific growth rate μ of the cells now depends on the extracellular glutamine concentration (GLN^x) instead of the glucose (GLC^x) concentration, as cells grew for a certain time span under low GLC^x levels:

$$\mu = \frac{\mu_{max}[GLN^x]}{k_{GLN^x}^m + [GLN^x]} \quad (A.2.1)$$

with $k_{GLN^x}^m = 0.04$ mmol/L as the Monod constant for GLN^x . Under low concentrations of GLC^x , the uptake may also depend on the affinity of the glucose transporter, which can yield smoother depletion dynamics. To account for such an effect, both uptake rates for GLC^x were extended by a Michaelis-Menten kinetic [320]:

$$r_{X/GLC^x} = \mu(X_1 f + \sum_{i=2}^{N_c} X_i) Y_{X/GLC^x} \frac{[GLC^x]}{k_{GLC^x}^m + [GLC^x]} \quad (A.2.2)$$

$$r_{m/GLC^x} = m_{GLC^x} V^C \frac{[GLC^x]}{k_{GLC^x}^m + [GLC^x]} \quad (A.2.3)$$

where $k_{GLC^x}^m = 0.24$ mmol/L is the new affinity constant for glucose. Except of Y_{X/GLN^x} which increases to 5.92×10^{-7} mmol/L/cell, all other parameter values were taken from the original model (Table C.4) while initial conditions were derived during model fitting (Table C.3).

Cell number, diameter and volume dynamics

These minor changes allow capturing the growth dynamics of adherent MDCK cells in numbers and mean cell diameter (Fig. A.2). Similarly to the growth of MDCK cells in GMEM-Z, the growth phases were identified based on the relative number of growing cells (b_{syn} , Eq. 3.1.94) with: growth phase 0 – 40 h (0 – 5 % growth inhibition), intermediate growth phase 40 – 75 h (5 – 95 % growth inhibition), and stationary growth phase 75 – 200 h (95 – 100 % growth inhibition). A total cell number of 2.80×10^6 is reached towards the end of cultivation, which is lower compared to the GMEM-Z cultures (Fig. 4.7A). The mean cell diameter starts with 15 μm and reaches a maximum of 19 microm at 24 h of cultivation, which is within the range we described for MDCK cells for cultivations in GMEM-Z medium (Fig. 4.7).

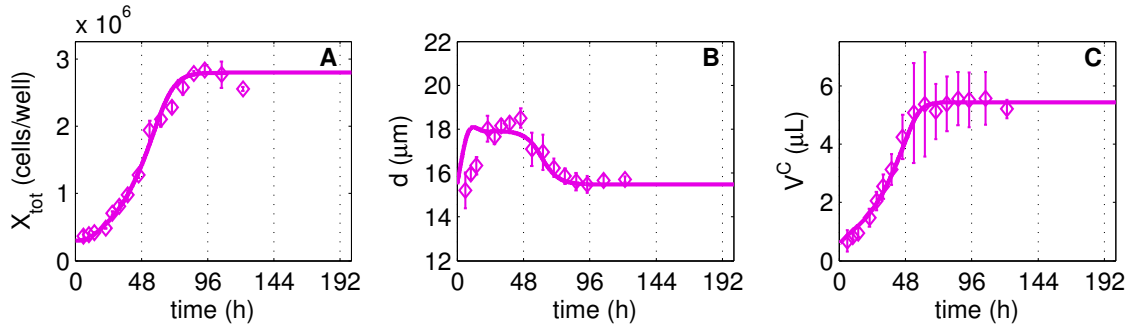


Figure A.2.: MDCK cell growth with DMEM (2 mmol/L GLC^x) in six-well plates. (A) cell number. (B) mean cell diameter. (C) the volume of all cells calculated from the mean cell diameter and the cell number. Data was taken from [23] and indicated as diamond (\diamond). Error bars represent mean and standard deviation of three wells (in case of V^C error bars were calculated according to the error propagation law). Lines represent the corresponding model simulation (parameters of Table C.3 and Table C.4 with modifications described in the text).

Extracellular metabolite pool dynamics

The level of GLC^x starts at low levels (2.3 mmol/L) and decreases fast due to an exponentially increasing demand by the cells (Fig. A.3A). The original data for GLC^x is

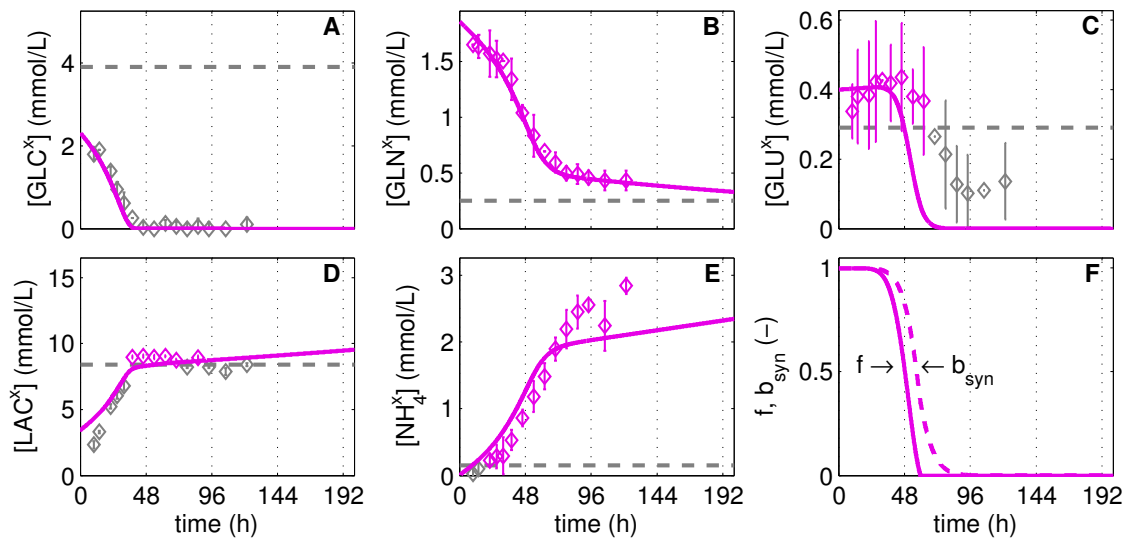


Figure A.3.: Concentrations of extracellular substrates and by-products during MDCK cell cultivation in DMEM (2 mmol/L GLC^x). Extracellular glucose (A), glutamine (B), glutamate (C), lactate (D) and ammonia (E) concentration. Data (\diamond) and error bars, which represent mean and standard deviation of three wells, were taken from [23]. The extracellular glucose concentration was shifted by -1.41 mmol/L to achieve a real depletion and to properly fit the model. F: cell volume-dependent growth inhibition f and relative biosynthesis activity b_{syn} of the cells. Data and corresponding model simulations (based on parameters of Table C.3 and C.4 and modifications described in the text) are shown in the color code of Figure A.2. Grey dashed lines are the limit of quantification (LOQ; data below LOQ marked in gray)

about 1.41 mmol/L higher (but still below the LOQ) and thus constantly high between 40 – 200 h of cultivation. As this neither fits to the observation that MDCK cells require GLC^x nor that V^C still increases after 40 h of cultivation we decided to shift the GLC^x concentration such that it depletes during cultivation. However, in both cases GLC^x levels remain constant after 40 h of cultivation while the total cell volume still increases (until 58 h of cultivation, Fig. 4.7C). Presumably, the cells use stored internal precursors and take up more GLN^x to meet their demands in biomass precursor. So the reduction in the final level of V^C may thus either be explained with the differences between media or be attributed to a delayed effect of the glucose limitation. The increased uptake of GLN^x is captured by the model (Fig. A.3B) and also agrees with the NH_4^x release (Fig. A.3E). The uptake of GLU^x depends on the growth inhibition of the cells and are similar to cell growth in GMEM-Z (Fig. A.3C, A.3F).

A.3. Fit of segregated cell growth model to MDCK.SUS growth

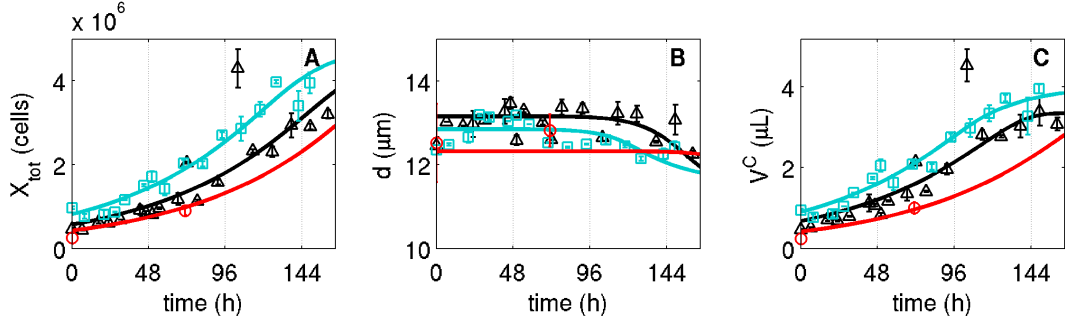


Figure A.4.: MDCK suspension cell growth in stirred tank bioreactors with SMIF08 medium. (A) Cell concentration. (B) Mean cell diameter. (C) Volume concentration of all cells calculated from the mean cell diameter and the cell number. Data of three independent experiments are indicated as triangle (Δ), rectangle (\square) and circle (\circ). Error bars represent mean and standard deviation of three technical replicates (in case of V^C error bars were calculated according to the error propagation law). Lines represent the corresponding model simulation.

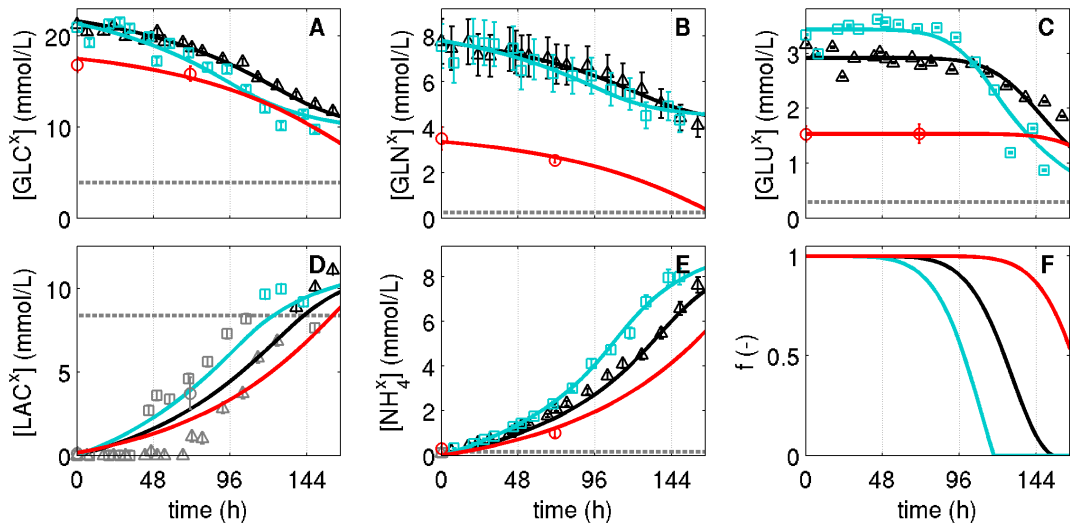


Figure A.5.: Concentration of extracellular substrates and byproducts. Glucose (A), glutamine (B), glutamate (C), lactate (D) and ammonia (E) during MDCK suspension growth in stirred tank bioreactors with SMIF08 medium. Data (Δ , \square , \circ) and error bars represent mean and standard deviation of three technical replicates. F: cell volume-dependent growth inhibition. Data and corresponding model simulations are shown in the color code of Fig. A.4. Grey dashed lines are the limit of quantification (LOQ; data below LOQ marked in gray).

A.4. Parameter correlation analysis

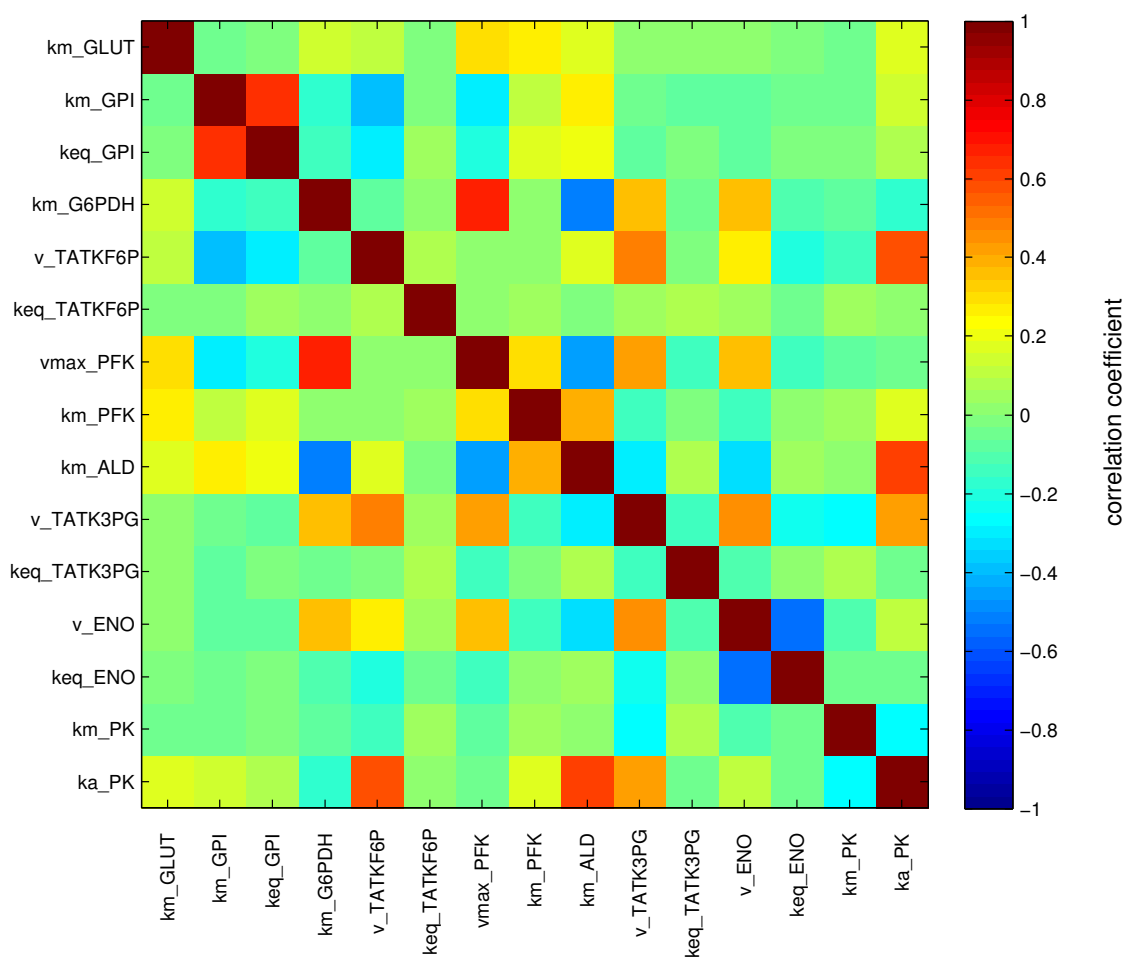


Figure A.6.: Pairwise linear correlation coefficient of model parameters for glycolysis that were estimated in this study (Cult1–3, Lim1, Lim2, Pulse). The coefficient is determined from 2000 parameter sets (Θ), which were generated by the bootstrap method (see section 3.3.2), and given as color code.

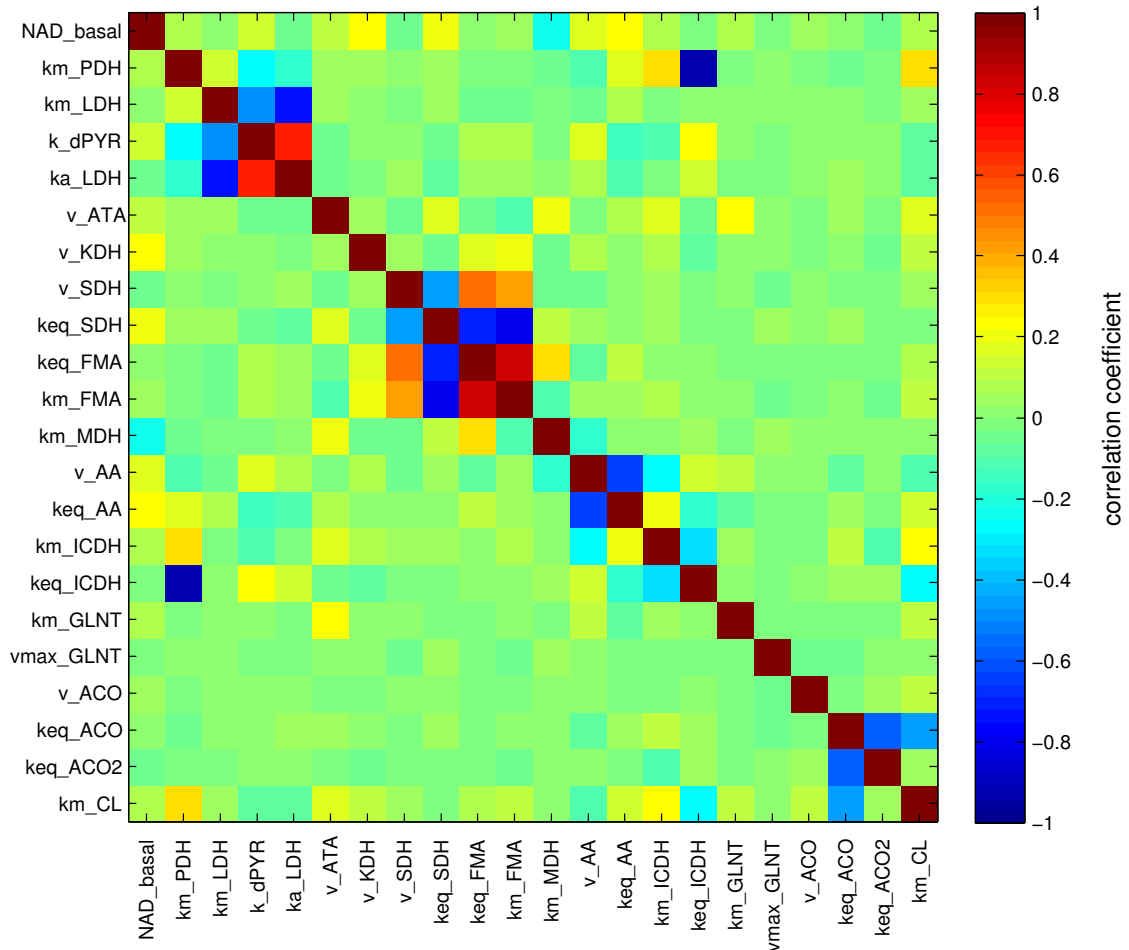


Figure A.7.: Pairwise linear correlation coefficient of model parameters for glutaminolysis that were estimated in this study (Cult1–3, Lim1, Lim2, Pulse). The coefficient is determined from 2000 parameter sets (Θ), which were generated by the bootstrap method (see section 3.3.2), and given as color code.

B Appendix

Supplementary data

B.1. Limits of quantification for metabolite measurements

Table B.1.: Limit of quantification for intracellular and extracellular metabolites (Max Planck Institute for Dynamics of Complex Technical Systems Magdeburg, not published)

Metabolite	LOQ	Unit	Metabolite	LOQ	Unit
2PG	3.75E-008	mmol	GLU ^x	0.29	mmol/L
3PG	3.75E-008	mmol	GMP	3.75E-008	mmol
α KG	1.50E-007	mmol	GTP	1.19E-007	mmol
ADP	3.00E-007	mmol	ICIT	3.75E-008	mmol
AMP	1.50E-007	mmol	LAC ^x	8.4	mmol/L
ATP	6.00E-007	mmol	MAL	3.00E-007	mmol
CDP	3.75E-008	mmol	NH ₄ ^x	0.15	mmol/L
CAC	3.75E-008	mmol	PEP	3.75E-008	mmol
CIT	5.78E-007	mmol	PYR	3.00E-007	mmol
CMP	3.75E-008	mmol	R5P	3.75E-008	mmol
CTP	6.00E-008	mmol	SUC	3.00E-007	mmol
F16BP	3.42E-007	mmol	UDP	3.75E-008	mmol
F6P	5.25E-008	mmol	UDP-GalNAc	9.00E-008	mmol
FUM	7.50E-008	mmol	UDP-GlcNAc	3.00E-007	mmol
GDP	6.00E-008	mmol	UGLC	1.05E-007	mmol
G6P	5.25E-008	mmol	UMP	3.75E-008	mmol
GLC ^x	3.9	mmol/L	UTP	3.00E-007	mmol
GLN ^x	0.25	mmol/L			

B.2. Adenosine pool dynamics during substrate perturbation

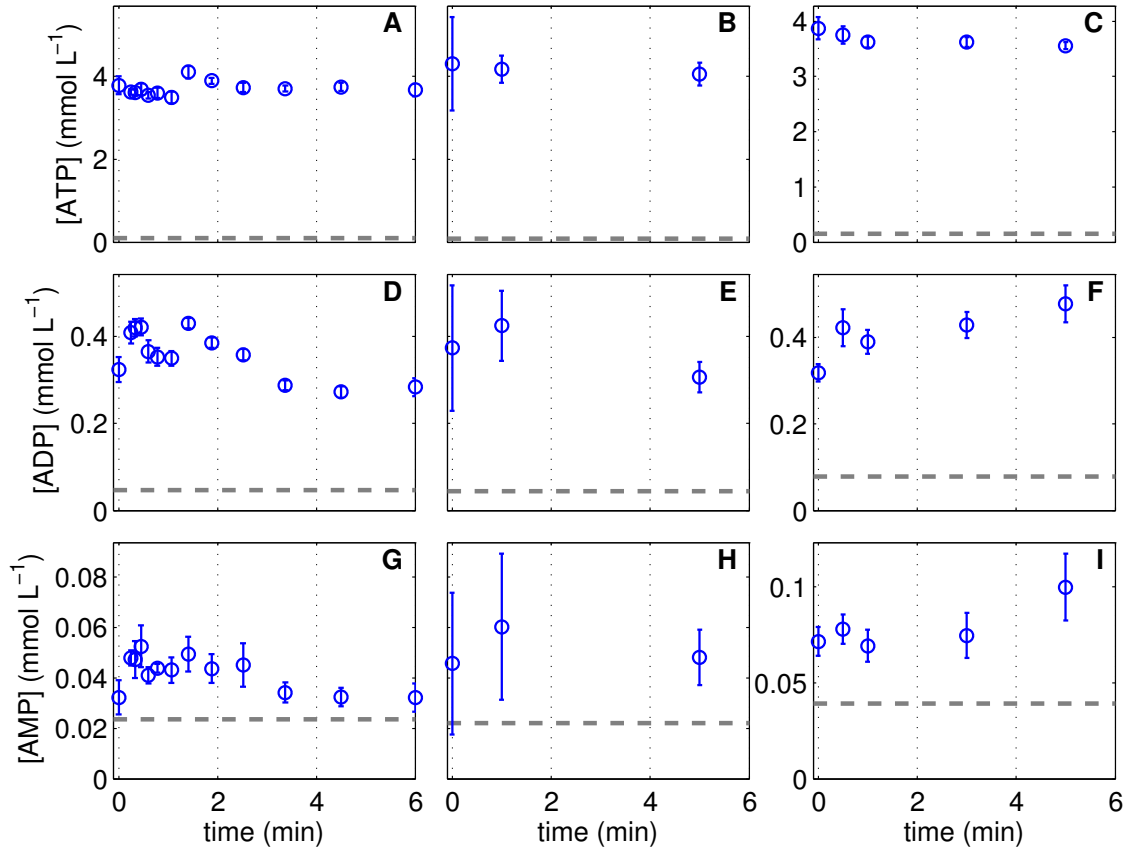


Figure B.1.: Adenosine-based nucleotide pools during during substrate limitation and substrate pulse. ATP (A – C), ADP (D – F) and AMP (G – I) concentrations of three independent perturbation experiments with MDCK cells in 6-well plates. Cells, originating from a cultivation experiment (see Table C.2) were deprived of extracellular nutrients by removal of medium and addition of phosphate buffered saline (PBS), shown in the first column (Lim1) and second column (Lim2). After a 2 h limitation, PBS was exchanged by fresh medium, shown in the third column (Pulse). Data (○) and error bars represent mean and standard deviation of three wells and were taken from Ritter [23]. Dashed lines are the limit of quantification (LOQ).

C

Appendix

Local and global model parameters

Table C.1.: Initial conditions and experiment-specific parameters for the structured model comprising the metabolic status, growth status and culture conditions relevant for simulation of the cultivation experiments (Cult1–3, Pred.). The metabolic status is derived by steady state simulation (see section 3.2).

	Cult1 (Δ)	Cult2 (\square)	Cult3 (\circ)	Pred. (\diamond)	Unit
	Initial metabolic status				
[αKG]		3.26×10^{-1}			mmol/L
[3PG]		5.12×10^{-2}			mmol/L
[ATP]		3.48			mmol/L
[ADP]		2.94×10^{-1}			mmol/L
[AMP]		5.09×10^{-2}			mmol/L
[CAC]		5.54×10^{-3}			mmol/L
[CIT]		5.71×10^{-1}			mmol/L
[F16BP]		9.88×10^{-2}			mmol/L
[F6P]		6.66×10^{-3}			mmol/L
[FUM]		5.76×10^{-2}			mmol/L
[G6P]		1.46×10^{-2}			mmol/L
[GLC]		1.18×10^{-4}			mmol/L
[GLU]		0			mmol/L
[ICIT]		1.83×10^{-2}			mmol/L
[IMP]		1.81			mmol/L
[MAL]		4.59×10^{-1}			mmol/L
[PEP]		1.49×10^{-2}			mmol/L
[PYR]		5.81×10^{-1}			mmol/L
[R5P]		5.74×10^{-3}			mmol/L
[SUC]		1.53×10^{-1}			mmol/L
[UGLC]		2.54×10^{-1}			mmol/L

(continued on next page)

Initial growth status		
γ_{GLNT}		-
γ_{GLUT}		-
μ^a	(calculated by	1/min
b_{syn}	segregated cell growth model)	-
f		-
V_S^C		L/cell
X_{tot}		cells
Initial culture condition		
$[GLC^x]$		mmol/L
$[GLN^x]$		mmol/L
$[GLU^x]$	(see Table C.3)	mmol/L
$[LAC^x]$		mmol/L
$[NH_4^x]$		mmol/L
V^M		L
E_{level}		-

^a note that μ is here used in minutes to be consistent with intracellular reaction rates

Table C.2.: Initial conditions and experiment-specific parameters for the structured model comprising the metabolic status, growth status and culture conditions relevant for simulation of the perturbation experiments derived from the cell's cultivation history.

	Lim1 (○)	Lim2 (○)	Pulse (○)	Unit
history:	Cult1 at $t^*= 52$ h	Cult1 at $t^*= 61$ h	Cult1 at $t^*= 34$ h ^a	
Initial metabolic status				
[3PG]	7.95×10^{-2}	6.10×10^{-2}	9.03×10^{-2}	mmol/L
[αKG]	5.28×10^{-1}	3.58×10^{-1}	1.29×10^{-1}	mmol/L
[ATP]	3.15	3.36	7.21×10^{-1}	mmol/L
[ADP]	3.32×10^{-1}	3.01×10^{-1}	1.13	mmol/L
[AMP]	5.87×10^{-2}	5.39×10^{-2}	1.03×10^{-1}	mmol/L
[CAC]	5.61×10^{-3}	5.56×10^{-3}	9.78×10^{-3}	mmol/L
[CIT]	5.79×10^{-1}	5.73×10^{-1}	1.01	mmol/L
[F16BP]	5.91×10^{-1}	2.66×10^{-1}	1.54×10^{-3}	mmol/L

(continued on next page)

C. Local and global model parameters

[F6P]	1.19×10^{-2}	8.86×10^{-3}	2.31×10^{-3}	mmol/L
[FUM]	1.29×10^{-1}	7.24×10^{-2}	3.65×10^{-2}	mmol/L
[G6P]	6.02×10^{-2}	3.24×10^{-2}	1.15×10^{-3}	mmol/L
[GLC]	7.96×10^{-4}	3.30×10^{-4}	0.00	mmol/L
[GLU]	4.50×10^{-1}	1.03×10^{-1}	0.00	mmol/L
[ICIT]	1.65×10^{-2}	1.75×10^{-2}	2.63×10^{-2}	mmol/L
[IMP]	2.09	1.92	3.68	mmol/L
[MAL]	7.46×10^{-1}	5.06×10^{-1}	1.81×10^{-1}	mmol/L
[PEP]	1.09×10^{-2}	1.28×10^{-2}	3.42×10^{-2}	mmol/L
[PYR]	4.79×10^{-1}	5.07×10^{-1}	1.66	mmol/L
[R5P]	2.35×10^{-2}	1.27×10^{-2}	4.53×10^{-4}	mmol/L
[SUC]	4.23×10^{-1}	2.15×10^{-1}	1.29×10^{-1}	mmol/L
[UGLC]	3.63×10^{-1}	3.38×10^{-1}	1.96×10^{-1}	mmol/L
Initial growth status				
γ_{GLNT}	3.69×10^{-2}	1.44×10^{-2}	6.19×10^{-2}	-
γ_{GLUT}	5.36×10^{-1}	2.84×10^{-1}	7.92×10^{-1}	-
b_{syn}	6.02×10^{-1}	2.71×10^{-1}	9.69×10^{-1}	-
f	1.62×10^{-1}	4.37×10^{-4}	8.82×10^{-1}	-
X_{tot}	2.10×10^6	2.69×10^6	1.11×10^6	cells
V_S^C	3.04×10^{-12}	2.53×10^{-12}	3.46×10^{-12}	L/cell
Initial culture condition				
[GLC ^x]	2.42×10^1	2.26×10^1	^b 3.00×10^1	mmol/L
[GLN ^x]	9.53×10^{-1}	8.43×10^{-1}	^b 1.61	mmol/L
[GLU ^x]	1.45×10^{-1}	1.85×10^{-2}	^b 5.80×10^{-1}	mmol/L
[LAC ^x]	1.85×10^1	2.22×10^1	^b 0.00	mmol/L
[NH ₄ ^x]	1.36	1.46	^b 0.00	mmol/L
E_{level}	1.08	1.08	1.08	-
V^M	3.00×10^{-7}	3.00×10^{-7}	^b 4.00×10^{-3}	L

^a followed by 2 h substrate limitation

^b manually adjusted

Table C.3.: Estimated initial conditions and experiment-specific parameters of the segregated cell growth model and enzyme level (E_{level}) for simulation adherent MDCK cell growth in 6-well plates with GMEM-Z medium.

Local parameter	Cult1 Δ	Cult2 \square	Cult3 \circ	Pred. \diamond	Unit
$[GLC^x](t = 0)$	31.04	29.25	31.95	2.31	mmol/L
$[GLN^x](t = 0)$	1.61	1.78	1.82	1.86	mmol/L
$[GLU^x](t = 0)$	0.58 ^a	0.54 ^a	0.48 ^a	0.40	mmol/L
$[LAC^x](t = 0)$	3.25	3.74	1.25	3.42	mmol/L
$[NH_4^x](t = 0)$	0.76 ^a	0.74 ^a	0.74 ^a	0.00	mmol/L
d_c	22.93	24.86	20.98	21.12	μm
d_m	15.68	15.31	14.34	15.48	μm
E_{level}	1.08	1.04	0.92	1.00	-
V^M	0.004 ^b	0.004 ^b	0.004 ^b	0.004 ^b	L
$X_1(t = 0)$	0.40×10^6	0.41×10^6	0.48×10^6	0.30×10^6	cells
$X_{2,\dots,N^c}(t = 0)$	0	0	0	0	cells
Precult. system	T-flask	T-flask	Roller bottle	T-flask	
Precult. duration	3 days	6 days	4 days	-	

^a taken from Wetzel [280]

^b manually adjusted

Table C.4.: Estimated global parameters of the segregated cell growth model (for adherent MDCK cells cultivated in 6-well plates with GMEM-Z medium) on the basis of three cultivation experiments with confidence intervals between 0.025-quantile ($Q_{0.025}$) and 0.975-quantile ($Q_{0.975}$) and respective relative sensitivities $\chi^2(\phi)$. Note that parameter values are used in minute units during simulation

Global param.	Value	$Q_{0.025} - Q_{0.975}$	$\chi^2(\phi)$	Unit
μ_{max}	0.039	0.036 – 0.051	0.74	1/h
F_{evap}	^a 2.75×10^{-6}	-	-	L/h
k_{dGLN^x}	^a 3.60×10^{-3}	-	-	1/h
$k_{GLC^x}^m$	0.923	0.000 ^c – 9.974 ^c	0.03	mmol/L
m_{GLC^x}	1.06×10^{-2}	$(0.92 - 1.19) \times 10^{-2}$	0.05	mmol/L/ μ L/h
m_{GLN^x}	5.29×10^{-9}	$(0.00^c - 2.83) \times 10^{-6}$	≈ 0	mmol/L/ μ L/h
$m_{NH_4^x}$	3.33×10^{-12}	$(0.00^c - 1.00^c) \times 10^{-10}$	≈ 0	mmol/L/ μ L/h
N^c	^b 5	-	-	-
s	2.752	2.140 – 4.145	0.26	-
v_{GLT}	3.33×10^{-10}	$(2.53 - 3.83) \times 10^{-10}$	0.22	L/cell/h
V_*^C	6.804	6.568 – 6.969	0.36	μ L
Y_{LAC^x/GLC^x}	2.140	2.034 – 2.283	0.08	-
Y_{X/GLC^x}	3.57×10^{-6}	$(3.18 - 3.96) \times 10^{-6}$	0.09	mmol/L/cell
Y_{X/GLN^x}	0.27×10^{-6}	$(0.25 - 0.28) \times 10^{-6}$	0.10	mmol/L/cell
Y_{X/NH_4^x}	3.5×10^{-7}	$(3.09 - 3.72) \times 10^{-7}$	0.04	mmol/L/cell

^a estimated experimentally (F_{evap} by Ritter [23], k_{dGLN^x} by Bock et al. [212])

^b estimated in separate simulation studies

^c value at parameter bound

Table C.5.: Estimated global parameters of the structured model (for glycolysis, pentose phosphate pathway and glycogenesis) on the basis of three cultivation experiments and three perturbation experiments with confidence intervals between 0.025-quantile and 0.975-quantile ($Q_{0.025} - Q_{0.975}$).

Parameter	Value	$Q_{0.025} - Q_{0.975}$	Unit	Parameter	Value	$Q_{0.025} - Q_{0.975}$	Unit
k_{PK}^a	6.56×10^{-1}	0.57 – 1.21	mmol ² /L ²	v_{ALD}^{max}	$^{a}2.36 \times 10^{-11}$	-	mmol/cell/min
k_{GPI}^{eq}	1.78	(0.03 – 1.00 ^d) $\times 10^1$	-	v_{GLUT}^{max}	$^c1.60 \times 10^{-11}$	-	mmol/cell/min
k_{ENO}^{eq}	3.80×10^{-1}	(2.10 – 5.19) $\times 10^{-1}$	-	v_{G6PDH}^{max}	$^a5.81 \times 10^{-11}$	-	mmol/cell/min
$k_{TATK3PG}^{eq}$	9.84	(0.00 – 9.69 ^d) $\times 10^3$	-	v_{GPI}^{max}	$^a2.72 \times 10^{-10}$	-	mmol/cell/min
$k_{TATK3PG}^{eq}$	1.01×10^{-1}	(0.00 – 9.31 ^d) $\times 10^2$	-	v_{HK}^{max}	$^a1.92 \times 10^{-11}$	-	mmol/cell/min
k_{ALD}^m	1.77	1.29 – 2.52	mmol/L	v_{PFK}^{max}	1.00×10^{-11}	(0.79 – 1.15) $\times 10^{-11}$	mmol/cell/min
k_{GLUT}^m	6.60	(0.18 – 3.59) $\times 10^1$	mmol/L	v_{PK}^{max}	$^a1.23 \times 10^{-9}$	-	mmol/cell/min
k_{GPI}^m	2.41	0.10 – 2.89	mmol/L	v_{UT}^{max}	8.17×10^{-15}	(0.07 – 1.00) $\times 10^{-13}$	mmol/cell/min
k_{G6PDH}^m	3.98	(0.12 – 1.05) $\times 10^1$	mmol/L	v_{ENO}	2.34×10^{-10}	(2.42 – 5.81) $\times 10^{-10}$	L/cell/min
k_{HK}^m	$^b0.02$	-	mmol/L	v_{GLYS}	1.91×10^{-14}	(0.17 – 2.74) $\times 10^{-13}$	L/cell/min
k_{PFK}^m	1.08×10^{-2}	(0.94 – 1.38) $\times 10^{-2}$	mmol/L	v_{RDPK}	3.69×10^{-11}	(1.09 – 9.38) $\times 10^{-11}$	L/cell/min
k_{PK}^m	1.66×10^{-3}	(0.11 – 9.99 ^d) $\times 10^{-3}$	mmol/L	$v_{TATK3PG}$	3.73×10^{-14}	(0.03 – 1.00) $\times 10^{-12}$	L/cell/min
k_{UT}^m	9.96×10^{-3}	(0.13 – 2.12) $\times 10^{-2}$	mmol/L	$v_{TATK3PP}$	5.60×10^{-13}	(0.00 – 1.12) $\times 10^{-11}$	L/cell/min

^a value taken from Janke et al. [22]; ^b value taken from Tsai and Wilson [321]; ^c value taken from [104];

^d value at parameter bound

Table C.6.: Estimated global parameters of the structured model (for citric acid cycle, pyruvate metabolism and energy metabolism) on the basis of three cultivation and three perturbation experiments with confidence intervals between 0.025-quantile and 0.975-quantile ($Q_{0.975} - Q_{0.025}$).

Parameter	Value	$Q_{0.025} - Q_{0.975}$	Unit	Parameter	Value	$Q_{0.025} - Q_{0.975}$	Unit
k_{dPYR}	9.09×10^{-2}	$(0.00^c - 3.97^c) \times 10^3$	1/min	k_{PDH}^m	2.94×10^1	$(1.05 - 3.99^c) \times 10^1$	mmol/L
k_{mATP}	3.82×10^{10}	$(0.02 - 1.23) \times 10^{11}$	cell/L/min	NAD_{basal}	5.97×10^{-2}	$(0.00^c - 1.36) \times 10^{-1}$	-
$k_{X/ATP}$	3.08	$(2.06 - 3.38)$	1/min	v_{AAex}	5.91×10^{-13}	$(4.36 - 7.99) \times 10^{-13}$	L/cell/min
k_{LDH}^a	1.67×10^1	$(0.13 - 3.91^c) \times 10^1$	mmol ² /L ²	v_{ACO}	3.12×10^{-10}	$(1.07 - 9.99^c) \times 10^{-10}$	L/cell/min
k_{AAex}^{eq}	1.80	$0.78 - 9.97^c$	-	v_{AT4}	2.48×10^{-12}	$(0.01 - 9.20^c) \times 10^{-11}$	L/cell/min
k_{ACO}^{eq}	9.69×10^{-3}	$(0.87 - 1.15) \times 10^{-2}$	-	v_{ATPase}	5.79×10^{-13}	$(2.77 - 8.14) \times 10^{-13}$	L/cell/min
k_{ACCO2}^{eq}	2.67	$2.12 - 2.92$	-	v_{GLT}	5.55×10^{-12}	$(4.22 - 6.38) \times 10^{-12}$	L/cell/min
k_{ADK}^{eq}	1.73×10^{-1}	$(1.49 - 1.85) \times 10^{-1}$	-	v_{KDH}	4.29×10^{-12}	$(3.80 - 4.98) \times 10^{-12}$	L/cell/min
k_{ICDH}^{eq}	1.24×10^{-3}	$(0.11^c - 9.97^c) \times 10^{-2}$	-	v_{PSP}	7.36×10^{-8}	$(0.00 - 1.19^c) \times 10^{-7}$	L/cell/min
k_{FMA}^{eq}	8.36	$(0.57 - 1.27) \times 10^1$	-	v_{SDH}	1.56×10^{-11}	$(0.09 - 6.56) \times 10^{-10}$	L/cell/min
k_{PSP}^{eq}	3.56×10^1	$(2.95 - 4.94) \times 10^1$	-	v_{ADK}^{max}	1.20×10^{-13}	$(0.00^c - 3.68) \times 10^{-8}$	mmol/cell/min
k_{SDH}^{eq}	3.85×10^{-1}	$(2.81 - 4.78) \times 10^{-1}$	-	v_{CL}^{max}	5.87×10^{-12}	-	mmol/cell/min
k_{ADK}^m	0.00	$(0.00 - 4.05) \times 10^1$	mmol/L	v_{FMA}^{max}	9.23×10^{-11}	-	mmol/cell/min
k_{CL}^m	7.23	$6.44 - 7.63$	mmol/L	v_{GLNT}^{max}	9.76×10^{-12}	$(0.44 - 9.99^c) \times 10^{-12}$	mmol/cell/min
k_{FMA}^m	2.50	$1.20 - 3.83$	mmol/L	v_{ICDH}^{max}	4.30×10^{-13}	-	mmol/cell/min
k_{GLNT}^m	4.81×10^{-3}	$(0.00^c - 9.36^c) \times 10^{-1}$	mmol/L	v_{LDH}^{max}	9.48×10^{-10}	-	mmol/cell/min
k_{ICDH}^m	3.92×10^{-1}	$0.01^c - 8.30$	mmol/L	v_{MDH}^{max}	7.95×10^{-10}	-	mmol/cell/min
k_{LDH}^m	5.33	$(1.00^c - 9.86^c)$	mmol/L	v_{PDH}^{max}	2.50×10^{-13}	-	mmol/cell/min
k_{MDH}^m	2.61×10^2	$(1.99 - 3.00) \times 10^2$	mmol/L				

^a value taken from Janke et al. [22]; ^b value taken from [104]; ^c value at parameter bound

Markus Rehberg

Curriculum Vitae

Kontakt

Private Adresse: Peter-Paul Straße 9,
D-39106 Magdeburg, Deutschland

☎ +49-177-3005466

✉ Rehberg.M@gmail.com

Geburtsdatum: 14.08.1984

Familienstand: ledig, 1 Kind

Staatsangehörigkeit: deutsch

Profil

Bestrebt aussagekräftige Erkenntnisse an der Schnittstelle von Biotechnologie und Systembiologie zu gewinnen

Erfahrung

2009 – 2015 Dez – Feb	Doktorarbeit am Max Planck Institut, Magdeburg, Deutschland in der Arbeitsgruppe Bioprozesstechnik (Prof. Dr. U. Reichl) Thema: Dynamik im Zentralstoffwechsel von Säugerzellen Betreuer: PD. Dr. Y. Genzel, Prof. Dr. U. Reichl Tätigkeit: Entwicklung, Unterscheidung und Analyse von Enzymkinetiken und makroskopischer Wachstumsfunktionen; Modellierung verschiedener Skalen und Hierarchien; Optimierung und Identifizierbarkeitsanalyse von Parametern
2009 Feb – Nov	Diplomarbeit am Max Planck Institut, Magdeburg, Deutschland in der Arbeitsgruppe Molekularen Netzwerkanalyse (Prof. Dr. W. Marwan) Thema: Modellkopplung im Phototaxis-Signalweg von <i>H. salinarum</i> Betreuer: Jun. Prof. Dr. S. Streif Tätigkeit: Entwicklung mathematischer Modelle zur Beschreibung von Signalkaskaden; Modellkopplung; Verwendung systemtheoretischen Methoden zur Analyse von Robustheit und oszillatorischem Verhalten; Parameteroptimierung Abschlussnote: 1.0

2009 Feb – Sept	<p>Hilfswissenschaftler, Max Planck Institut, Magdeburg, Deutschland in der Arbeitsgruppe Systembiologie (Prof. Dr. mult. E.D. Gilles); 40 h im Monat</p> <p>Thema: Modellierung der <i>lac</i> Operon Induktion durch Laktose, IPTG und TMG in <i>E. coli</i></p> <p>Tätigkeit: Entwicklung mathematischer Modelle zur Beschreibung des zellulären Transkriptionssystems; Unterscheidung von “nested models” mittels gemischt ganzzahliger nicht linearer Optimierung</p>
2008 – 2009 Okt – Jan	<p>Praktikum, Sartorius-Stedim Biotech, Göttingen, Deutschland in der Forschungs- und Entwicklungsabteilung</p> <p>Thema: Evaluierung von Membranadsorbentien in biopharmazeutischen Prozessen</p> <p>Betreuer: Dr. A. Pastor</p> <p>Tätigkeit: Kultivierung von <i>P. pastoris</i> in Petrischalen und Schüttelkolben; rekombinante Proteinexpression; Proteinaufreinigung mittels Ionen-Austauscher FPLC; Proteinbestimmung mittels SDS-Gel, Bradford-Assay und HPLC</p>
2008 Feb – Sept	<p>Studienarbeit, IIM-CSIC, Vigo, Spanien in der Arbeitsgruppe Process Engineering (Prof. Dr. J. Banga)</p> <p>Thema: Modellselektion und Parameteridentifizierung mittels gemischt ganzzahliger nichtlinearer Optimierung (MINLP): eine Studie zum KdpD- / KdpE-System von <i>E. coli</i></p> <p>Betreuer: Dr. M. Rodriguez-Fernandez, Prof. Dr. A. Kremling</p> <p>Tätigkeit: Evaluierung globaler stochastischer Optimierungsalgorithmen; gemischt ganzzahlige nicht linearer Optimierung; Identifizierbarkeitsanalyse von Parametern</p> <p>Abschlussnote: 1.0</p>
2006 – 2008 Mai – Jan	<p>Hilfswissenschaftler, Max Planck Institut, Magdeburg, Deutschland in der Arbeitsgruppe Bioprozesstechnik (Prof. Dr. U. Reichl); 40 h im Monat</p> <p>Tätigkeit: Kultivierung und Quantifizierung von Säugerzellen in 6-Well Platten, T-Flaschen and Rollerflaschen; Metabolitmessungen; Probenahme und Probenvorbereitung von Influenzavirus Produktionsprozessen unter S2-Bedingungen</p>
2005 Jul – Okt	<p>Praktikum, Miltenyi-Biotech AG, Bergisch-Gladbach, Deutschland in der Produktionsabteilung</p> <p>Betreuer: Dr. G. Steinhilber</p> <p>Tätigkeit: Flusszytometrische Messungen; assistieren bei der Aufreinigung von Antikörpern mittels Größenausschlusschromatographie; assistieren bei der rekombinanten Proteinproduktion mit <i>E. coli</i></p>

Sprachkenntnisse

Deutsch	verhandlungssicher
Englisch	fließend
Latein	Latinum

Lehrtätigkeiten

Kurse	Modellierung von Bioprozessen (2012 – 2015) Leiten einer Übung zur mathematischen Modellierung und modellbasierten Optimierung von Batch, Fed-Batch und kontinuierlichen Kultivierungssystemen Cell culture engineering (2012 – 2014) Leiten einer Übung zur mathematischen Modellierung von Zellwachstum und Stoffwechsel, Modellunterscheidung und modellbasierter Optimierung Bioprozesstechnik (2010 – 2012) Leiten eines Praktikums zur Quantifizierung von Wachstum und Stoffwechsel von <i>S. cerevisiae</i> Zellen in Bioreaktoren
Betreuung	Maria Wetzel (Masterstudent) Thema der Arbeit: “Modellierung von Glutaminolyse und Zitronensäurezyklus zur Analyse von Energie- und Biomassegenerierung in MDCK Zellen” Jan Mares Klassen (Bachelorstudent) Thema der Arbeit: “Modellieren von Wachstum und Stoffwechsel kontinuierlich wachsender AGE1.HN.AAT Zellen”

Gewählte Positionen

2010 – 2014	Sprecher der Doktoranden Beteiligung am PhDnet; Organisation von Informationsveranstaltungen; Vermitteln zwischen Doktoranden und MPG Administration sowie der wissenschaftlichen Belegschaft
-------------	---

Ausbildung

2004–2009	Diplom (Dipl.-Ing.) in Biosystemtechnik Otto-von-Guericke Universität, Magdeburg, Deutschland Abschlussnote: 1.7
1991–2004	Abitur Maximillian-Kolbe-Gymnasium, Köln, Deutschland Abschlussnote: 2.7

Computerkenntnisse

Mathematisch	Deterministische Systeme partieller und gewöhnlicher Differentialgleichungen, stochastische Systeme, (mixed integer) linear and nonlinear programming, Modellunterscheidung und Identifizierbarkeitsanalyse von Parametern
Programmieren	MATLAB, C/C++, LaTeX, COPASI
Toolboxen	Curve Fitting Toolbox, Optimization Toolbox, Parallel Computing Toolbox, PottersWheel Toolbox, SBPD, SBTOOLBOX2, SimBiology, Statistics Toolbox
Software	Windows, Linux, MS Office, OpenOffice, Emacs, EndNote, JabRef und verschiedene Bildbearbeitungsprogramme

Publikationen

Paper	<p>Rehberg M., Ritter J.B., Reichl U., <i>Glycolysis Is Governed by Growth Regime and Simple Enzyme Regulation in Adherent MDCK Cells</i>, PLoS Computational Biology, 10/2014, 10(10):e1003885</p> <p>Rath A., Rehberg M., Janke R., Genzel Y., Scholz S., Noll T., Rose T., Sandig V., Reichl U., <i>The influence of cell growth and enzyme activity changes on intracellular metabolite dynamics in AGE1.hn.aat cells</i>, J. of Biotechnol., 2014, 178: 43–53</p> <p>Rehberg M., Rath A., Genzel Y., Ritter J.B., Reichl U., <i>Changes in intracellular metabolite pools during growth of adherent MDCK cells in two different media</i>, Appl. Microbiol. Biotechnol., 2014, 98(1): 385–397</p> <p>Rehberg M., Wetzel M., Ritter J.B., Reichl U., <i>The regulation of glutaminolysis and citric acid cycle activity during mammalian cell cultivation</i>, IFAC proceedings, 2013, 12(1): 48–53</p> <p>Rodriguez-Fernandez M., Rehberg M., Kremling A., Banga J.R., <i>Simultaneous model discrimination and parameter estimation in dynamic models of cellular systems</i>, BMC Systems Biology, 2013, 7(1): 76</p> <p>Rehberg M., Ritter J.B., Genzel Y., Flockerzi D., Reichl U., <i>The relation between growth phases, cell volume changes and metabolism of adherent cells during cultivation</i>, J. Biotechnol., 2013, 164: 498–499</p>
Vorträge	<p>The regulation of glutaminolysis and citric acid cycle activity during mammalian cell cultivation, Computer Applications in Biotechnology, 2013, Mumbai, Indien</p> <p>The modulation of central carbon metabolism during adherent MDCK cell growth, International Conference on Systems Biology, 2013, Kopenhagen, Dänemark</p> <p>Glycolysis of adherently growing mammalian cells - dynamics during cell growth and glucose limitation, 2012, Gastvortrag am Institut für experimentelle Physik, Otto-von-Guericke Universität, Magdeburg, Deutschland</p> <p>Inherent Dynamics of Glycolysis in MDCK Cells, Gastvortrag am Institut für Complex Systems and Mathematical Biology, 2010, University of Aberdeen, Schottland</p>
Poster	<p>Systems Biology of Mammalian Cells, 2014, Berlin, Deutschland</p> <p>ESACT meeting, 2013, Lille, Frankreich</p> <p>DECHEMA Himmelfahrtstagung, 2013, Bad-Wildungen, Deutschland</p> <p>Systems Biology of Mammalian Cells, 2012, Leipzig, Deutschland</p> <p>International Conference on Systems Biology, 2011, Heidelberg, Deutschland</p> <p>International Conference on Systems Biology, 2010, Edinburgh, Schottland</p> <p>Systems Biology of Mammalian Cells, 2010, Freiburg, Deutschland</p> <p>International Conference on Systems Biology, 2008, Göteborg, Schweden</p>